OFFICE OF CIVILIAN RADIOACTIVE WASTE MANAGEMENT
ANALYSIS/MODEL COVER SHEET

Complete Only Applicable Items

1. QA: QA

2. ☒ Analysis — Check all that apply

Type of Analysis	☒ Engineering ☐ Performance Assessment ☐ Scientific
Intended Use of Analysis	☒ Input to Calculation ☒ Input to another Analysis or Model ☒ Input to Technical Document ☒ Input to other Technical Products
Describe use:	
Input to Site Recommendation Design	

3. ☐ Model — Check all that apply

Type of Model	☐ Conceptual Model ☐ Abstraction Model ☐ Mathematical Model ☐ System Model ☐ Process Model
Intended Use of Model	☐ Input to Calculation ☐ Input to another Model or Analysis ☐ Input to Technical Document ☐ Input to other Technical Products
Describe use:	

4. Title:

Ground Control for Emplacement Drifts for SR

5. Document Identifier (including Rev. No. and Change No., if applicable):

ANL-EBS-GE-000002 REV 00 ICN 01

6. Total Attachments:

4

7. Attachment Numbers - No. of Pages in Each:

I-5; II-14; III-13; IV-12

	Printed Name	Signature	Date
8. Originator	Y. Sun	Yuanjian Sun	5/31/2001
9. Checker	D. Tang	David Tang	5/31/01
10. Lead/Supervisor	F. Duan	Fei Duan	5/31/01
11. Responsible Manager	R. Boutin	Robert S. Boutin	5/31/01

12. Remarks:

Additional Contributers of the Analysis:

A. Fei Duan: Contributed to the sections related to seismic analyses.

B. Ming Lin: Contributed to the Attachments I and IV.

C. Narayanan Doraswamy: Contributed to part of the Attachment II.

LWM-11 NNA5507

OFFICE OF CIVILIAN RADIOACTIVE WASTE MANAGEMENT
ANALYSIS/MODEL REVISION RECORD

Complete Only Applicable Items

2. Analysis or Model Title:

Ground Control for Emplacement Drifts for SR

3. Document Identifier (including Rev. No. and Change No., if applicable):

ANL-EBS-GE-000002 REV 00 ICN 01

4. Revision/Change No.	5. Description of Revision/Change
00	Initial Issue.
00/ICN 01	ICN to incorporate changes corresponding to low temperature repository design and sensitivity study. All changes are indicated by sidebars in the margin. The following sections are revised or added: 1, 2, 3, 4, 4.1.1, 4.1.2, 4.1.3, 4.1.4, 4.1.5, 4.1.6, 4.1.7, 4.1.8, 4.1.10, 4.1.12, 4.1.13, 4.1.14, 4.2, 4.3, 4.4, 5.1, 5.3, 5.4, 5.5, 5.6, 5.7, 5.8, 5.9, 5.10, 5.11, 5.12, 5.13, 5.14, 6.1, 6.2.1, 6.3.1, 6.3.3, 6.4.2.1, 6.4.2.2.1.1, 6.4.2.2.1.2, 6.4.2.2.2.3, 6.4.2.2.3, 6.5, 6.5.1, 6.5.1.1.2.2, 6.5.1.2.1.1, 6.5.1.2.1.2, 6.5.1.2.2.1, 6.5.1.2.2.2, 6.5.1.2.2.3, 6.5.2, 6.6.1.1, 6.6.1.2, 6.6.1.3, 6.6.2.1, 6.7, 7, Attachments I, II, III, and IV.

CONTENTS

Page

CONTENTS (Continued)

Page

CONTENTS (Continued)

Page

FIGURES

FIGURES (Continued)

Page

FIGURES (Continued)

Page

FIGURES (Continued)

FIGURES (Continued)

Page

FIGURES (Continued)

FIGURES (Continued)

TABLES

ACRONYMS

3DEC	3-Dimensional Distinct Element Code
ACI	American Concrete Institute
AISC	American Institute of Steel Construction
SCM	Software Configuration Management
ESF	Exploratory Studies Facility
FLAC	Fast Lagrangian Analysis of Continua
HT	High Temperature
LT	Low Temperature
NGI	Norwegian Geotechnical Institute
PDD	Project Description Document
PGA	Peak Ground Acceleration
PGV	Peak Ground Velocity
PTn	Paintbrush Nonwelded Tuff
RMQ	Rock Mass Quality
SDD	System Description Document
SR	Site Recommendation
TBM	Tunnel Boring Machine
TC	Thermal Condition
TCw	Tiva Canyon Welded Tuff
Tptpll	Topopah Spring Tuff Crystal-poor Lower Lithophysal Unit
Tptpmn	Topopah Spring Tuff Crystal-poor Middle Non-lithophysal Unit
TSw1	Topopah Spring Densely Welded Devitrified Lithophysal-rich Tuff
TSw2	Topopah Spring Densely Welded Devitrified Lithophysal-poor Tuff
UDEC	Universal Distinct Element Code

1. PURPOSE

The purpose of the analysis is to demonstrate that a satisfactory ground control system can be designed to ensure the stability of the emplacement and adjacent non-emplacement drifts and provide a technical basis for the design and selection of the ground support systems for these drifts. The analysis will provide inputs for the Site Recommendation (SR) design.

The objective of the analysis is to develop, describe and apply analytical methods and models to predict the behavior of repository drifts and ground support systems during the repository preclosure period. The analysis is limited to the thermal and mechanical effects of waste emplacement. Other effects such as hydrological and chemical effects are not considered in this analysis.

The analysis identifies the physical mechanisms and governing parameters related to drift stability, develops analytical methods for modeling them, and performs calculations for the SR design. The potential repository subsurface layout for the analysis is based on the Site Recommendation design. Numerical calculations are carried out using both qualified and unqualified codes. Use of the unqualified codes is identified with "To Be Verified" (TBV) in this analysis (see Section 3).

The scope of the work also includes a literature search of case histories, identification of input data, software, and references, as required. The primary tasks involved in the development of the analysis include the following, based on the *Development Plan for Ground Control for Emplacement Drifts for SR* (CRWMS M&O 1999f) and the *Technical Work Plan for Subsurface Design Section FY 01 Work Activities* (CRWMS M&O 2001, p. 13):

- Review case histories to identify relevant information on tunnel design and performance. Existing data collected from the Exploratory Studies Facility (ESF), the Enhanced Characterization of the Repository Block (ECRB), and the Drift Scale Test (DST) are included in this review.

- Identify input data, sources, and assumptions necessary to perform the analysis.

- Evaluate existing calculations and models relevant to drift stability. Revise existing models or develop new approaches, if necessary, to account for the latest design information, including the subsurface layout, rock properties, joint patterns, and ground support types.

- Perform analyses to evaluate the stability of emplacement and adjacent non-emplacement drifts subjected to in situ, thermal, and seismic loads during the preclosure period. Evaluate the performance of candidate ground supports. Thermal conditions considered for the SR design correspond to a high-temperature and a low-temperature operation mode. Effects of longer ventilation period under the low temperature operation mode on emplacement drift closures, stress redistributions, and ground support behavior are also evaluated.

- Perform sensitivity studies to assess the impact of variations of rock types, properties, joint patterns, loads, and model dimension on the drift and ground support behaviors.

2. QUALITY ASSURANCE

The emplacement drifts ground support system has been classified as QL-2 in the *Classification of the MGR Ground Control System* (CRWMS M&O 1999a, Table 1). Therefore, emplacement drifts ground support is subject to QA controls. In the same reference, ground control for the non-emplacement openings is classified as CQ (conventional quality) and, thus, is not subject to the requirements of the *Quality Assurance Requirements and Description* (QARD) (DOE 2000).

This design analysis activity has been evaluated (CRWMS M&O 1999d and CRWMS M&O 2001, p. A12) in accordance with the AP-2.21Q procedure, *Quality Determinations and Planning for Scientific, Engineering, and Regulatory Compliance Activities*, and it was determined that this analysis is subject to quality assurance controls. Therefore, this activity is subject to the requirements of the QARD.

Input data used in this analysis and their sources and qualification status are identified and documented in Sections 4 and 5 in accordance with the AP-3.15Q procedure, *Managing Technical Product Inputs*.

Results of the analysis, including input and output files of numerical analyses, are submitted to the Technical Data Management System (TDMS) and the Document Control (DC) for data management and retrieval, respectively, in accordance with the AP-SV.1Q procedure, *Control of the Electronic Management of Information*. There is no variance in the method used from that planned (CRWMS M&O 2001, Section 10, p. 19).

3. COMPUTER SOFTWARE AND MODEL USAGE

Four commercially available computer programs, ANSYS, FLAC (Fast Lagrangian Analysis of Continua), UDEC (Universal Distinct Element Code), and 3DEC (3-Dimensional Distinct Element Code), are used to perform thermal, mechanical, and seismic analyses. Descriptions of these codes and their qualification status are provided in the following subsections.

The modeling approaches used to perform the analyses with these computer programs do not constitute the development of a model as defined in the AP-3.10Q procedure, *Analyses and Models*. However, all of these programs are developed based on established mathematical and engineering theories and laws, such as Fourier's law, Hooke's law, and Mohr-Coulomb yield criterion. Selection of these programs or mathematical models for this analysis indicates the adoption of these underlying scientific and engineering laws. Since all of these software programs have been or are being validated and verified by the Project (discussed below), in addition to the rigorous validation conducted by the vendors before the release of the programs, the underlying mathematical models are determined valid as long as their intended use is within the range of validation.

3.1 ANSYS COMPUTER SOFTWARE

ANSYS Version 5.2 is a general purpose, finite-element analysis code, and is used in many disciplines of engineering such as structural, geotechnical, and mechanical, dealing with behavior of solids and fluids, including thermal response. ANSYS is installed on the Silicon Graphics (SGI) and Sun Microsystems workstations with the Unix operating system. ANSYS Version 5.2 has been verified and validated (CSCI#: 30013 V5.2SGI, CRWMS M&O 1997d) according to the AP-SI.1Q procedure, *Software Management*. ANSYS was used in this analysis in thermal and coupled thermomechanical analyses for the emplacement drifts. The input and output files generated by ANSYS are submitted as part of the records package for this analysis (DTNs: MO0004MWDEMP02.003 and MO0105MWDGRO02.008). The results are presented and described throughout Section 6.0. A detailed discussion of the general features and fields of application of the ANSYS code is presented in the user's manual (Swanson Analysis Systems 1995).

The ANSYS Version 5.2 software (CRWMS M&O 2000d) (CSCI#: 30013 V5.2SGI) was obtained from the Software Configuration Management (SCM) in accordance with the AP-SI.1Q procedure. The software was appropriate for the applications used in this analysis. The software was used only within the range of validation as specified in the software qualification report (CRWMS M&O 1997d).

3.2 FLAC COMPUTER SOFTWARE

FLAC Version 3.5 is a two-dimensional explicit finite difference code which simulates the behavior of structures built of soil, rock, or other materials subjected to static, dynamic, and thermally-induced loads (Itasca Consulting Group 1998). Modeled materials respond to applied forces or boundary restraints according to prescribed linear or non-linear stress/strain laws and undergo plastic flow when a limiting yield condition is reached. FLAC is based upon a "Lagrangian" scheme which is well suited for large deflections and has been used primarily for

analysis and design in mine engineering and underground construction. The explicit time-marching solution of the full equations of motion, including inertial terms, permits the analysis of progressive failure and collapse. A detailed discussion on the general features and fields of the FLAC computer software applications is presented in the user's manual (Itasca Consulting Group 1998). It is noted that the cited FLAC user's manuals are for the Version 3.4 because the FLAC Version 3.5 user's manuals are not available. The input and output files generated by FLAC are submitted as part of the record package for this analysis (DTNs: MO0004MWDEMP02.003 and MO0105MWDGRO02.008). The results are presented and described throughout Section 6.0 and its subsections.

FLAC Version 3.5 (CRWMS M&O 1999i) (Software Tracking Number (STN): 10167-3.5-00) was obtained from the SCM in accordance with the AP-SI.1Q procedure. FLAC is installed and run on Pentium PCs. FLAC Version 3.5 is qualified for use in design in accordance with the AP-SI.1Q procedure. The software was appropriate for the applications used in this analysis, and used only within the range of validation, as specified in the software qualification documentation.

3.3 UDEC COMPUTER SOFTWARE

UDEC Version 3.0 is a two-dimensional numerical program based on the distinct element method for discontinuum modeling (Itasca Consulting Group 1996b). The program simulates the response of discontinuous media (such as a jointed rock mass) subjected to thermal, static, or dynamic loading. In UDEC, the discontinuous medium is represented as an assemblage of discrete blocks. The discontinuities between blocks are treated as boundary conditions that permit large displacements along the discontinuities and block rotations. Individual blocks behave as either rigid or deformable material. Deformable blocks are subdivided into a mesh of finite difference elements, and each element responds according to a prescribed linear or non-linear stress-strain law. The relative motions at discontinuities are also governed by linear or non-linear force-displacement relations for movement in both the normal (perpendicular) and shear directions. UDEC has several built-in material behavior models for deformable blocks that simulate discontinuous geologic materials. UDEC is based on a Lagrangian calculation scheme that is well-suited to model the large movements and deformations of blocks in a system. A more detailed discussion of the general features and fields of applications of UDEC computer software is presented in the user's manual (Itasca Consulting Group 1996b). The input and output files generated by UDEC are submitted as part of the records package for this analysis (DTNs: MO0004MWDEMP02.003 and MO0105MWDGRO02.008). The results are presented and described in Section 6.0 and its subsections.

UDEC (CRWMS M&O 1999j) (STN: 10173-3.0-00) is installed and run on Pentium PCs. UDEC Version 3.0 is being processed for ultimate qualification for use in design in accordance with the AP-SI.1Q procedure, Rev. 3, ICN 1, Section 5.10, as "Interim Use of Unqualified Software to Support SR Products." UDEC was appropriate for the applications used in this analysis, and used only within the range of validation, which will be specified in the software qualification documentation (STN: 10173-3.0-00).

3.4 3DEC COMPUTER CODE

3DEC Version 1.5 is a three-dimensional computer code based on the distinct element method for discontinuum modeling. In 3DEC, the discontinuous medium is presented as an assemblage of discrete blocks. Individual blocks behave as either rigid or deformable material; deformable blocks are subdivided into a mesh of finite difference elements. 3DEC is based on a Lagrangian calculation scheme that is well-suited to model the large deformations of blocks in a system. A detailed discussion on the general features and fields of 3DEC computer software applications is presented in the user's manual (Itasca Consulting Group 1994). The input and output files generated by 3DEC are submitted as part of the records package for this analysis (DTN: MO0004MWDEMP02.003). The results are presented and described in Section 6.0 and its subsections.

3DEC Version 1.5 (CRWMS M&O 1994b) (CSCI#: B00000000-01717-1200-30013) was obtained from the SCM in accordance with the AP-SI.1Q procedure. 3DEC is installed and run on Pentium PCs. 3DEC Version 1.5 was qualified for use in quality affecting work in accordance with the AP-SI.1Q procedure (CSCI#: B00000000-01717-1200-30013, CRWMS M&O 1994a). 3DEC was appropriate for the applications used in this analysis, and used only within the range of validation as specified in the software qualification documentation (CRWMS M&O 1994a).

3.5 SPREADSHEET SOFTWARE

Microsoft Excel 97 spreadsheet software was used in displaying some of the ANSYS, FLAC, and UDEC results graphically and calculating the combined stresses in steel sets based on the results obtained from the ANSYS and FLAC analyses. In the former application, the results from these analyses, including drift closures, stresses in rock adjacent to drift openings, forces and bending moments in steel sets, and axial forces in rock bolts, were used as inputs. In the latter application, simple arithmetic operations, such as addition, subtraction, multiplication, and division, were used. User-defined formulas and/or algorithms are displayed where used. For example, Equation (6-6) was used to compute the combined stresses in steel sets with Excel. The outputs are presented in the form of figures in Section 6 and Attachments I through IV. Both the inputs and outputs used in Excel are contained in DTNs: MO0004MWDEMP02.003 and MO0105MWDGRO02.008.

Microsoft Excel 97 is an exempt software product in accordance with the AP-SI.1Q procedure, Rev. 3, ICN 1, Section 2.1.1.

4. INPUTS

This section presents the data and parameters, criteria, and codes and standards used in the analysis. Some of the input data presented in this section are considered unqualified, and obtained from TDMS. Justification for use of these data in the analysis will be provided in accordance with the AP-3.10Q procedure. The outputs from this analysis cannot be used for procurement, fabrication, or construction prior to qualification of all input data.

4.1 DATA AND PARAMETERS

4.1.1 Average Ground Surface Temperature and In Situ Thermal Gradient

The average ground surface rock temperature is 18.7°C (CRWMS M&O 1999c, Section 5.1.2). The rock thermal gradients (CRWMS M&O 1999c, Section 5.1.2) are listed in Table 4-1. The source data are based on the tempature profile in borehole USW G-4 (Sass et al. 1988, p. 48 and Figure 1-12). For use of these data, see Assumption 5.8.

Table 4-1. Rock In Situ Thermal Gradient

Depth (m)	Value (°C /m)
0 - 150	0.020
150 - 400	0.018
400 - 700	0.030

Source: CRWMS M&O 1999c, Section 5.1.2, which is based on Sass et al. 1988, p. 48 and Figure 1-12.

4.1.2 Depths of Rock Units and Emplacement Drifts

The thicknesses of the lithostratigraphic rock units are listed in Table 4-2. These are the average values at the point (N233,760 m, E170,750 m) of the emplacement area (CRWMS M&O 1999b; DTN: SN0003T0571897.013). The average elevations of the surface and the repository levels (invert) at this point are 1421.28 m (CRWMS M&O 1999b) and 1072.30 m (CRWMS M&O 1998b, Figure 4-1, p. 19), respectively. Therefore, the depth of the repository level (the invert) at this point is at 348.98 m (1421.28 – 1072.30 = 348.98 m) from the surface. It is noted that the elevations of the ground surface and emplacement drift invert and stratigraphy were taken from the most recent of the references available when the numerical modeling for this analysis started. These values may slightly differ from those in the subsurface layout design for SR. However, minor changes are not significant to the results of this analysis.

The depth of each rock unit listed in Table 4-3 is calculated based on the elevations of the surface (1421.28 m) and the top of the Tpcpv2 unit (1306.98 m), and the thickness of each rock unit (CRWMS M&O 1999b). The top of the Tpcpv2 unit is at depth 114.30 m (1421.28–1306.98=114.30 m). The information is then used to determine the vertical (y) coordinates (see Table 4-3) of the top and bottom of the units lying above and below the emplacement drifts, respectively. The origin of the coordinates is set at the center of the emplacement drifts.

For use of these data, see Assumption 5.9.

Table 4-2. Thermal Modeling Parameters by Stratigraphic Unit

T/M Unit	USGS Unit		ISM 3.0	Thickness	Saturated Bulk Density[a]	Thermal Conductivity		Specific Heat		
						T≤100°C	T>100°C	T≤95°C	95°C<T≤114°C	T>114°C
				(m)	(kg/m^3)	(W/m·K)		(J/kg·K)		
TCw	Tpcpv	3	Tcpv3	0.0	1890	0.98	0.54	857	4570	857
		2	Tcpv2	5.49						
PTn	Tpcpv1		Tcpv1	4.69	1890	1.07	0.50	1037	6048	1037
	Tpbt4		Tcbt4	0.53	1720	0.5	0.35	1077	21976	1077
	Tpy		Yucca	7.05	1860	0.97	0.44	849	16172	849
	Tpbt3		Tcbt3_dc	4.58	1710	1.02	0.46	1016	20669	1016
	Tpp		Pah	14.09	1630	0.82	0.35	1330	25560	1330
	Tpbt2		Tpbt2	9.69	1730	0.67	0.23	1224	23878	1224
	Tptrv3		Tptrv3	4.58	1730	1.00	0.37	834	5137	834
	Tptrv2		Tptrv2	0.53						
TSw1	Tptrv1		Tptrv1	1.06						
	Tptrn		Tptrn	46.85	2310	1.62	1.06	866	5629	866
	Tptrl		Tptrl	8.98	2250	1.58	0.89	882	5693	882
	Tptpul		Tptpul	77.68	2260	1.80	0.71	883	5694	883
TSw2	Tptpmn		Tptpmn	29.94	2360	2.33	1.56	948	4568	948
	Tptpll		Tptpll	106.21	2360	2.02	1.20	900	4663	900
	Tptpln		Tptpln	47.73	2410	1.84	1.42	865	4523	865
TSw3	Tptpv3		Tptpv3	20.61	2360	2.08	1.69	984	1958	984
CHn1	Tptpv2		Tptpv2	2.99						
	Tptpv1		Tptpv1	11.27						
	Tpbt1		Tpbt1	3.35	1850	1.31	0.7	1057	21076	1057
	Tac5	Tac(v)	Calico	84.37	1880	1.17	0.58	1201	23863	1201
	Tac4									
	Tac3									
	Tac2	Tac(z)			1880	1.2	0.61	1154	22086	1154
	Tac1									
CHn2	Tacbt				1880[b]	1.35	0.73	1174	13561	1174

Note: [a] Saturated bulk density is based on DTN: MO9911SEPGRP34.000 (CRWMS M&O 1999h, Table 9).
[b] Assumed the same as Tac(z).
For use of these data, see Assumption 5.9.
Source: DTN: SN0003T0571897.013 (CRWMS M&O 1999b) and DTN: MO9911SEPGRP34.000 (CRWMS M&O 1999h, Table 9)

Table 4-3. Depths and Vertical Coordinates of Stratigraphic Units

USGS Unit	Depth (m)	Vertical (Y) Coordinate (m)
Tcpv3_top	0	346.23
Tcpv2_top	114.30	231.93
Tpcpv1_top	119.79	226.44
Tpbt4_top	124.48	221.75
Tpy_top	125.01	221.22
Tpbt3_top	132.06	214.17
Tpp_top	136.64	209.59
Tpbt2_top	150.73	195.50
Tptrv3_top	160.42	185.81
Tptrv2_top	165.00	181.23
Tptrv1_top	165.53	180.70
Tptrn_top	166.59	179.64
Tptrl_top	213.44	132.79
Tptpul_top	222.42	123.81
Tptpmn_top	300.10	46.13
Tptpll_top	330.04	16.19
Tptpll_bottom	436.25	-90.02
Tptpln_bottom	483.98	-137.75
Tptpv3_bottom	504.59	-158.36
Tptpv2_bottom	507.58	-161.35
Tptpv1_bottom	518.85	-172.62
Tpbt1_bottom	522.20	-175.97
[Combined Tac(v), Tac(z), and Tacbt]_bottom	606.57	-260.34

Note: For use of these data, see Assumption 5.9.
Source: CRWMS M&O 1998b, Figure 4-1 and DTN: SN0003T0571897.013 (CRWMS M&O 1999b)

4.1.3 Rock Thermal Properties

The rock saturated bulk density, thermal conductivity, and specific heat values are used in the thermal modeling. The values of these properties for each rock unit are listed in Table 4-2 based on the *Thermal Modeling Parameters by Stratigraphic Unit* (CRWMS M&O 1999b; DTN: SN0003T0571897.013). For use of these data, see Assumption 5.9.

4.1.4 Intact Rock Mechanical Properties

The thermomechanical analysis models involve only the Topopah Spring Crystal-poor middle non-lithophysal unit (Tptpmn) and the Topopah Spring Crystal-poor lower lithophysal unit

(Tptpll). The intact rock mechanical properties for these units are given in Table 4-4 (DTN: MO0003RIB00079.000, Tables 2 through 5). For use of these data, see Assumption 5.10.

Table 4-4. Intact Rock Mechanical Properties for Non-Lithophysal and Lithophysal Units

Parameter	Non-lithophysal Unit (Tptpmn)	Lithophysal Unit (Tptpll)
Elastic Modulus (GPa)	32.93	27.54
Poisson's Ratio	0.21	0.21
Cohesion (MPa)	36.90[a]	36.90[b]
Friction Angle (degrees)	50	50[b]
Tensile Strength (MPa)	11.56	8.29

Note: [a] Minimum value (lower bound of range)
[b] Assumed the same as Tptpmn.

Source: DTN: MO0003RIB00079.000, Tables 2 through 5

4.1.5 Rock Mass Mechanical Properties

The rock mass parameters and properties for the non-lithophysal and lithophysal units used in the analyses are provided in Tables 4-5a and 4-5b, respectively. These values are selected based on DTN: MO0001SEPSRMPC.000. For use of these data, see Assumption 5.11.

Table 4-5a. Rock Mass Mechanical Properties for the Non-Lithophysal Unit

Parameter		Non-lithophysal Rock (Tptpmn)				
Rock Mass Quality Category		1	2	3	4	5
Cumulative Frequency Distribution (%)		5	20	40	70	90
Rock Mass Quality (Q)		0.53	1.20	2.00	5.40	12.00
Elastic Modulus (GPa)		9.32	12.51	15.21	19.56	25.83
Poisson's Ratio		0.21	0.21	0.21	0.21	0.21
Cohesion (MPa)	Confining Stress = 0 – 3 MPa	2.0	2.4	2.7	3.3	4.1
	Confining Stress = 0 - 42 MPa	8.1	8.9	9.5	10.4	11.6
Friction Angle (degrees)	Confining Stress = 0 – 3 MPa	56	57	57	58	58
	Confining Stress = 0 - 42 MPa	37	39	39	41	42
Tensile Strength (MPa)	Confining Stress = 0 – 3 MPa	1.21	1.41	1.59	1.89	2.33
	Confining Stress = 0 - 42 MPa	8.03	8.55	8.94	9.53	10.33

Source: DTN: MO0001SEPSRMPC.000.

Table 4-5b. Rock Mass Mechanical Properties for the Lithophysal Unit

Parameter		Lithophysal Rock (Tptpll)				
Rock Mass Quality Category		1	2	3	4	5
Cumulative Frequency Distribution (%)		5	20	40	70	90
Rock Mass Quality (Q)		0.67	2.45	4.58	8.45	14.82
Elastic Modulus (GPa)		9.74	14.57	19.26	25.50	27.54[a]
Poisson's Ratio		0.21	0.21	0.21	0.21	0.21
Cohesion (MPa)	Confining Stress = 0 – 3 MPa	2.0	2.6	3.2	4.0	5.1
	Confining Stress = 0 - 42 MPa	8.2	9.3	10.3	11.5	13.0
Friction Angle (degrees)	Confining Stress = 0 – 3 MPa	56	57	58	58	58
	Confining Stress = 0 - 42 MPa	37	39	41	42	43
Tensile Strength (MPa)	Confining Stress = 0 – 3 MPa	1.23	1.55	1.87	2.30	2.91
	Confining Stress = 0 - 42 MPa	8.10	8.85	9.49	10.29	11.29

Note: [a] Used same value as for intact rock.

Source: DTN: MO0001SEPSRMPC.000.

4.1.6 Rock Mass Coefficient of Thermal Expansion

The temperature-dependent coefficients of thermal expansion used in the analyses for the non-lithophysal and lithophysal units are listed in Table 4-6 and are based on DTN: MO0004RIB00035.001, Table 13. These values were the mean values obtained from laboratory tests using small rock samples from the non-lithophysal and lithophysal units, and were based on saturated rock samples during heat-up. Other data are also available, including those using dry rock samples during heat-up or cool-down and saturated rock samples during cool-down (DTN: MO0004RIB00035.001, Tables 13 and 14). The measured data vary slightly with the saturation state and the thermal loading stages (heat-up or cool-down). Since the saturated bulk density is used (see Table 4-2), and the focus of the analysis is on the response of the rock mass to the temperature increase after the waste emplacement, the values for the saturated rock samples during heat-up are selected for this analysis.

The coefficients of thermal expansion used were obtained from laboratory tests using small rock samples. These coefficients are for intact rock and higher than those for rock mass containing fractures and joints, which may close during heating, resulting in lower effective thermal expansivity. Therefore, use of the coefficients of thermal expansion for intact rock to evaluate the thermally-induced deformation and stress in rock mass is conservative.

Though the coefficients of thermal expansion for the non-lithophysal and lithophysal units are not identical, the differences are very small, according to the results from the laboratory tests (CRWMS M&O 1997a, Table 5-15). Therefore, the use of the average values of the coefficients

of thermal expansion for both the non-lithophysal and lithophysal units is reasonable, and not expected to have significant impact on the results of the analysis.

Table 4-6. Mean Rock Mass Coefficient of Thermal Expansion for Non-Lithophysal and Lithophysal Units

Temperature Range (°C)	Value (10^{-6}/°C)
25 - 50	7.14
50 - 75	7.47
75 - 100	7.46
100 - 125	9.07

Source: DTN: MO0004RIB00035.001, Table 13

4.1.7 Properties for Rock Joints in Non-Lithophysal and Lithophysal Units

Rock joint parameters and properties include joint geometry, strengths, and stiffness values. The rock joint parameter and property values are listed in Table 4-7. The mechanical property values are either based on the *Yucca Mountain Site Geotechnical Report* (CRWMS M&O 1997a, Tables 5-39 and 5-40) or assumed. For conservatism, the cohesion and normal stiffness values used are lower than those provided. The source DTNs for the joint mechanical properties are SNL02112293001.002, SNL02112293001.003, SNL02112293001.005, and SNL02112293001.007.

The joint spacing and orientation, as listed in Table 4-7, for the horizontal joint set are taken from DTN: MO0002SPAFRA06.002. The combined joint spacing and orientation for the vertical joint set are calculated based on the information provided in DTN: MO0002SPAFRA06.002. Details of the calculations for the combined joint spacing and orientation of the vertical joint set are given in Attachment I. For use of these data, see Assumption 5.7.

Table 4-7. Properties for Rock Joints in Non-Lithophysal and Lithophysal Units

Parameter	Non-Llithophysal Unit	Lithophysal Unit
Cohesion (MPa)	0.1	0.1[d]
Friction Angle (degrees)	41	41[d]
Tensile Strength (MPa)	0[a]	0[d]
Normal Stiffness (MPa/m)	5×10^{4}	5×10^{4}[d]
Shear Stiffness (MPa/m)	5×10^{4}[b]	5×10^{4}[d]
Dilation Angle (degrees)	20.5[c]	20.5[d]
Orientation (Dip)	83.5° for vertical joint set 9° for horizontal joint set	80.5° for vertical joint set 5° for horizontal joint set
Spacing (m)	0.54 for vertical joint set 0.56 for horizontal joint set	1.93 for vertical joint set 2.94 for horizontal joint set

Note: [a] Assumed value; [b] Used the same as the normal stiffness; [c] Used half of the friction angle; [d] Used the same as non-lithophysal unit.

Source: DTN: SNL02112293001.002, SNL02112293001.003, SNL02112293001.005, and SNL02112293001.007 (CRWMS M&O 1997a, Tables 5-39 and 5-40) and DTN: MO0002SPAFRA06.002

4.1.8 Steel Set Dimensions and Thermal and Mechanical Properties

The steel set used is W6×20, ASTM A36 (ASTM A 36/A 36M-00a 2000). For W6×20, a cross-sectional area of 3.7871×10^{-3} m^2 and a corresponding moment of inertia of 1.72320×10^{-5} m^4 are taken from the American Institute of Steel Construction (AISC) *Manual of Steel Construction - Allowable Stress Design* (AISC 1997, p. 1-32).

The thermal and mechanical properties for steel sets are listed in Table 4-8. The shear allowable stress is not included because the shear forces in the steel sets installed to support circular underground openings like the emplacement drifts are usually very low, and the compliance of this requirement is expected. For the two-dimensional numerical modeling the mechanical properties will be divided by the 1.5-m spacing of the steel sets along the drift.

Table 4-8. Steel Set Thermal and Mechanical Properties

Parameter	Value	Source
Density (kg/m^3)	7,859	ASM 1978, p. 145
Thermal Conductivity (W/m·K)	50.67	ASM International 1990, p. 197 (averaged value for AISI-SAE grade 1025 for temperatures from 0°C to 200°C)
Specific Heat (J/kg·K)	502.5	ASM International 1990, p. 198 (averaged value for AISI-SAE grade 1025 for temperatures from 50°C to 200°C)
Elastic Modulus E (GPa)	200	AISC 1997, p. 1-117 (converted from 29,000 ksi)
Poisson's Ratio ν	0.3	Merritt 1983, p. 6-8
Coefficient of Thermal Expansion (10^{-6}/°C)	11.24 at 25°C 11.40 at 50°C 11.71 at 100°C 12.01 at 150°C 12.32 at 200°C	Merritt 1983, Eq. 9-75, p. 9-67
Allowable Stress (MPa)	164	AISC 1997, p. 1-7 for yield limit and p. 5-45 for allowable stress of steel sets with compact section (converted from $0.66\sigma_y=0.66\times36/145\times1000=164$)
Shear Modulus G (GPa)	76.92	Calculated using $G=E/[2(1+\nu)]$, based on Goodman 1980, pp. 172-173

4.1.9 Steel Set-Rock Surface Contact Element Parameters

Contact element parameters are needed to model the circumferential interface (discontinuity) between the steel sets and the rock surface. This interface maintains the physical contact between the steel and the rock so that any deformation of the rock due to in situ stress or temperature increase will induce stresses in the steel sets. In addition, the interface also allows the steel sets and the rock to slide relative to each other. The following parameters are associated with the interface: (1) coefficient of friction, (2) penetration tolerance, (3) normal contact stiffness, and (4) sticking contact stiffness (Swanson Analysis Systems 1995, Volume III,

p. 4-332). The values for these parameters used in the analyses are listed in Table 4-9, along with the basis for each value. Additional details of the bases are presented below.

(1) The coefficient of friction between the steel sets and the rock is set to be 1.0. Based on Beer and Johnston (1977, Table 8.1), approximate values of the coefficient of static friction for dry surfaces (metal on stone) range from 0.3 to 0.7. For conservatism, a higher value is used in this analysis because the loads on the steel sets increase with the friction. The remaining parameters are determined using procedures presented in the *ANSYS User's Manual for Revision 5.2* (Swanson Analysis Systems 1995, Volume I, pp. 3-143 to 3-145), as described below.

(2) The parameter "penetration tolerance" is used to determine if penetration compatibility is satisfied during a model run. According to the *ANSYS User's Manual for Revision 5.2* (Swanson Analysis Systems 1995, Volume I, p. 3-145), the tolerance is typically about 1 percent of the size of the elements on contact surfaces. The penetration tolerance value used in the analysis, as determined by trial-and-error runs to minimize the penetration and at the same time to achieve numerical convergence, is 0.1 mm. This value would be less than 0.1 percent of the size of the contact surface elements if the contact ring should be divided into 48 elements with a length of about 0.36 m for each element ($\pi \times 5.5/48 = 0.36$).

(3) The normal contact stiffness is used to determine contact forces. Based on the *ANSYS User's Manual for Revision 5.2* (Swanson Analysis Systems 1995, Volume I, p. 3-143), the value for normal contact stiffness is equal to the rock mass modulus of elasticity, E, multiplied by the characteristic contact length, h, multiplied by the penetration compatibility factor, f (0.01 to 100). The stiffness value used in this analysis was determined by setting $f = 1$ (per Swanson Analysis Systems 1995, Volume I, Page 3-144) and performing trial-and-error runs in which the compatibility factor was varied to achieve numerical convergence.

(4) The sticking contact stiffness is used if the elastic Coulomb friction behavior is sought, i.e., where the coefficient of friction is larger than zero. Based on trial-and-error runs, the value required to avoid numerically ill-conditioning in the analyses was determined.

Table 4-9. Steel Set-Rock Surface Contact Element Parameters

Parameter	Contact between Steel and Rock	Basis
(1) Coefficient of Friction	1.0	Based on Beer and Johnston (1977, Table 8.1), the coefficient of friction for surfaces of metal on stone ranges from 0.3 to 0.7. For conservatism, a higher value of 1.0 is used.
(2) Penetration Tolerance (mm)	0.1	Trial & error (See Section 4.1.9)
(3) Normal Contact Stiffness (N/m)	1×10^9	Trial & error (See Section 4.1.9)
(4) Sticking Contact Stiffness (N/m)	1×10^9	Trial & error (See Section 4.1.9)

4.1.10 Rock Bolt and Grout Material Properties

Steel rock bolts are proposed for zones needing rock reinforcement. Their thermal and mechanical properties are the same as those for the steel sets (Table 4-8). The dimensions and property values used in the analyses for the rock bolts and grout are listed in Table 4-10. For the bond stiffness and strength of grout, the following expressions are used based on Itasca Consulting Group (1996a, p. G-30):

$$K_{bond} = \frac{2\pi G}{10\ln(1+2t/D)} \qquad \text{(Eq. 4-1)}$$

and

$$S_{bond} = \pi(D+2t)\tau_{peak} \qquad \text{(Eq. 4-2)}$$

where
- K_{bond} = grout bond stiffness, N/m/m
- G = grout shear modulus, N/m^2, $G=E/[2(1+\upsilon)]$
- t = grout annulus thickness, m
- D = rock bolt diameter, m
- S_{bond} = grout cohesive (shear) strength per meter of bolt, N/m
- τ_{peak} = grout peak shear strength, N/m^2
- E = grout modulus of elasticity, N/m^2
- υ = Poisson's ratio, dimensionless

In estimating the grout cohesive strength using Equation (4-2), it is assumed that failure occurs at the bolt/grout interface. Thus, the maximum bond force per length is calculated with $D+2t$ replaced by D. In addition, the peak shear strength of the grout is set to be half of its unconfined compressive strength. The allowable shear strength is estimated by dividing the peak shear strength by a safety factor of 2. The bond stiffness and strength of grout are calculated as follows:

$$G = \frac{E}{2(1+\upsilon)} = \frac{14}{2(1+0.25)} = 5.6 \quad GPa$$

$$K_{bond} = \frac{2\pi G}{10\ln(1+2t/D)} = \frac{2\pi \times 5.6\times 10^9}{10\ln\left(1+\frac{2\times 0.00635}{0.0254}\right)} = 8.68\times 10^9 \quad N/m/m$$

and

$$S_{bond} = \pi(D+2t)\tau_{peak} = \pi \times 0.0254 \times \frac{90}{2\times 2} = 1.795\times 10^6 \; N/m$$

Table 4-10. Dimensions and Properties for Rock Bolts and Grout

Parameter	Value	Source
Diameter of Rock Bolt (m)	0.0254	Converted from a diameter of 1 inch (1 in × 0.0254 m/in = 0.0254 m)
Thickness of Grout Annulus (m)	0.00635	Converted from a thickness of 0.25 in (0.25 in × 0.0254 m/in = 0.00635 m)
Perimeter of Rock Bolt (m)	0.08	Calculated: $p = \pi D = 3.1415 \times 0.0254 = 0.08$ m
Allowable Axial Force (kN)	160.2	Based on the yield strength (force) of 267 kN (Williams Form Engineering Corporation 1997, p. 8) and a strength reduction factor of 0.6 (AISC 1997, p. 5-40) ($0.6F_y$=0.6×267=160.2)
Modulus of Elasticity of Grout (GPa)	14	Onofrei et al. 1993, Figure 33, p. 60. A low bounding value is used because it corresponds to the expected spherical stress around the drift opening.
Poisson's Ratio of Grout	0.25	Set to be the same as concrete (see Table 4-11)
Grout Unconfined Compressive Strength (MPa)	90	Onofrei et al. 1993, Figure 27b, p. 52
Bond Stiffness of Grout (N/m/m)	8.68×10^{9}	Calculated using Equation (4-1).
Bond Strength of Grout (cohesion) (N/m)	1.795×10^{6}	Calculated using Equation (4-2) with $D+2t$ replaced by D.
Frictional Strength of Grout (Friction Angle) (Degrees)	10	Based on Beer and Johnston (1977, Table 8.1), the coefficient of friction for surfaces of metal on stone ranges from 0.3 to 0.7. For conservatism, a lower value of 0.18 or tan10° is used.

For use of these data, see Assumption 5.12.

4.1.11 Concrete Lining Dimensions and Thermal and Mechanical Properties

The thickness of concrete lining proposed for the exhaust main is 0.3 m. Its cross-sectional area and corresponding moment of inertia are 0.3 m^2/per linear meter and 2.25×10^{-3} m^4/per linear meter, respectively.

The specified (nominal) compressive strength of concrete used in this analysis is 5,000 psi. This is a design parameter, and can be changed depending on the calculated loads and stresses in the concrete lining. For example, if the calculated stresses in the concrete lining exceed the allowable design strength, the specific compressive strength of concrete should be increased by selecting a high strength concrete. The allowable design strength of concrete is defined as the nominal compressive strength multiplied by a strength reduction factor, which is always less than one (ACI 1999, Section R9.3). The strength reduction factor is selected in accordance with the requirements specified in the American Concrete Institute (ACI) *Building Code Requirements for Structural Concrete (ACI 318-99) and Commentary (ACI 318R-99)* (ACI 1999, Section 9.3). Since axial loads with flexure are anticipated in the concrete lining (with wire mesh reinforcement) for the exhaust main and other non-emplacement drifts, the strength reduction factor shall be 0.7 according to ACI (1999, Section 9.3.2.2). The thermal and mechanical properties for concrete are listed in Table 4-11.

Table 4-11. Concrete Thermal and Mechanical Properties

Parameter	Value	Source
Density (kg/m^3)	2,323	Merritt (1983, p. 8-4)
Elastic Modulus *E* (GPa)	27.58	ACI 1999, Section 8.5. (converted from $E=4\times10^6$ psi which is based on a compressive strength of 5,000 psi and $E=57{,}000\times5{,}000^{1/2}$)
Poisson's Ratio ν	0.25	Merritt (1983, p. 6-8)
Coefficient of Thermal Expansion (10^{-6}/°C)	9.9	Merritt (1983, p. 5-13)
Allowable Strength (MPa)	24.14	ACI 1999, Section 9.3 for strength reduction factor (converted from $0.7\sigma_y=0.7\times5{,}000/145=24.14$, based on a compressive strength of 5,000 psi)

4.1.12 Time Histories of Model Boundary Temperatures

Time histories of rock temperatures on the model boundaries (drift wall and horizontal boundaries at 50 or 100 meters above and 50 or 100 meters below the drift center, or at the TSw2/TSw3 contact) used in the thermomechanical calculations for the emplacement drifts are listed in Tables 4-12a and 4-12b (DTNs: MO9911SPAWAQ01.000 and MO0105MWDTHE05.009) for a high temperature condition and a low temperature condition, respectively. All the temperature inputs are obtained by downloading the ANSYS output files from the Technical Data Management System (TDMS), and then extracted using the ANSYS code.

Time histories of average rock temperatures at the emplacement level and at the 50 meters above and 50 meters below the Exhaust Main are also given in Table 4-12a. These temperatures are used for the thermomechanical analyses for the Exhaust Main.

For use of these data, see Assumption 5.14.

Table 4-12a. Boundary Temperatures for Thermomechanical Models

Time (Year)	Temperature (°C)						
	At ED Wall	At 50-m above ED Center	At 50-m below ED Center	At Middle of Pillar	At ED Level	At 50-m above EM Center	At 50-m below EM Center
0	27.33	26.62	28.10	27.33	27.33	26.85	28.36
1	99.78	26.62	28.10	27.33	63.56	26.85	28.36
5	123.30	26.73	28.18	28.30	75.80	27.73	28.36
10	124.94	27.78	29.09	32.79	78.87	30.43	28.44
15	120.36	29.45	30.60	37.73	79.04	33.43	28.80
20	113.78	31.26	32.27	41.91	77.85	36.21	29.45
30	101.79	34.70	35.47	47.82	74.80	40.74	31.28
40	94.53	37.65	38.23	51.42	72.98	44.06	33.33
50	87.32	40.04	40.48	53.55	70.43	46.41	35.29
60	81.14	41.88	42.23	54.56	67.85	47.93	37.03
70	75.92	43.22	43.53	54.87	65.40	48.85	38.50
80	71.59	44.16	44.46	54.74	63.17	49.33	39.70
90	67.97	44.79	45.11	54.36	61.16	49.51	40.65
100	64.89	45.19	45.53	53.82	59.36	49.48	41.40
150	57.56	45.56	46.09	51.28	54.42	48.45	43.22
200	52.05	44.91	45.62	48.98	50.52	46.97	43.58

Note: ED stands for emplacement drift; EM stands for exhaust main.

Source: DTN: MO9911SPAWAQ01.000

4.1.13 Peak Ground Velocity (PGV) and Peak Ground Acceleration (PGA)

PGV values presented in Table 4-13 are used as input to account for seismic effects in performing dynamic analyses for the emplacement drifts; while PGA values shown in Table 4-14 are used as input to account for seismic effects in performing quasi-static analyses for the non-emplacement drifts. Data in both tables come from an AP-3.14Q design input transmittal from NEPO to EBSO (CRWMS M&O 1999g, Attachment 1: p. A1-1; pp. A1-13 through A1-16; pp. A1-18 through A1-21; DTN: MO0004SEPPGVRB.006, MO0003SEPSDARS.002 and MO0003SEPSDATH.003). Values in Table 4-14 are for 100 Hz. These data correspond to the seismic events of the Frequency Category 1 (mean annual exceedance probability of 0.001) and the Frequency Category 2 (mean annual exceedence probability of 0.0001).

For use of these data, see Assumption 5.3.5.

Table 4-12b. Boundary Temperatures for Low Temperature Thermomechanical Models

Time (Year)	Temperature (°C)					
	At ED Wall	At 50-m above ED Center	At 50-m below ED Center	At 100-m above ED Center	At 100-m below ED Center	At TSw2 & TSw3 Contact Boundary
0	25.27	25.00	25.00	25.00	25.00	25.00
1	46.89	25.00	25.00	25.00	25.00	25.00
5	54.55	25.02	25.02	25.00	25.00	25.00
10	55.25	25.24	25.23	25.00	25.00	25.00
15	53.49	25.67	25.66	25.01	25.00	25.01
20	51.32	26.17	26.15	25.03	25.02	25.03
25	49.29	26.65	26.63	25.08	25.06	25.08
30	47.46	27.10	27.09	25.15	25.14	25.16
40	45.20	27.86	27.87	25.37	25.37	25.42
50	42.84	28.47	28.50	25.66	25.69	25.76
60	57.57	29.07	29.12	25.96	26.05	26.14
70	64.65	29.94	30.02	26.27	26.44	26.55
80	66.47	30.96	31.07	26.63	26.86	26.99
90	65.34	32.05	32.19	27.03	27.33	27.49
100	63.22	33.07	33.26	27.50	27.85	28.05
125	66.92	35.31	35.64	28.79	29.29	29.57
150	67.41	37.26	37.74	30.12	30.80	31.15
200	65.78	40.25	41.04	32.63	33.70	34.13
250	63.38	42.15	43.20	34.71	36.13	36.59
300	60.94	43.27	44.53	36.31	37.99	38.45

Note: ED stands for emplacement drift.

Source: DTN: MO0105MWDTHE05.009

Table 4-13. Peak Ground Velocity Values

Frequency	Annual Frequency of Exceedance			
	10^{-3} (a 1,000-year return period)		10^{-4} (a 10,000-year return period)	
	Horizontal	Vertical	Horizontal	Vertical
1-2 Hz Earthquake	16.3 cm/sec	9.3 cm/sec	46.9 cm/sec	28.0 cm/sec
5-10 Hz Earthquake	15.2 cm/sec	7.9 cm/sec	38.9 cm/sec	22.2 cm/sec

Source: CRWMS M&O 1999g, Attachment 1, p. A1-1; DTN: MO0004SEPPGVRB.006

Table 4-14. Peak Ground Acceleration Values

Frequency	Annual Frequency of Exceedance			
	10^{-3} (a 1,000-year return period)		10^{-4} (a 10,000-year return period)	
	Horizontal	Vertical	Horizontal	Vertical
1-2 Hz Earthquake	0.10g	0.09g	0.26g	0.24g
5-10 Hz Earthquake	0.14g	0.13g	0.43g	0.44g

Source: CRWMS M&O 1999g, Attachment 1, pp. A1-13 through A1-16; pp. A1-18 through A1-21; DTN: MO0003SEPSDARS.002 and MO0003SEPSDATH.003

4.1.14 Rock Mass Thermal and Mechanical Properties for the TCw, PTn and TSw1 Thermal/Mechanical Units

In addition to the TSw2 unit, the TCw, PTn, and TSw1 units are also included in constructing numerical models for performing dynamic analyses for seismic effects. Table 4-15 lists the mechanical properties for these three units (CRWMS M&O 1999h, Tables 10 through 13 and Table 15, DTN: MO9911SEPGRP34.000 and DTN: MO0004RIB00035.001, Table 13).

Table 4-15. Rock Mass Mechanical Properties for the TCw, PTn, and TSw1 Units

Thermal/Mechanical Unit	TCw		PTn		TSw1	
Density[a] (kg/m^3)	1890		1750		2273	
Thermal Conductivity[a] W/m·K)	0.98		0.88		1.72	
Specific Heat[a] (J/kg·K)	857		1086		877	
Rock Mass Quality (RMQ)	1	5	1	5	1	5
Coefficient of Thermal Expansion for Temperature at 25 – 50°C (10^{-6}/°C)	7.09		4.46		6.56	
Modulus of Elasticity (GPa)	7.33	29.36	2.54	2.54	9.03	20.36
Poisson's Ratio	0.21	0.21	0.23	0.23	0.23	0.23
Cohesion (MPa)	1.5	3.9	0.5	1.0	1.1	2.9
Friction Angle (degree)	54	57	33	56	44	47
Tensile Strength (MPa)	0.97	2.35	0.52	0.67	0.90	2.26

Note: [a] Weighted average based on Table 4-2.

Source: DTN: MO9911SEPGRP34.000, CRWMS M&O 1999h for the mechanical properties
DTN: MO0004RIB00035.001 for the coefficient of thermal expansion

4.2 CRITERIA

The criteria that are related to this analysis are listed in the following subsections, based on the *Ground Control System Description Document* (SDD) (CRWMS M&O 2000a) and the *Requirements and Criteria for Implementing a Repository Design that can be Operated Over a Range of Thermal Modes* (BSC 2001).

4.2.1 Ground Control System Functions

4.2.1.1 The system provides structural support for the subsurface repository openings (CRWMS M&O 2000a, Section 1.1.1).

4.2.1.2 The system provides protection against rock fall, loosening of blocks, and fracturing and surface deterioration of the rock mass surrounding each opening (CRWMS M&O 2000a, Section 1.1.2).

4.2.1.3 The system maintain adequate subsurface operating envelopes (CRWMS M&O 2000a, Section 1.1.3).

4.2.1.4 The system provides for monitoring of ground control performance parameters (CRWMS M&O 2000a, Section 1.1.4).

4.2.2 Ground Support System Design Criteria for Performance

4.2.2.1 The system shall maintain the operating envelopes specified in Table 4-16, while allowing for the expected variations in excavated dimensions, lining thickness, alignment, and deformation (CRWMS M&O 2000a, Section 1.2.1.1, Table 1). For use of these data, see Assumption 5.13.

Table 4-16. Operating Envelopes for Emplacement and Non-Emplacement Drifts

Type of Drifts	Dimensions and Shape of Envelope
Emplacement Drifts	5.1 m diameter circle
Access and Exhaust Mains	7.02 m diameter circle
Emplacement Drift Turnouts	7.6 m wide × 5.9 m high rectangle with rounded upper corners for the curved portion 7.6 m wide × 6.5 m high horseshoe for the straight portion

Source: CRWMS M&O 2000a, Table 1

4.2.2.2 The system shall accommodate geologic mapping of emplacement drifts so that the maximum distance between mapped emplacement drifts does not exceed 300 meters, geologic mapping of 100 percent of non-emplacement drift openings, and observation/recording of rock mass conditions during construction (CRWMS M&O 2000a, Section 1.2.1.2).

4.2.2.3 The system shall provide for the monitoring of ground control performance parameters including, as a minimum, opening convergence, ground support and rock temperatures, and ground support loads (CRWMS M&O 2000a, Section 1.2.1.3).

4.2.2.4 Emplacement drift ground support shall be carbon steel (steel sets and/or rock bolts and mesh) (CRWMS M&O 2000a, Section 1.2.1.4).

4.2.2.5 The system shall use cementitious grout to anchor the permanent rock bolts (CRWMS M&O 2000a, Section 1.2.1.5).

4.2.2.6 The system shall be designed for the appropriate worst case combination of in situ rock stresses, construction, operational, and thermal loads (CRWMS M&O 2000a, Section 1.2.1.6).

4.2.2.7 The system design shall allow the repository to remain open for up to 300 years following final waste emplacement, with appropriate monitoring and maintenance, and could allow closure of the repository 30 years following final waste emplacement, with variations in thermal management via operational flexibility (BSC 2001, Section 5.1.1.1).

4.2.3 Ground Support System Design Criteria for Safety

4.2.3.1 The system shall be designed to prevent a 6 metric ton or greater rock from falling more than 3.3 meters in the emplacement drifts during the preclosure period (CRWMS M&O 2000a, Section 1.2.2.1.1).

4.2.3.2 The system shall use materials having acceptable (i.e., acceptability based on the results of waste isolation site impact evaluations) long-term effects on waste isolation (CRWMS M&O 2000a, Section 1.2.2.1.2).

4.2.3.3 The system's structures, systems, and components (SSCs) important to safety shall be designed to withstand a design basis earthquake of Frequency Category 1 or Frequency Category 2, as appropriate to the seismic frequency classification assigned to a specific structure, system, and component (CRWMS M&O 2000a, Section 1.2.2.1.3).

4.2.3.4 The system shall be designed to prevent rock falls that could potentially result in personnel injury (CRWMS M&O 2000a, Section 1.2.2.2.1).

4.2.3.5 The system shall use noncombustible and heat resistance material as defined by "Standard Test Method for Behavior of Material in a Vertical Tube Furnace at 750°C" (CRWMS M&O 2000a, Section 1.2.2.2.3).

4.2.4 Ground Support System Design Criteria for Interfacing

4.2.4.1 The system shall interface with the following systems: Subsurface Facility, Emplacement Drift, MGR Operations Monitoring and Control, Waste Emplacement/Retrieval, and Subsurface Excavation (CRWMS M&O 2000a, Section 1.2.4).

4.2.5 Ground Support System Design Criteria for Maintenance

4.2.5.1 The system shall be designed to function without planned maintenance during the operational life while providing for the ability to perform unplanned maintenance on an as-needed basis (CRWMS M&O 2000a, Section 1.2.5.1).

4.2.5.2 The system shall accommodate maintenance of non-emplacement openings (CRWMS M&O 2000a, Section 1.2.5.2).

4.3 CODES AND STANDARDS

The codes and standards, applicable to this analysis, are as listed below.

4.3.1 AISC (American Institute of Steel Construction) 1997. *Manual of Steel Construction - Allowable Stress Design,* 9th Edition, 2nd Revision, 2nd Impression.

4.3.2 ACI 318-99 (American Concrete Institute) 1999. *Building Code Requirements for Structural Concrete (318-99) and Commentary (318R-99).*

4.3.3 ASTM A 36/A 36M-00a (American Society for Testing and Materials) 2000. *Standard Specification for Carbon Structural Steel.*

4.4 CONSTRAINTS

The following design constraints are specified in the *Requirements and Criteria for Implementing a Repository Design that can be Operated Over a Range of Thermal Modes* (BSC 2001, Section 5.2).

4.4.1 Drift Spacing: The approximate emplacement drift spacing shall be 80 meters, drift center to drift center (BSC 2001, Section 5.2.1).

4.4.2 Excavated Diameter: The nominal excavated diameter of the emplacement drift shall be 5.5 meters (BSC 2001, Section 5.2.5).

4.4.3 Ground Support Types: The ground support in the potential repository emplacement drift shall be carbon steel (e.g., steel sets and/or rock bolts and mesh) with cementitious grout allowed, where necessary, to anchor the rock bolts (BSC 2001, Section 5.2.6).

4.4.4 Ground Support Functionality: With periodic maintenance, if necessary, the emplacement drift ground support shall keep the emplacement drift open and stable for the entire preclosure period (BSC 2001, Section 5.2.7).

4.4.5 The maximum linear heat load shall not exceed 1.5 kW/m, averaged over a fully loaded emplacement drift at the time of completion of loading an entire emplacement drift (BSC 2001, Section 5.2.10).

4.4.6 The repository design shall ensure that the maximum emplacement drift wall temperature, shall not exceed 96°C during normal preclosure operations, nor, at any position or any time, exceed 200°C (BSC 2001, Section 5.2.24).

4.4.7 The system shall be designed to maintain WP surface temperature below 85°C (low end of range) (BSC 2001, Section 5.1.1.3).

5. ASSUMPTIONS

The following assumptions have been made in order to complete this analysis:

5.1 INITIAL GROUND RELAXATION

5.1.1 Emplacement Drifts

An initial ground relaxation value of 60 percent is assumed and used in the ground support analysis of emplacement drifts. This results in 40 percent of the pre-excavation in situ stress being imposed on the ground support system, providing a reasonably conservative upper bound to the loading recommended in earlier studies conducted by Hardy and Bauer (1991, Table 8-1). It is recommended that 15 percent of the pre-excavation in situ stress be applied to steel sets and 25 percent be applied to rock bolts for the Yucca Mountain Project (Hardy and Bauer 1991, Table 8-1). Thus, this assumption does not need to be confirmed by further study. Used in Sections 6.3.1, 6.4.2, and 6.5.2.

5.1.2 Non-Emplacement Drifts

An initial ground relaxation value of 100 percent is assumed and used in the ground support analysis for the final cast-in-place concrete lining in non-emplacement drifts. This value is considered to be reasonable because the cast-in-place concrete lining will usually be installed months or even years after the drift excavation. Any rock deformation induced by the excavation will most likely be complete before the installation of the concrete lining. Thus, this assumption does not need to be confirmed by further study. Used in Sections 6.3.1, 6.4.2, and 6.6.2.

5.2 DRIFT WALL TEMPERATURE IN NON-EMPLACEMENT DRIFTS

The maximum temperature on the drift walls of non-emplacement drifts, including the access mains, ventilation exhaust main, and turnout drifts, is assumed to be 50°C during the potential repository preclosure period. The rationale for this assumption is that the non-emplacement drifts should be accessible by personnel during the preclosure period. To achieve this, a sufficient ventilation rate will be used to ensure the temperature to be maintained within an allowable range. Therefore, a wall temperature of 50°C is considered as an upper bound. Further confirmation of this assumption is not required. Used in Sections 6.4.2 and 6.6.1.

5.3 SEISMIC LOADS

5.3.1 Representation of Seismic Waves

Seismic waves are represented as velocity waves that are assumed to be sinusoidal in shape, with the amplitude equal to the PGV value. This assumption is based on common practice in lieu of ground motion time histories. This assumption leads to a repetitive peak vibratory ground motion as design input at the potential repository host horizon. Since the peak ground velocity in an actual seismic event just occurs once at one location, this assumption is conservative. Thus, this assumption does not require confirmation. Used in Sections 6.4.2, 6.5.1, and 6.5.2.

5.3.2 Frequencies of Seismic Waves

A proper value of frequency is required to generate the sinusoidal velocity waves that are used as the dynamic load input. Since earthquakes generally excite a broad range of frequencies, a frequency of 10 Hz is assumed for this analysis. A rationale for this assumption is that a 10-Hz frequency results in a wave length value of a few hundred meters based on the shear wave velocities of approximately 3,000 m/s (CRWMS M&O 1999g, Attachment 4) for the rock units involved. Since seismic waves generally have large wave lengths, this assumption is appropriate. This assumption does not require confirmation. Used in Sections 6.4.2, 6.5.1, and 6.5.2.

5.3.3 Duration of Ground Shaking

A duration of 3 seconds is assumed for accounting for seismic effects. This assumption is based on the rationale that a 3-second duration at a frequency of 10 Hz will result in 30 vibration cycles propagating through the rock. This is a conservative number of cycles, since the rock formation does not show significantly nonlinear behavior during seismic loading. Thus, this assumption does not require confirmation. Used in Sections 6.4.2, 6.5.1, and 6.5.2.

5.3.4 Incidence Angle

For this analysis, seismic waves are assumed to propagate vertically upwards, i.e., the incidence angle is zero with respect to the vertical direction. This is conservative as the vertically-propagating P- and S-waves are the major ones to cause dynamic effects. Therefore, this assumption does not require confirmation. Used in Sections 6.4.2, 6.5.1, and 6.5.2.

5.3.5 Peak Ground Velocity and Peak Ground Acceleration

PGV and PGA values used are listed in Tables 4-13 and 4-14, respectively. These values are considered bounding in the corresponding frequency categories. Therefore, further confirmation is not required. Used in Section 4.1.13.

5.4 ROCK IN SITU STRESSES

The upper bound vertical stress value of 10 MPa at the repository drifts is assumed based on the *Repository Ground Support Analysis for Viability Assessment* (CRWMS M&O 1998b, Section 7.4.2). The range of the ratio (K_o) of horizontal stress to vertical stress is given in the same reference (CRWMS M&O 1998b, Section 7.4.2) as 0.3 to 1.0. According to the *In Situ Rock Conditions* (DTN: MO0007RIB00077.000, Table 1), the vertical stresses at the repository horizon vary from 6.46 MPa to 7.65 MPa, while the minimum and maximum horizontal-to-vertical stress ratios range from 0.37 to 0.41 and 0.75 to 0.82, respectively. Therefore, the vertical stress (10 MPa) and horizontal-to-vertical stress ratios (0.3 and 1.0) used are bounding. No confirmation is required. Used in Sections 6.3, 6.4, 6.5, and 6.6.

5.5 PROPERTIES FOR ARTIFICIAL COMPUTATIONAL JOINTS

In the UDEC and 3DEC models, some artificial joints are used to assist the model generation. For example, the boundaries which divide the subregion with joints and the subregion without

joints are artificial joints. These joints are assigned with the high property values listed in Table 5-1. These values are assumed and not significant to the results. Therefore, no further confirmation is required. Used in Sections 6.5.1 and 6.6.1.

Table 5-1. Properties for Artificial Computational Joints

Parameter	Value
Cohesion (MPa)	1×10^{4}
Friction Angle (degrees)	60
Tensile Strength (MPa)	1×10^{4}
Normal Stiffness (MPa/m)	1×10^{6}
Shear Stiffness (MPa/m)	1×10^{6}

5.6 FRACTURE TRACE AND GAP LENGTHS

Through-going continuous fractures with constant dipping angle were used in the UDEC discontinuum analyses to represent fractures within each joint set. In order to evaluate the impact of the variation of joint continuity and joint orientation, the statistical joint-set generator in UDEC was used to generate a more realistic joint pattern as described in Attachment IV. The statistical joint-set generator requires inputs of angles of joints, joint spacing, joint trace and gap lengths (Itasca Consulting Group 1996b, p. E-2). Fracture trace length data from mapping of the ESF main drift and the ECRB cross drift are summarized in DTN: MO0002SPAFRA06.002 and listed in Table IV-1. Following the conservative approach in the *Drift Degradation Analysis* (CRWMS M&O, 2000b, Section 5.1), the modeled trace lengths are assumed to be four (4) times the mapped trace lengths listed in Table IV-1. Data for the continuity of fracture (defined as the trace length divided by the total length) was reported in the *Drift Design Methodology and Preliminary Application for the Yucca Mountain Site Characterization Project* (Hardy and Bauer 1991, p. 12-12 and Table 12-8) based on the joint trace photographs of pit walls excavated in TSw2. The reported mean continuity for the horizontal and vertical joint set are 41.5 and 51.8 percent respectively. The continuity of joints is conservatively assumed to be within 80 to 90 percent. Continuity data from the ESF mapping are not available. Based on the visual inspection of the joint trace maps, the range of 80 and 90 percent continuity is conservative. The values for the maximum deviation are assumed to be approximately 10 to 20 percent of the mean values for the dip angle, trace length, and spacing. Zero deviation is assumed for gap length to enhance the computational efficiency. Therefore, use of these data in this analysis is appropriate and adequate. Used in Attachment IV.

5.7 MECHANICAL PROPERTIES OF ROCK JOINTS

Rock joint parameters and properties include joint geometry, strengths, and stiffness values. The rock joint parameter and property values are listed in Table 4-7. For conservatism, the cohesion and normal stiffness values used are lower than those provided in the references listed in Section 4.1.7. Also, for conservatism, the highest combined joint frequency, or the minimum combined joint spacing, as listed in references given in Section 4.1.7, was selected in the two-dimensional

numerical analysis (Attachment I, p. I-2). Therefore, the properties as listed in Table 4-7 are bounding values and adequate and appropriate for use in this analysis. Used in Section 4.1.7.

5.8 GROUND SURFACE TEMPERATURE AND IN SITU THERMAL GRADIENT

Ground surface temperature and in situ thermal gradient are listed in Section 4.1.1. Emplacement drifts are located at about 300 m below the ground surface. Spatial variations of the ground surface temperature above the repository footprint are within a few degrees at most. For the thermal load considered for SR, it takes much longer for the heat to get close to the ground surface than for the drift wall temperature to reach its peak. The peak drift wall temperature is considered to be the key factor in defining the maximum load on ground support under the thermal loading condition. Spatial variations of the ground surface temperature are inconsequential. Use of a constant ground surface temperature in the ground control analysis is considered to be adequate and appropriate. Used in Section 4.1.1.

5.9 ROCK THERMAL PROPERTIES

Rock thermal properties are used as listed in Table 4-2 of Section 4.1.3. Among these data, thermal conductivity and specific heat values have been superseded by DTN: SN0011T0571897.014. Though the newer data for thermal conductivity and specific heat are not identical to the older values listed in Table 4-2, differences are not substantial, and impact of these differences on the results is considered insignificant. In addition, the ground support analysis for the high temperature condition was based on the older data, and in order to compare the results for the high temperature condition with those for the low temperature condition, use of consistent data is necessary.

Rock thermal properties presented in DTNs: SN0003T0571897.013 and SN0011T0571897.014 were both based on laboratory tests using small rock samples, and are for intact rock. Thermal conductivity values for intact rock are higher than those for rock mass containing fractures and voids. Use of the thermal conductivity values for intact rock is considered not conservative in terms of temperature prediction. However, the boundary temperatures used in this analysis were given as inputs (see Section 4.1.12). The thermal properties were used in thermomechanical models for regenerating the temperature distributions based on the given drift wall and other boundary temperatures. Change in the thermal properties may have some impact on the temperature distribution within rock, but consequently will not alter the drift wall and other boundary temperatures. Therefore, overall impact on the thermally-induced mechanical response of rock mass and ground support is considered minimal.

The use of the data as provided in DTN: SN0003T0571897.013 for this analysis is adequate and appropriate. Used in Sections 4.1.2 and 4.1.3.

5.10 INTACT ROCK MECHANICAL PROPERTIES

The intact rock mechanical properties for the Tptpmn and Tptpll units are listed in Table 4-4. These data are assumed based on DTN: MO0003RIB00079.000. They represent the currently available data and are preliminary in nature, pending the on-going activities including evaluating the data adequacy, identifying the needs for additional laboratory and/or field tests, and

finalizing the design parameters for the License Application design. Use of these data in this analysis is considered appropriate. Used in Section 4.1.4.

5.11 ROCK MASS MECHANICAL PROPERTIES

The rock mass parameters and properties for the non-lithophysal and lithophysal units used are provided in Tables 4-5a and 4-5b, respectively. These values are selected based on DTN: MO0001SEPSRMPC.000. They are empirically derived values and are preliminary in nature, pending the on-going activities including evaluating the data adequacy, identifying the needs for additional laboratory and/or field tests, and finalizing the design parameters for the License Application design. Use of these data in this analysis is considered appropriate. Used in Section 4.1.5.

5.12 ROCK BOLT AND GROUT MATERIAL PROPERTIES

Steel rock bolts are proposed for zones needing rock reinforcement. Their thermal and mechanical properties presented in Section 4.1.10 are assumed to be the same as those for the steel sets (Table 4-8). The dimensions and property values used in the analyses for the rock bolts and grout are listed in Table 4-10. The bond stiffness and strength of grout are assumed to be adequately quantified using expressions developed by Itasca Consulting Group (1996a, p. G-30). At this time this is the best information available for this application. It is considered adequate and appropriate for use in this document. Used in Section 4.1.10.

5.13 OPERATING ENVELOPES FOR REPOSITORY OPENINGS

The operating envelopes listed in Table 4-16 for emplacement and non-emplacement drifts are obtained from the *Ground Control System Description Document* (CRWMS M&O 2000a, Table 1). These are design outputs, and therefore no confirmation is required. Used in Section 4.2.2.1.

5.14 TIME HISTORIES OF MODEL BOUNDARY TEMPERATURES

Time histories of rock temperatures on the model boundaries used are listed in Tables 4-12a and 4-12b for the high temperature and the low temperature conditions, respectively (DTNs: MO9911SPAWAQ01.000 and MO0105MWDTHE05.009). The high temperature condition uses an initial linear heat load of 2.0 kW/m and a preclosure ventilation rate of 10 m^3/s for 200 years following waste emplacement. The selection of this for this analysis is intended to bound the ground control analysis and address some uncertainties associated with variations in design parameters. The low temperature condition considered uses an initial linear heat load of 1.0 kW/m and a preclosure forced ventilation rate of 15 m^3/s for 50 years after waste emplacement followed by a natural ventilation rate of 3 m^3/s from 50 to 100 years and 1.5 m^3/s from 100 to 300 years. Use of these two cases can accommodate the flexible repository design, and cover the range of thermal conditions anticipated during the repository preclosure period. It is considered adequate and appropriate for use in this document. Used in Section 4.1.12.

6. ANALYSIS/MODEL

6.1 INTRODUCTION

This analysis provides the technical basis for the design of the ground control systems for the potential repository drifts for Site Recommendation (SR). In the design of permanent underground facilities, the ground support needs are determined using several available methods. Generally, the nature and importance of the underground facility, the cost, and the risk associated with such factors as personnel safety, loss of function or service, and other indirect losses, play an important role in determining the design criteria for the ground support system. The design and construction of an underground high-level nuclear waste repository facility introduce unique challenges that are not commonly experienced for other subsurface facilities. For example, the presence of high level nuclear waste and the resultant thermal loading conditions introduce a series of additional requirements to the overall design and construction of the facility in addition to the waste isolation requirements. In situ (excavation) loads, construction loads, potential loads from repository operations, and loads due to seismic loading conditions during an earthquake must also be addressed in the design.

In order to meet the repository ground control design requirements, a comprehensive and effective methodology must be adopted. The repository ground control design effort for SR will focus mainly on analytical methods, using computer programs, due to the complexity of the problem. This engineering analysis for the SR design presents the application of analytical methods in the design of the ground support systems for both repository emplacement drifts and adjacent non-emplacement drifts. The overall ground support design methodology has been addressed in the *Drift Ground Support Design Guide* (CRWMS M&O 1998c). The emplacement drifts will contain the nuclear waste packages and will comprise the majority of the repository openings. The non-emplacement drifts include all other repository underground openings that will not be used for waste emplacement, such as mains, exhaust mains, ventilation raises, emplacement drift turnouts, and intersections between turnouts and mains. For the emplacement drifts, the types of final ground support system concepts considered for SR analysis are steel sets with welded wire fabric and fully-grouted rock bolts. These ground support systems should be designed to mitigate the need for routine maintenance and, thus, access to the emplacement drifts which will experience severe environmental conditions. Also, a service life up to 300 years following initiation of waste emplacement is required for the emplacement drifts (see Section 4.2.2.7). During this time, the drifts will be monitored and, if necessary, a retrieval capability for the waste packages and maintenance of ground supports must be provided (Section 4.2.1.4). The steel sets and rock bolts systems are also well suited for tunnel boring machine (TBM) construction and can be installed quickly after excavation to provide personnel safety during construction. In addition, these systems can also facilitate the performance confirmation mapping activities (Section 4.2.2.2).

The non-emplacement drifts represent openings of different sizes and shapes, including various drift intersections. For the non-emplacement drifts, an initial and a final ground support system will be required. The initial ground support system will be needed to allow for safe construction and to accommodate performance confirmation mapping requirements. The turnouts and intersections are most likely to be excavated using roadheaders. This is the same equipment as

used for alcove construction in the ESF. A rock bolt and welded wire fabric ground control system was used during the construction of the ESF Main Loop, the alcoves, and the alcove/main loop intersections.

For non-emplacement drifts an initial ground support system comprised of rock bolts and welded wire fabric with occasional shotcrete application is proposed because this will provide the required support for the anticipated geologic conditions during construction and access to accommodate performance confirmation geologic mapping. The use of steel sets will be required to address more difficult localized geologic conditions, as was experienced in the ESF construction. The experience gained from the ESF construction will be incorporated into the design of the ground support system for the non-emplacement drifts to further accommodate constructibility and performance confirmation requirements. The final ground support system will incorporate a full lining system such as cast-in-place concrete lining to accommodate the different sizes and shapes of non-emplacement drift openings.

The ground support systems designed for emplacement and non-emplacement drifts will be addressed separately in this analysis. The final ground support systems for the emplacement drifts will also serve as the initial ground support systems because a single-pass operation is recommended, and the initial ground support system for the non-emplacement drifts will be similar to the ESF ground support system. Therefore, discussion of the ground support system design for both emplacement and non-emplacement drifts will focus on the final ground support systems. The analysis depends heavily on the analytical methods used to address the in situ stress, thermal, and seismic loading conditions. The thermal load will induce the dominant design loads. The empirical design approach, mainly used for design of the initial ground support subjected to in-situ stress and excavation loads, will not be discussed in this analysis.

This analysis evaluates the ground control systems for both emplacement and non-emplacement drifts. These are related to "Other Factors," according to AP-3.15Q, Attachment I, and are assigned Level 3 importance.

6.2 REPOSITORY GROUND CONTROL SYSTEM

Repository ground control systems for SR are divided into two groups: (1) the emplacement drift ground support system, and (2) the non-emplacement drift ground support system. The emplacement drifts include all drifts in which the waste packages will be placed for disposal. The non-emplacement drifts comprise all other repository drifts such as mains, exhaust mains, ventilation raises, emplacement drift turnouts, and intersections between turnouts and mains.

6.2.1 Ground Control for Emplacement Drifts

As discussed above, two types of final ground support system concepts are evaluated in the SR analysis for the repository emplacement drifts. These concepts include steel sets with welded-wire fabric, with and without fully-grouted rock bolts as the final ground support system. As stated above, the final ground support system will also serve as the initial ground support system for the emplacement drifts.

6.2.1.1 Steel Sets with Welded-Wire Fabric

An all-steel lining for emplacement drift support is installed in a single-pass operation and consists of rolled-steel ring beams or ribs and welded-wire fabric. The fabric is installed between the ribs and the rock, to prevent movement of the rock blocks into the drift. Following the installation of a steel invert section between the previously placed invert and the tunnel boring machine (TBM), steel rib sections are bolted together, set in place, and tie rods inserted between the ribs. A partial shield protects the assembly area from rock fall. The welded-wire fabric is installed behind the shield with steel pins holding it against the exposed rock. The rib is expanded against the fabric with the use of hydraulic jacks as the machine moves forward. Steel sets are recommended for the emplacement drifts excavated in various rock units including the lithophysal and non-lithophysal rocks. Figure 6-1 illustrates the use of steel sets for the lithophysal rock.

6.2.1.2 Fully-Grouted Rock Bolts

A rock bolt system consists of a pattern of steel rock bolts installed through the welded-wire fabric and grouted with cementitious material to hold the rock bolts in place. The rock bolts will only be installed in areas with massively-jointed rock to prevent any key blocks from loosening or where falling key blocks formed by joints are mobilized by excavation and have the potential of falling. These conditions are anticipated primarily in non-lithophysal rock areas. Therefore, rock bolts are recommended for the emplacement drifts excavated in non-lithophysal rock units. Figure 6-2 illustrates the use of fully-grouted rock bolts with steel sets for the non-lithophysal rock.

6.2.2 Ground Control for Non-Emplacement Drifts

The non-emplacement drifts have openings of different sizes and shapes, including various drift intersections. For the non-emplacement drifts, separate initial and a final ground support systems will be required. The initial ground support system will be needed to allow for safe construction and to accommodate performance confirmation mapping requirements. The turnouts and intersections are most likely to be excavated using mechanical mining technology. Rock bolts with welded-wire fabric and occasional shotcrete application was used in the construction of the ESF alcoves and main/alcove intersections. An initial ground support system comprising rock bolts and welded-wire fabric with occasional shotcrete application will be recommended. The other non-emplacement drifts will be excavated mainly with a TBM (e.g., at mains) or a roadheader (e.g., at alcoves). Initial ground support systems using rock bolts and welded-wire fabric will suit both types of excavation. This ground support system provides immediate support as the excavation proceeds and certainly accommodates performance confirmation mapping needs. For initial support, shotcrete application may be required to address localized geologic conditions, mainly for roadheader excavation. For the TBM excavations, the use of steel sets may be required in extensively blocky and fractured areas, as was experienced in the ESF construction, to address personnel safety immediately after excavation.

For the non-emplacement drifts, cast-in-place concrete lining will be recommended for the final ground support system. This cast-in-place concrete lining can be installed after the completion

of the performance confirmation mapping activities. It can accommodate different sizes and shapes of non-emplacement drift openings. Figure 6-3 illustrates the use of a cast-in-place concrete lining for the ventilation exhaust main.

6.3 DESIGN LOADS

In designing the potential repository openings, stresses resulting from four sources must be considered: in situ (including excavation effects), construction and operation activities, thermal (nuclear waste), and seismic. In situ stresses are present before drift excavation and will be altered in the vicinity of openings during repository excavation. The stresses during construction, such as installation activities (e.g. jacking process) or stresses due to equipment movement such as TBM weight during mining, must be considered in the design of the ground support systems. The stresses due to repository operations such as loads caused by gantry weight or waste package weight may also need to be considered in the design. Thermal stresses will occur after waste emplacement, and the timing and magnitude of the temperature-induced loads at any particular location in the potential repository are primarily dependent upon the position relative to the stored waste packages. The magnitude of earthquake-induced stress and the duration of the earthquake event are a function of the intensity of the earthquake, the distance from the event to the repository, and the direction and size of the seismic wave relative to the opening. The applicability and magnitude of some of the design loads will vary depending on the type of ground support system. Some of the loads, such as thermal loads, will only apply to the final ground support system. In the following sections, a description for each design load type is presented. The magnitude and method of application of specific loads in the design are presented in detail in the applicable sections of this analysis.

6.3.1 In Situ Loads

The virgin stress field existing before excavation is the in situ or geostatic state of rock stress. Excavation of repository openings will disturb the surrounding in situ stress field. The stability of the opening will depend on the concentrations of excavation-induced stress and rock mass deformation behavior. For repository openings, computer simulation of the excavation process will be used to assess the stability. In situ stress estimates, opening dimensions, rock mass bulk density, rock mass elastic moduli, and rock mass strength parameters for the failure or yield criteria are required to perform the analyses.

The in situ stress state at the repository has not been measured directly and will vary from location to location. In situ stress values to be used for the repository design will be determined in accordance with the procedure discussed in this section.

For the initial state of stress, the vertical stress (σ_v) at some point caused by the overburden weight is given as (Goodman 1980, Eq. 4.1)

$$\sigma_v = -\sum_{i=1}^{n} \rho_i g h_i \qquad \text{(Eq. 6-1)}$$

where ρ_i = average bulk density of the ith layer of rock mass, kg/m^3

h_i = thickness of the ith layer of rock mass above an opening, m
g = gravitational acceleration, m/s^2
n = total number of overlaying layers of rock mass, dimensionless

Assuming that lateral displacements are prevented, linear elasticity theory predicts that the horizontal stress (σ_h) is determined by (Goodman 1980, Eq. 4.2 and p. 101)

$$\sigma_h = \frac{\upsilon}{1-\upsilon}\sigma_v \qquad \text{(Eq. 6-2)}$$

where υ = Poisson's ratio, dimensionless

This formula is derived from the assumption that gravity is suddenly applied to an elastic mass of material in which lateral movement is prevented. This condition hardly ever applies in practice due to repeated tectonic movements, overburden removal, material failure, and locked-in stresses due to localized geologic heterogeneous conditions and faulting. Studies on the Yucca Mountain Project have estimated the relationship between horizontal and vertical stresses (CRWMS M&O 1997b, p. 1; DTN: SNF37100195002.001). The in situ stress measurements by hydraulic fracturing in a test borehole drilled from the ongoing Thermal Test Facility at ESF, located in the TSw2 unit, have shown that at an approximately 4.7 MPa vertical stress level, the two mutually orthogonal horizontal stresses are 1.7 (±0.1) and 2.9 (±0.4) MPa, respectively (CRWMS M&O 1997b, pp. 1 and 15; DTN: SNF37100195002.001). Accordingly, the minimum K_o value is 0.34 [=(1.7-0.1)/4.7] and the maximum K_o value is 0.70 [=(2.9+0.4)/4.7]. In addition, the data in *In Situ Rock Conditions* (DTN: MO0007RIB00077.000, Table 1) show that the minimum and maximum horizontal-to-vertical stress ratios range from 0.37 to 0.41 and 0.75 to 0.82, respectively. These K_o values indicate that the K_o values of 0.3 and 1.0 are lower and upper bounds and, therefore, are proper for bounding analyses. Therefore, the lower and upper bound K_o values of 0.3 and 1.0 are used for ground support analyses (Section 5.4).

In order to perform these analyses, a vertical stress value must also be estimated. Considering a repository drift located at 346.23 m from the surface, the vertical stress at the drift center will be equal to about 7.2 MPa. This value is obtained using the thicknesses and bulk densities of the respective lithostratigraphic units and Equation 6-1 (see Tables 4-2 and 4-3). In order to provide a reasonably conservative upper bound for the repository ground support SR design, the vertical stress value of 10 MPa is used (Section 5.4). The lower and upper bound K_o values of 0.3 and 1.0 are used to estimate the horizontal stresses.

In evaluation of the stresses induced by excavation in the ground support components for the emplacement drifts, an initial ground relaxation value of 60 percent is used (Section 5.1.1). This results in 40 percent of the pre-excavation in situ stress being imposed on the ground support system, providing a reasonably conservative upper bound to the loading recommended in earlier studies (see Section 5.1). For the non-emplacement drifts, the initial ground relaxation value of 100 percent is used for the final cast-in-place concrete lining (Section 5.1.2). This value is considered to be reasonable because the cast-in-place concrete lining will usually be installed months or even years after drift excavation. Any rock deformation induced by the excavation will most likely be complete before the installation of the concrete lining.

6.3.2 Construction and Operation Loads

Two invert designs are being considered for the emplacement drifts:

I. Steel beam inverts placed between the ground support steel sets and supported by direct contact with the rock surface forming the floor and sidewalls of the drift.

II. Crushed rock ballast invert spread over the rock surface and the lower surface of the ground support steel set ring beams.

For Invert Design I, the weights of construction and waste transport equipment and the waste packages will be transferred to the rock surface without loading the ground support steel sets. For Invert Design II, these weights will load the upper surface of the ballast, and a portion of this load will be transferred to the ground support steel sets. If this invert design is selected, the load transferred will be considered in a future analysis of ground support.

6.3.3 Thermal Loads

Thermally induced stresses are generated by thermal expansion of the rock mass due to the thermal energy released from the stored nuclear waste. Thermal stresses at any location depend on the proximity and timing of waste emplacement, the waste heat generation, the age of the waste, packaging and emplacement configuration, and the thermomechanical properties of the rock mass. Therefore, thermal loads are time-dependent, and are modeled for a preclosure period of up to 300 years, to meet the system performance requirement (Section 4.2.2.7), and to capture the behavior during the thermal pulse.

The current design requirements for the repository system performance include the limit of the emplacement drift wall temperature to 96°C or less (BSC 2001, Section 5.2.24) during the preclosure period and the limit of WP surface temperature to 85°C or less (BSC 2001, Section 5.1.1.3). These requirements specify a flexible repository design with a variable thermal load. Two initial linear thermal loads corresponding to two operation modes have been considered for the subsurface layout design, one at 1.45 kW/m (high-temperature operation mode) and the other at 1.0 kW/m (low-temperature operation mode).

To accommodate these operational scenarios, two different thermal conditions are incorporated in the ground control design. The first thermal condition uses an initial linear heat load of 2.0 kW/m and a preclosure ventilation rate of 10 m^3/s for 200 years following waste emplacement. This high-temperature thermal selection is intended to bound the ground control analysis and address some uncertainties associated with variations in design parameters. The time histories of rock temperatures associated with this thermal condition are presented in Table 4-12a. The second thermal condition considered corresponds to the low-temperature mode, with an initial linear heat load of 1.0 kW/m and a preclosure forced ventilation rate of 15 m^3/s for 50 years after waste emplacement combined with a natural ventilation rate of 3 m^3/s from 50 to 100 years and 1.5 m^3/s from 100 to 300 years. According to DTN: MO0105MWDTHE05.009, the initial linear heat load will be likely limited to about 1.0 kW/m in order to maintain the WP surface temperature below 85°C during the repository life time. The time histories of rock temperatures for this low-temperature condition are listed in Table 4-12b.

The two thermal operating modes considered in this analysis apply only to normal preclosure operating conditions. For any abnormal condition, the maximum emplacement drift wall temperature is limited to 200°C (BSC 2001, Section 5.2.24). Since an abnormal condition could be caused by any unpredictable event, such as an earthquake or a volcano eruption, response to such kinds of events will be dependent on the magnitude of damages caused. The time required to bring the repository system back to normal operation mode, for example to have ventilation fans operating, will determine the magnitude of any temperature increase, and has not been analyzed. Therefore, this analysis only considers the thermal requirements for the normal operation modes.

6.3.4 Seismic Loads

Ground motions associated with earthquakes are required to be considered in the design of the repository underground openings. The critical ground motions for subsurface design are ground velocity and acceleration.

In contrast to surface structures, underground structures such as tunnels and their lining or reinforcement systems are constrained by the surrounding medium and do not move independently of the surrounding rock. In reality, the underground structures display significantly greater degrees of redundancy due to the confinement from the ground compared to surface structures, which are generally unsupported above their foundation. Therefore, for underground openings, the surrounding rock acts as a support during a seismic event. Case history studies of underground openings which have been subjected to seismic activities are generally used in practice to provide a basis for ground support design. Forty-one (out of seventy-one) cases of observed damage to rock tunnels from earthquake movements were compared to calculate peak surface motions to determine damage thresholds (Dowding 1979, p. 15). The tunnels were built between late 1800s and the 1960s, and, thus, represent a wide variety of construction methods. It is shown that peak surface accelerations which cause heavy damage to surface structures, cause only minor damage to tunnels. For accelerations up to 0.19g and velocities up to 20 cm/s, no damage was experienced even for unsupported openings. Minor damage (new cracks and minimal rock fall) was observed for accelerations up to 0.5g and velocities up to about 90 cm/s (Dowding 1979, p. 17 and Figure 5).

Other than case history studies, there are no empirical or closed-form solutions available to assess seismic effects on underground openings. Limited progress has been made in seismic design methodology for underground tunnels, possibly because of favorable performance data. The lack of applicable codes in the past has led to widely varied measures of precaution taken by different engineers. Recent earthquake awareness in the United States, since the Loma Prieta earthquake of 1989, has lead to a rethinking of seismic design practices for underground tunnels, and especially for transportation systems. Moreover, the development of pertinent computer codes, as well as vast improvements in computational capacities of hardware, are providing effective tools for seismic design of underground openings. For ground support analysis for SR, both quasi-static and fully dynamic analyses will be performed to simulate seismic effects and assess opening stability.

In general, the following information on vibratory ground motions (often referred to as ground shaking) may be required for performing design analysis: PGA, PGV, peak ground displacement,

duration of shaking, and time histories of acceleration, velocity, and displacement, depending on the structural characteristics (e.g., stiffness) of the system, structure, or component to be analyzed.

For a dynamic loading approach, only PGV values are used in this analysis to generate seismic velocity waves in forms of primary (P) and shear (S) waves that propagate vertically upwards from below the potential repository host horizon, through the emplacement drift area, and towards the ground surface. Velocity waves (P-wave and S-wave) are generated with amplitudes equal to PGV values, in conjunction with assumed frequency and duration values. Since the S-wave causes horizontal ground vibration (shaking) and is a leading cause of structural damage while the P-wave oscillates the ground in compression and tension, both types of waves are considered simultaneously in this analysis for analyzing the emplacement drift behavior.

For a quasi-static loading approach, the PGA values from design basis seismic events are used. PGA values are converted into additional body forces, much like extra gravitational forces, and are instantly applied to the rock mass under consideration. The basis of the quasi-static approach is that the size of the opening is much smaller than the predominate wave length of the seismic event, that is, a large ratio of wavelength to drift diameter. The response is effectively static, corresponding to a long duration loading. Therefore, the application of static load corresponding to peak dynamic load is a reasonable approximation of the actual dynamic response.

6.4 DESIGN APPROACHES

The repository ground support design effort includes analytical methods, coupled with the lessons learned from the design and construction of the ESF. Analytical methods are used to evaluate the stability of the repository openings under in situ, seismic, and thermal loading conditions. The response of the surrounding rock subjected to excavation, seismic, and thermal loads is determined and incorporated into the design of the final ground support system. The effects of the construction and repository operation loads on the final ground support system are discussed and will be evaluated in detail and addressed in LA design efforts, as these loads do not govern design of the ground support systems. As indicated earlier, the ground support designs for the emplacement drifts and the non-emplacement drifts focus on the performance of the final ground support systems. Results presented in the following sections will be based on analytical methods.

6.4.1 Rock Mass Classification

Rock mass classification systems allow rock properties and geologic conditions shown in samples taken from boreholes, scanline, full-peripheral mapping, detailed test surveys, and certain outcrops at the planned site, to be compared with similar information compiled and categorized from existing underground facilities. Based on this comparison, rock mass properties for use in analyses can be estimated.

To date, many rock mass classification systems have been proposed, the better known being systems by Terzaghi (1968), Deere and Deere (1988), Wickham et al. (1972), Bieniawski (1988), and Barton (1988). Two common classification systems were recommended and used in the design and construction of the ESF openings (CRWMS M&O 1995, Sections 7.5 and 7.6).

These two classification systems are the Geomechanics classification system or rock mass rating (RMR) developed by Bieniawski (1988), and the Norwegian Geotechnical Institute (NGI) classification system developed by Barton (Barton 1988). The latter system was used in designing the ESF, and the successful performance of that facility has lead to adoption of this system for analysis of ground control elements for SR. A detailed description of this classification systems can be found in Barton (1988), and an overview is presented below.

6.4.1.1 NGI Rock Mass Classification System

The NGI rock mass classification or the rock mass quality Q system, developed in Norway in 1974 by Barton (1988), is commonly used in the design of rock support for tunnels and large underground chambers. The six parameters in the NGI system include (Barton 1988, p. 63):

- Rock Quality Designation (*RQD*)
- Joint Set Number (*Jn*)
- Joint Roughness Number (*Jr*)
- Joint Alteration Number (*Ja*)
- Joint Water Reduction Factor (*Jw*)
- Stress Reduction Factor (*SRF*)

The parameters are combined in the following way:

$$Q = \left(\frac{RQD}{J_n}\right)\left(\frac{J_r}{J_a}\right)\left(\frac{J_w}{SRF}\right) \qquad \text{(Eq. 6-3)}$$

where Q = final classification value, dimensionless
(RQD/J_n) = block size parameter, dimensionless
(J_r/J_a) = interblock shear strength parameter, dimensionless
(J_w/SRF) = active stress parameter, dimensionless

The rock mass descriptions and ratings for each of the six parameters are given in Barton (1988, p. 63). The NGI system is logarithmic with possible Q values ranging from 0.001 (exceptionally poor) to 1,000 (exceptionally good), encompassing the whole spectrum of rock mass qualities from heavily squeezed ground to sound unjointed rock. As in the Geomechanics classification system, the nature of the joints plays a major role in estimating Q values.

The NGI rock mass classification system provides guidance on bolt spacing, bolt length, and shotcrete thickness, based on the rock mass quality index (Q) and the opening dimensions.

The rock mass quality index (Q) was used as a tool to estimate ground support requirements for the ESF openings. The Q estimates from surface-based drilling were used to establish ground support classes for the ESF prior to construction. During construction, estimates of Q values were obtained from mapping activities that followed the TBM excavation. A comparison of field data and borehole estimates, for the most part, shows a relatively close correlation between both estimates.

The rock mass quality index (Q) was used to estimate rock mass properties based on the mapping data from the ESF tunnel and the Cross Block Drift. Five RMQ categories were defined, corresponding to the cumulative frequencies of occurrence of 5 percent, 20 percent, 40 percent, 70 percent and 90 percent of the rock mass quality index, using the approach suggested by Hardy and Bauer (1991, Table 12-3, p. 12-9). The quality of the rock mass was classified based on its estimated Q value as extremely poor for RMQ=1, very poor for RMQ=2, poor for RMQ=3, fair for RMQ=4, and good for RMQ=5. For each rock mass quality category, the corresponding bounding values of rock mass properties were estimated. Tables 4-5a and 4-5b in Section 4-1.6 give the values of rock mass properties corresponding to the five rock mass quality categories for the non-lithophysal (Tptpmn) and lithophysal (Tptpll) rock units. These values were considered to bound the variations in rock mass properties for the corresponding unit and, therefore, were used in the ground control analyses.

6.4.2 Analytical Design Approach

The computer modeling techniques serve as an analytical basis for assessing the opening shape and determining the general stress distribution around the tunnel opening in underground design. In repository ground support design, numerical analyses will play an important role in determining and evaluating the effects of the seismic and thermal loading conditions. As indicated earlier, design of the repository openings introduces new challenges due to the presence of high temperatures and resultant thermal loading conditions. There are many unknown factors involved in the design of such openings and, presently, no known tunnels exist or operate under such high temperatures. The computer simulation of repository openings subjected to high temperatures due to waste emplacement will provide an analytical basis for the design of the openings and the ground support systems. An in situ thermal test is being conducted in the ESF to provide an experimental basis for evaluating the thermal-hydrological-geomechanical-geochemical behavior at the site. The response of the host rock and ground support components in temperatures higher than the anticipated repository temperatures is being measured and monitored. The test is a drift-scale test that represents in-drift emplacement of large waste packages. The drift-scale test is being conducted in the heated drift portion of the Thermal Test Alcove located in the middle non-lithophysal (Tptpmn) unit. The Heated Drift contains a row of large heaters, and is flanked, on either side, by arrays of borehole-emplaced "wing" heaters. The results of the tests will provide additional knowledge about the response of the surrounding rock and the ground support components when subjected to high temperatures.

For the SR analysis, a series of computer analyses are conducted and presented here to simulate the in situ, seismic, and thermal loading conditions, and to assess the stability of the repository openings. First, the unsupported openings are analyzed using continuum and discontinuum models, with rock mass properties corresponding to Rock Mass Categories 1 and 5. Then, the final ground support systems are incorporated into the computer models and are analyzed for applicable loading conditions. It is noted that a rock mass with or without an initial ground support will behave differently. However, the initial ground support is not credited in modeling the final ground support for the purpose of conservatism. Emplacement drift analyses include computer simulation of the excavation of the repository openings in a gravity-stressed rock medium, followed by the introduction of high temperatures to simulate the waste emplacement process. The resultant thermal stresses are superimposed onto the stresses due to the excavation and, finally, the model is subjected to seismic loading. For supported opening analyses, the final

ground support system is incorporated into the model during the excavation process and, therefore, is subjected to in situ, thermal, and seismic loading. The thermal effects on non-emplacement drifts will depend on the location of the drift with respect to the waste emplacement area as well as the repository ventilation scheme. It is clear that the temperatures and the thermal effects on the non-emplacement drifts will be much lower than those experienced by the emplacement drifts. In what follows, the general concepts and approaches for the analysis of the ground support systems for the emplacement and non-emplacement drifts will be discussed. The application of these approaches and the results will be presented in Sections 6.5 and 6.6.

6.4.2.1 Thermal Analysis

Before performing a thermomechanical analysis on a given thermomechanical model, the model is first subjected to a thermal analysis to determine the time history of the temperature at all points in the model. This requires that the time-dependent temperatures at the temperature-controlled boundaries of the model are known. The boundaries of the thermomechanical models used in the analysis of emplacement drifts are listed in Table 6-1.

Table 6-1. Temperature-Controlled Boundaries of the Thermomechanical Models

Thermal Model	Thermomechanical Model Static Conditions	Thermomechanical Model Seismic Conditions
Upper Boundary	Horizontal Plane 50 Meters Above Drift Center	Ground Surface Above Drift Center[a]
Drift Wall Boundary	5.5-Meter Diameter Drift	5.5-Meter Diameter Drift
Lower Boundary	Horizontal Plane 50 Meters Below Drift Center	Horizontal Plane 50 Meters Below Drift Center

Note: [a] Model extends to ground surface to capture dynamic effects of overburden layers.

The temperature at the ground surface is given in Section 4.1.1. The time histories of temperature at the other temperature-controlled boundaries are presented in Tables 4-12a and 4-12b, and are used as known inputs to the thermomechanical analyses.

For non-emplacement drifts, such as access mains, ventilation exhaust main, emplacement turnout drifts, ventilation raises, and intersections formed by emplacement and non-emplacement drifts, the rock temperature on the drift walls is assumed to be maintained at or below 50°C by ventilation during the repository preclosure period. Since the Exhaust Main is located only 10 m below the emplacement drifts (from the crown of the Exhaust Main to the invert of the emplacement drifts), the temperature condition in the emplacement drifts will affect the behavior of the ground supports in the Exhaust Main, and must be taken into account.

Four prescribed temperature boundaries are used in the models: (I) the upper boundary, located at 50 m above the center of the Exhaust Main or at 33.44 m above the center of the emplacement drift; (II) the lower boundary, located at 50 m below the center of Exhaust Main or 66.56 m below the center of the emplacement drifts; (III) the horizon of the center of the emplacement drifts, which is 16.56 m above the center of the Exhaust Main; and (IV) the drift wall of the Exhaust Main. Except the constant temperature on the wall of the Exhaust Main, the temperatures on the boundaries, I, II, and III, are time-dependent (see Section 4.1.12). These are

the average rock temperatures at the corresponding horizons. For example, at the emplacement drift horizon, the drift wall temperature is 99.78°C at 1 year after waste emplacement, and the rock temperature at the middle of the drift pillar is 27.33°C. Thus, the average rock temperature at this level is 63.56°C at 1 year. The time histories of temperature at the model boundaries are given in Table 4-12a.

Use of the average rock temperatures instead of the wall temperatures of the emplacement drifts to account for the temperature effect on the Exhaust Main can be justified. First, the emplacement drifts have a drift spacing of 81 m. This wide spacing results in a great temperature gradient soon after waste emplacement (see Table 4-12a). The effects of elevated temperatures on rock mass expansion and behavior of the ground support for the Exhaust Main are likely close to that for the condition in which an average temperature is assumed for the entire emplacement drift horizon. Second, the ventilation raises are constructed at the end the emplacement drifts, and the drift rock temperatures near the ventilation raises are expected to be relatively lower as a result of edge effects. Third, the input temperatures selected for this analysis are very conservative in order to address some uncertainties, as discussed in Section 4.1.12. Therefore, the thermal loading condition used for the Exhaust Main is conservative.

6.4.2.2 Thermomechanical Analysis

The physical process in the rock mass near an emplacement drift with an emplaced waste package involves coupling the effects of thermal loading with excavation- and seismic-induced stress and deformation. The temperature increase in the rock mass and ground supports, caused by the waste package emplacement, will result in deformation and stress. Depending on the mechanical properties and the magnitude of the induced response, the rock mass and the ground support may behave elastically or elasto-plastically, with the results being judged by appropriate criteria, such as the Mohr–Coulomb yield criterion for the rock mass and joint (see Section 6.4.2.4 below).

The thermomechanical analyses are performed for both unsupported and supported emplacement and non-emplacement drifts based on their corresponding thermal loading conditions. The numerical approaches used in the thermomechanical models are described in the following subsections.

6.4.2.2.1 Modeling of Unsupported Emplacement Drifts

Unsupported emplacement drifts are modeled to predict the thermomechanical behavior of the rock mass, especially near the drift openings. The rock mass considered is either equivalently continuous or jointed. Two-dimensional models are used to perform the analysis.

6.4.2.2.1.1 Continuum Modeling

For an equivalently continuous rock mass, the FLAC code is employed. In a FLAC model, the rock joint properties are not considered explicitly, but are reflected in the rock mass properties that are used as inputs. The mechanical properties for the rock mass include the elastic modulus and Possion's ratio for deformation, and cohesion, friction angle, and tensile strength for strength. The Mohr–Coulomb yield criterion is used in the FLAC model to judge the stability

performance of the rock mass. Symmetrical conditions, both thermal and mechanical, with respect to drift layout and loading, are incorporated in the model. Figure 6-4 shows the configuration of a FLAC model.

The unsupported emplacement drift is modeled first as subjected to an in situ stress load, including effects of excavation, and then to a thermal loading period of 200 or 300 years, depending on the thermal (high temperature or low temperature) conditions analyzed. During the thermal loading period, the analysis involves both the thermal and mechanical calculations.

In the thermal phase of the modeling, the boundary temperatures include those for the opening wall and the model upper and lower boundaries, and are time-dependent except on the boundary of the ground surface. With the boundary temperatures as input, the rock temperature distributions over time are determined. The temperature calculation in the FLAC model involves thermal conduction only.

With the temperature distributions at a given time being determined, the mechanical phase of the modeling is turned on and thermally-induced rock stresses and displacements are calculated. The rock stresses and displacements at a given time are obtained when force equilibrium is reached. Then the mechanical phase is turned off and the thermal phase is turned on to calculate the rock temperature distributions at a later time. This process is repeated over a simulated time period of 200 or 300 years. The results of the thermomechanical calculation with FLAC include the time histories of rock stresses and displacements, such as the principal (tangential) stresses near the opening and the opening closures. The rock strength-to-stress ratio contours at a given time are also generated from the results to evaluate the opening stability, such as the potential rock mass yield, under the combined in-situ stress and thermal loads.

6.4.2.2.1.2 Discontinuum Modeling

The discontinuum modeling approach considers the rock mass to be a discontinuum composed of individual blocks which interact with their neighbors through elastic and plastic deformation of the intervening joints. The UDEC code is employed for this analysis.

As shown in Figure 6-5, a UDEC model is constructed to contain a single emplacement drift. The mutual effect of adjacent emplacement drift excavation is neglected because the drift spacing, 81 m, is considered wide enough to preclude significant mutual effect. The model is divided into two subregions, one with joints and the other without joints, in order to reduce the number of zones generated in the model and to increase the efficiency of the problem solving. The dimension of the subregion with joints is determined by trial-and-error to ensure that the results are not substantially affected by the subregion size. The subregion without joints encloses the jointed subregion, as shown in Figure 6-5; the drift is located at the center of the jointed interior subregion.

In the subregion with joints, joint patterns and properties are considered explicitly, and intact rock blocks that are bounded by joints are treated as deformable. In the subregion without joints, the presence and effect of joints are considered implicitly by using the rock mass properties. Therefore, the properties of joint, rock mass, and intact rock are required for the UDEC model. For rock joints, the deformation properties are given in terms of the normal and shear stiffness

values. The Mohr–Coulomb yield criterion is used for judging the performance of both rock joints and intact rock blocks. Also, temperature-dependent properties, such as thermal conductivity, specific heat, and the coefficient of thermal expansion, as listed in Tables 4-2 and 4-6, are used to determine the temperature distribution and rock block expansion.

Two joint sets, one nearly vertical and the other nearly horizontal, are modeled. The joint dip angles and spacings vary with the rock units (see Table 4-7). A fine mesh is used in the region close to the opening since this region is the focus of the numerical investigation. Intact rock properties obtained from laboratory testing are assigned to these rock blocks. Joints are given deformation properties in terms of horizontal and vertical stiffness values, and strength properties in terms of cohesion and friction.

The analyses are conducted for an unsupported emplacement drift opening. The emplacement drift to be modeled is first subjected to in situ stress load upon excavation. Then, the temperature, stress, and displacement distributions in the joints, intact rock blocks, and rock mass are calculated for a period of 200 or 300 years. The computational process is similar to that for the continuum model with FLAC (see Section 6.4.2.2.1.1 for details). The most important information obtained from a UDEC model is the potential rock block movement near the drift opening, which is extracted from the predicted joint closure and shear displacement under the combined in-situ and thermal loads.

6.4.2.2.2 Modeling of Supported Emplacement Drifts

Supported emplacement drifts may be subjected to in-situ, thermal, and seismic loads. The FLAC code is employed to model the rock bolts, and the ANSYS code is used for steel sets. Two-dimensional models are used for ground support modeling. The modeling approaches for the supported emplacement drifts subjected to these loading conditions are described separately in the following two subsections.

6.4.2.2.2.1 Representation of Ground Support Components

Steel sets are modeled as a lining ring with two-dimensional beam elements in both the ANSYS and FLAC codes. The beam element is defined by two nodes, together with the cross-sectional area, the area moment of inertia, and the material properties. The beam ring is subdivided into a number of beam segments. With the beam elements, the bending resistance of the lining is considered. The results are the thrust and bending moment within the beam ring. In modeling the steel sets, the mechanical properties such as the modulus of elasticity of steel are scaled by dividing by the spacing of the sets along the drift. Thrust and bending moment outputs from the model are then multiplied by the spacing to obtain the actual loads.

Rock bolts are modeled in the FLAC code only. The bolts are simulated by one-dimensional cable elements. The cable element is defined by two nodes, together with the cross-section area and the material properties. The cable is divided into a number of segments that are grouted along its length to provide bonding to the rock. The cable element is an axial member, meaning that only the uniaxial resistance, compression or tension, is taken into account. Similar to the modeling of steel sets, the mechanical properties such as the modulus of elasticity and the

strength of the bolts are also scaled by the spacing. Axial forces from the model are then multiplied by the spacing to obtain the actual loads.

6.4.2.2.2.2 In-Situ Stress Loading Condition

In the design of tunnel supports, it is important to determine the amount of initial ground relaxation that takes place before installing the support. Since some relaxation actually takes place before installation, the loads on the ground support will be over-estimated if no relaxation is allowed in the model. It is difficult to accurately estimate the amount of initial relaxation, since it depends on the distance and the timing of the support installation with respect to the advancing of the tunnel face. In TBM excavation, steel sets will be installed behind the TBM shield and by the time they are jacked in place, most of the initial ground relaxation has most likely been completed. Based on Assumption 5.1.1, a 60 percent relaxation value is used in analyzing the emplacement drift ground support systems (see Section 5.1.1). Based on Assumption 5.1.2, a 100 percent relaxation value is used for non-emplacement drifts (see Section 5.1.2).

6.4.2.2.2.3 Thermal Loading Condition

Under combined in-situ stress and thermal loading conditions, there are two major factors that contribute to the stress and strain in the ground support during the heating process: (1) rock mass deformation, including thermal expansion of the rock, and (2) thermal expansion of the ground support materials. As a result, the stress in the ground support may be several times higher than when it is subjected to in-situ stress load alone. As an analogy, consider a beam with its two ends fixed. When the temperature rises, the beam will tend to expand. Due to the restraint at its two ends, no expansion is allowed and, therefore, a compressive stress is induced in the beam (even with no measurable strain detected). A ground support lining ring in the emplacement drifts will behave similarly. It will expand when the temperature increases so that the gap between the rock and the steel sets, if any, will get smaller or be closed. Since the drift wall rock will act as a confinement to the lining ring, preventing it from expanding, thermal stress will be induced in the steel sets. In addition, the rock will also expand when it is heated, and transfer additional load to the lining through its deformation once the lining is in full contact with the rock wall.

In modeling ground support subjected to combined in-situ stress and thermal loads, different approaches are used depending on the type of support. Details on the numerical approach used for each type of ground support used are discussed in the following two subsections.

6.4.2.2.2.3.1 Modeling of Steel Sets

Steel sets installed as a circular ring will neither bond nor conform perfectly to the bored surface of the opening. The joint connection between two steel set segments may also allow some relative displacement. Areas with gaps or no contact between the steel sets and the rock exist. These factors will alter the load condition on the steel sets, producing lower stresses than for the perfect contact condition. Therefore, an approach which takes into account the gaps between the steel sets and the rock is proposed and used in this analysis when modeling steel sets subjected to combined in situ and thermal loads.

The interface or gaps between the steel sets and the rock surface are represented by the two-dimensional circumferential point-to-surface contact elements provided in the ANSYS code. The interface may separate the steel sets from the rock or maintain physical contact between them, depending on the loading condition. It may also allow the steel sets and the rock to slide relative to each other. Therefore, the contact elements are capable of supporting compression in the direction normal (perpendicular) to the surfaces and shear in the tangential direction. Behavior of the circumferential contact elements is governed by their stiffness and frictional resistance.

An initial "gap" is assigned to the contact elements, representing an initial mismatch between the steel set ring and the rock surface. The initial "gap" is not uniform along the circular ring, varying from the greatest at the crown to zero at the invert. Figure 6-6 shows a sketch of the model representation for the steel sets with the circumferential gap elements. The only physical property of the contact elements is the coefficient of friction. Its value depends on the types of materials which form the interface. For numerical analysis purposes, two numerical parameters, called normal contact stiffness (k_n) and sticking contact stiffness (k_t) are also associated with the contact elements. The values of these parameters are related to the stiffness of the system being modeled and determine the amount of the so-called "penetration" in the normal (perpendicular) direction and the relative displacement (sliding) between two surfaces. The values of these parameters used in the ANSYS models are provided in Section 4.1.9.

It is noted that introduction of the circumferential interface is intended to simulate the interaction between the steel sets and the rock more realistically. No perfect fit will be achieved during excavation. Any small degree of mismatch will yield gaps between the steel sets and the rock. When the steel sets and the rock are heated by the emplaced waste, they will expand without resistance initially, owing to the presence of these gaps. With the increase in temperature and the decrease in the size of gaps, the gaps may be closed completely under combined loading conditions, depending on the magnitude of the thermal load or temperature increase and the size of the mismatch.

The approach discussed here applies only to the steel sets under combined in-situ stress and thermal loads using the ANSYS code. For seismic loading conditions, the steel sets are modeled as perfectly bonded to the rock surface since any gap left after ground relaxation will most likely be reduced or closed due to thermal expansion of steel sets and rock mass at elevated temperatures. In addition, gaps, voids or soft contact between the steel sets and the rock would help dissipate the dynamic energy and lessen the effect of seismic loading on the steel sets. Therefore, the approach used for seismic loading condition is conservative.

As indicated earlier, the steel sets are modeled with two-dimensional beam elements (see Section 6.4.2.2.2.1).

6.4.2.2.2.3.2 Modeling of Fully-Grouted Rock Bolts

A rock bolt fully grouted with cement will bond to the rock to reinforce the rock mass along its length. The fully-grouted rock bolt is judged to fail when either the bond yields or the rock bolt material itself yields. Of these two strength factors, the grout bonding (shear) strength is considered more critical to the performance of the rock bolt system subjected to thermal loading

because of the difference in the coefficients of thermal expansion of the bolt steel and the grout material. This difference may result in a shear stress at the bolt/grout interface that could be high enough to exceed the grout shear strength.

As stated in Section 6.4.2.2.2.1, rock bolts are modeled with one-dimensional cable elements using the FLAC code. The axial stiffness of the cable elements is described in terms of the bolt cross-sectional area and Young's modulus of the bolt material. Both a tensile yield-force limit and a compressive yield-force limit are assigned to the cable. Once the tensile or compressive limits are reached, no higher cable forces can develop and the bolt is considered to yield.

The maximum shear force that can be developed in the grout, per length of element, is a function of the cohesive strength of the grout and the stress-dependent frictional resistance of the grout. The relation used to determine the maximum shear force is given as follows (Itasca Consulting Group 1996a, Eq. G.11, p. G-28):

$$\frac{F_s^{\max}}{L} = S_{bond} + p' \times \tan\left(S_{friction}\right) \times perimeter \qquad \text{(Eq. 6-4)}$$

where
F_s^{max} = maximum shear force along a bolt, N
L = length of a bolt, m
S_{bond} = intrinsic shear strength or cohesion, N/m
p' = mean effective confining stress normal to the element, N/m^2
$S_{friction}$ = friction angle, degrees
$perimeter$ = exposed perimeter of the element, m

6.4.2.2.3 Modeling of Non-Emplacement Drifts

The non-emplacement drifts considered in this analysis consist mainly of access mains, ventilation exhaust main, emplacement drift turnouts, ventilation raises, and intersections formed by emplacement and non-emplacement drifts. These drifts are modeled to evaluate their behavior under in-situ stress, thermal, and seismic loads, and to establish their ground support needs. The in-situ stress and seismic loading for the non-emplacement drifts are assumed to be the same as those for the emplacement drifts, but the thermal load is different. Therefore, additional modeling efforts are still needed. Both two- and three-dimensional analyses are performed for the non-emplacement drifts.

For the access mains and the ventilation exhaust main, a 300-mm-thick cast-in-place concrete lining is recommended as the final support (see Section 4.1.11). As indicated in Table 4-16, the diameters of the ventilation exhaust main and the access mains are the same (7.62 m). The ground support selection for the exhaust main should be conservatively applicable to the access mains. Therefore, only the ventilation exhaust main is modeled in the analysis.

For both unsupported and supported exhaust main drifts, the FLAC code is used to perform the two-dimensional analysis. In the modeling, the concrete lining is treated as a continuous lining ring with beam elements and is considered to be bonded perfectly to the rock wall. Figure 6-7 illustrates the model configuration using FLAC. It is noted that a symmetrical condition with

respect to the exhaust main drift geometry and loading condition is assumed. Also, the lateral thermal boundaries are assumed to be adiabatic.

A three-dimensional 3DEC model is constructed to examine the stress concentration and stability at the intersection area formed by emplacement and non-emplacement openings. One typical area to be concerned is the emplacement drift turnout where large roof spans and wedge-shaped pillars are present. A three-dimensional modeling representation is necessary for this area. Figures 6-8a and 6-8b illustrate the 3DEC model for the intersection region formed by an access main and emplacement turnout drift. An intersection angle of 75 degrees as shown in Figure 6-8b is used in the model. It is noted that the numerically constructed model implies that there is turnout drift on each side of an emplacement drift. Though this numerical model is not representative for the subsurface layout, its use, contributing to a reduction in computational efforts, is considered conservative in terms of the stability evaluation of the intersection.

In performing the numerical analysis, only in-situ stress and seismic loads are considered in this 3DEC model. Any thermal effect on the excavation stability and ground support at this intersection after waste emplacement in emplacement drifts is expected to be insignificant, since the temperature surrounding this intersection and non-emplacement openings will be much lower than that for emplacement drifts. If necessary, thermomechanical analysis for these non-emplacement openings will be performed in the future design efforts for the License Application. Rock mass properties are assigned to deformable rock blocks and no joints are explicitly modeled in the 3DEC model.

6.4.2.3 Seismic Analysis

Seismic loads in forms of sinusoidal velocity waves are applied to both the continuum and discontinuum models after the in situ and thermal loads have been considered. Figure 6-9 shows a FLAC model configuration for the continuum modeling approach. The model upper boundary extends from below the emplacement drift horizon all the way to the ground surface. Therefore, the model contains the TCw, PTn, TSw1 and TSw2 thermal/mechanical units. The two vertical lateral boundaries are set to be in viscous or quiet boundary conditions to prevent the outwardly-propagating waves from reflecting back into the model at these two boundaries. The top of the model corresponds to the ground surface where waves can reflect back to the model. Seismic waves are applied at the bottom of the model. Applied waves propagate vertically upwards.

To help visualize the dynamic response of an emplacement drift to seismic loads in a straightforward manner, the resultant displacement caused by both excavation under the in situ load and subsequent thermal loads is zeroed out prior to the application of seismic loads. Therefore, the output from the model upon the application of seismic loads is in forms of purely dynamic displacement and total stress.

6.4.2.4 Rock Failure Criterion

The Mohr-Coulomb failure criterion is used in this analysis to judge whether the stresses in the rock mass or on joints surrounding the emplacement and non-emplacement drifts reach the magnitude of the yield limit. The Mohr-Coulomb failure criterion is defined as (Owen and Hinton 1980, pp. 218-220):

$$\tau_f = c - \sigma_n \tan\phi \qquad \text{(Eq. 6-5)}$$

where τ_f = shear stress on a failure plane, N/m^2
c = cohesion, N/m^2
σ_n = normal stress on a failure plane, N/m^2
ϕ = angle of internal friction, degrees

6.4.2.5 Sign Convention

The sign convention for normal stresses, as shown in Figure 6-10, is "tension is positive and compression is negative." For shear stresses, a positive shear tends to cause two positive normal stress axes to rotate toward each other. All stress components shown in the figure are in the positive sense. This sign convention applies to the rock stresses calculated with ANSYS, FLAC, UDEC, and 3DEC, and the steel set stresses calculated with ANSYS. For axial forces in both the beam and cable elements analyzed with FLAC, a compressive force (thrust) is positive while a tensile force is negative. In this analysis, all stresses in steel sets and rock bolts are plotted as positive in compression and negative in tension. For drift opening closures (changes in diameter), a positive closure indicates that two reference points move toward to each other, resulting in a reduction in the distance between these two points.

6.5 EVALUATION OF EMPLACEMENT DRIFT GROUND SUPPORTS

The design of the final ground support systems in the emplacement drifts will incorporate analytical methods to address in situ, seismic, and thermal loading conditions. In applying numerical modeling techniques, first the unsupported drifts are analyzed to assess opening stability under in situ, seismic, and thermal loading conditions. Then, the final ground support system is incorporated into the model and analyzed to assess its performance.

For the emplacement drifts, the two types of final ground support system concepts considered for SR design are steel sets with welded-wire fabric, with and without fully-grouted rock bolts. Analytical methods using numerical modeling techniques are implemented to demonstrate the design approach for ground support under combined in situ stress, thermal, and seismic loading conditions, to assess emplacement drift long-term stability, and to evaluate the performance of the steel sets and rock bolts. Use of the continuum and discontinuum models in evaluating underground opening stability under in situ loading conditions is a common practice in the industry. For seismic analyses, the emplacement drift opening is analyzed using dynamic and quasi-static approaches. The thermal loading is unique to the repository design and the design approach and methodology are still under development. The thermal analyses presented here will demonstrate an approach which will be refined as the design proceeds, especially when more experimental data become available from programs such as thermal testing in the ESF. Coupled thermomechanical analyses to determine time-dependent temperatures, displacements, and stresses within the rock mass were performed using ANSYS and FLAC for continuum modeling and UDEC for discontinuum modeling.

Rock mass properties representing Categories 1 and 5 are used in the analyses to simulate the worst and best expected rock conditions, respectively, in the middle non-lithophysal (Tptpmn) and lower lithophysal (Tptpll) units. Though the majority of emplacement drifts will be located

in the lower lithophysal unit (Tptpll), the rest will be excavated in the middle non-lithophysal unit (Tptpmn), the upper lithophysal unit (Tptpul), and the lower non-lithophysal unit (Tptpnl). The rock conditions between two lithophysal units, Tptpll and Tptpul, and between two non-lithophysal units, Tptpmn and Tptpln, are comparable. Therefore, the rock mass properties for the Tptpll and Tptpmn units are considered applicable to the overall rock mass conditions anticipated at the emplacement drift horizon.

As indicated in Tables 4-5a and 4-5b, mechanical properties for these two rock units show no significant difference. Overall, the properties of the lower lithophysal unit (Tptpll) appear to be better than those of the middle non-lithophysal unit (Tptpmn), though the elastic modulus and tensile strength of the intact non-lithophysal unit are slightly higher than those of the lithophysal unit (Table 4-4). The only significant difference clearly indicated is the joint spacing, as shown in Table 4-7, for these rock units. The joint spacing for the Tptpmn unit is much smaller, about 0.5 m for both vertical and horizontal sets, than that for the Tptpll unit, about 2 m for the vertical sets and 3 m for the horizontal sets. The ground supports for the Tptpmn unit should represent the worst case scenario and be applicable to all other units in evaluating the suitability of a single system. Therefore, the modeling efforts for this analysis are focused on the middle non-lithophysal unit, with additional efforts on the lower lithophysal unit for the purpose of sensitivity study and completeness only.

To accommodate the flexible repository design, two thermal conditions corresponding to the high and low temperature modes discussed in Section 6.3.3 are considered in the evaluating the performance of ground support in emplacement drifts. Since the temperature loads and the lengths of preclosure period associated with these thermal modes are different, discussion will be provided separately in the subsections 6.5.1 and 6.5.2 for the high and low temperature modes, respectively.

6.5.1 Ground Control under High Temperature Condition

Temperature loads associated with the high temperature mode are provided in Table 4-12a. The model configurations and boundary conditions used to perform the analyses using ANSYS, FLAC, and UDEC are shown in Figures 6-4 and 6-5 for continuum and discontinuum models, respectively.

6.5.1.1 Results for Unsupported Emplacement Drifts

Two-dimensional models with the FLAC and UDEC codes are used to perform the analyses for the unsupported emplacement drifts. Thermally-induced displacements and stresses in the rock mass are calculated for up to 200 years after waste emplacement. Seismically-induced response of the rock mass is evaluated using the dynamic approach. Details on the numerical approaches are discussed in Section 6.4.2.

6.5.1.1.1 In Situ Stress Loading Condition

6.5.1.1.1.1 Non-lithophysal (Tptpmn) Unit

Continuum modeling using FLAC was performed for the unsupported emplacement drifts in the Category-1 and Category-5 rock masses of the Tptpmn unit subjected to in-situ stress load. The

results are summarized in Table 6-2 for drift closures and rock stresses. As expected, rock deformation and stress are shown to be sensitive to the mechanical properties and the initial horizontal-to-vertical stress state (K_o value). It can been seen that the worst case in terms of vertical closure (10.1 mm), is associated with rock mass Category 1 and K_o=0.3. An opening of rock mass Category 1 and K_o=1.0 shows the largest horizontal closure of 7.1 mm. The negative horizontal drift closure indicates an increase in the distance between two opposite points at the springline and the drift shows a horizontal ovaling.

Contour plots of Mohr–Coulomb strength-to-stress ratios indicating potential yield zones around the unsupported drift opening are presented in Figures 6-11a through 6-11d. For the Category 1 rock mass and K_o=0.3, the potential yield zone is approximated about 1.0 m into the rock, and a potential tensile yield may occur at the crown. For all other cases, the analyzed potential yield zone around the opening is less than 1.0 m. The results indicate that the emplacement drifts are expected to be relatively stable after excavation. Any potential instability near the skin of the opening can be controlled by minimal support, such as timely installation of rock bolts advanced through the finger shield of the TBM, or installed with welded-wire fabric immediately after advance of the TBM.

The results of modeling the rock mass as a discontinuum using UDEC are illustrated in Figures 6-12a and 6-12b in terms of the rock block displacement, joint shear movement, and yield zone development surrounding an unsupported emplacement opening. Individual rock block displacements are plotted as vectors. The magnitude of the displacement is proportional to the vector length. The arrow points in the direction of rock movement. As shown in Figure 6-12a, for a K_o of 0.3 the maximum rock block displacement (downward) near the crown is about 33 mm. The maximum joint shear displacement detected is about 27 mm. For a K_o of 1.0 (Figure 6-12b), the maximum rock block displacement near the crown is about 24 mm, while the maximum joint shear displacement is about 20 mm. Joints within the width of the emplacement drift displace the most. It is indicated that more rock block displacements are induced when a relatively low horizontal stress field exists (Figures 6-12a and 6-12b).

In addition, Figures 6-12a and 6-12b show some tensile failure zones developed around the emplacement drift following excavation. These tensile failure zones are caused by the potential falling key blocks above the springline. The results suggest that the use of ground supports to maintain the stability of the emplacement drifts in the heavily jointed rock mass like the non-lithophysal unit is necessary.

Table 6-2. Unsupported Emplacement Drift – Results from FLAC for In Situ Stress Loading Condition

Items	RMQ=1		RMQ=5	
	K_o=0.3	K_o=1.0	K_o=0.3	K_o=1.0
	Non-Lithophysal Unit (Tptpmn)			
Horizontal Closure (mm)	-0.5	7.1	-0.2	2.5
Vertical Closure (mm)	10.1	7.4	3.6	2.6
Major Principal (Tangential) Stress near Crown (MPa)	-0.9	-17.9	-1.1	-18.4
Minor Principal (Radial) Stress near Crown (MPa)	-0.1	-1.6	-0.2	-1.6
Major Principal (Tangential) Stress near Springline (MPa)	-22.0	-18.0	-22.6	-18.3
Minor Principal (Radial) Stress at Springline (MPa)	-2.0	-1.6	-1.9	-1.9
	Lithophysal Unit (Tptpll)			
Horizontal Closure (mm)	-0.5	6.9	-0.2	1.9
Vertical Closure (mm)	10.0	7.0	2.7	2.0
Major Principal (Tangential) Stress near Crown (MPa)	-1.0	-18.0	-10.9	-18.4
Minor Principal (Radial) Stress near Crown (MPa)	-0.3	-1.6	-0.2	-1.6
Major Principal (Tangential) Stress near Springline (MPa)	-21.9	-17.9	-22.6	-18.4
Minor Principal (Radial) Stress at Springline (MPa)	-2.0	-1.8	-1.9	-1.9

6.5.1.1.1.2 Lithophysal (Tptpll) Unit

As indicated in Tables 4-5a and 4-5b, the values of the mechanical properties such as the modulus of deformation, cohesion and friction angle, for the lithophysal (Tptpll) unit are close to or slightly higher than those for the non-lithophysal (Tptpmn) unit. Therefore, it is predicable that the behavior of an emplacement drift in the Tptpll unit should generally be similar to that in the Tptpmn unit. As part of a sensitivity study, numerical modeling using FLAC for the unsupported emplacement drifts in the Tptpll unit was also performed. The results including the drift closures and stresses from these models are summarized in Table 6-2. These results suggest that numerical modeling using FLAC or ANSYS to model the Tptpll unit as a continuum medium is not necessary, and that use of the mechanical properties for the Tptpmn unit is considered conservative and bounding.

The lithophysal rock unit is also modeled as a discontinuum using UDEC for the sensitivity study. The results shown in Figures 6-13a and 6-13b indicate that the maximum rock block displacements are about 7 mm and 6 mm for the horizontal-to-vertical stress ratios K_o of 0.3 and 1.0, respectively. The maximum joint shear displacements are about 4 mm and 2 mm, respectively for these two stress ratios. These shear displacements are small, with insignificant joint slippage. It is indicated that some potential yield zones are predicted around the drift opening, but unlikely cause substantial instability. These results are comparable to those from the FLAC continuum models for the rock mass Category 1 (see Table 6-2).

6.5.1.1.2 Thermal Loading Condition

Time-dependent rock temperatures at the model boundaries are shown in Figure 6-14. These temperatures, for a period of 200 years, were obtained from DTN: MO9911SPAWAQ01.000 (Section 4.1.12), based on an initial linear heat load of 2.0 kW/m and a preclosure ventilation rate of 10 m^3/s. The maximum temperature at the drift wall is about 125°C, occurring at about 10 years after waste emplacement.

6.5.1.1.2.1 Rock Mass Deformation

Based on the boundary temperatures shown in Figure 6-14, thermally-induced rock mass displacements and stresses were evaluated using FLAC. The results for the opening closures are presented in Figures 6-15a and 6-15b for the non-lithophysal unit. It is indicated that as the rock temperature increases, the vertical closure (the relative displacement between the invert and crown) decreases, while the horizontal closure (the relative displacement between two opposite drift walls at the springline) increases. This suggests that thermally-induced rock deformation will offset a certain amount of the deformation induced by excavation. The maximum vertical and horizontal closures offset by temperature are estimated to be about 2.7 mm and 3.4 mm, respectively, for all cases considered. These thermally-induced deformations are considered small and insignificant in causing any potential instability of the drift opening.

The results of the analyses indicate that the horizontal displacements induced by elevated temperatures are higher than the vertical ones, suggesting that thermally-induced loads are predominantly in the horizontal direction.

6.5.1.1.2.2 Rock Mass Stresses

Time histories of major (tangential) and minor (radial) principal stresses near the drift crown and springline are shown in Figures 6-16a through 6-17b for the non-lithophysal rock unit. Both tangential and radial compressive stresses increase with temperature, and reach their maximum values at about 10 years following waste emplacement. Once temperature starts to decrease, these stresses drop as well.

It is noted that the significant decrease in the tangential stress near the springline during heating is also due to the horizontal inward displacement of the rock because of thermal expansion. The magnitude of the stresses may eventually drop below the level the rock has experienced under the in-situ loading condition.

The results indicate that the maximum stresses induced by elevated temperatures are higher either near the crown or near the springline, depending on the in situ horizontal-to-vertical ratios. The maximum major (tangential) compressive stress near the crown is predicted to be about -44 MPa for RMQ=5 and K_o=1.0 under combined in-situ and thermal loads (see Figure 6-17b). This value is about 2.4 times the in situ stress value. The maximum minor (radial) compressive stress near the crown, on the other hand, is calculated to be about -4.3 MPa.

Distributions of major and minor principal stresses within the rock mass near the crown and springline are plotted in Figures 6-18a through 6-21b for 0, 10, and 150 years after waste emplacement. These plots predict the depth of the rock mass zone that is affected by the

elevated temperatures. One interesting observation is that once the temperature starts to decrease, the maximum major (tangential) principal stress close to the drift skin drops much faster than at about 1 m into the rock. This suggests that cooling of the emplacement drifts may result in a reduction in confinement stress near the periphery of the drift opening. This confirms the need for ground support, such as steel sets and/or rock bolts.

6.5.1.1.2.3 Rock Mass Potential Yield Zones

Rock mass yield is indicated in Figures 6-22a through 6-23d, which give strength-to-stress-ratio contour plots and failure surface envelopes at 10 and 100 years after emplacement for rock mass Categories of 1 and 5. These plots indicate that a potential rock yield occurs to a depth of about 1 m into the rock for all cases considered, irrespective of the initial horizontal-to-vertical stress ratio (K_o) and the rock mass properties. These plots also confirm the observation discussed in Section 6.5.1.2.2 that a drop in temperature with time may cause some reduction in the confinement stress around the opening. (See Figures 6-22c and 6-22d, for example.)

It is noted that the strength-to-stress ratio in more than 50 percent of the rock pillar cross-section is at or above a value of 2 for all cases. This suggests that the rock mass is, in general, in an elastic state and that modest ground support should ensure drift stability under combined in-situ and thermal loading conditions.

6.5.1.1.2.4 Rock Joint Behavior

The thermal loading condition was also used in the previously-mentioned discontinuum model for the unsupported emplacement drifts in the non-lithophysal (Tptpmn) unit using UDEC. Figures 6-24a through 6-25b illustrate the rock block displacement vectors, joint shear displacements, and failure zone development near the opening after 10 and 100 years of thermal loading for K_o=0.3 and K_o=1.0, respectively.

For K_o=0.3, the maximum rock block displacement due to waste emplacement is about 66 mm at 10 years and about 124 mm at 100 years (Figures 6-24a and 6-24b), compared to about 33 mm near the crown due to excavation (Figure 6-12a). For K_o=1.0, the corresponding maximum block displacements are about 59 mm at 10 years and about 139 mm at 100 years (Figures 6-25a and 6-25b), compared to about 24 mm near the crown due to excavation (Figure 6-12b). It appears that the thermally-induced rock displacement increases with time and is over an order of magnitude greater than that induced by excavation. Similar phenomena may also be observed for shear displacement on joints (Figures 6-24a and 6-24b).

As shown in Figures 6-24a and 6-24b, a potential yield zone extending about 2.0 m into the rock surrounding the emplacement drift is predicted. This potential yield zone was indicated less than 1.0 m under the in situ stress loading condition (Figure 6-12a). Comparing Figures 6-24a and 6-24b for K_o=0.3 to Figures 6-25a and 6-25b for K_o=1.0 indicates that the depth of potential yield zone is also sensitive to the initial horizontal-to-vertical stress ratio.

A number of blocks near the springline and the crown are subject to tensile failure as indicated in Figures 6-24a through 6-25b by an "o" symbol. This limited tension is due to the joint separation occurring in these regions. Also, noticeable shear displacements on joints are predicted where rock blocks yield according to the Mohr–Coulomb yield criterion.

6.5.1.1.3 Seismic Loading Condition

Seismic loading condition is analyzed for the unsupported emplacement drifts using both the FLAC and UDEC codes for continuum and discontinuum rock masses, respectively. Both the Frequency Category 1 and 2 seismic events are considered in the models. The corresponding peak ground velocities for these frequency categories are provided in Table 4-13. As indicated, a 3-second duration is used in the seismic analyses. For a strong earthquake motion, this duration is too brief, as can be seen from the ground motion time histories available. However, as mentioned in Assumption 5.3.3, a 3-second duration for the peak velocity is considered adequate for examining dynamic response of the drift to the seismic load.

6.5.1.1.3.1 Continuum Modeling

Under the Frequency Category 2 seismic event with a PGV value equal to 46.9 and 28.0 cm/sec in the horizontal and vertical direction respectively (Section 4.1.13), Figure 6-26a shows the drift closures under the 3-second seismic load. The vertical closure is measured between the crown and invert while the horizontal closure is measured across the springline. The maximum variation of the dynamic drift closures during seismic loading is about 3.3 mm for the vertical closure and about 1.0 mm for the horizontal closure. The dynamic closures vanish rapidly beyond the duration of seismic loads, indicating that the drift vicinity remains largely in the elastic domain of deformation. Figure 6-26b monitors the stress fluctuation at the crown and the springline under the seismic load. This stress component is the tangential stress, and it is shown to oscillate between -9.2 MPa and -11.7 MPa (compression) while the static stress is about -10.3 MPa at the crown. The tangential stress at the springline oscillates from -11.0 MPa to -20.0 MPa, compared to the static stress of about -16.0 MPa. The seismic load induces a momentary fluctuation in stress of about +5.0 MPa at the springline where the positive sign means the tensile stress. Such a stress fluctuation is about 31 percent of the static stress which exists prior to the application of the seismic load. The drift stability is not compromised by the introduction of seismic loads, as shown in Figure 6-27.

6.5.1.1.3.2 Discontinuum Modeling

Two episodes of seismic events are imposed on the UDEC model after a 20-year thermal loading period has been simulated. The first episode in forms of sinusoidal velocity waves lasts for 3 seconds while the second episode is applied at 2 seconds after the first one, leading to an evaluation of repetitive seismic loading effects in a simple manner. It should be pointed out that the likelihood for the jointed rock mass within the repository block to experience damaging seismic loads more than once or twice during the preclosure period is negligible.

Figure 6-28a shows the dynamic response of tangential stress near the drift wall to seismic loads. Stress time histories are taken at two points: one is at the crown and the other is at the springline. Similar to the results (Figure 6-26b) obtained using the continuum model approach, during the seismic loading, the stress at the two monitored points fluctuates about the static stress existing prior to the seismic loading. The stress rebounds to the static value shortly after seismic waves are turned off, indicating an insignificant impact to the drift stability. The second episode of seismic load results in a similar stress response as the first one.

Figures 6-28b through 6-28d illustrate the movement of jointed rock blocks surrounding the drift. Figure 6-28b corresponds to the one prior to the application seismic load, Figure 6-28c is taken after the first episode of seismic loading, and Figure 6-28d is taken after the second episode of seismic load. A visual comparison among these figures indicates that the seismic load facilitates the fall of rock blocks that have been loosened prior to the seismic loading. Seismically-induced stresses are not shown to be significant enough to cause additional rock fall, as shown by no change in the potential yield zone development even under the seismic loading condition. The potential yield zone remains within 2 m into rock.

6.5.1.2 Results for Supported Emplacement Drifts

Supported emplacement drifts are modeled with ANSYS for steel sets (W6×20) and FLAC for fully-grouted rock bolts (3-m long) under combined in situ and thermal loading conditions. The impact of seismic load on the steel sets and rock bolts is evaluated with FLAC. Details of the approaches for modeling the ground supports are discussed in Section 6.4.2. It is noted that no credit or account is given for rock bolts in modeling the steel sets using ANSYS or for steel sets in modeling the rock bolts with FLAC, which is conservative.

6.5.1.2.1 Performance of Steel Sets

According to the *EFS Design Confirmation Steel Set Loads Analysis* (CRWMS M&O 1998a, p. 73) and the *Constructibility Considerations for Repository Drifts for Viability Assessment* (CRWMS M&O 1997c, Section 4.3.7.5), the design for the steel sets included a tolerance of the steel set diameter of about 50 mm to account for the need to accommodate the steel lagging and to provide clearance for maneuvering the steel sets into place. Even after the expansion of the steel sets by jacking, areas with gaps between the steel sets and the rock remained.

In order to account for the initial gap or mismatch between the steel sets and the rock surface, steel sets are modeled with circumferential gap elements of various thickness. The magnitude of the initial gap is varied along the steel set ring, and the maximum gap dimensions used in the models are 13 mm and 15 mm in order to evaluate the effect of gap size on the stress predicted in the steel sets.

It is noted that the gap dimensions used in this analysis are the design values. These values are selected based on the anticipated design tolerance of the steel set diameter discussed above and the computer trial-and-error runs. The results based on an initial gap less than 13 mm do not meet the allowable stress for steel, and, thus, are excluded in this analysis.

To judge whether the stresses in the steel sets remain below the allowable stress specified in Table 4-8, the maximum combined stresses at a given cross-section are considered. The following equation is used to calculate the combined stresses in the steel sets (MacGregor 1997, Eq. 11-2, p. 425):

$$\sigma_{combined} = \frac{F}{A} \pm \frac{M}{I} y \qquad \text{(Eq. 6-6)}$$

where $\sigma_{combined}$ = combined stress, N/m^2

F = axial force in steel sets, N
A = area of the cross-section, m^2
M = bending moment in steel sets, N-m
I = moment of inertia of the cross-section, m^4
y = distance from the centroidal axis to the most outer surface, m

6.5.1.2.1.1 In Situ Stress Loading Condition

Results of the stresses induced in the steel sets by residual loading following excavation are presented in Figures 6-29a and 6-29b for an initial gap of 13 mm. It is indicated that stresses for W6×20 steel sets with a spacing of 1.5 m are estimated to be dependent on the variation of rock mass properties under in situ loads. The distribution of the stresses along the ring is non-uniform. The maximum stresses, in general, occur at the springline, and are compressive stresses for both rock mass Categories 1 and 5. The stresses at the crown of the steel sets are tensile stresses under the in situ loading condition. These stresses are low and well below an allowable stress of 164 MPa (see Section 4.1.8). The results also suggest that the initial gap is closed at the crown under the in situ load.

When the initial gap increases to 15 mm, the stresses at the crown and springline of the steel sets, as shown in Figures 6-30a and 6-30b, remain nearly unchanged compared to those for the initial gap of 13 mm. This may indicate that the sizes of gap (13 mm and 15 mm) are comparable to the amount of rock deformation induced by excavation.

6.5.1.2.1.2 Thermal Loading Condition

Time histories of the stresses and the safety factor for steel sets subjected to combined in situ and thermal loads are shown in Figures 6-29a and 6-29b for an initial gap of 13 mm. The results indicate that stresses induced by elevated temperatures are sensitive to the surrounding rock mass categories (e.g. 1 versus 5); i.e., to the modulus of elasticity. The stress values are calculated to be greater for the weaker rock (RMQ=1) than for the stronger rock (RMQ=5). This is because the magnitude of stresses induced in the steel sets is dependent on the amount of rock deformation, and the weaker rock experiences the greater deformation. The maximum stresses in the steel sets installed in an emplacement drift located in Category 1 rock are about 109 and 65 MPa at the crown and springline, respectively. These calculated stress values remain below the allowable stress of 164 MPa, with a minimum safety factor of 1.5. It is noted that the safety factor plotted in Figures 6-29a and 6-29b is defined as the ratio of the allowable stress to the calculated stress in the steel sets. Generally, the safety factor is defined as the ratio of the yield limit to the calculated stress. Therefore, actual safety factor in the steel sets with respect to the yield stress can be obtained by dividing those provided in Figures 6-29a and 6-29b by a strength reduction factor of 0.66 for steel indicated in Table 4-8.

Figures 6-30a and 6-30b show the time histories of stresses and safety factor in steel sets for an initial gap of 15 mm. It is indicated that the stresses are very sensitive to the size of initial gap when the modulus of rock is low (RMQ=1), but are not sensitive when the modulus is high (RMQ=5).

An interaction (thrust-moment) diagram for the steel sets is plotted in Figure 6-31 for RMQ=1 and an initial gap of 13 mm. This diagram illustrates the interaction between moments and axial forces in the steel sets, and may provide additional information on the loading path during heating. Points on the lines plotted in this diagram represent combinations of axial force and moment, corresponding to the resistance of the steel sets. An envelope is also plotted in the diagram, and represents the combinations of allowable axial force and moment. The relationship of the axial force and moment for the envelope is defined by the interaction equation as (MacGregor 1997, Eq. 11-3, p. 426)

$$\frac{F}{F_{allowable}} + \frac{M}{M_{allowable}} = 1 \qquad \text{(Eq. 6-7)}$$

where F = axial force in steel sets, N
$F_{allowable}$ = allowable axial force for steel sets, N
M = bending moment in steel sets, N-m
$M_{allowable}$ = allowable bending moment for steel sets, N-m

Since the steel has the same compressive and tensile strength, the envelope contains two parts, one line lying above the moment-axis for compression and the other below the moment-axis for tension. A point inside the envelope represents a combination of axial force and moment that will not exceed the allowable resistance of the steel sets. Since the steel has the same compressive and tensile strength, as shown, all loading curves calculated fall inside the allowable envelope, indicating that the combinations of axial force and moment in the steel sets are satisfactory. The same conclusion can be drawn for RMQ=5 with an initial gap of 13 mm and for RMQ=1 and RMQ=5 with an initial gap of 15 mm, when examining Figures 6-29b through 6-30b.

6.5.1.2.1.3 Seismic Loading Condition

The seismic loading condition is modeled for steel sets using FLAC. Different from the approach used for the in situ and thermal loading conditions, the steel sets are modeled as perfectly bonded to the underlying rock during seismic motions. As part of the sensitivity study, the seismic velocities for both the Frequency Category-1 and Category-2 (see Table 4-13) are considered. These seismic velocities are applied to the bottom of the model boundary at 10 years after heating.

The results shown in Table 6-3 indicate that the stresses induced in the steel sets by seismic ground velocities are dependent on the category, i.e., the magnitude of PGV, and the location. The values given in Table 6-3 are the maximum fluctuations (plus and minus) of the stresses at the crown and the springline due to the sinusoidal waves applied. The positive sign indicates a change in compression, while the negative sign indicates a change in tension. The maximum variations of the combined stresses at the springline are greater than that at the crown. For the Frequency Category-2 seismic event, the induced stresses are predicted to be about 38 MPa and 116 MPa at the crown and the springline, respectively.

By superimposing the stresses induced by seismic velocities over those induced by combined in situ and thermal loads, the stresses in the steel sets are about 147 MPa and 181 MPa at the crown

and the springline, respectively. According to AISC (1997, Section A5.2, p. 5-30), the allowable stresses may be increased 1/3 above the values otherwise provided (164 MPa). Therefore, an allowable stress of 219 MPa (164×1/3+164=219) can be used for the combined in situ, thermal, and seismic loading conditions. With this increased allowable stress, the minimum factor of safety for the steel sets is calculated to be 1.2.

Table 6-3. Maximum Variations of Combined Stress in Steel Sets Due to Seismic Load

Frequency Category	Item	Location			
		Crown		Springline	
1	Combined Stress (MPa)	11.1	-13.1	38.4	-42.1
2		38.0	-36.1	116.1	-124.7

In summary, the steel sets with welded-wire fabric can be designed for use in emplacement drifts, subjected to combined in situ, thermal (high temperature condition), and seismic loads, to provide desired functionality of preventing any potential rock falls during the preclosure period as long as the longevity of steel sets materials is guaranteed.

6.5.1.2.2 Performance of Fully-Grouted Rock Bolts

Fully-grouted rock bolts are modeled with FLAC. The rock bolts used are 3 m long, spaced at 1.5 m in the tunnel longitudinal direction, with typical bolt pattern illustrated in Figure 6-2. Both bond strength and frictional resistance for the bolt/grout interface are included in the models. The grout annulus is not modeled explicitly in FLAC, and its presence is represented by its bond stiffness and strength.

6.5.1.2.2.1 In Situ Stress Loading Condition

Figures 6-32a through 6-32d illustrate the distributions of axial forces in rock bolts subjected to the in situ load for the non-lithophysal rock with the rock mass Categories of 1 and 5, and the initial horizontal-to-vertical stress ratios of 0.3 and 1.0. It is seen that axial forces in the bolts are sensitive to the rock mass modulus (e.g. 1 versus 5). The axial forces in the bolts installed near the springline are usually greater than in those near the crown. The maximum force is about -12.2 kN (-8.153×1.5=-12.2, where 1.5 is the bolt spacing) in tension, occurring in a bolt installed near the springline (labeled No. 2 bolt in Figure 6-32b). This force is well below the allowable force of 160.2 kN given in Table 4-10. The rock bolts are generally in tension under the in situ load because the rock moves inward after excavation and pulls the bolts bonded perfected to the rock. As a result, the tensile force is induced in the rock bolts.

Bonding condition at the bolt/grout interface is also shown in Figures 6-32a through 6-32d. The interface where the shear force exceeds the allowable bond shear strength is marked with a symbol "x". It is indicated that the shear force at the interface is within the allowable bond shear strength specified in Section 4.1.10 for the cases considered.

In case of a potential rock fall, the allowable weight of a rock block that a single rock bolt can support is about 160.2 kN or 16.3 metric tons, which is the yield strength of a rock bolt (see Section 4.1.10). This weight is much greater than that of a six metric ton rock, as specified in Section 4.2.3.1, giving a factor of safety of about 2.7, calculated based on a very conservative estimation by ignoring all other contributing elements for ground control, such as the strength of grout.

6.5.1.2.2.2 Thermal Loading Condition

Time histories of the axial forces induced by elevated temperatures in the rock bolts are plotted in Figures 6-33a through 6-34b for the non-lithophysal rock unit. Results indicate that the thermally-induced axial forces are not very sensitive to the rock mass modulus, which is different from what is observed for the in situ loading condition. These forces are generally compression when the rock is heated up, but become tension in the bolts placed near the crown when the rock cools down (see Figure 6-14 for the temperature histories). The axial force in the rock bolts changes from tension under the in situ load to compression under the thermal load due mainly to the higher coefficient of thermal expansion of the bolts than the rock.

The maximum axial force during heating is about 38.7 kN, experienced in the bolt installed near the crown. This force is also low compared to the allowable force of 160.2 kN, with a safety factor of 4.1.

Figures 6-35a through 6-35d illustrate the distributions of axial forces in rock bolts placed at different locations around the opening at 10 years after waste emplacement. Results indicate that the magnitude of the axial force experienced during heating is not very sensitive to the location where the bolt is installed, meaning that the elevated temperatures create a nearly hydrostatic stress state in the upper periphery of the opening.

Bonding condition at the bolt/grout interface is also shown in Figures 6-35a through 6-35d. It is indicated that the shear force at the interface is within the allowable bond shear strength specified in Section 4.1.10 for the cases considered.

6.5.1.2.2.3 Seismic Loading Condition

A row of six fully-grouted rock bolts is inserted into the seismic FLAC model after the 60 percent of drift closure due to excavation has been completed (Section 5.1.1). Upon the completion of drift closure, installed bolts will sustain the reinforcing loads which are in tension. Similar to the seismic analyses for the steel sets, the seismic velocities for both the Frequency Category-1 and Category -2 seismic events are considered. These seismic velocities are applied to the model after a 10-year thermal loading. Table 6-4 summarizes the axial load fluctuations due to the imposition of seismic loads. Similar to the steel sets mentioned in Section 6.5.2.1.3, the values given in Table 6-4 are the maximum fluctuations (plus and minus) of the axial forces near the crown and the springline. The positive sign indicates a change in compression, while the negative sign indicates a change in tension.

Table 6-4. Maximum Variations of Axial Force in Rock Bolts Due to Seismic Load

Frequency Category	Item	Location			
		Crown		Springline	
1	Axial Force (kN)	2.9	-2.9	2.8	-1.8
2		8.6	-8.5	8.1	-5.0

Sinusoidal velocity waves are generated at a 10-Hz frequency. It takes one tenth of a second to complete one oscillating cycle. The load fluctuation in rock bolts follows closely the wave cycle. The maximum increase in bolt load is approximately ±8.6 kN near the crown. The application of seismic loads has a greater impact on bolts installed near the crown than those near the springline. By superimposing the loads induced by seismic velocities over those induced by combined in situ and thermal loads, the maximum axial forces in the rock bolts are about 47.3 kN, well below the allowable force of 160.2 kN.

In summary, the load increase caused by the Frequency Category 2 seismic events is not considered significant from the viewpoint of ground control. Therefore, fully-grouted rock bolts can be designed for use in emplacement drifts, subjected to combined in situ, thermal, and seismic loads, to provide desired functionality of preventing potential rock block loosening and falling during the preclosure period as long as their material longevity is guaranteed.

6.5.2 Ground Control under Low Temperature Condition

The low temperature repository design requires an extended period of preclosure ventilation, including both forced and natural ventilation, in order to keep the maximum waste package surface below 85°C (BSC 2001, Section 5.1.1.3). Though this low temperature condition will be more favorable to the performance of ground support, compared to the high temperature condition, the extended period of ventilation will require a longer service life of ground support. Additional analyses are needed to ensure that the ground support will provide the necessary control of emplacement drift openings over the extended ventilation period. The duration of the extended preclosure ventilation considered in this analysis is 300 years following the completion of waste emplacement.

Temperature loads associated with the low temperature mode are provided in Table 4-12b. The drift wall temperature is compared with that for the high temperature condition in Figure 6-36. The peak wall temperature is about 67°C, occurring during the natural ventilation period at about 150 years after waste emplacement, compared to the peak wall temperature of about 125°C occurring at about 10 years for the high temperature condition (see Table 4-12a). Due to the use of forced ventilation throughout the preclosure period under the high temperature condition, the drift wall temperature beyond 100 years is observed to be lower than that under the low temperature condition. Therefore, analyzing and understanding the ground support performance and drift behavior under the low temperature condition may also be important if they are controlled by the extended period of heating instead of the peak rock temperature. The model

configurations and boundary conditions used to perform these analyses are shown in Figures 6-4 and 6-5.

6.5.2.1 Results for Unsupported Emplacement Drifts

6.5.2.1.1 Rock Mass Deformation

Rock mass deformations in the form of the drift vertical and horizontal closures are presented in Figures 6-37a and 6-37b, respectively. Similar to those under the high temperature condition (see Figures 6-15a and 6-15b), the vertical closures decrease while the horizontal closures increase as the rock temperature increases. Though the drift wall temperature is expected to drop after 150 years (see Figure 6-36), the rock does not stop deforming until about 200 years, owing to continuously rising temperatures at the upper and lower boundaries over the entire preclosure period. The thermally-induced closure for all cases analyzed is about 2.4 mm in both the vertical and horizontal directions, which is judged insignificant from the drift stability point of view.

In general, the drift closures are smaller under the low temperature condition than those under the high temperature condition (see Figures 6-15a and 6-15b), indicating that the rock deformation is expected to be determined by the magnitude of increasing temperature.

6.5.2.1.2 Rock Mass Stresses

Time histories of major (tangential) and minor (radial) principal stresses near the drift crown and springline are presented in Figures 6-38a through 6-39b. The maximum stresses induced by elevated temperatures are higher either near the crown or near the springline, depending on the in situ horizontal-to-vertical stress ratios (K_o). The higher the stress ratio (K_o), the higher the stresses near the crown than those near the springline. The major (tangential) principal stresses are shown to reach their peaks before or about 200 years, suggesting that extended duration of preclosure is not expected to cause any potential instability of the drift openings.

A comparison of the rock stresses illustrated in Figures 6-38a through 6-39b for the low temperature condition with those shown in Figures 6-16a through 6-17b for the high temperature condition indicates that the magnitude of thermally-induced rock stresses are also dependent on the magnitude of temperature increase. The rock stresses under the low temperature condition are generally lower.

6.5.2.1.3 Rock Joint Behavior

Unsupported emplacement drifts in jointed rock masses are modeled using UDEC. The rock block displacement vectors, joint shear displacements, and failure zone development near the drift opening at 10, 100, 150, and 300 years after waste emplacement are shown in Figures 6-40a through 6-41d for K_o=0.3 and K_o=1.0, respectively.

Modeling indicates that throughout heating, rock block displacements increase with time, even after the drift wall temperature starts to level off or drop. This observation is different from what is predicted from the continuum models using FLAC. As shown in Figures 6-40a through 6-41d, a few key blocks near the left shoulder of the opening have a potential to fall under the increased thermal load. The large displacements of about ten centimeters indicated in these

figures are primarily caused by these key blocks. By ignoring the displacements of these falling key blocks, the maximum rock displacement induced by elevated temperatures is estimated to be only a few centimeters. Similar observations apply to the shear displacements on joints (see Figures 6-40a through 6-41d).

Rock potential yield zones around the emplacement drift under the low temperature condition are also shown in Figures 6-40a through 6-41d. Compared to those under the high temperature condition (see Figure 6-24a through 6-25b), these potential yield zones are shallower, due to a lower rock temperature.

In short, more stable and favorable conditions are expected for the emplacement drifts if the rock temperatures are lower. The extended duration of preclosure period or ventilation to maintain the low temperature may require additional monitoring of the behavior of emplacement drifts as well as maintenance if necessary.

6.5.2.2 Results for Supported Emplacement Drifts

Similar to the analyses for the high temperature condition, supported emplacement drifts are modeled with ANSYS for steel sets (W6×20) and FLAC for fully-grouted rock bolts (3-m long) under the low temperature condition. Both the steel sets and rock bolts have a spacing of 1.5 m in the tunnel axial direction.

6.5.2.2.1 Performance of Steel Sets

As mentioned in Section 6.5.1.2.1, an initial gap of 13 mm between the steel sets and the rock surface is used in analyzing the steel set performance under the high temperature condition. Since lower rock temperatures are anticipated under the low temperature condition (see Figure 6-36), less thermal expansion in both steel sets and rock mass is expected and the initial gap can be reduced. In this analysis, the minimum gap dimensions used for the low temperature condition are 8 mm and 4 mm for the rock mass categories of 1 and 5, respectively, to keep the maximum stress below the allowable stress of 164 MPa for steel (see Section 4.1.8).

Figures 6-42a and 6-42b show the time histories of stresses in steel sets subjected to combined in situ stress and low temperature thermal loads. The results indicate that the stresses in steel sets reach their peaks at about 150 years. In terms of the stresses, the extended duration of ventilation or preclosure is not expected to have any negative impact on the steel set performance. For the Category 1 rock, the predicted maximum stresses in the steel sets with a gap of 8 mm are about 117 and 63 MPa at the crown and springline, respectively. For the Category 5 rock, the gap is reduced to 4 mm, and the maximum stresses with this gap size are expected to be about 102 and 37 MPa at the crown and springline, respectively. These stresses are low compared to the allowable stress of 164 MPa, indicating that the steel sets are expected to perform satisfactorily under the low temperature condition, even with a smaller gap.

In general, the lower the rock temperatures or the stronger the rock mass, the smaller the required dimensions of the gap. If a single steel set design is intended for all rock conditions, the minimum gap dimension should be determined by the highest temperature and the weakest rock

conditions anticipated, meaning that the high temperature condition controls the design (see Section 6.5.1.2.1).

6.5.2.2.2 Performance of Fully-Grouted Rock Bolts

Time histories of the axial forces in the rock bolts installed near the crown and the springline under the in situ stress and low temperature conditions are shown in Figures 6-43a and 6-43b for the rock mass categories of 1 and 5, respectively. The axial forces increase with temperature. The predicted maximum axial force during heating is about 22 kN, well below the allowable axial force of 160.2 kN (Section 4.1.10).

Similar to the stresses in steel sets, the weaker the rock mass, the greater the thermally-induced forces in rock bolts. Again, from the axial force point of view, the extended period of ventilation is not expected to have any unfavorable effect on the rock bolt performance. Therefore, the high temperature condition controls the design (see Section 6.5.1.2.2).

6.5.3 Effects of Variations in Modeling Parameters

As part of sensitivity studies, the effects of variations in modeling parameters, such as rock mass mechanical properties, model dimensions, and joint patterns, on the thermal/mechanical response of emplacement drifts are analyzed. The results are summarized in the following subsections 6.5.3.1 through 6.5.3.3. Details are presented in Attachments II through IV.

6.5.3.1 Variation of Rock Mass Mechanical Properties

Variation in rock mass mechanical properties includes changes in the modulus of deformation, cohesion, friction angle, and tensile strength. Two scales of changes are used. One represents a limited degree of change to address some variation in the strength parameter values due to the sensitivity of these values to assumptions and approaches employed to determine them. For clarity, this kind of change is called the normal variation in rock mass properties. The other represents a great degree of change to account for some possible effects of the heat on the long-term values of some mechanical properties. This kind of change is called the heat-induced variation in rock mass properties.

6.5.3.1.1 Normal Variation of Rock Mass Strength Properties

The general variation in rock mass properties is accounted by the use of rock mass categories 1 through 5. However, as indicated in Tables 4-5a and 4-5b, the strength parameter values for a given rock mass category are also sensitive to the range of confining stress developed. For example, the rock mass cohesion for the Category 1 non-lithophysal rock varies from 2.0 MPa at a confining stress of 0 to 3 MPa to 8.1 MPa at a confining stress of 0 to 42 MPa, while the friction angle changes from 56 degrees to 37 degrees, respectively. To evaluate the effects of variation of these strength properties on the rock mass thermomechanical response, eight different cases were analyzed. Details are presented in Attachment II.

Results indicate that rock mass deformations and stresses are very sensitive to the variation of strength properties, either cohesion or friction angle, especially under the thermal loading condition. Larger deformations combined with lower stresses are expected when the strength

values are reduced. As a result, an increase in the potential yield zone around an opening may occur.

However, the combination of a low friction angle with a high cohesion appears to have an equivalent effect on the rock mass thermomechanical response as that of a high friction angle combined with a low cohesion. Therefore, use of either set of strength properties provided in Tables 4-5a and 4-5b is expected to give equivalent results.

6.5.3.1.2 Heat-Induced Variation of Rock Mass Properties

The effect of elevated temperatures on the mechanical properties of intact welded tuff has been evaluated (CRWMS M&O 1997a, Section 5.3.2.4 and Table 5-34). Seventeen confined compression tests were performed at a temperature of 150°C and nine at room temperature, both series at effective confining pressures of 1, 5, and 10 MPa. The test results indicated that the effect of temperature on the strength of welded tuff from the thermomechanical unit TSw2 is small. It is also indicated that Young's modulus and Poisson's ratio measured at elevated temperatures are not significantly different from those measured at room temperature. The results of field-scale tests to evaluate the effects of elevated temperatures (up to 143°C) on in situ tuff are also available (CRWMS M&O 1999e, Table 9-6, p. 9-18). These results again indicate no general trend of reduction in stiffness due to temperature increases and, in some cases, show an apparent increase in modulus. The tests were not run to failure, but constant or increasing values of stiffness are generally associated with similar behaviors for strength. Some of the rock tested was fractured, supporting the conclusion that joint properties are also little affected by the temperatures imposed. Therefore, the effect of heat-induced variation in rock mass properties is not considered in this analysis.

6.5.3.2 Variation of Model Dimensions

Most thermomechanical models in this analysis use the configuration illustrated in Figure 6-4. In this configuration, the vertical dimension is 100 m, and both the upper and lower boundaries are set at 50 m from the drift center. Though these boundaries are located at a distance about 10 times the drift diameter (5.5 m), the question remains whether this distance is adequate to limit or eliminate the boundary effect on the displacements and stresses near the drift openings. Therefore, additional analyses were conducted to evaluate the effects of variation of model vertical dimension on the thermomechanical response of rock mass adjacent to unsupported emplacement drifts by extending the upper and lower boundaries. Details are presented in Attachment III.

In this study, two additional configurations were examined: (A) both the upper and lower boundaries were extended from 50 m to 100 m measured from the drift center; and (B) the upper boundary was extended to the ground surface, about 346 m from the drift center, and the lower boundary was set at the TSw2 and TSw3 contact, about 138 m from the drift center. These two configurations as well as their corresponding boundary conditions are illustrated in Figures III-1 and III-2, respectively. For convenience of discussion, the configuration shown in Figure 6-4 is called the Base Configuration.

Results indicate that as long as the loading conditions are equivalent (Base Configuration versus Configuration A), extending the upper and lower boundaries is not expected to have a substantial effect on the thermomechanical response of emplacement drifts. The maximum difference in drift closures is only about 0.3 mm for all related cases analyzed. This difference is primarily contributed by the overall rock deformation under the in situ load, and not seen to increase with temperature.

On the other hand, the drift closures and rock stresses near the drift opening are shown to differ greatly if different configurations imply different loading conditions, such as the Base Configuration versus Configuration B. The vertical stress at the elevation of the drift center is 10 MPa for the Base Configuration, compared to about 7 MPa for the Configuration B (see Attachment III). As a result, the calculated drift closures, especially the vertical, using the Base Configuration are much larger that those based on the Configuration B. In terms of the thermomechanical response, use of the Base Configuration will clearly lead to conservative results.

It is further confirmed that the upper and lower boundaries located at a distance of about 10 times the drift diameter are not expected to have a substantial impact on the rock mass response adjacent to the drift opening as long as the associated loading conditions are equivalent. Therefore, use of the base configuration for thermomechanical analyses is considered adequate.

6.5.3.3 Variation of Joint Patterns

As stated in Section 6.4.2.2.1.2, discontinuum models for jointed rock masses are based on regular or ubiquitous joint pattern with through-going continuous fractures and constant joint spacing (see Figure 6-5). The primary reason for using the regular joint pattern in this analysis is to reduce the computational efforts associated with the discontinuum analyses. In reality, joints are randomly distributed, and their trace lengths and spacings also vary greatly at different locations. To evaluate the effects of variation of joint patterns on the thermomechanical response of jointed rock masses around emplacement drifts, analyses using statistically-generated random joint patterns were performed using UDEC. These analyses were then compared with those based on the regular joint pattern.

Three joint patterns were used based on the parameters listed in Table IV-1. Among these joint patterns, one is regular and the other two are random. Figure IV-2 illustrates the model configuration and a close-view of these joint patterns. The model dimensions and boundary conditions are identical to those shown in Figure III-2. Details are provided in Attachment IV.

Results indicate that both the vertical and horizontal closures predicted using the regular joint pattern are larger than those predicted using the random joint patterns, which is due mainly to the continuity of joints associated with the regular joint pattern compared to the discontinuity of joints with the random joint patterns. On the other hand, the rock block stresses predicted based on all three joint patterns are in general comparable, with a slightly higher stress calculated using the random joint patterns.

Therefore, use of the regular joint pattern to predict the rock mass response under combined in situ stress and thermal loading conditions is judged to be appropriate and generally conservative.

Due to the stochastic nature of joint network, it is impossible to consider all possible combinations of joint patterns in the analysis. The limited number of simulations used in this study is intended to represent the best estimate of the joint footprints on a two-dimensional cross section.

6.6 EVALUATION OF NON-EMPLACEMENT DRIFT GROUND SUPPORTS

The non-emplacement openings considered in this analysis consist mainly of emplacement drift turnouts, ventilation exhaust main, ventilation raises, and intersections formed by emplacement and non-emplacement drifts. In this section, the assessment of final ground support systems for the non-emplacement drifts is presented. Some of the initial ground support systems for the non-emplacement drifts, such as the East Main, have already been installed during the ESF construction. The rest can be determined by using knowledge and lessons learned from the ESF construction. The final ground support needs are established, based on the analytical approach similar to that used for the emplacement drift ground supports. The analytical approach is presented in detail in Section 6.4.2.

6.6.1 Results for Unsupported Non-Emplacement Drifts

A two-dimensional model using FLAC, as shown in Figure 6-7, was employed to evaluate the unsupported opening stability of a ventilation exhaust main subjected to excavation-induced and thermal loads. As mentioned, the exhaust main has a diameter of 7.62 m and is assumed to experience a maximum wall temperature of 50°C during the repository preclosure period. In addition, three prescribed temperature boundaries are also used in the models to take into account the effects of the rock temperature increases due to waste emplacement, as discussed in Section 6.4.2.1.

For the seismic loading condition, a three-dimensional model with the 3DEC code was used for the intersections of non-emplacement drifts. The analysis used a quasi-static approach, as discussed in Section 6.4.2.2.3. Given the rock mass categories and in situ stress ranges, the least favorable combination is when the rock representing the rock mass Category 1 is subjected to the K_o=0.3 in situ stress condition under seismic loads.

6.6.1.1 In Situ Stress Loading Condition

Table 6-5 summaries the FLAC analysis results of unsupported Exhaust Main for drift closures and rock stresses induced by excavation. The horizontal closure varies from 9.8 mm for rock mass Category 1 and K_o=1.0 to –0.4 mm for rock mass Category 5 and K_o=0.3. The vertical closure is estimated to be 15.5 mm for rock mass Category 1 and K_o=0.3 and 4.2 mm for rock mass Category 5 and K_o=1.0, showing the effect of rock mass quality on the drift deformation.

The maximum tangential stress varies from about –18 MPa in compression for the rock mass category 1 and K_o=1.0 to about –22 MPa in compression for the rock mass category 5 and K_o=0.3, occurring near the skin of springline. The stresses at the crown are low when K_o=0.3 and high when K_o=1.0. These values are comparable to those for the emplacement drifts with a smaller diameter (5.5 m) (see Table 6-2).

Contours of the Mohr–Coulomb strength-to-stress ratios for all four cases are presented in Figures 6-44a through 6-44d. These plots indicate that for unsupported openings, a rock mass yield zone of approximately 1 m in depth is predicted for the rock mass Category 1 and K_o=0.3. The yield zone is estimated to be less than 1 m for the other cases considered. For the rock mass Category 1 and K_o=0.3, a potential tension failure may occur at the crown within a very shallow depth. The results show that the installation of ground support in the non-emplacement drifts is necessary, especially when an area with a rock mass category of 1 is encountered.

Table 6-5. Unsupported Exhaust Main – Results from FLAC for In Situ Stress Loading Condition

Items	RMQ=1		RMQ=5	
	K_o=0.3	K_o=1.0	K_o=0.3	K_o=1.0
Horizontal Closure (mm)	-0.9	9.8	-0.4	3.5
Vertical Closure (mm)	15.5	10.4	5.3	4.2
Major Principal (Tangential) Stress near Crown (MPa)	-0.9	-15.3	-1.1	-17.6
Minor Principal (Radial) Stress near Crown (MPa)	-0.2	-1.0	-0.2	-1.0
Major Principal (Tangential) Stress near Springline (MPa)	-21.1	-17.6	-21.6	-17.9
Minor Principal (Radial) Stress at Springline (MPa)	-2.5	-1.9	-2.4	-2.1

Numerical results from the 3DEC model of the intersection region formed by the access main (AM) and emplacement drift turnout (EDT) were obtained by sequentially excavating the AM and EDT under the K_o=0.3 in situ stress field. Upon the completion of AM and EDT, the 3DEC model predicts approximately 14 mm of displacement (closure) at the crown of the center of the intersection. At two other crown locations which are about 4 and 10 m away from the intersection along the access main, a vertical displacement of 14 and 2 mm (closure) is predicted by the model respectively. Results indicate that the intersection region experiences a noticeably larger closure than anywhere else in the access main or the turnout drift.

Figures 6-45a through 6-45d reveal in sectional views the redistributed stress state against the Mohr-Coulomb yield criterion. These two-dimensional views correspond to the cross-sections cut in the access main at 0, 5.5, 6, and 8 m away from the center of the intersection. The wedged-shaped pillar between the AM and EDT becomes wider and wider as the cross-section moves farther away from the intersection. Failure indicators on each view point out that, although the rock mass surrounding the excavation still remains in the elastic range of deformation, a potential plastic zone up to 1 m deep could develop. The narrow portion of the pillar between the access main and turnout drift will be subjected to a higher stress concentration. But for a 75-degree intersection, the wedge-shaped pillar becomes wider rapidly, therefore, becomes stable quickly. Generally, the smaller the intersection angle is, the larger the narrow portion of the pillar will be, and thus, additional ground support measures will be required to maintain its stability.

6.6.1.2 Thermal Loading Condition

Maximum drift closures and rock stresses due to combined in situ stress and thermal loads are listed in Table 6-6. By comparing Table 6-6 with Table 6-5, the stress results indicate that drift openings experience, in general, a greater increase of the stresses at the crown than at the springline, as a result of the predominant horizontal thermal loading condition. This is also confirmed by the greater increase of the horizontal closures with the elevated temperatures.

Figures 6-46a through 6-46d present the contours of Mohr–Coulomb strength-to-stress ratios for combined in situ stress and thermal loads. When compared to Figures 6-44a through 6-44d, it appears that there is no noticeable extension to the potential rock mass yield zones due to thermal loads for all rock mass categories.

Table 6-6. Unsupported Exhaust Main – Results from FLAC for Combined In Situ Stress and Thermal Loading Conditions

Items	RMQ=1		RMQ=5	
	K_o=0.3	K_o=1.0	K_o=0.3	K_o=1.0
Horizontal Closure (mm)	3.7	14.4	4.2	8.1
Vertical Closure (mm)	15.6	10.4	5.3	4.2
Major Principal (Tangential) Stress near Crown (MPa)	-8.4	-22.1	-22.0	-36.6
Minor Principal (Radial) Stress near Crown (MPa)	-0.5	-1.2	-1.2	-1.9
Major Principal (Tangential) Stress near Springline (MPa)	-22.4	-19.1	-25.7	-22.1
Minor Principal (Radial) Stress at Springline (MPa)	-2.6	-2.2	-3.0	-2.7

6.6.1.3 Seismic Loading Condition

Seismic effects on the stability of this intersection area are examined in a quasi-static approach. Additional body forces corresponding to PGA values are superimposed onto the 3DEC model both in the horizontal and vertical directions after the excavation-induced stress redistribution surrounding the intersection has been completed under the in situ load. Numerical iteration continues until a new equilibrium state is reached under these additional static body forces. Quasi-static superimposition of seismic loads is made in such a way that an increase in the verti

results indicate that the intersection region experiences a noticeably larger closure than anywhere else in the access main or the turnout drift.

Figures 6-47a through 6-47d reveal in sectional views the redistributed stress state against the Mohr-Coulomb yield criterion. These two-dimensional views correspond to the cross-sections cut in the access main at 0, 5.5, 6, and 8 m away from the center of the intersection. These are the same locations examined under the in situ load. The potential overstressing patterns surrounding the intersection and pillar areas appear the same as those under the in situ load, supporting that additional ground support measures will be required to maintain its stability.

6.6.2 Results for Supported Exhaust Main

The ground support system for non-emplacement drifts, such as access and exhaust mains, will consist of initial and final systems. A 7.62-meter diameter opening representing access/service mains is similar to the ESF Main Drift that was excavated in the TSw2 unit. A ground support system comprised mainly of rock bolts and welded wire fabric was used to support the ESF Main Drift. Steel sets and partial lagging were also used in more difficult tunneling areas to address personnel safety behind the TBM trailing shield. Similar types of initial ground supports can be used in the main drifts including the ventilation exhaust main with a diameter of 7.62 m. In turnout areas and small portions of the rock bolted sections, application of shotcrete may be needed for ground stabilization. For the intersections, any potential plasticity zones near the openings can be stabilized effectively by rock bolt installation, shotcrete application, and steel set installation. Therefore, the initial ground support for non-emplacement drifts will include mainly rock bolts with welded wire fabric, limited shotcrete application, and limited installation of steel sets.

The discussion presented in this subsection is focused on the evaluation of the final cast-in-place concrete lining recommended for the exhaust main. Since the exhaust main represents the opening with the hottest environment among the non-emplacement drifts considered for the SR design, any conclusions concerning the feasibility of designing ground control systems for non-emplacement openings for the Yucca Mountain site, based on the calculation for this drift, should be conservatively applicable to other drifts.

The supported exhaust main was modeled with FLAC for in situ stress and thermal loading cases. As discussed in Section 5.1.2, 100 percent relaxation of in situ stress was allowed prior to installation of the final ground support system in the exhaust main. Therefore, the stresses in the concrete lining induced by excavation are not relevant and will not be discussed in this analysis. Thermally-induced stresses and displacements are predicted for a preclosure period of 200 years. In the models, the concrete lining is perfectly bonded to the rock surface, a conservative condition.

6.6.2.1 Thermal Loading Condition

Table 6-7 presents the maximum and minimum stresses in a 300-mm-thick concrete lining for the rock mass Categories 1 and 5, and K_o=0.3 and 1.0. The results indicate that the stresses are sensitive to the rock mass properties, but less sensitive to the initial stress state. The former is

because the concrete lining is bonded to the rock, and the latter is due to the assumption of 100 percent ground relaxation prior to lining placement.

Figures 6-48a through 6-49d illustrate the distributions of axial forces and bending moments along the concrete lining ring. It is indicated that the calculated axial forces at the crown of the concrete lining are compression while those at the springline are tension for all cases considered. Combined stresses at the crown and springline are calculated using the corresponding axial force and bending moment values, and are given in Table 6-7. The maximum combined compressive stress in the concrete lining, corresponding to combining the maximum axial force with the maximum bending moment, is estimated to be 23.2 MPa. As indicated, the calculated compressive stresses for all cases are below the allowable strength for concrete of 24.14 MPa (see Table 4-11). The maximum combined tensile stress in the concrete lining is predicted to be -10.0 MPa. This magnitude of tensile stress is not negligible and may result in cracks in the concrete lining, suggesting that the use of reinforcement to prevent potential tensile failure of the concrete lining is necessary.

Table 6-7. Stresses in Concrete Lining for Exhaust Main – Results from FLAC for Thermal Loading Condition

Items	RMQ=1		RMQ=5	
	K_o=0.3	K_o=1.0	K_o=0.3	K_o=1.0
Axial Force at Crown (kN)	4.74×10^3	4.74×10^3	6.21×10^3	6.21×10^3
Bending Moment at Crown (kN-m)	25.19	25.48	24.24	24.40
Axial Force at Springline (kN)	-1.38×10^3	1.37×10^3	-2.26×10^3	2.26×10^3
Bending Moment at Springline (kN-m)	25.68	29.22	36.79	36.49
Max. Axial Force (kN)	4.74×10^3	4.74×10^3	6.21×10^3	6.21×10^3
Max. Bending Moment (kN-m)	25.78	29.27	36.84	36.55
Combined Stress at Crown (MPa)	17.5	17.5	22.3	22.3
Combined Stress at Springline (MPa)	-6.3	-6.5	-10.0	-9.9
Potential Maximum Combined Stress (MPa)	17.5	17.7	23.2	23.1

6.7 APPROPRIATENESS AND CONFIDENCE OF THE ANALYSIS

The analysis presented in this document uses numerical approaches to predict the performance of ground support and repository openings. These numerical approaches are based on widely accepted mathematical or engineering laws, such as the Mohr-Coulomb failure criterion (see Equation 6-5), and were executed using ANSYS, FLAC, UDEC, and 3DEC computer codes. Use of the numerical approaches and these computer codes is considered appropriate for this analysis.

In addition, some assumptions and preliminary data were used due to a lack of sufficient qualified data or additional tests and studies pending. Use of these assumptions or preliminary

data does not necessarily undermine the confidence of the analysis because they are supported by solid basis and engineering judgement. Change of these assumptions or preliminary data may ultimately affect the results of the analysis and require a reevaluation of the conclusions. This impact should be judged acceptable and does not indicate any inappropriateness of the analysis. This analysis is appropriate for use in the SR design.

7. CONCLUSIONS

7.1 SUMMARY

This analysis demonstrates that a satisfactory ground control system for the potential repository with flexible operational conditions can be designed for an extended service life of up to 300 years. It provides the technical basis for the design of ground support systems to be used in repository emplacement and non-emplacement drifts. The repository ground support design was based on analytical methods using acquired computer codes, and focused on the final support systems.

A literature review of case histories, including the lessons learned from the design and construction of the ESF, the studies on the seismic damages of underground openings, and the use of rock mass classification systems in the ground support design, was conducted (Sections 6.3.4 and 6.4). This review provided some basis for determining the inputs and methodologies used in this analysis.

Stability of the supported and unsupported emplacement and non-emplacement drifts was evaluated in this analysis. The excavation effects (i.e., state of the stress change due to excavation), thermal effects (i.e., due to heat output from waste packages), and seismic effects (i.e., from potential earthquake events) were evaluated, and stress controlled modes of failure were examined for two in situ stress conditions (K_o=0.3 and 1.0) using rock properties representing rock mass categories of 1 and 5. Variation of thermal conditions, such as the high and low temperature conditions, rock mass units such as the non-lithophysal (Tptpmn) and lithophysal (Tptpll), rock mass strength properties such as cohesion and friction angle, and rock joint patterns such as regular or random were considered in the analysis. The focus was on the non-lithophysal unit because this unit appears to be relatively weaker and has much smaller joint spacing. Therefore, the drift stability and ground support needs were considered to be controlled by the design for this rock unit.

The ground support systems for both emplacement and non-emplacement drifts were incorporated into the models to assess their performance under in situ, thermal, and seismic loading conditions. Both continuum and discontinuum modeling approaches were employed in the analyses of the rock mass behavior and in the evaluation of the stability of the openings. No credit or account was given for the initial ground support in modeling the final ground support systems for both emplacement and non-emplacement drifts in this analysis.

7.2 STABILITY OF UNSUPPORTED OPENINGS

Under the in-situ stress, rock deformation and stress were shown to be especially sensitive to rock mass modulus and the initial horizontal-to-vertical stress state (K_o value). The worst case was associated with the Category 1 rock mass and the initial stress state of K_o=0.3. Overall, the emplacement drifts are expected to be stable after excavation.

Under the thermal load (either the high temperature condition or the low temperature condition), Category 1 rock properties resulted in the greatest deformation. The thermally-induced deformations were relatively small and insignificant to cause any substantial instability of the

drift opening. Major (tangential) principal stresses or confinement around the emplacement drifts increased substantially with temperature, especially for the Category 5 rock mass, while at the same time minor (radial) principal stresses increased only slightly. Overall, the emplacement drifts are stable and self-supporting under combined in situ and thermal loading conditions.

Results also indicate that cooling of the emplacement drifts will result in a reduction in tangential stresses or confinement, which could potentially lead to loosening near the periphery of the drift opening (Figures 6-16a through 6-21b). This will be counteracted by ground supports, such as steel sets and/or, if necessary, rock bolts.

Under the seismic load, the unsupported emplacement and non-emplacement drifts are expected to perform satisfactorily. Expected variations in the magnitude and duration time of seismic load do not have a significant impact on the rock mass behavior.

7.3 REPOSITORY GROUND SUPPORT

The final ground support for emplacement drifts will include two systems: steel sets (1) with and (2) without fully grouted rock bolts, dependent on the rock conditions. For massively jointed rock mass, such as the Tptpmn rock unit, use of the steel sets together with fully grouted rock bolts is recommended. For generally continuous rock mass, such as the Tptpll rock unit, use of the steel sets alone may be sufficient. These systems also serve as the initial ground support during excavation. It can be concluded that the ground support system of choice will have to be structurally flexible to accommodate deformations mainly caused by thermal loading, to ensure that induced stresses in the ground support components remain within allowable limits.

The final ground support system for non-emplacement drifts will include a cast-in-place concrete lining.

7.3.1 Steel Sets

In reality, full bonding between rock and the steel sets will not occur. For the jacking loads to be used to expand the steel sets against the rock surface, gaps will remain along the steel/rock interface due to the mismatch between the bored surface and the steel set ring. Therefore, an approach which accounts for this mismatch was developed and used to assess the performance of steel sets (W6×20 spaced at 1.5 m, ASTM A36 steel) for the emplacement drifts.

Results indicate that the stresses in the steel sets induced by in situ and thermal loads are sensitive to rock mass properties, such as the modulus of deformation. The calculated stresses are greater for weaker rock (RMQ=1) than for stronger rock (RMQ=5). The maximum stresses in steel sets under thermal loading condition, either the high or the low temperature condition, are predicted to be dependent on the size of an initial gap. Their values will remain within an allowable stress of 164 MPa based on ASTM A36 steel (see Section 4.1.8) as long as an appropriate size of the initial gap is considered.

It is also indicated that the stresses in steel sets induced by the seismic load are significant and sensitive to the magnitude of the seismic velocities. The maximum stresses under combined in situ, thermal, and seismic loads are calculated to be below the increased allowable stress for the earthquake loading condition.

Overall, the steel sets together with welded-wire fabric can be designed for use in emplacement drifts, subjected to in situ, thermal, and seismic loads, to provide desired functionality of preventing potential rock falls during the preclosure period.

7.3.2 Fully-Grouted Rock Bolts

Fully grouted rock bolts, 3-m long spaced at 1.5 m, were modeled using FLAC under in situ stress and thermal conditions. Both bond strength and frictional resistance for the bolt/grout interface were included in the models. The grout annulus was not modeled explicitly; its presence was represented by its bond stiffness and strength.

Results show that under combined in situ, thermal, and seismic loads, the axial forces in rock bolts are not very sensitive to the rock mass properties and location where the bolts are installed. The maximum axial force in rock bolts was predicted to be well below an allowable force of 160.2 kN (see Table 4-10).

Therefore, the fully-grouted rock bolts can be designed for use in emplacement drifts, subjected to in situ, thermal, and seismic loads, to provide desired functionality of preventing potential rock loosening and falls during the preclosure period.

7.3.3 Cast-In-Place Concrete Lining

A cast-in-place concrete lining with a thickness of 300 mm is recommended for the main drifts including access mains and ventilation exhaust main. Thermally-induced stresses and displacements were calculated using FLAC for a temperature increase on drift walls from 25°C to 50°C. In the models, the concrete lining was assumed to be bonded perfectly to the rock surface.

Results indicate that an increase in rock temperatures is predicted to cause an increase in the stress in the lining (see Table 6-7). The magnitude of increase is dependent on the rock mass modulus. The maximum combined stress in the concrete lining was estimated to be below a concrete allowable strength of 24.2 MPa (see Table 4-11). The tensile stress was also predicted in the concrete lining when experiencing the elevated temperatures. Therefore, the use of reinforcement in the cast-in-place concrete lining will be necessary for the non-emplacement drifts subjected to the thermal loading condition.

7.4 SITE SUITABILITY

The analysis supports the conclusion that satisfactory ground control systems can be designed for the emplacement drifts and the non-emplacement openings planned for the Yucca Mountain Site.

7.5 UNCERTAINTY AND RESTRICTION

Uncertainties associated with the input data, such as thermal and mechanical properties of rock, mechanical properties of rock joints, still remain. Results and conclusions discussed in this analysis are based on the input data presented in Section 4 and the assumptions discussed in Section 5. Any change in the input data may have an impact on the conclusions of this analysis, and therefore, a re-evaluation may be required.

This document may be affected by technical product input information that requires confirmation. Any changes to the document that may occur as a result of completing the confirmation activities will be reflected in subsequent revisions. The status of the technical product input information quality may be confirmed by review of the DIRS database.

7.6 MODEL WAREHOUSE DATA

The electronic inputs and outputs from software used in Section 3 are found in two model warehouse DTNs: MO0004MWDEMP02.003 and MO0105MWDGRO02.008. These DTNs contain the outputs, such as the drift closures, stresses in rock adjacent to drift openings, axial forces, bending moments, and combined stresses in steel sets, axial forces in rock bolts, displacements of rock blocks, and shear displacements of rock blocks on joints.

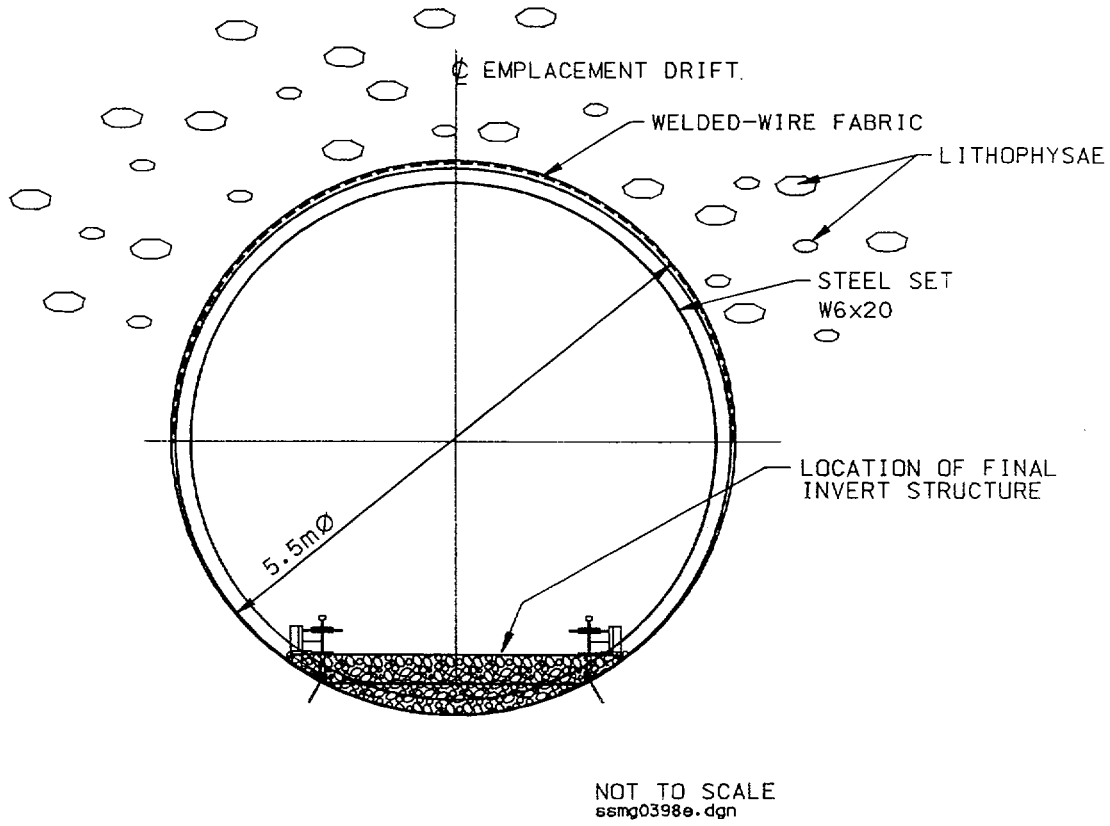

Figure 6-1. Steel Sets With Welded-Wire Fabric for Lithophysal Rock Unit

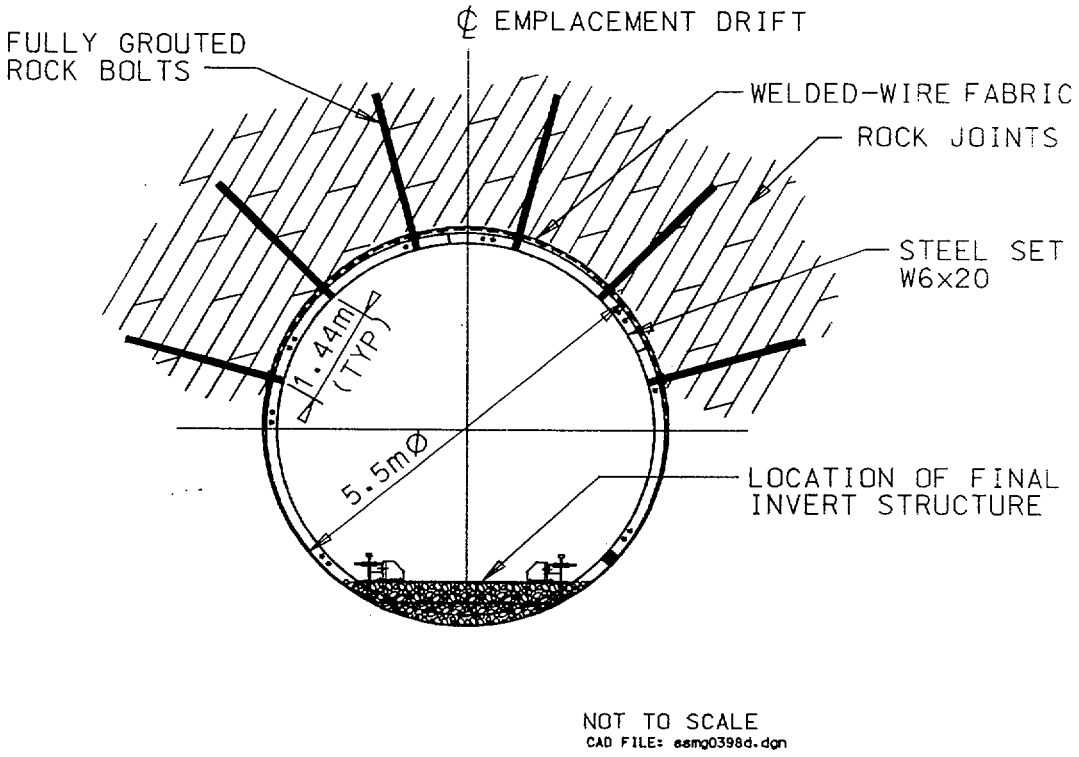

Figure 6-2. Fully Grouted Rock Bolts With Steel Sets for Non-lithophysal Rock Unit

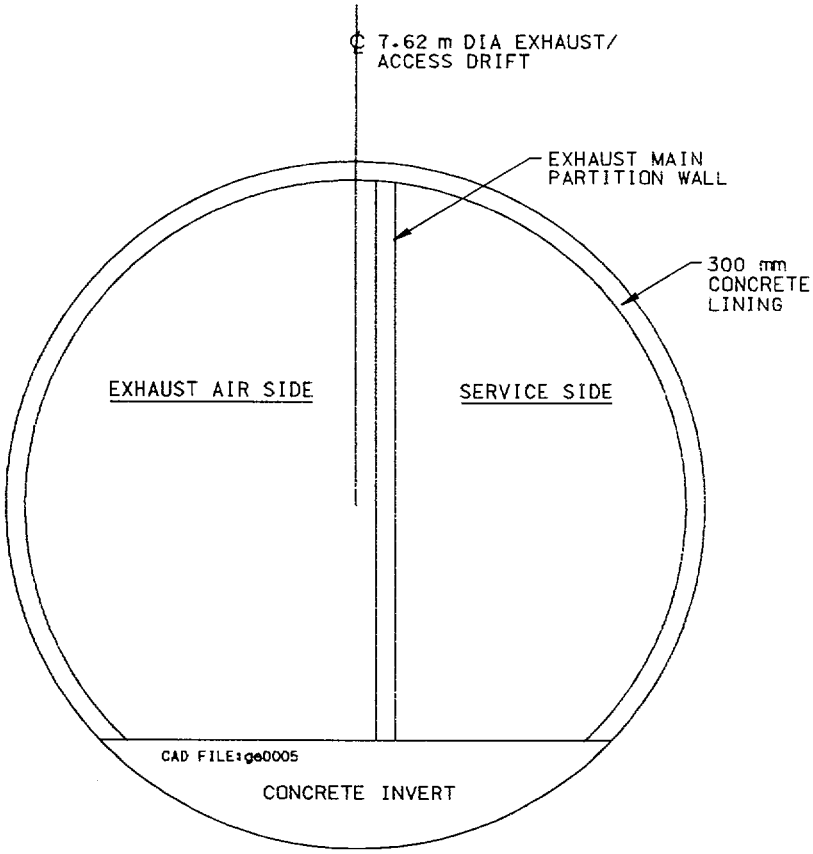

Figure 6-3. Cast-in-Place Concrete Lining for Exhaust Main

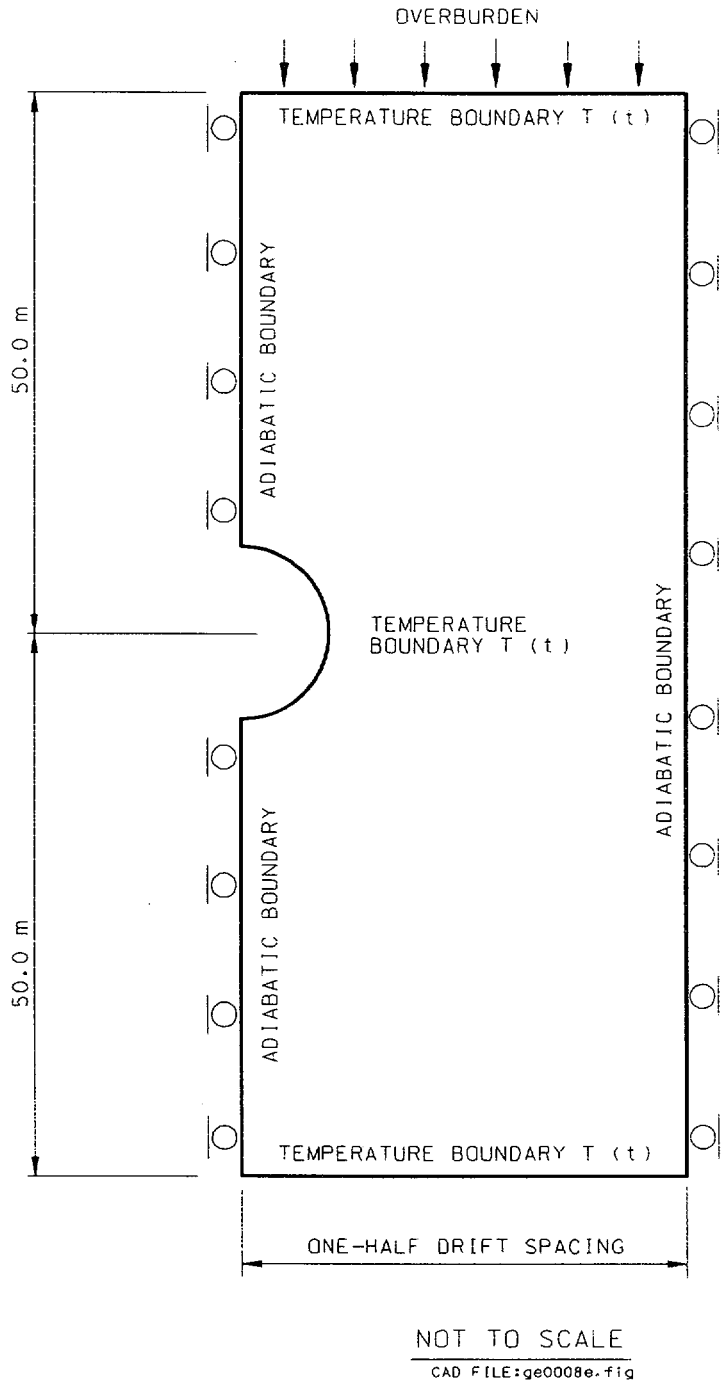

Figure 6-4. Geometry and Boundary Conditions for Thermomechanical Modeling for Emplacement Drifts Using ANSYS and FLAC

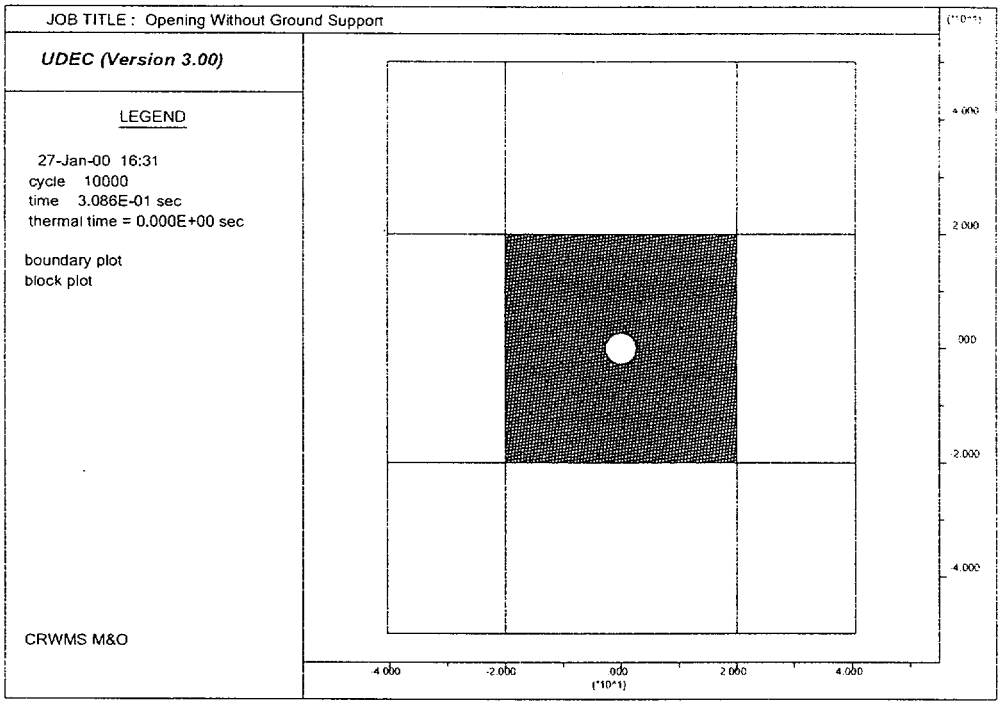

Figure 6-5. Geometry and Zones for Thermomechanical Modeling for Emplacement Drifts Using UDEC

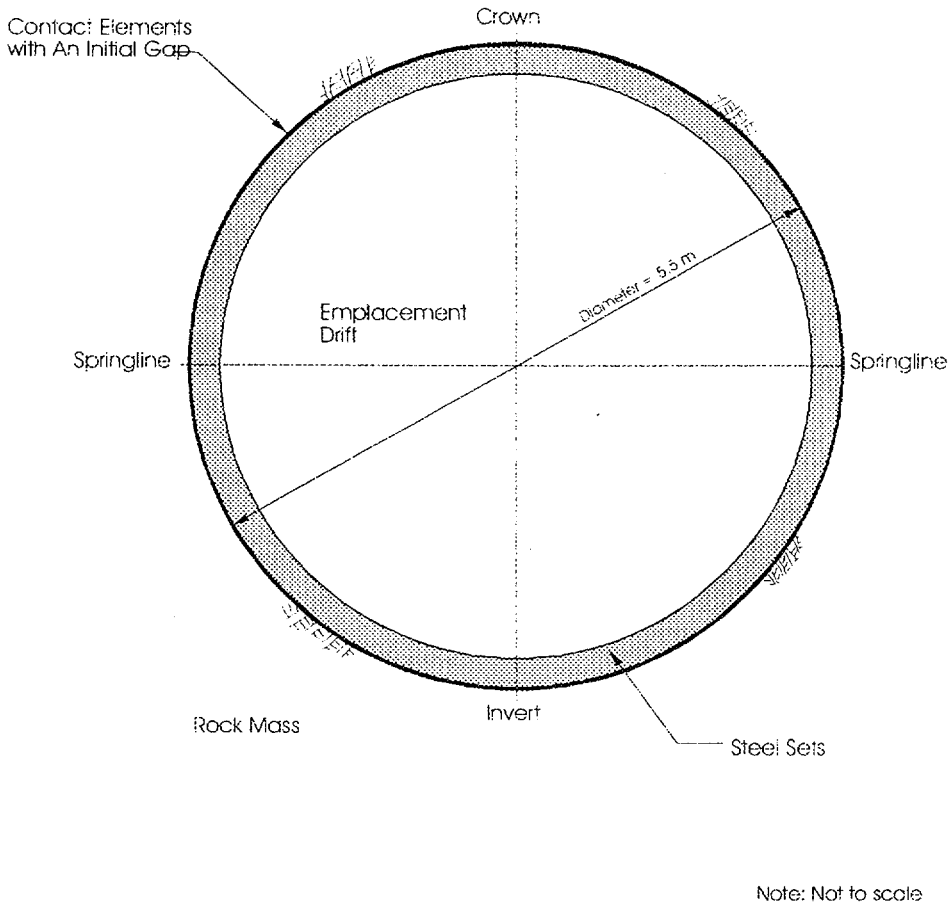

Figure 6-6. Illustration of Contact (Gap) Element Concept for Steel Sets

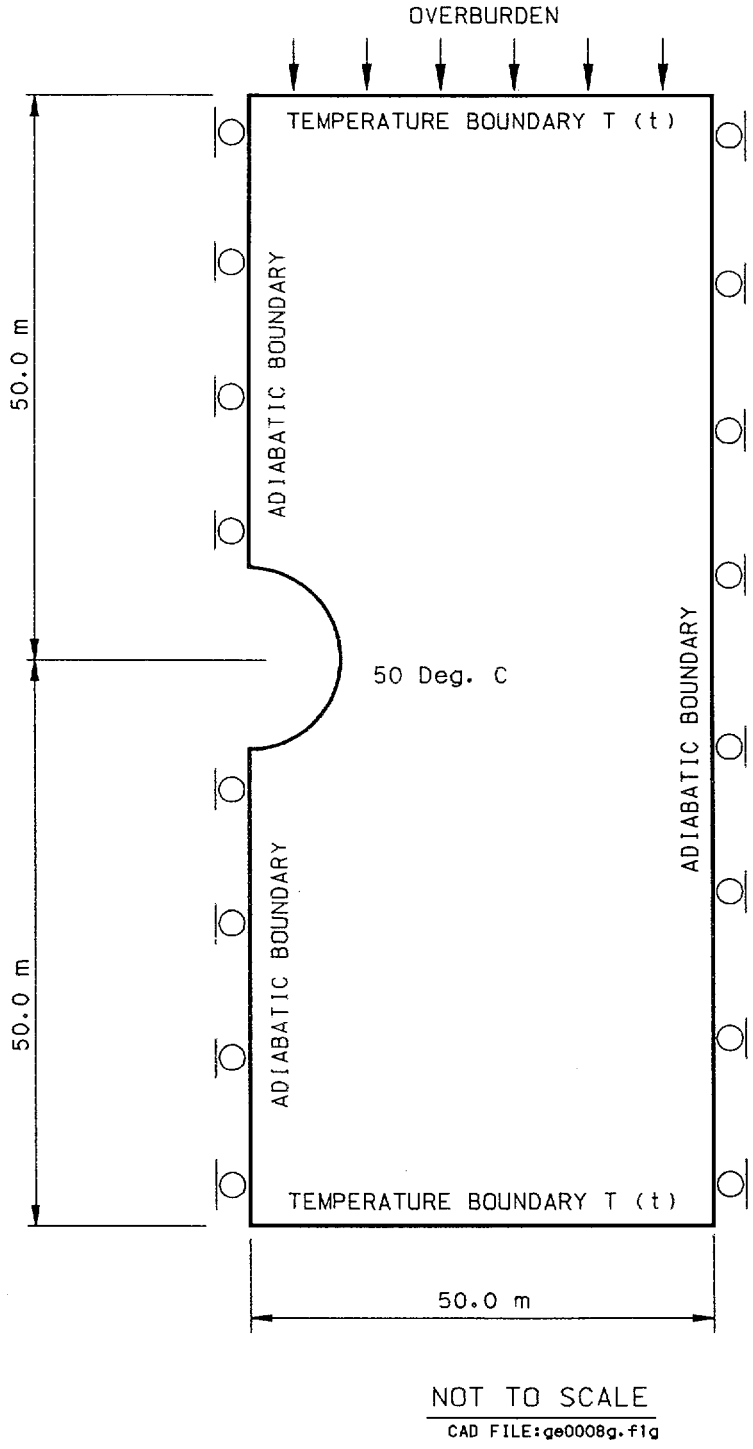

Figure 6-7. Geometry and Boundary Conditions for Thermomechanical Modeling for Exhaust Main Using FLAC

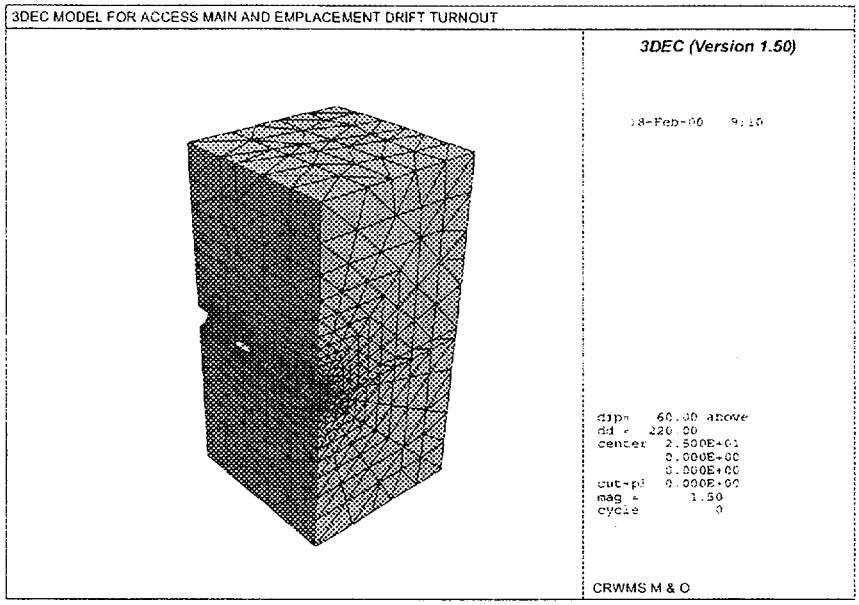

(a)

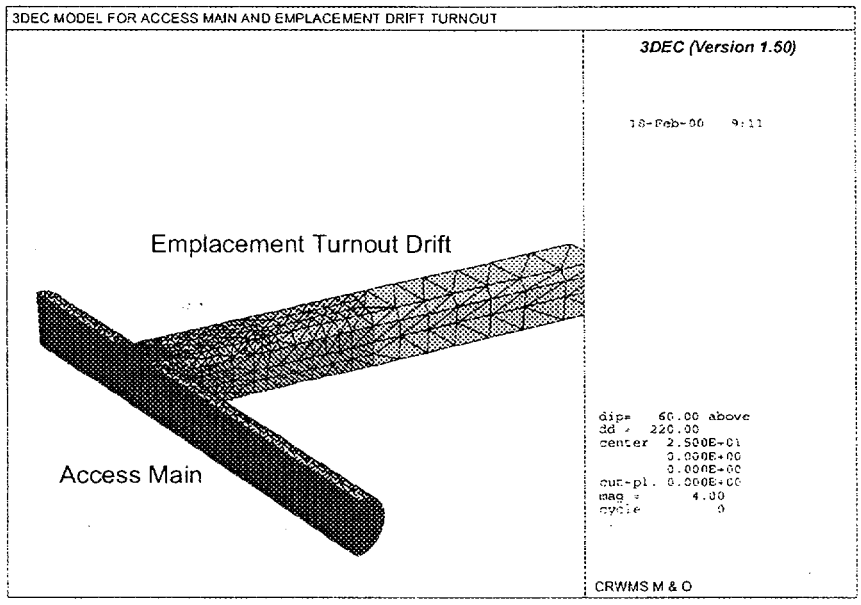

(b)

Figure 6-8. A 3DEC Model of Access Main and Emplacement Turnout Drift: (a) Whole Model; (b) Close-up of Opening

Note: Model Dimensions Are 60-m Wide, 120-m High, and 60-m Long.

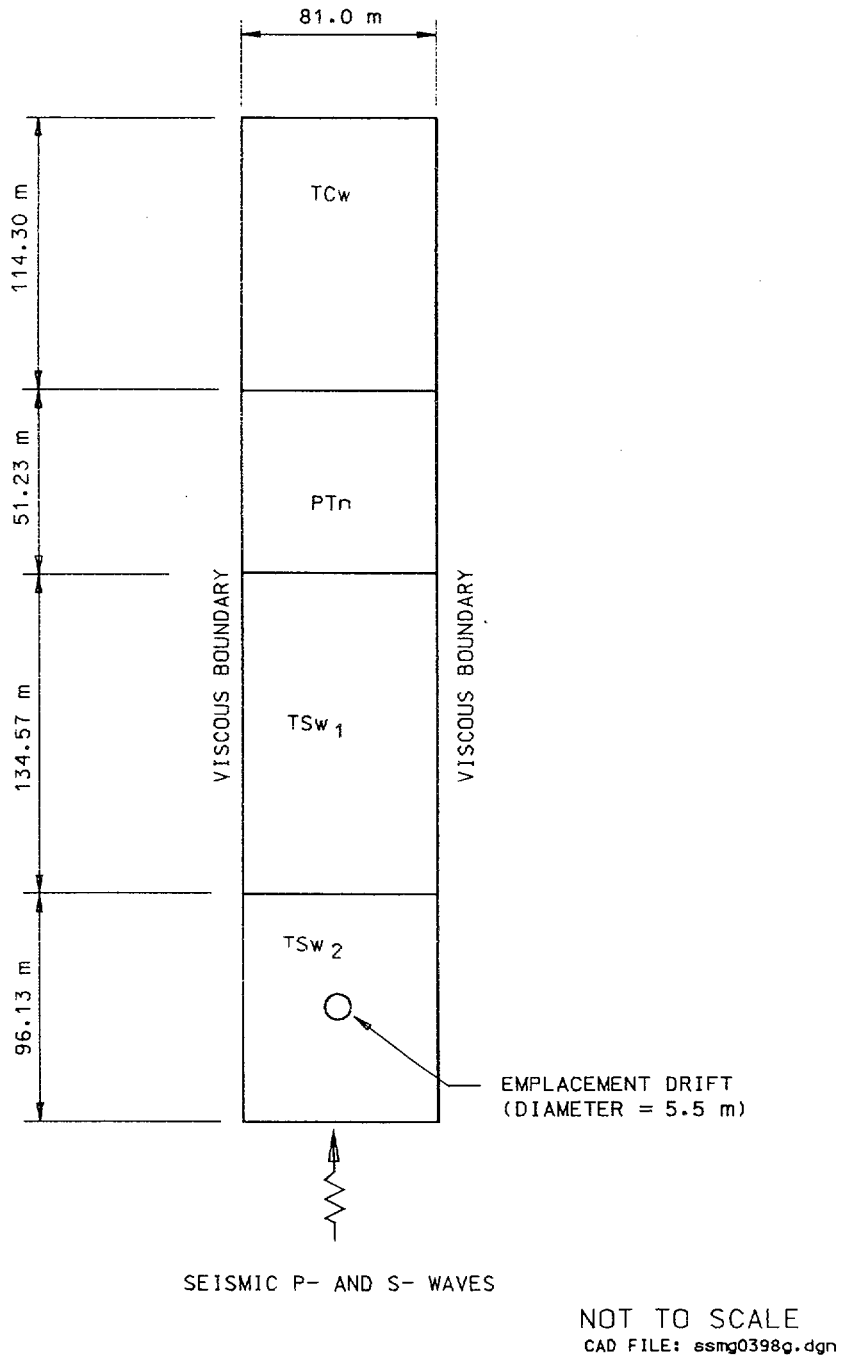

Figure 6-9. Model Configuration of Emplacement Drifts for Seismic Loading Condition Using FLAC and UDEC

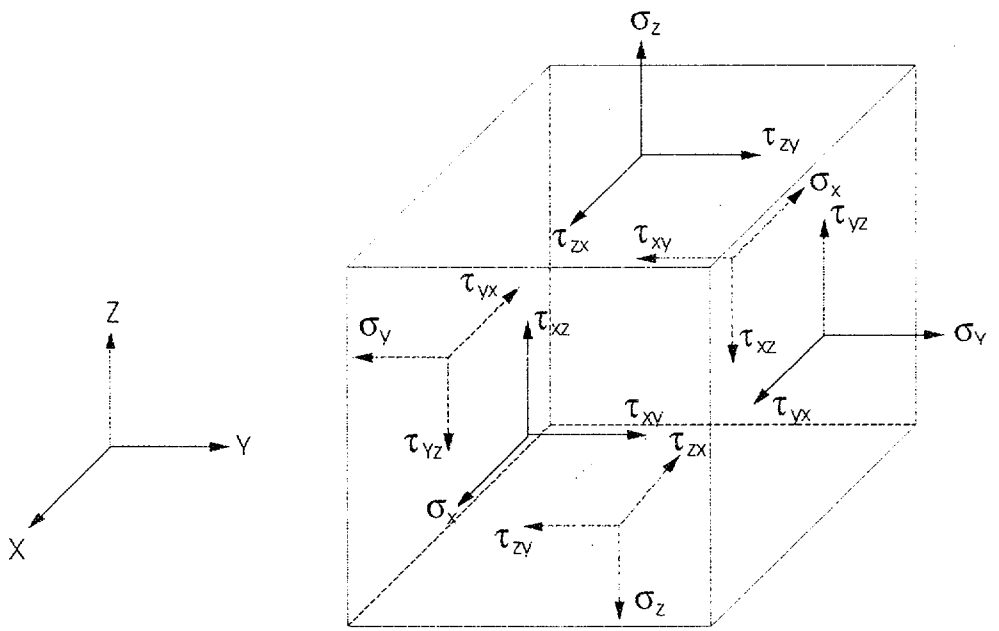

Figure 6-10. Sign Convention for Positive Stresses

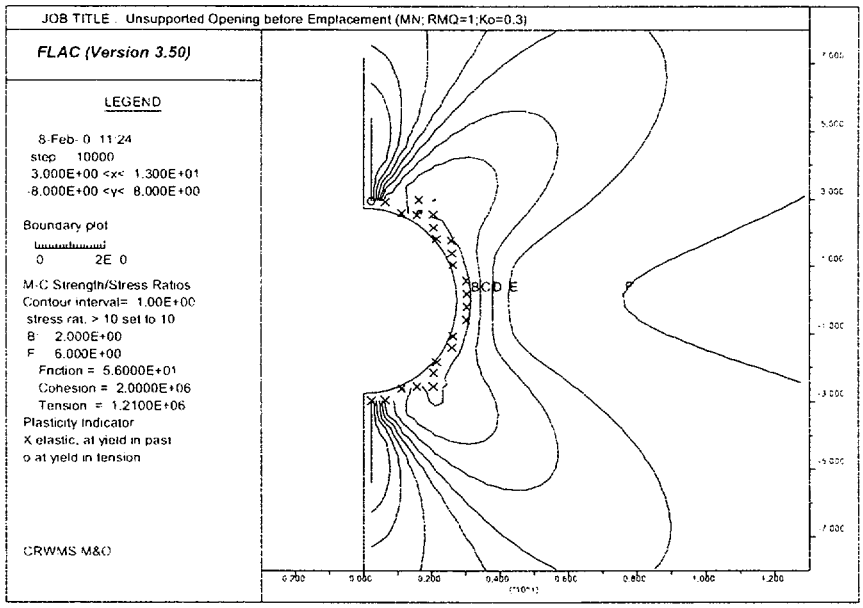

(a)

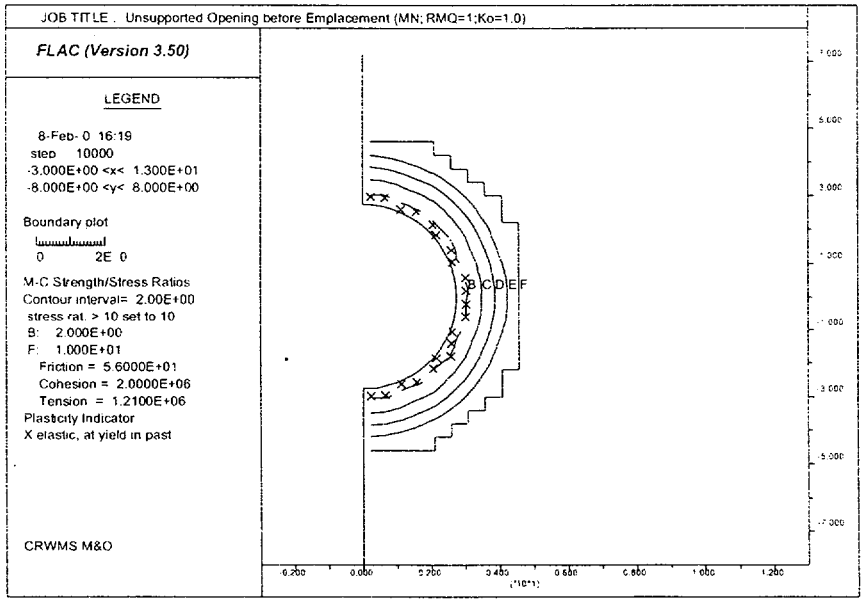

(b)

Figure 6-11. Strength/Stress Ratio Contours and Plasticity Indicators for Unsupported Emplacement Drifts for In Situ Stress Load, Different RMQ Categories, and In Situ Stress Ratio K_o: (a) RMQ=1, K_o=0.3; (b) RMQ=1, K_o=1.0; (c) RMQ=5, K_o=0.3; (d) RMQ=5, K_o=1.0

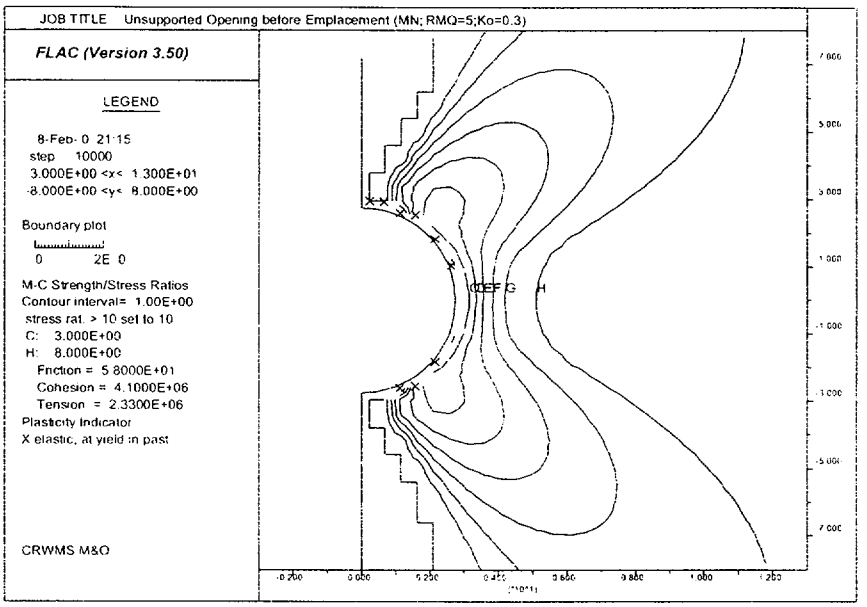

(c)

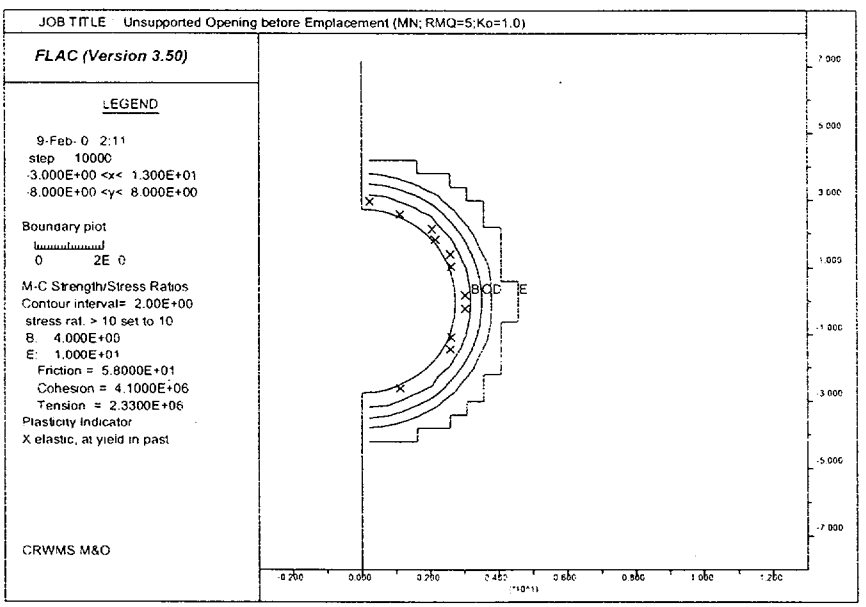

(d)

Figure 6-11 (Continued). Strength/Stress Ratio Contours and Plasticity Indicators for Unsupported Emplacement Drifts for In Situ Stress Load, Different RMQ Categories, and In Situ Stress Ratio K_o: (a) RMQ=1, K_o=0.3; (b) RMQ=1, K_o=1.0; (c) RMQ=5, K_o=0.3; (d) RMQ=5, K_o=1.0

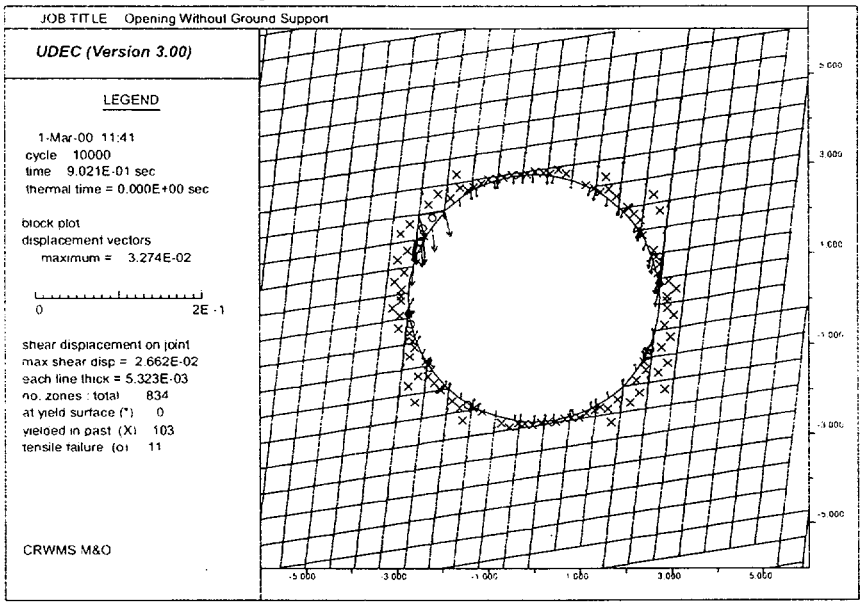

(a)

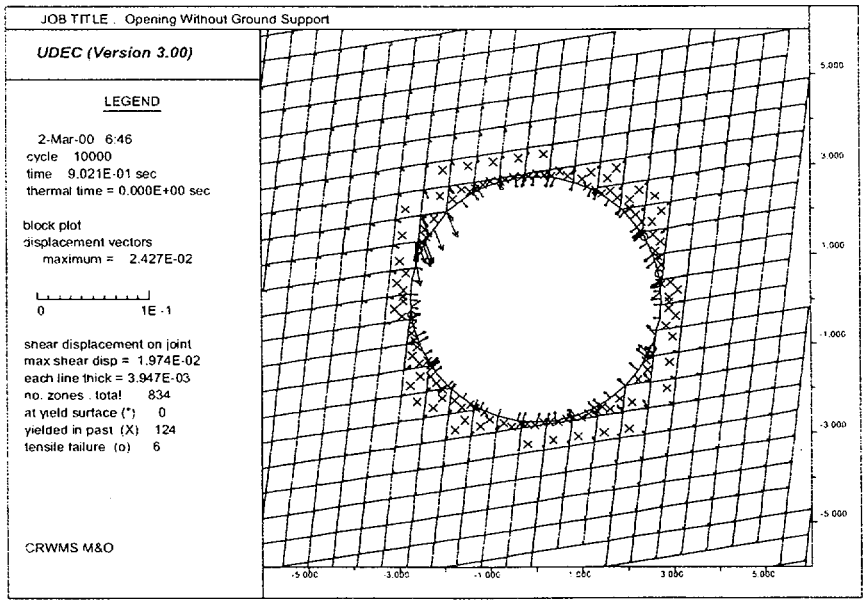

(b)

Figure 6-12. Rock Block Displacements, Shear Displacement on Joints, and Failure Zone Development Around an Emplacement Drift in Non-Lithophysal Rock Under In Situ Stress Load for Different K_o Values: (a) K_o=0.3; (b) K_o=1.0

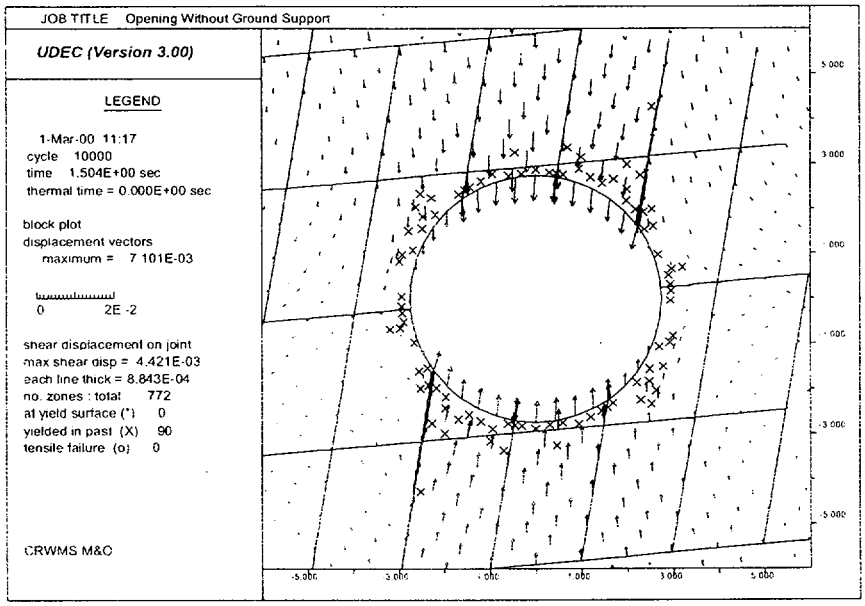

(a)

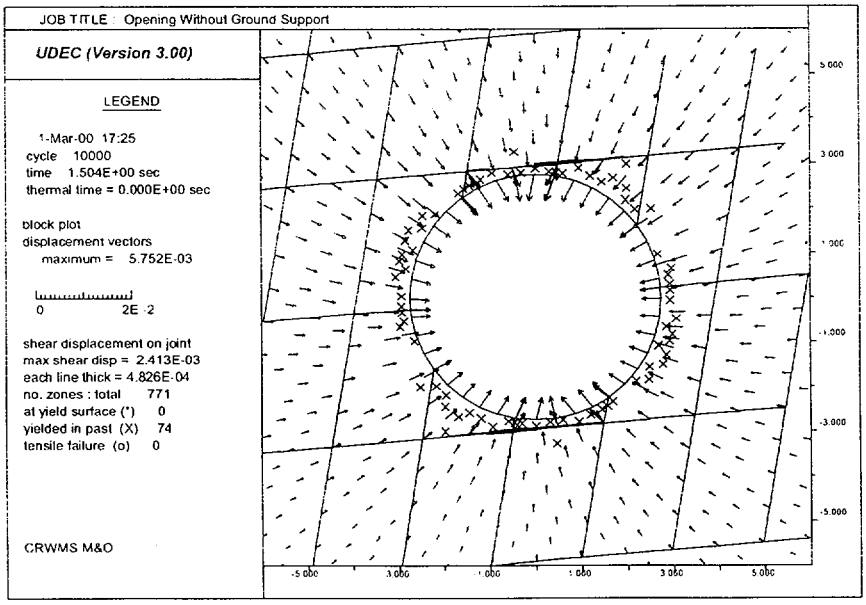

(b)

Figure 6-13. Rock Block Displacements, Shear Displacement on Joints, and Failure Zone Development Around an Emplacement Drift in Lithophysal Rock Under In Situ Stress Load for Different K_o Values: (a) K_o=0.3; (b) K_o=1.0

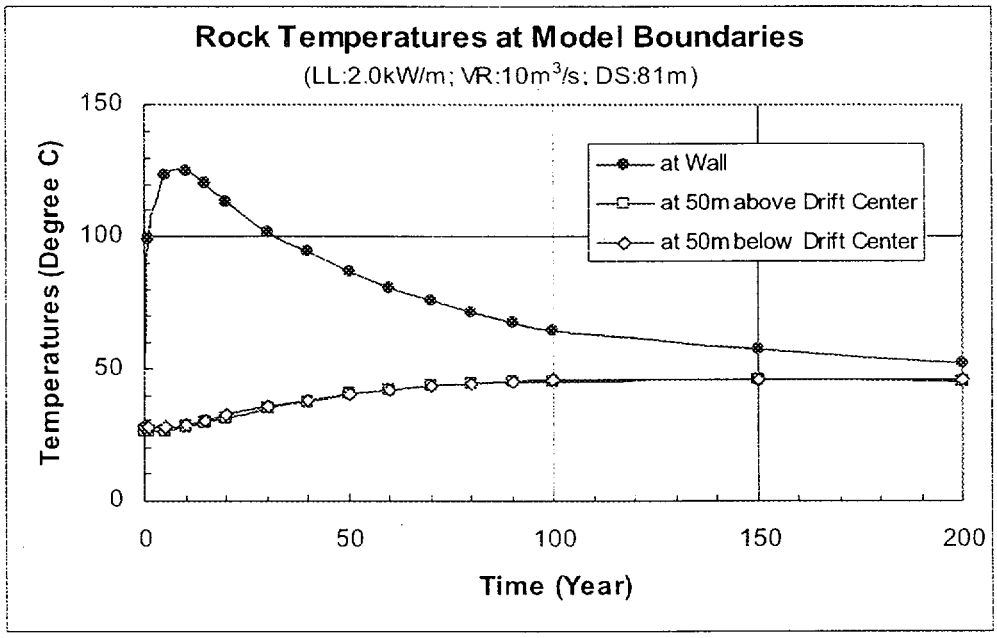

Figure 6-14. Time Histories of Temperatures on Drift Wall and Model Upper and Lower Boundaries for High Temperature Condition

Note: LL=Linear Load; VR=Ventilation Rate; DS=Drift Spacing.

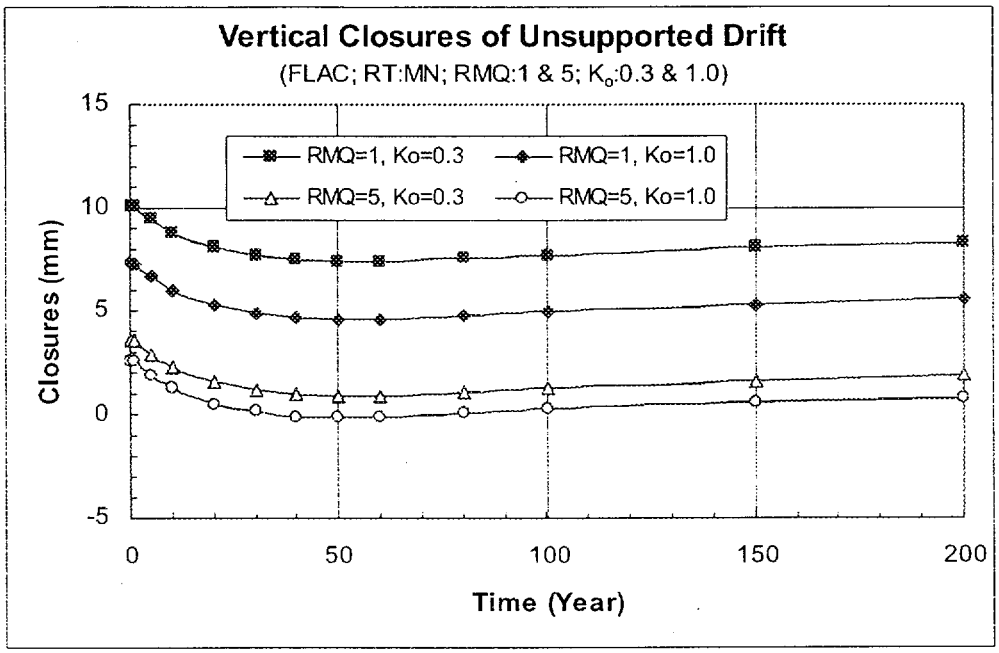

(a)

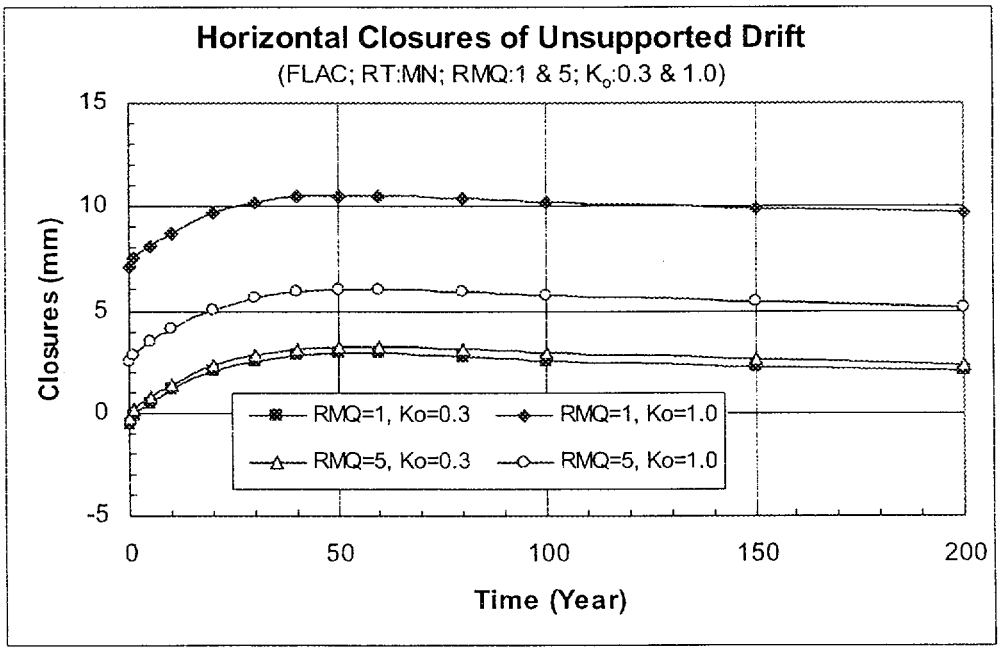

(b)

Figure 6-15. Time Histories of Drift Closures for Non-Lithophysal Rock and RMQ Categories 1 and 5: (a) Vertical Closures; (b) Horizontal Closures

Note: RT=Rock Type; MN=Middle Non-Lithophysal Unit; RMQ=Rock Mass Quality Category; K_o=In Situ Horizontal to Vertical Stress Ratio.

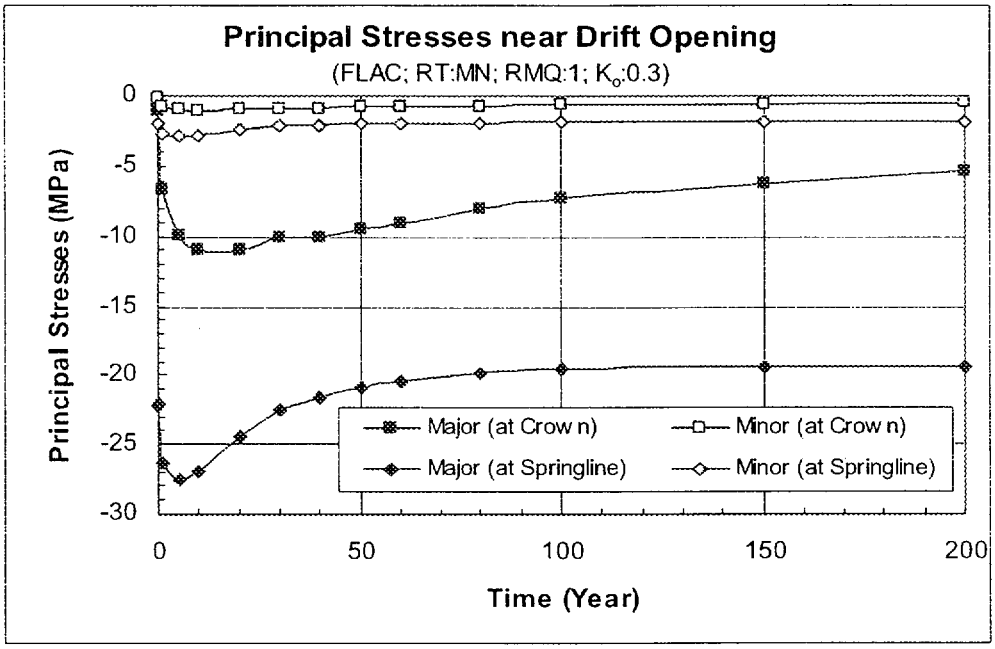

(a)

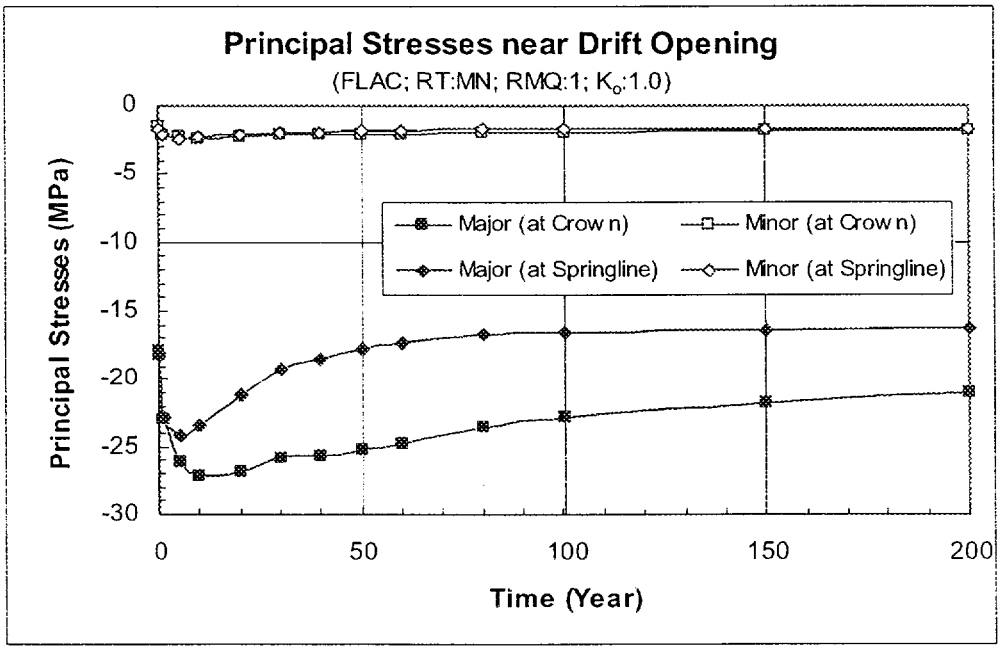

(b)

Figure 6-16. Time Histories of Major and Minor Principal Stresses at Crown and Springline for Non-Lithophysal Rock and RMQ Category 1: (a) K_o=0.3; (b) K_o=1.0

Note: RT=Rock Type; MN=Middle Non-Lithophysal Unit; RMQ=Rock Mass Quality Category; K_o=In Situ Horizontal to Vertical Stress Ratio.

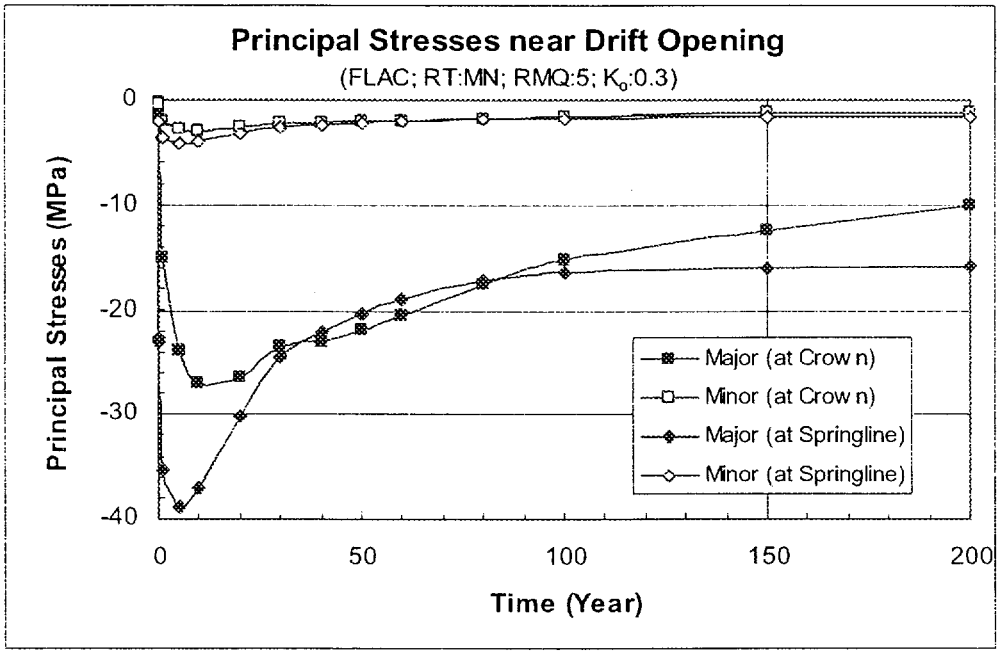

(a)

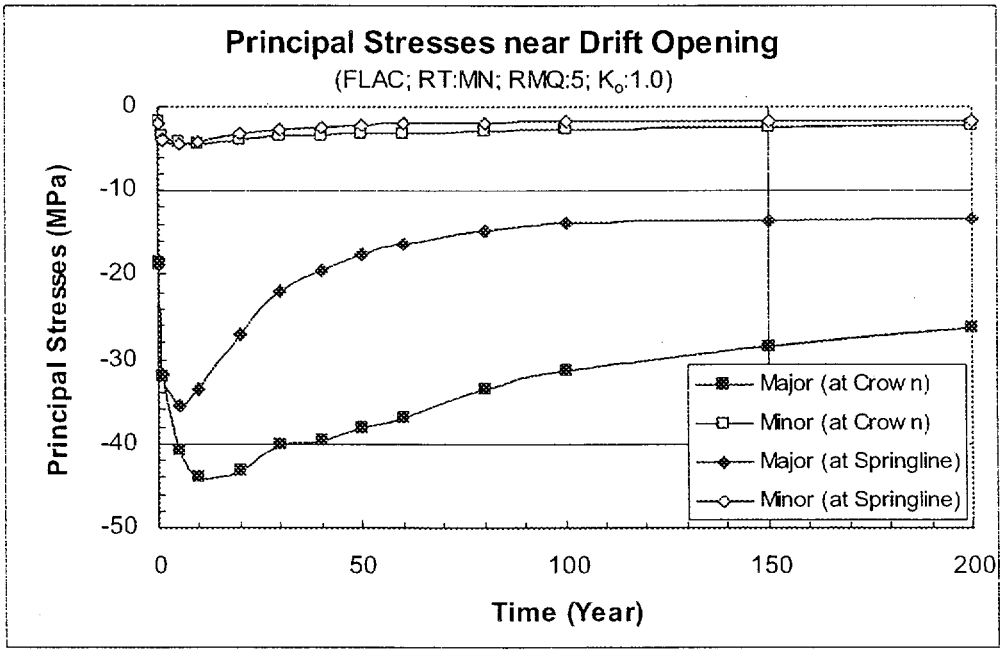

(b)

Figure 6-17. Time Histories of Major and Minor Principal Stresses at Crown and Springline for Non-Lithophysal Rock and RMQ Category 5: (a) K_o=0.3; (b) K_o=1.0

Note: RT=Rock Type; MN=Middle Non-Lithophysal Unit; RMQ=Rock Mass Quality Category; K_o=In Situ Horizontal to Vertical Stress Ratio.

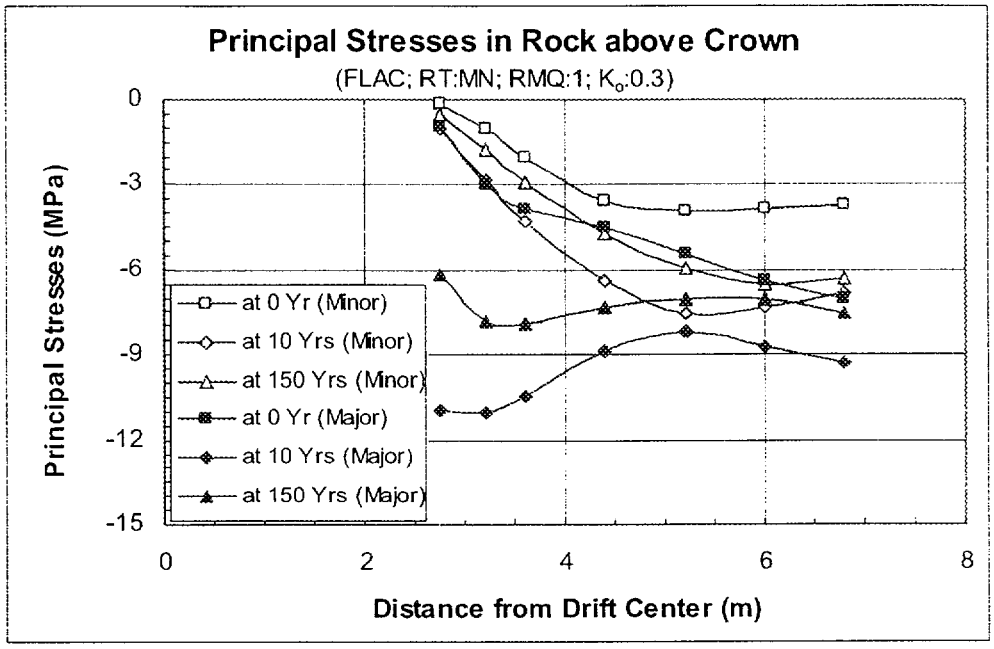

(a)

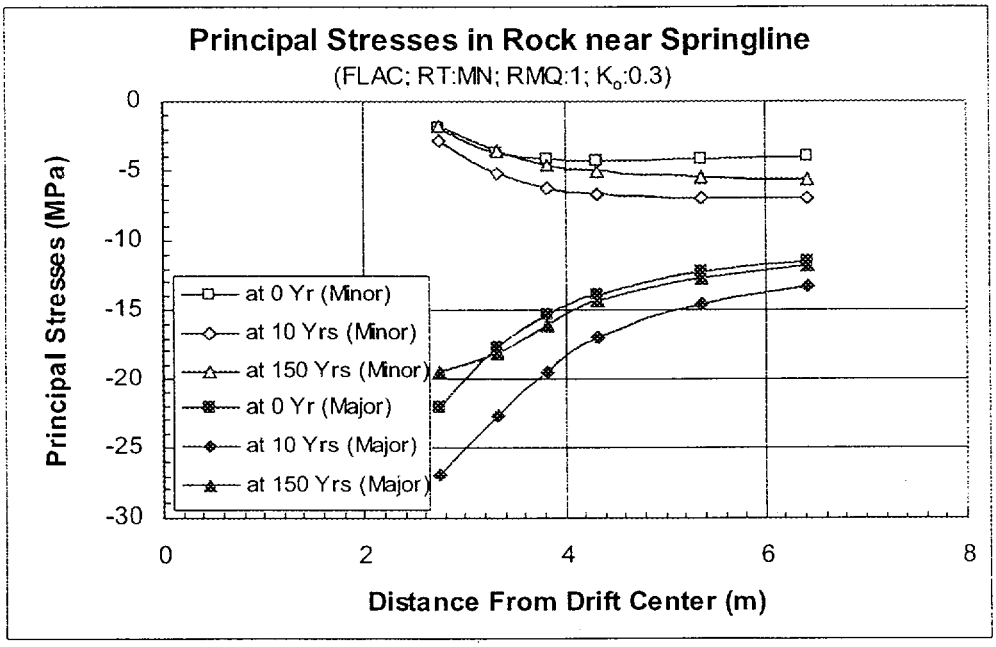

(b)

Figure 6-18. Distributions of Major and Minor Principal Stresses Near Crown and Springline for Non-Lithophysal Rock and RMQ Category 1 and K_o=0.3: (a) Above Crown; (b) Near Springline

Note: RT=Rock Type; MN=Middle Non-Lithophysal Unit; RMQ=Rock Mass Quality Category; K_o=In Situ Horizontal to Vertical Stress Ratio.

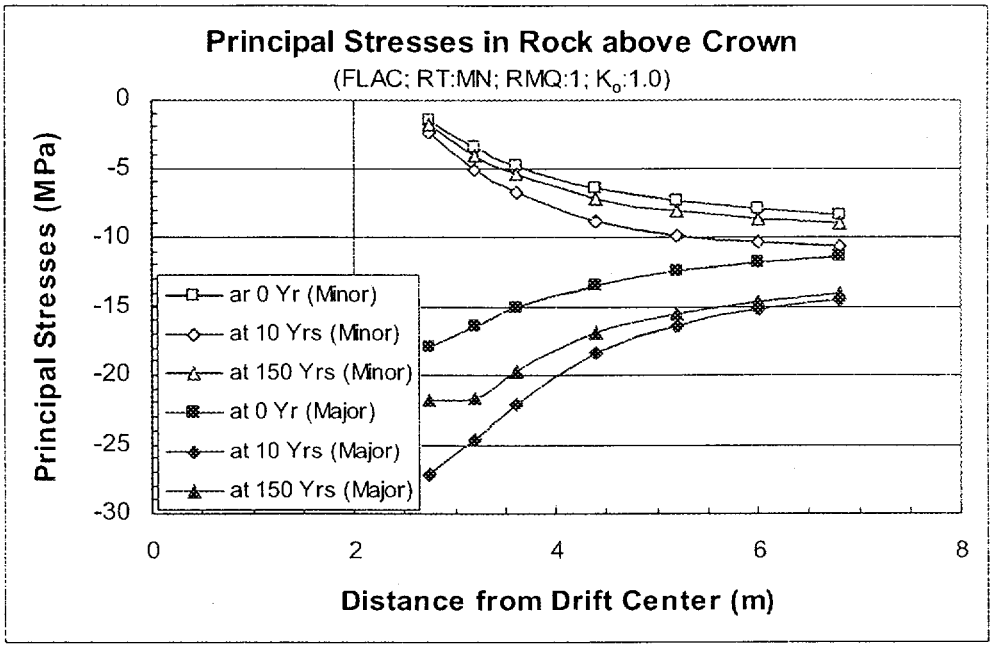

(a)

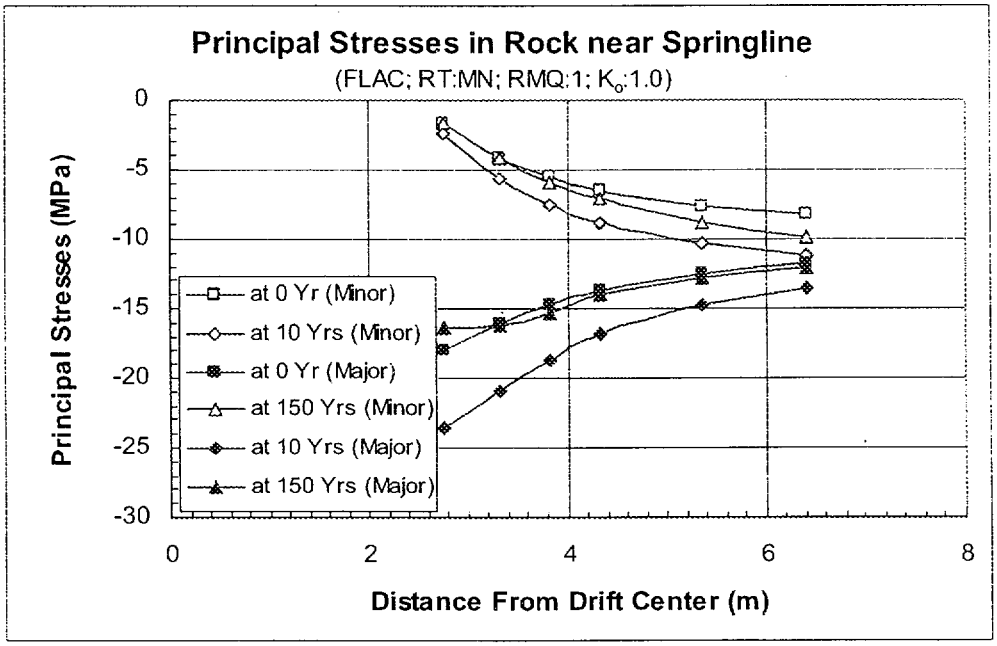

(b)

Figure 6-19. Distributions of Major and Minor Principal Stresses Near Crown and Springline for Non-Lithophysal Rock and RMQ Category 1 and K_o=1.0: (a) Above Crown; (b) Near Springline

Note: RT=Rock Type; MN=Middle Non-Lithophysal Unit; RMQ=Rock Mass Quality Category; K_o=In Situ Horizontal to Vertical Stress Ratio.

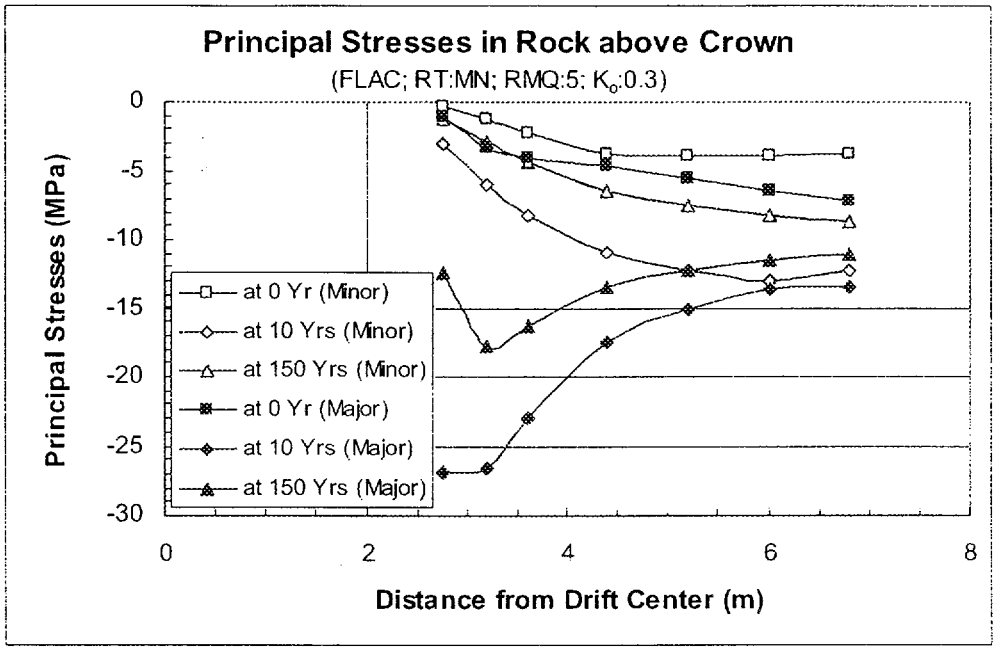

(a)

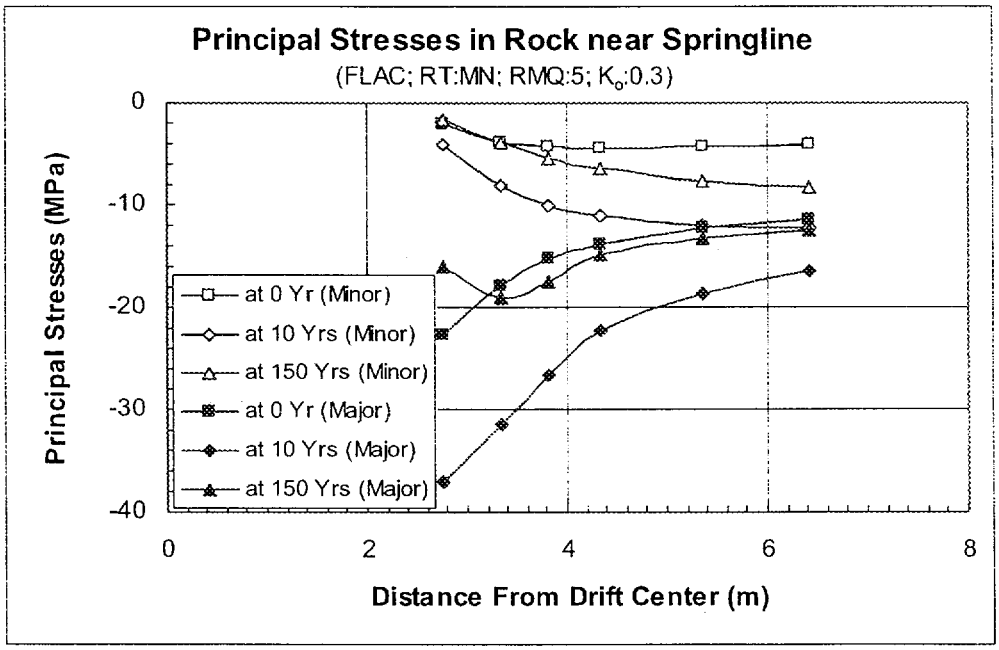

(b)

Figure 6-20. Distributions of Major and Minor Principal Stresses Near Crown and Springline for Non-Lithophysal Rock and RMQ Category 5 and K_o=0.3: (a) Above Crown; (b) Near Springline

Note: RT=Rock Type; MN=Middle Non-Lithophysal Unit; RMQ=Rock Mass Quality Category; K_o=In Situ Horizontal to Vertical Stress Ratio.

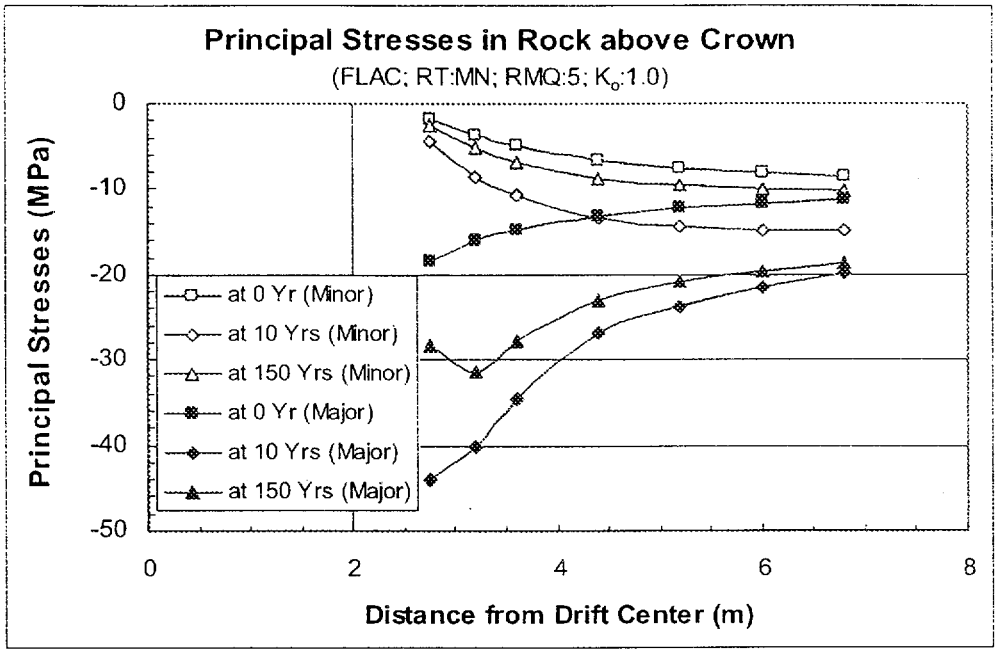

(a)

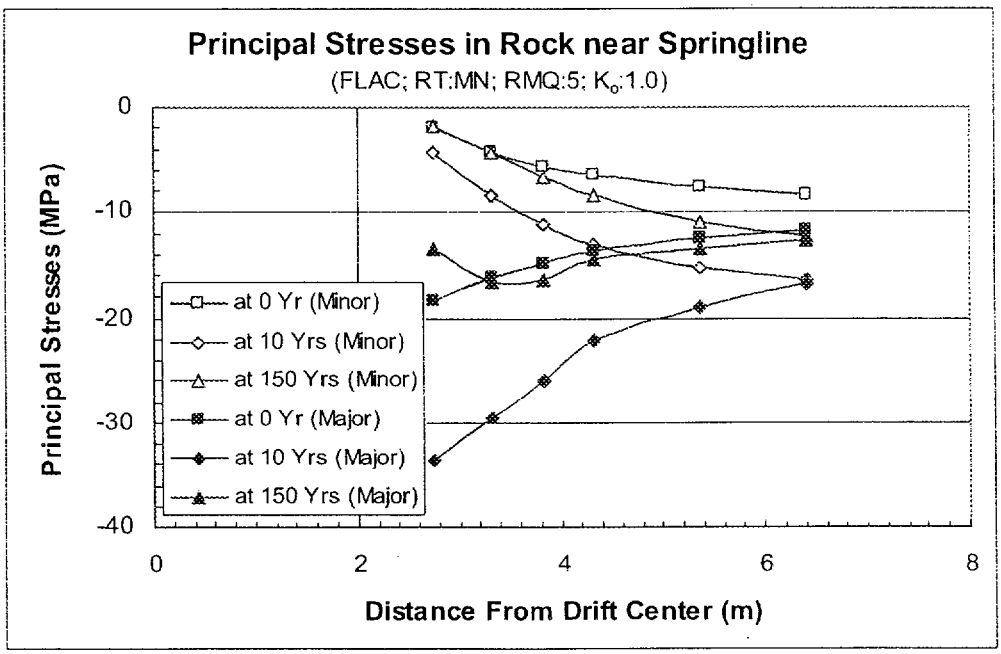

(b)

Figure 6-21. Distributions of Major and Minor Principal Stresses Near Crown and Springline for Non-Lithophysal Rock and RMQ Category 5 and K_o=1.0: (a) Above Crown; (b) Near Springline

Note: RT=Rock Type; MN=Middle Non-Lithophysal Unit; RMQ=Rock Mass Quality Category; K_o=In Situ Horizontal to Vertical Stress Ratio.

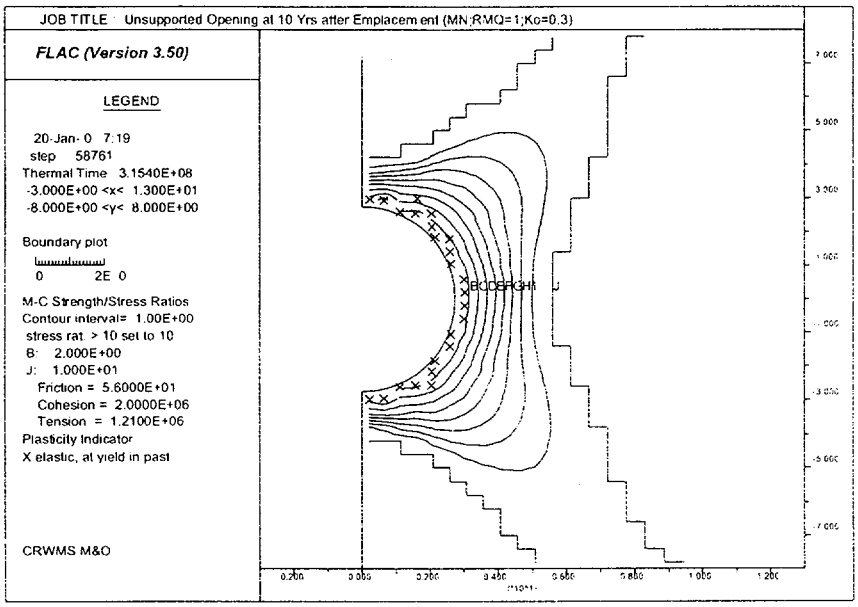

(a)

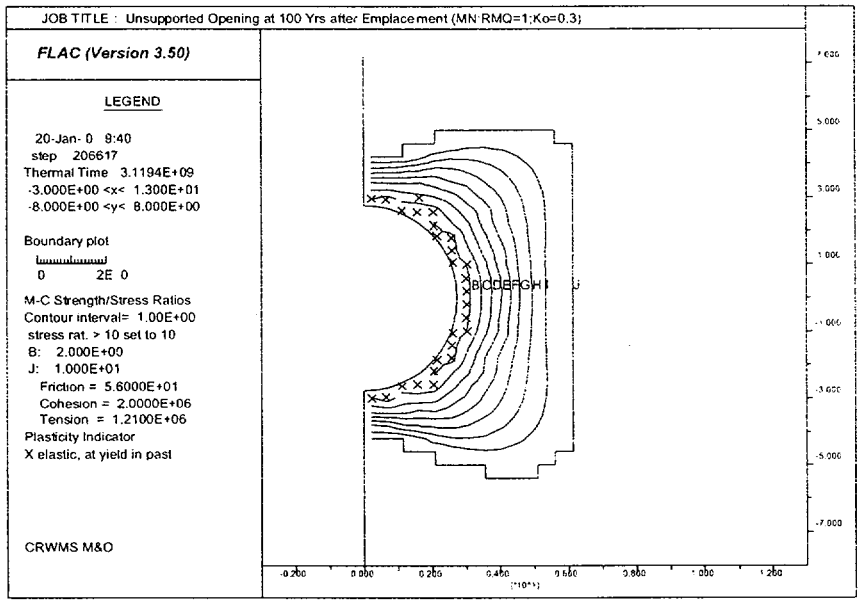

(b)

Figure 6-22. Strength/Stress Ratio Contours and Plasticity Indicators for Unsupported Emplacement Drifts for Combined In Situ Stress and Thermal Loads, RMQ Category 1, and In Situ Stress Ratios K_o of 0.3 and 1.0: (a) at 10 Years After Heating and K_o=0.3; (b) at 100 Years After Heating and K_o=0.3; (c) at 10 Years After Heating and K_o=1.0; (d) at 100 Years After Heating and K_o=1.0

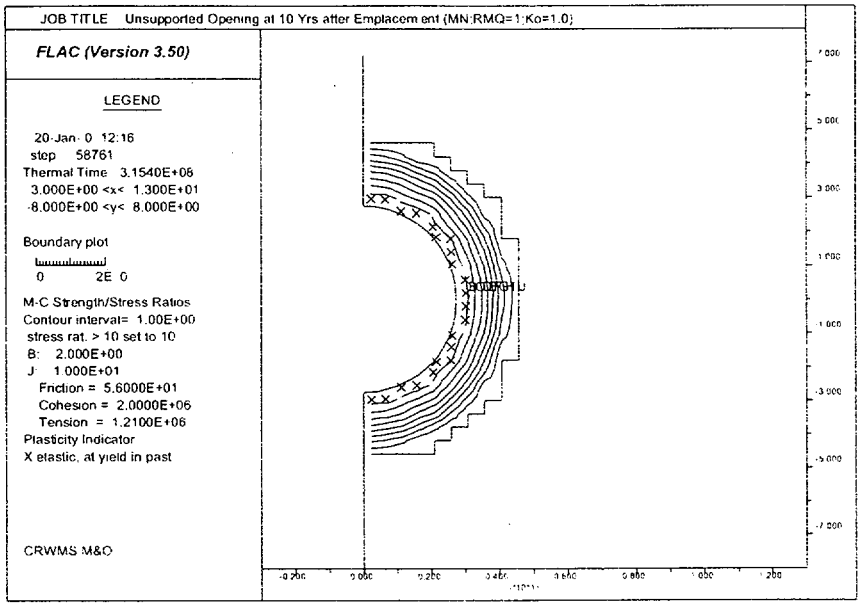

(c)

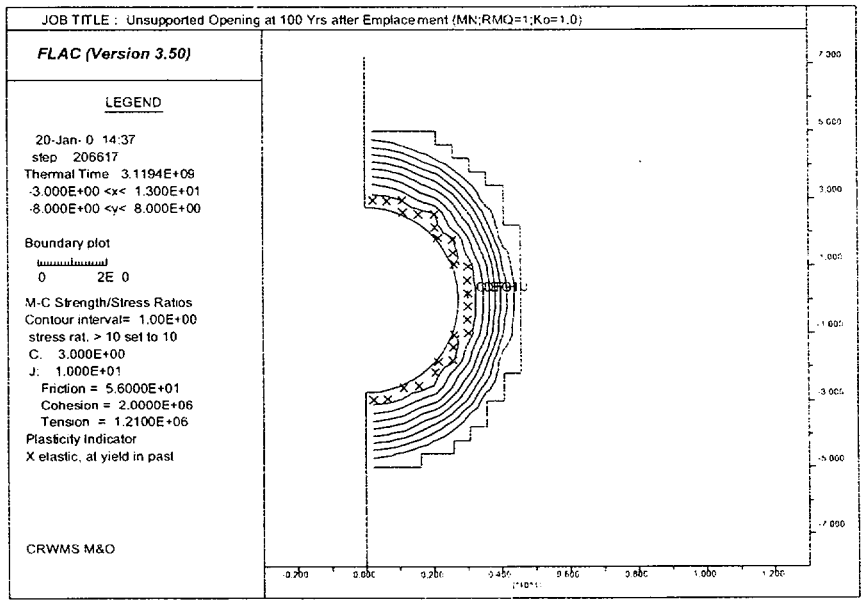

(d)

Figure 6-22 (Continued). Strength/Stress Ratio Contours and Plasticity Indicators for Unsupported Emplacement Drifts for Combined In Situ Stress and Thermal Loads, RMQ Category 1, and In Situ Stress Ratios K_o of 0.3 and 1.0: (a) at 10 Years After Heating and K_o=0.3; (b) at 100 Years After Heating and K_o=0.3; (c) at 10 Years After Heating and K_o=1.0; (d) at 100 Years After Heating and K_o=1.0

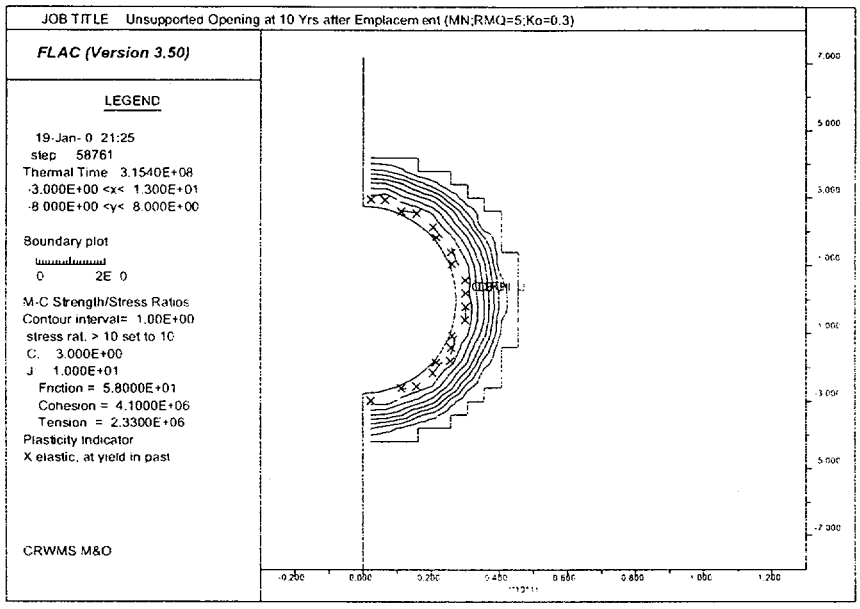

(a)

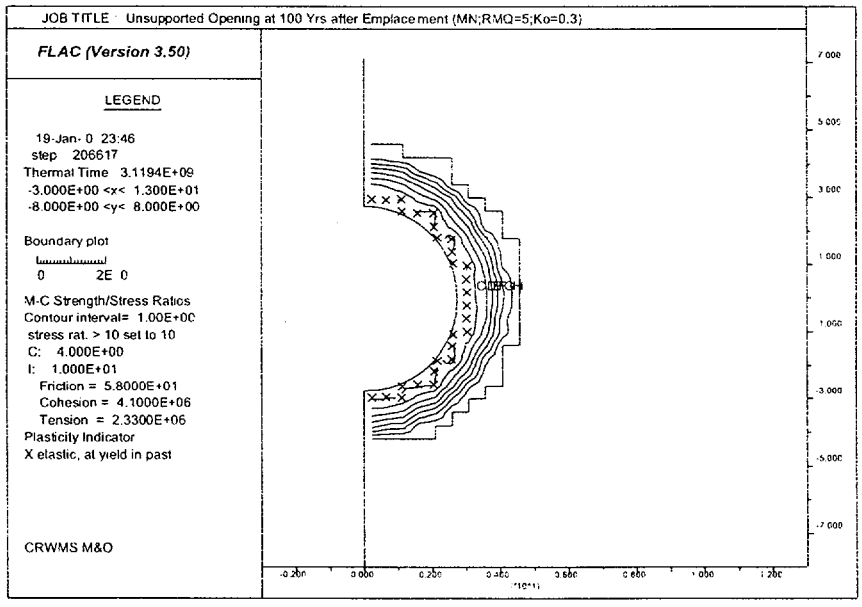

(b)

Figure 6-23. Strength/Stress Ratio Contours and Plasticity Indicators for Unsupported Emplacement Drifts for Combined In Situ Stress and Thermal Loads, RMQ Category 5, and In Situ Stress Ratios K_o of 0.3 and 1.0: (a) at 10 Years After Heating and K_o=0.3; (b) at 100 Years After Heating and K_o=0.3; (c) at 10 Years After Heating and K_o=1.0; (d) at 100 Years After Heating and K_o=1.0

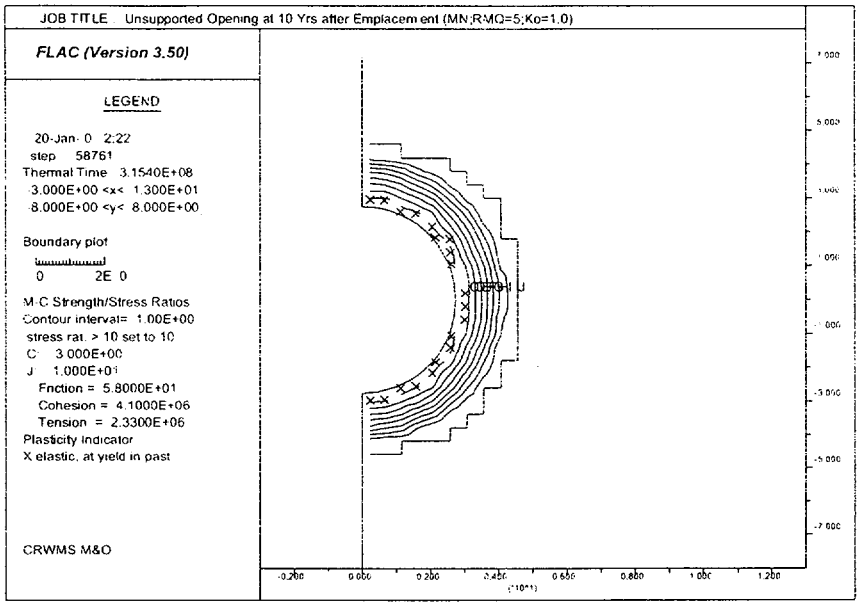

(c)

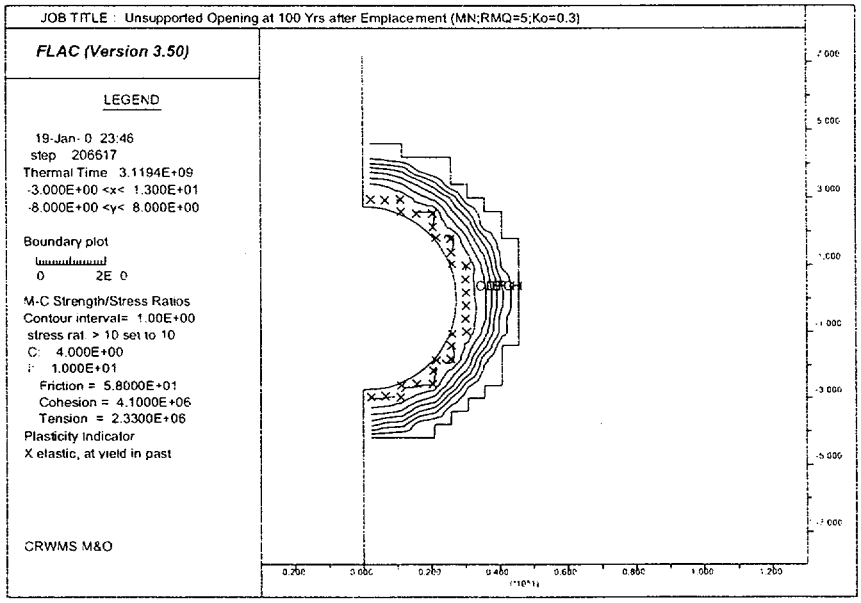

(d)

Figure 6-23 (Continued). Strength/Stress Ratio Contours and Plasticity Indicators for Unsupported Emplacement Drifts for Combined In Situ Stress and Thermal Loads, RMQ Category 5, and In Situ Stress Ratios K_o of 0.3 and 1.0: (a) at 10 Years After Heating and K_o=0.3; (b) at 100 Years After Heating and K_o=0.3; (c) at 10 Years After Heating and K_o=1.0; (d) at 100 Years After Heating and K_o=1.0

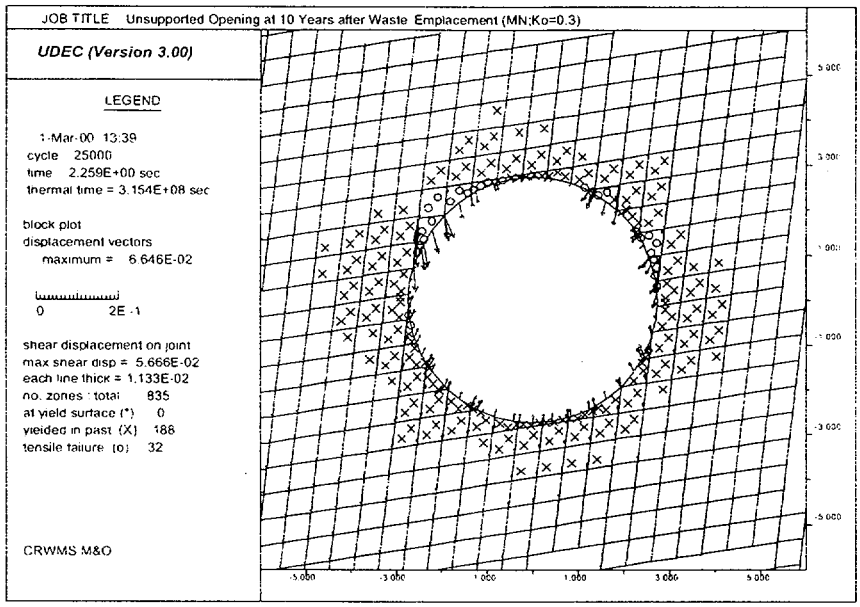

(a)

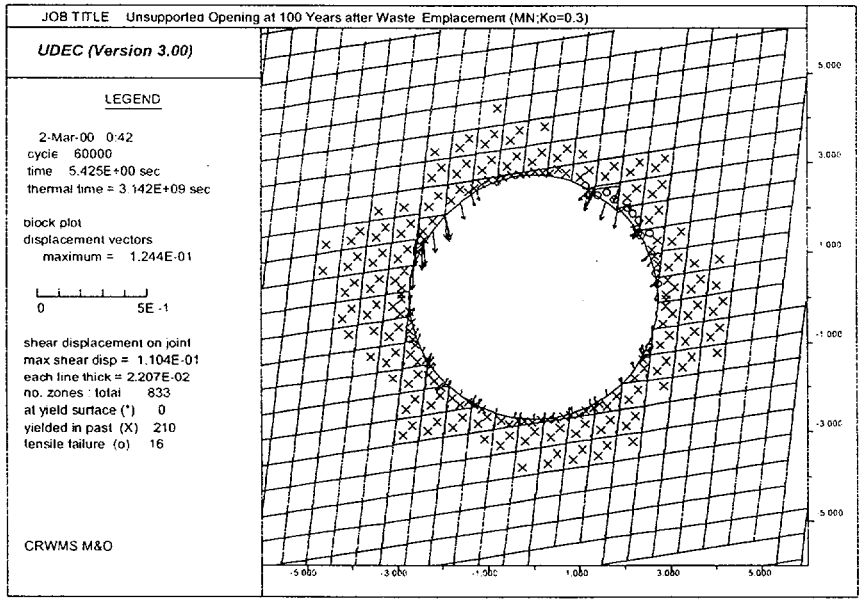

(b)

Figure 6-24. Rock Block Displacements, Shear Displacement on Joints, and Failure Zone Development Around an Emplacement Drift in Non-Lithophysal Rock Under Combined In Situ Stress and Thermal Loads for K_o=0.3: (a) at 10 Years After Heating; (b) at 100 Years After Heating

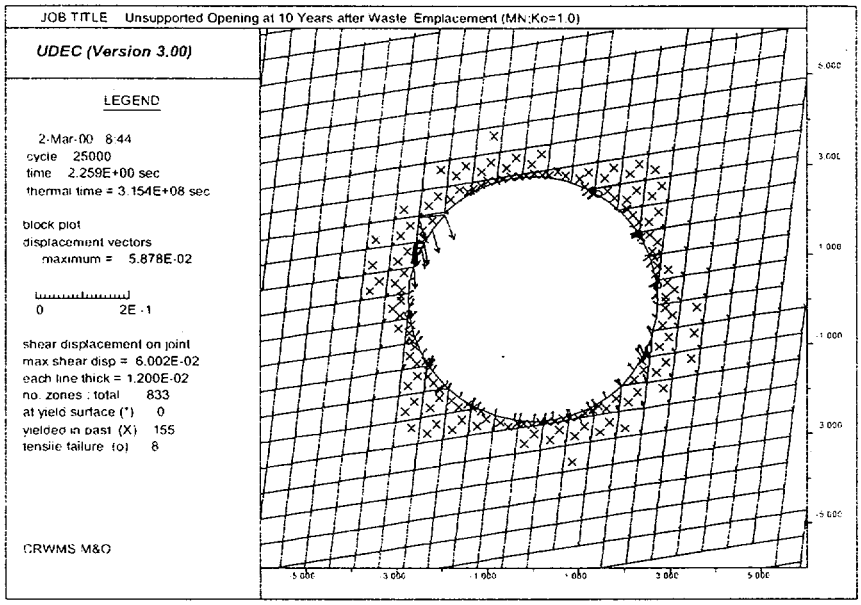

(a)

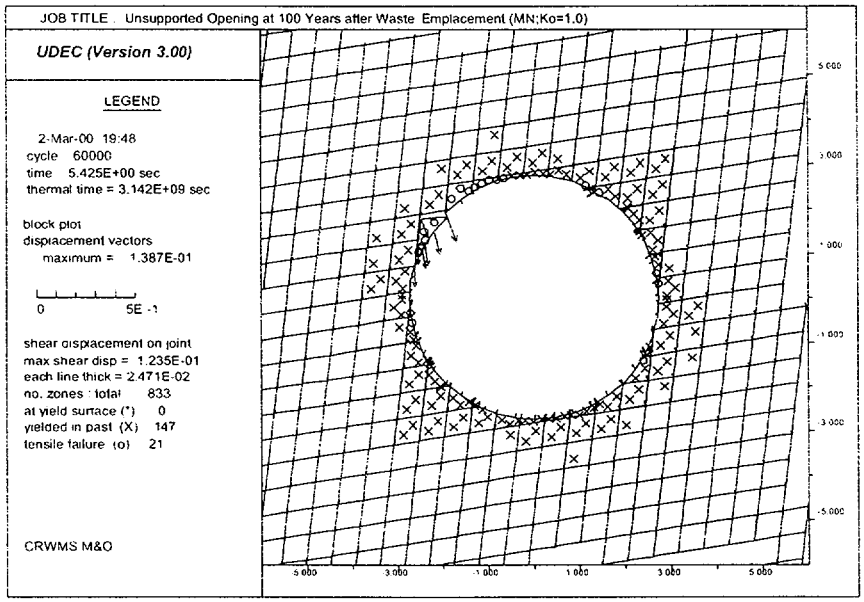

(b)

Figure 6-25. Rock Block Displacements, Shear Displacement on Joints, and Failure Zone Development Around an Emplacement Drift in Non-Lithophysal Rock Under Combined In Situ Stress and Thermal Loads for K_o=1.0: (a) at 10 Years After Heating; (b) at 100 Years After Heating

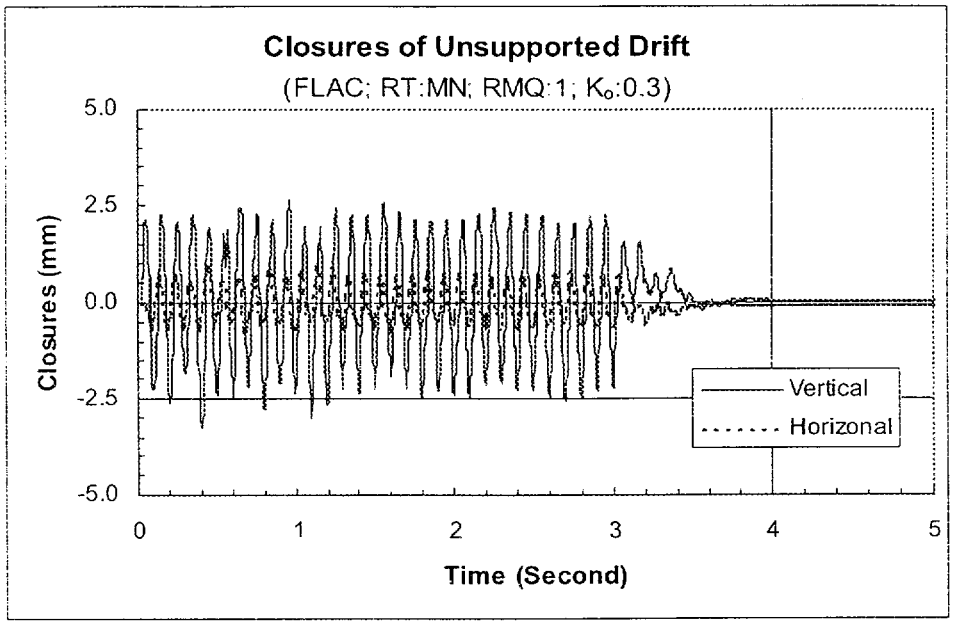

(a)

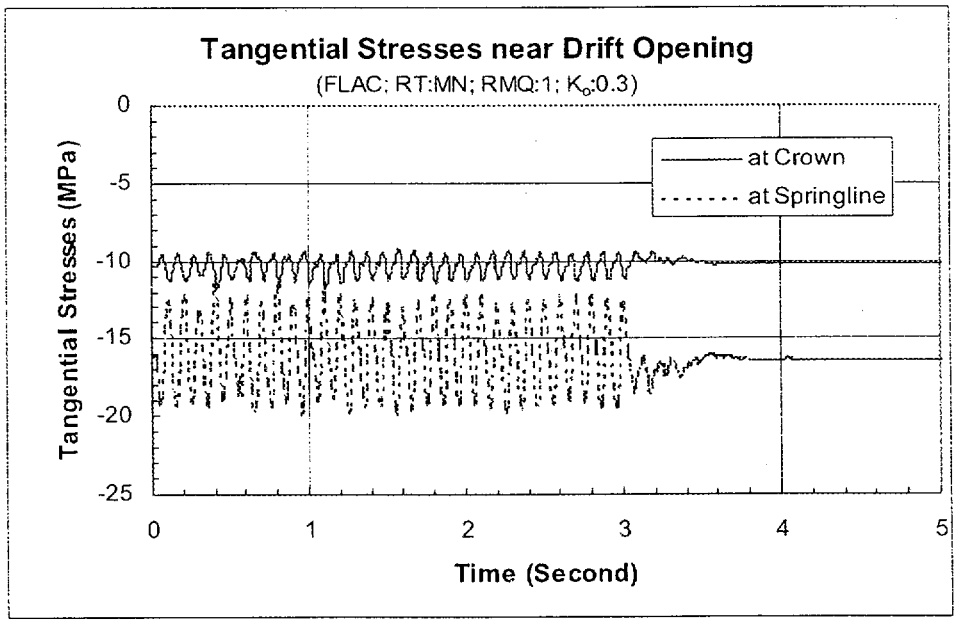

(b)

Figure 6-26. Drift Closures and Stresses Under In Situ, Thermal, and Seismic Loads RMQ Category 1 and K_o=0.3: (a) Dynamic Closures Induced by Seismic Load Only; (b) Tangential Stresses at Crown and Springline After 20-Year Heating and 3-Second Seismic Motion

Note: RT=Rock Type; MN=Middle Non-lithophysal Unit; RMQ=Rock Mass Quality Category; K_o=In Situ Horizontal to Vertical Stress Ratio.

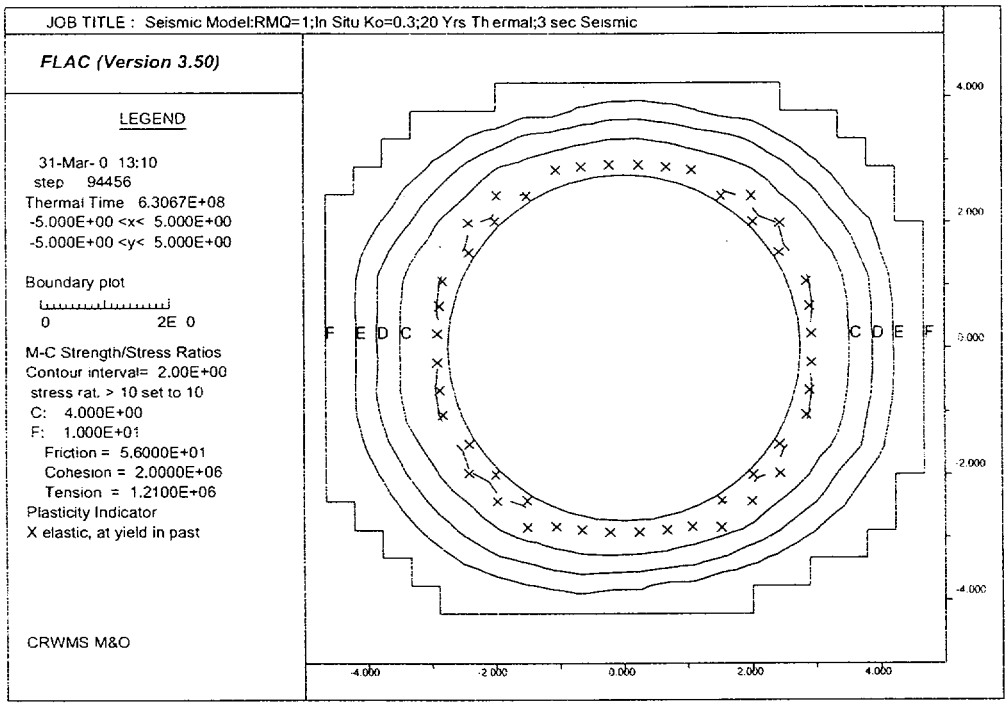

Figure 6-27. Strength/Stress Ratios for Unsupported Emplacement Drifts Under In Situ, Thermal, and Seismic Loads for RMQ Category 1 and K_o=0.3 after 20-Year Heating and 3-Second Seismic Motion

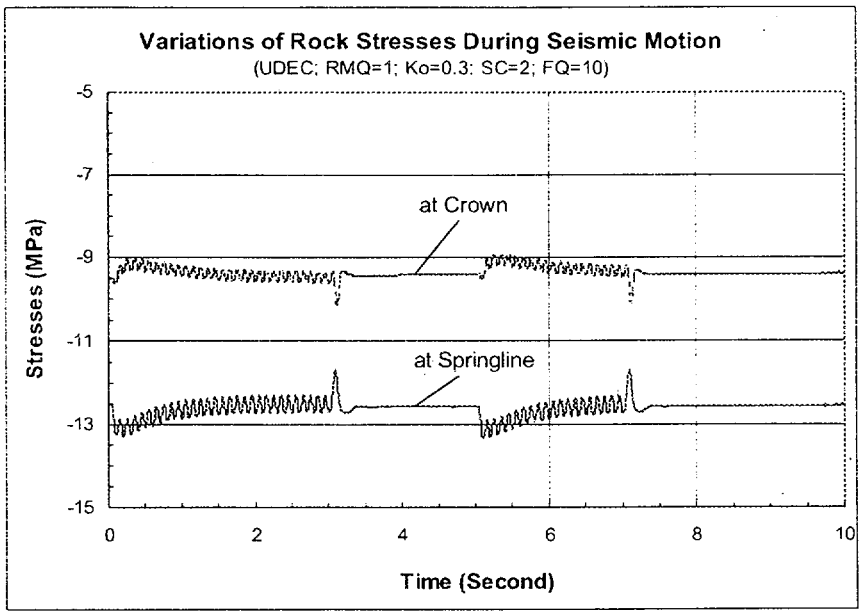

(a)

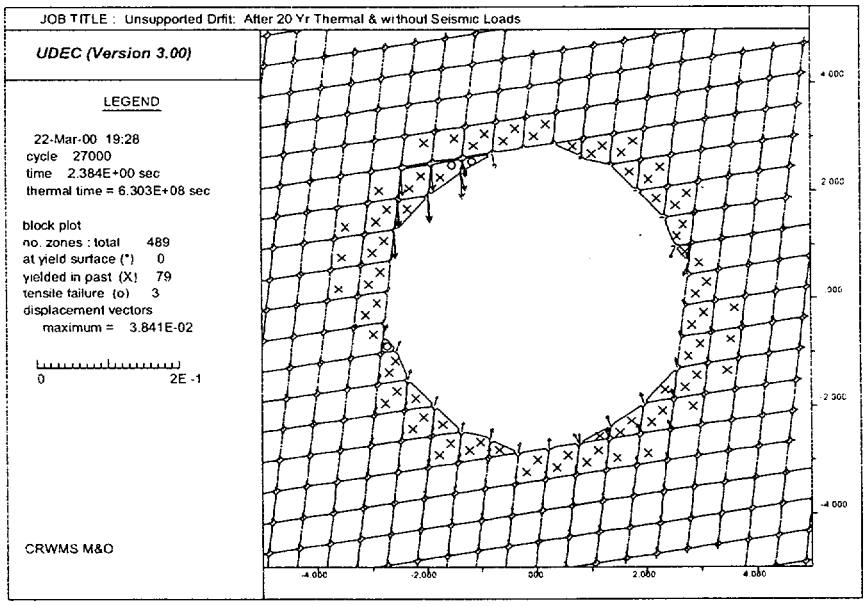

(b)

Figure 6-28. Rock Stress Variations, Block Displacements, and Failure Zone Development Around an Emplacement Drift in Non-Lithophysal Rock Under In Situ and Thermal Loads With and Without Seismic Events for RMQ=1 and K_o=0.3: (a) Stress Variations During Seismic Events; (b) Displacements and Failure Zone Development Before Seismic Events; (c) Displacements and Failure Zone Development After One Seismic Event; (d) Displacements and Failure Zone Development After Two Seismic Events

Note: SC=Seismic Frequency Category; FQ=Seismic Velocity Frequency.

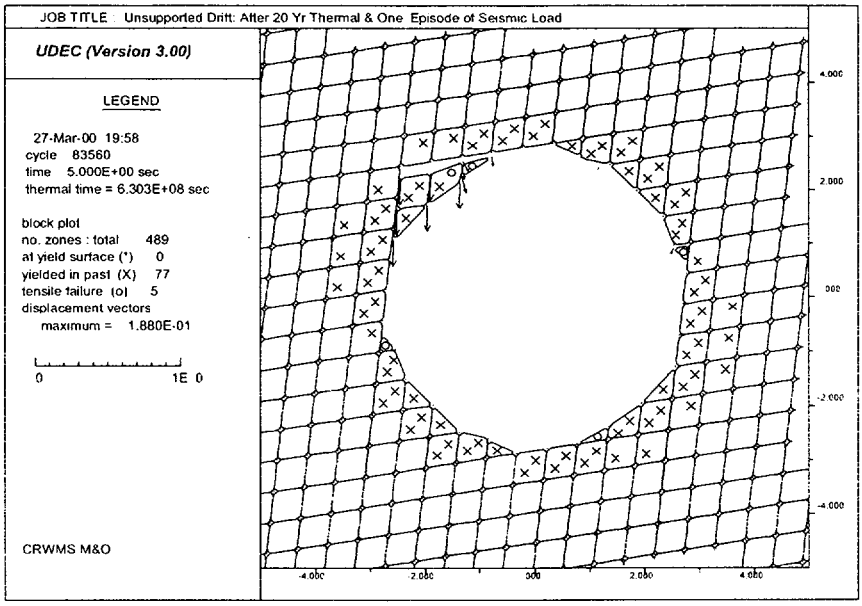

(c)

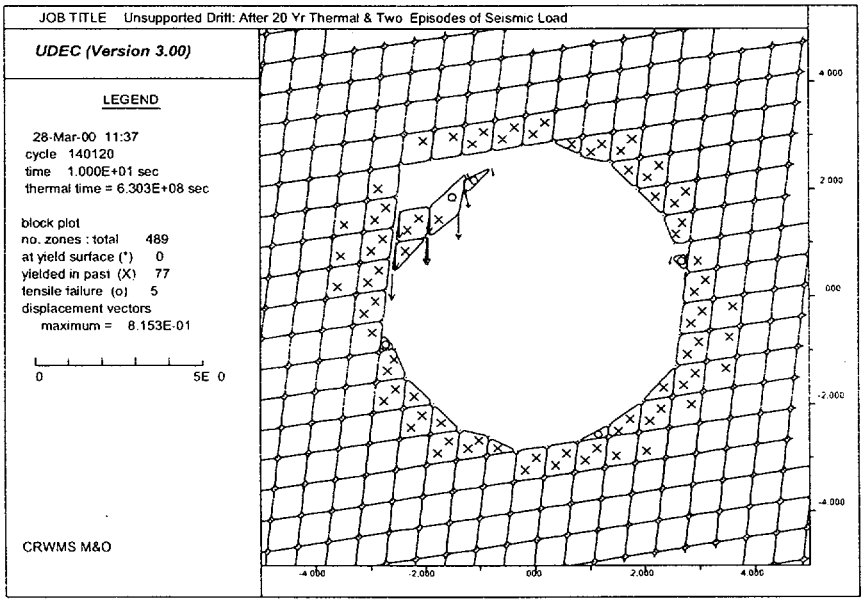

(d)

Figure 6-28 (Continued). Rock Stress Variations, Block Displacements, and Failure Zone Development Around an Emplacement Drift in Non-Lithophysal Rock Under In Situ and Thermal Loads With and Without Seismic Events for RMQ=1 and K_o=0.3: (a) Stress Variations During Seismic Events; (b) Displacements and Failure Zone Development Before Seismic Events; (c) Displacements and Failure Zone Development After One Seismic Event; (d) Displacements and Failure Zone Development After Two Seismic Events

Note: SC=Seismic Frequency Category; FQ=Seismic Velocity Frequency.

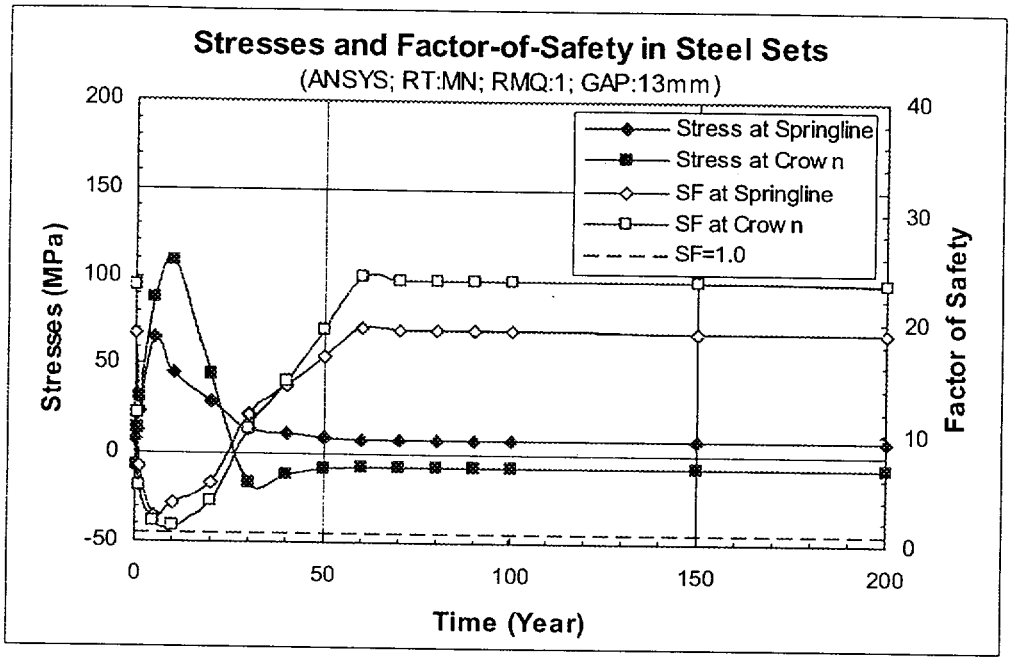

(a)

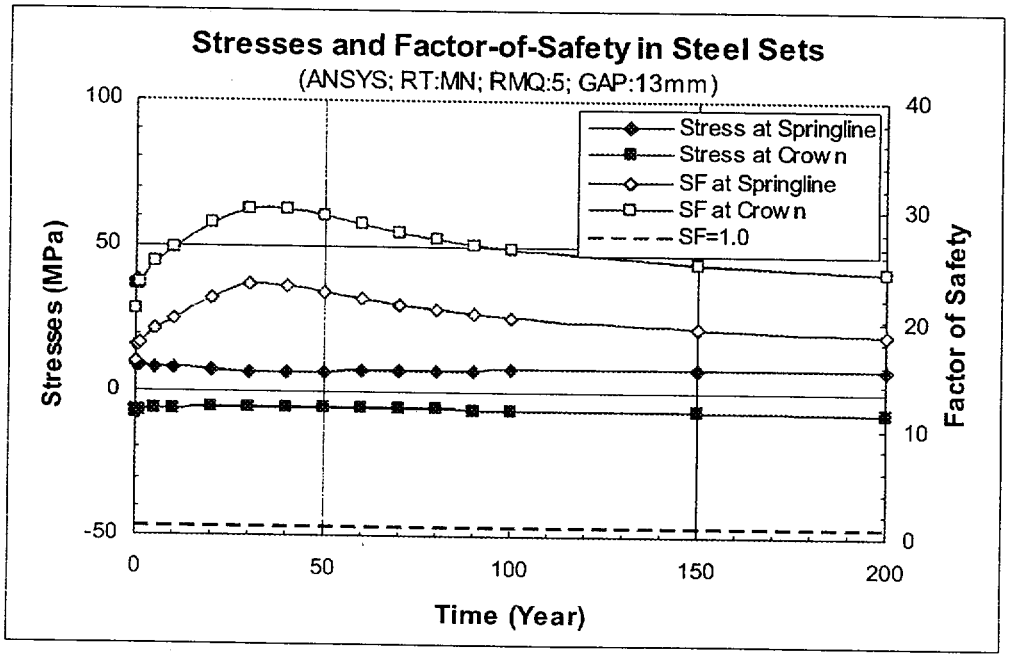

(b)

Figure 6-29. Time Histories of Stresses and Factor-of-Safety at Crown and Springline of Steel Sets With an Initial Gap of 13 mm for RMQ Categories 1 and 5: (a) RMQ=1; (b) RMQ=5

Note: RT=Rock Type; MN=Middle Non-lithophysal Unit; RMQ=Rock Mass Quality Category.

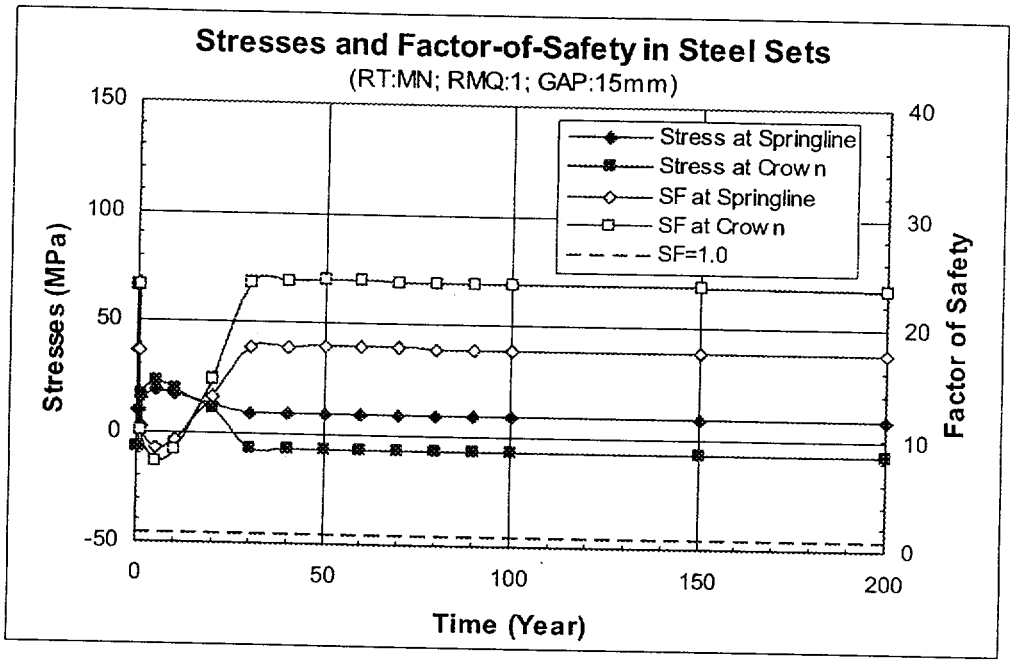

(a)

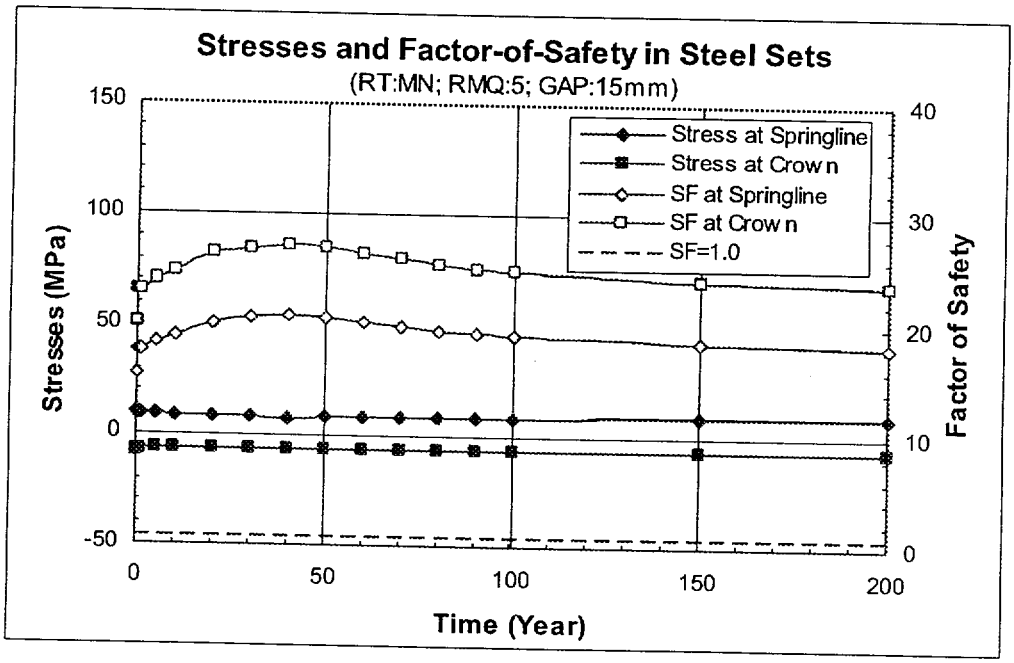

(b)

Figure 6-30. Time Histories of Stresses and Factor-of-Safety at Crown and Springline of Steel Sets With an Initial Gap of 15 mm for RMQ Categories 1 and 5: (a) RMQ=1; (b) RMQ=5

Note: RT=Rock Type; MN=Middle Non-lithophysal Unit; RMQ=Rock Mass Quality Category.

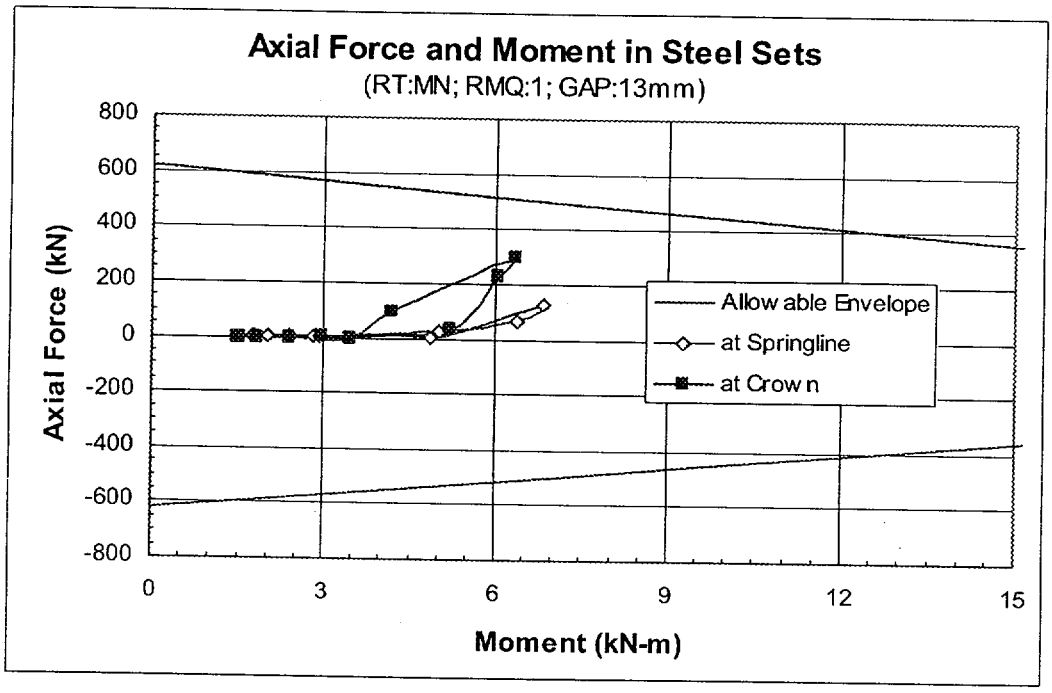

Figure 6-31. Axial Force and Moment Diagram for Steel Sets With an Initial Gap of 13 mm for RMQ Category 1

Note: RT=Rock Type; MN=Middle Non-lithophysal Unit; RMQ=Rock Mass Quality Category.

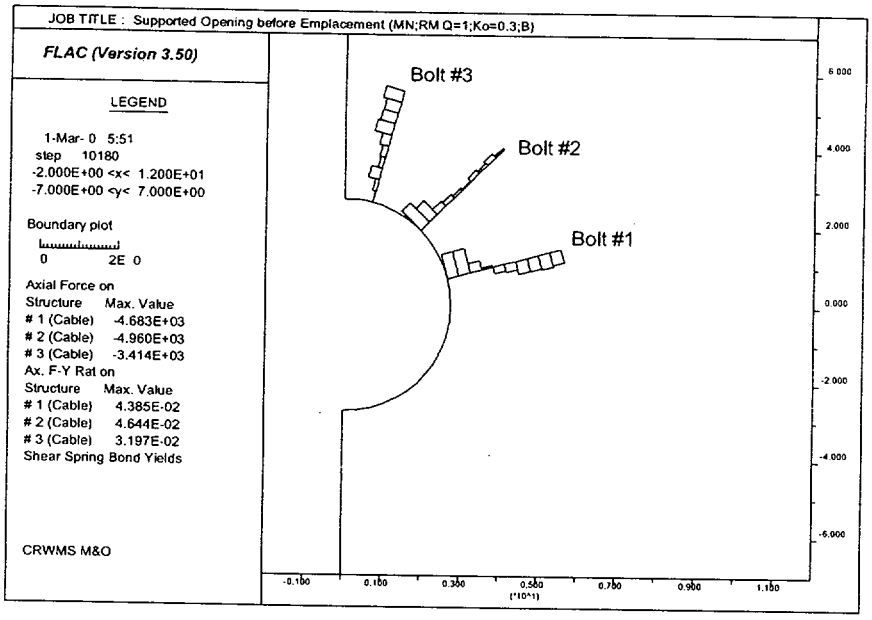

(a)

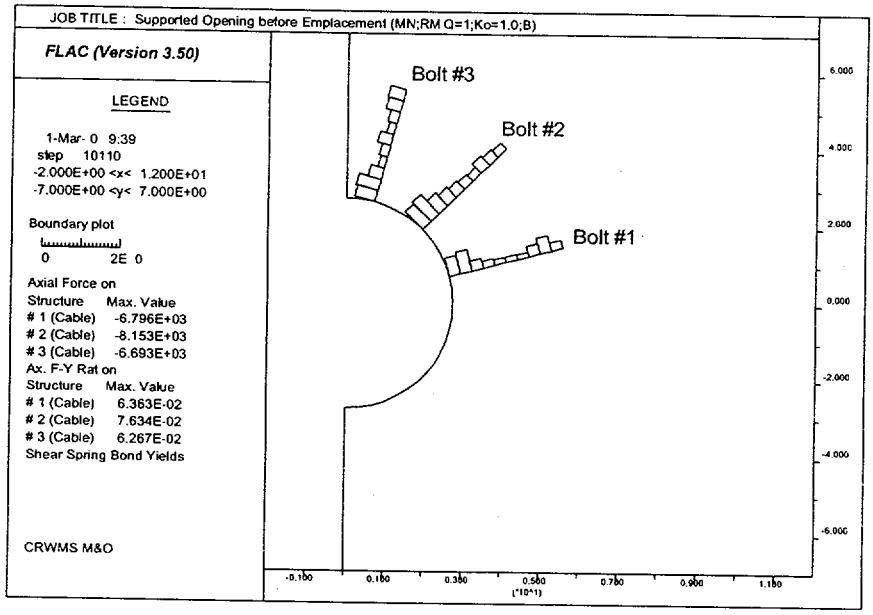

(b)

Figure 6-32. Distributions of Axial Force Along Rock Bolts for Emplacement Drift in Non-Lithophysal Rock Under In Situ Load for Different RMQ Categories and K_o: (a) RMQ=1 and K_o=0.3; (b) RMQ=1 and K_o=1.0; (c) RMQ=5 and K_o=0.3; (d) RMQ=5 and K_o=1.0

Note: MN=Middle Non-lithophysal Unit; B=Bolt.

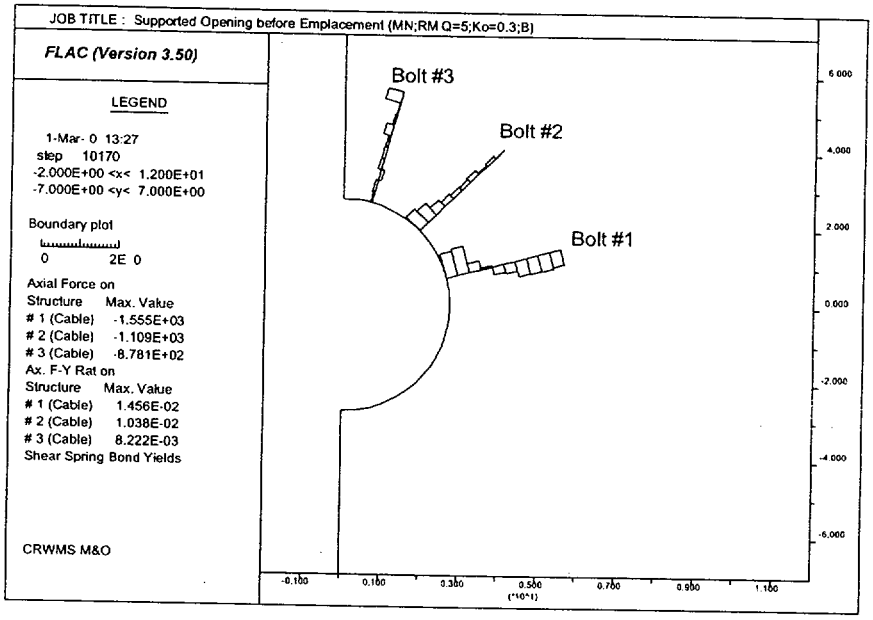

(c)

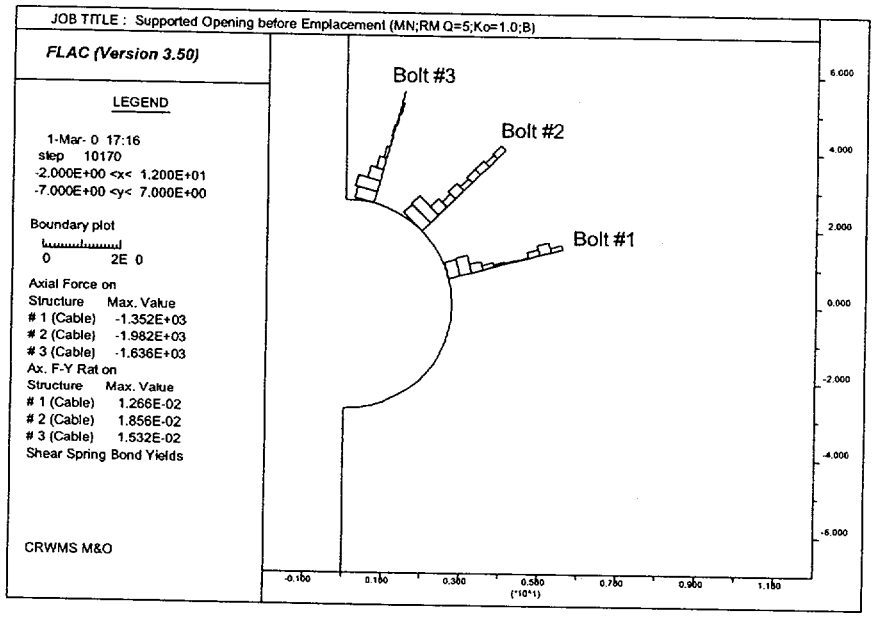

(d)

Figure 6-32 (Continued). Distributions of Axial Force Along Rock Bolts for Emplacement Drift in Non-Lithophysal Rock Under In Situ Load for Different RMQ Categories and K_o: (a) RMQ=1 and K_o=0.3; (b) RMQ=1 and K_o=1.0; (c) RMQ=5 and K_o=0.3; (d) RMQ=5 and K_o=1.0

Note: MN=Middle Non-lithophysal Unit; B=Bolt.

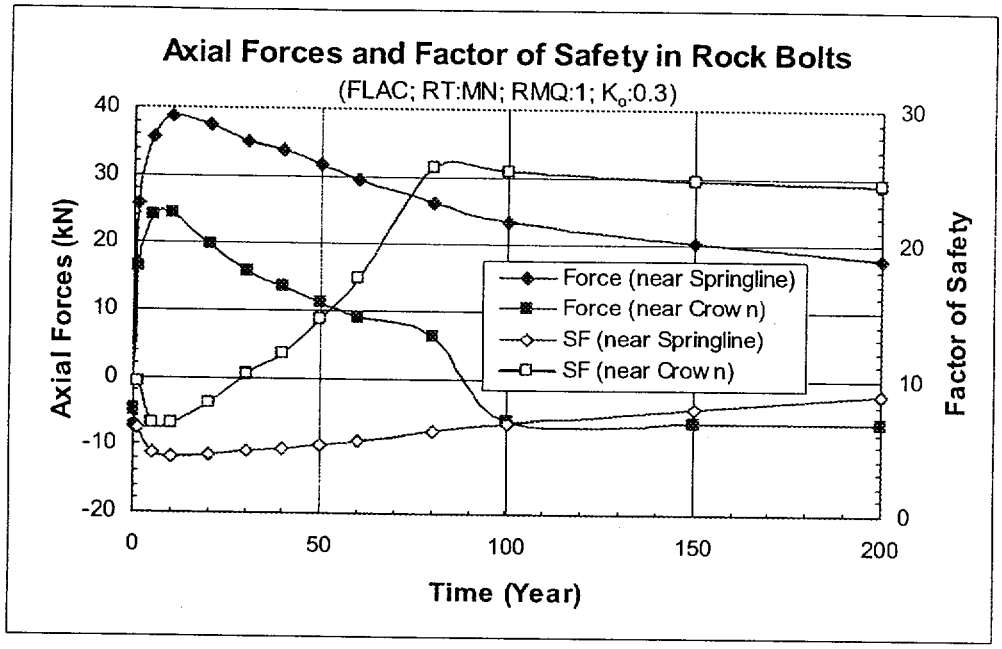

(a)

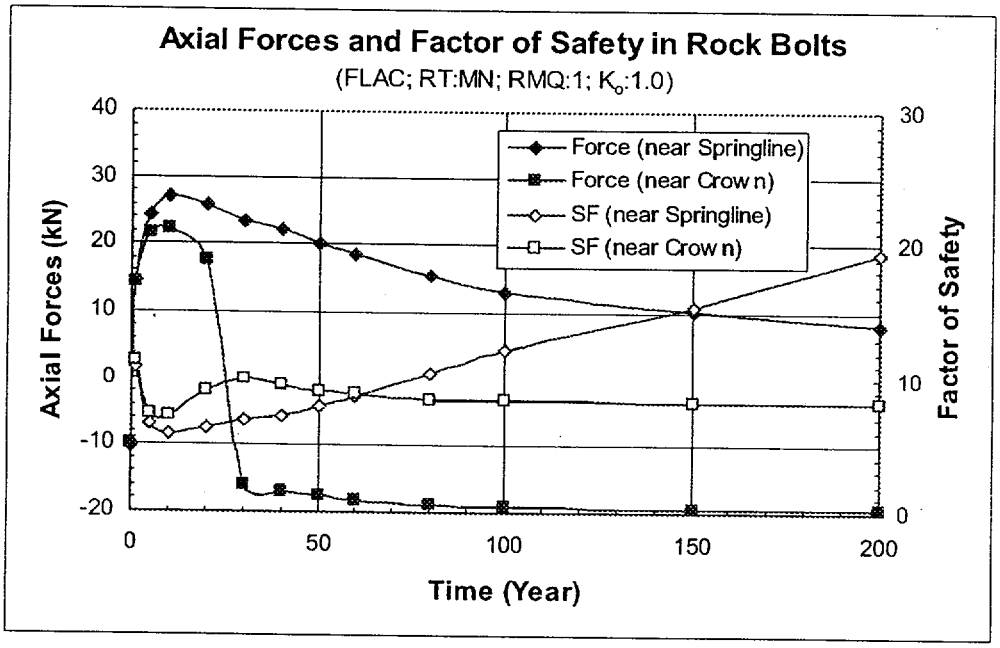

(b)

Figure 6-33. Time Histories of Axial Forces and Factor-of-Safety in Rock Bolts Near Crown and Springline of Emplacement Drifts for RMQ Category 1 and Different K_o: (a) K_o=0.3; (b) K_o=1.0

Note: RT=Rock Type; MN=Middle Non-lithophysal Unit; RMQ=Rock Mass Quality Category.

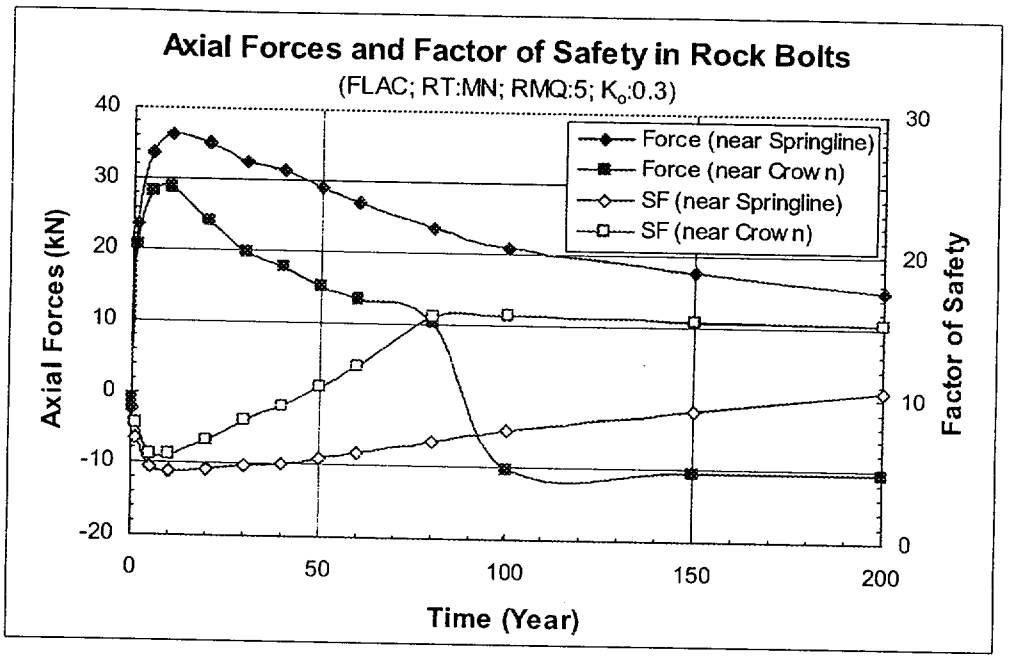

(a)

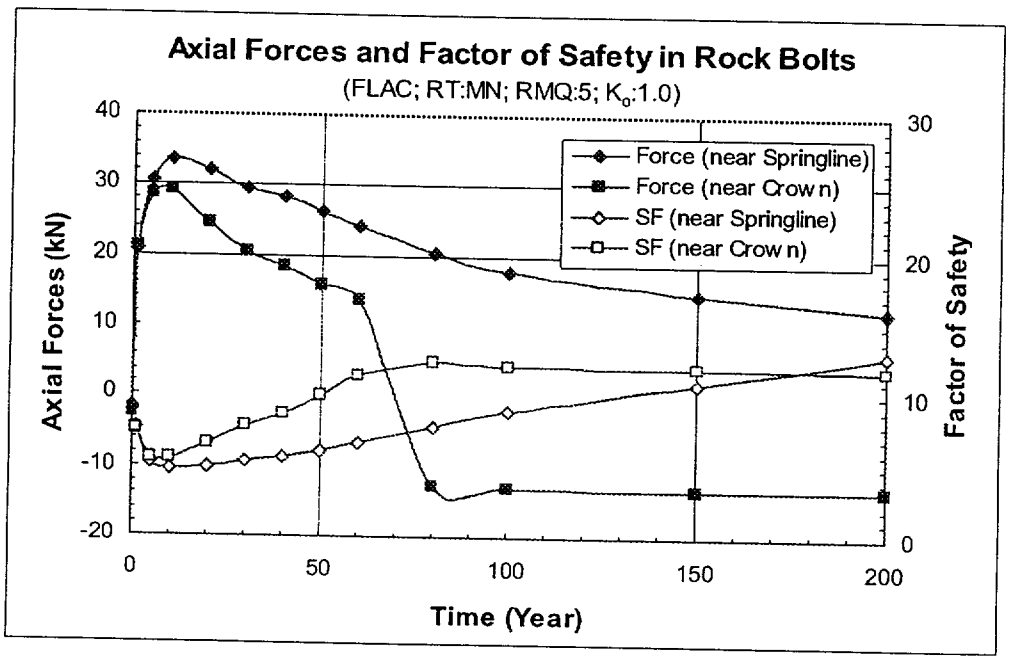

(b)

Figure 6-34. Time Histories of Axial Forces and Factor-of-Safety in Rock Bolts Near Crown and Springline of Emplacement Drifts for RMQ Category 5 and Different K_o: (a) K_o=0.3; (b) K_o=1.0

Note: RT=Rock Type; MN=Middle Non-lithophysal Unit; RMQ=Rock Mass Quality Category.

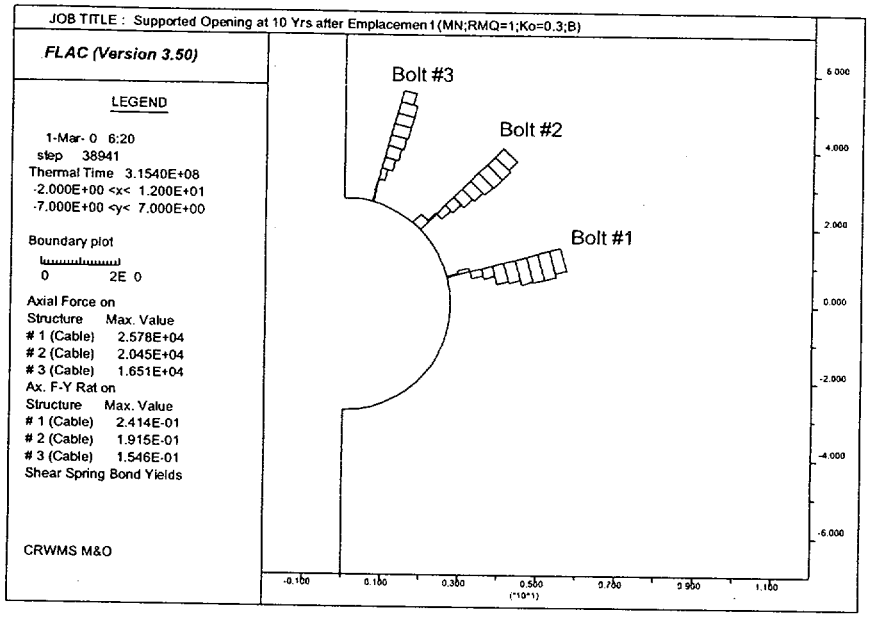

(a)

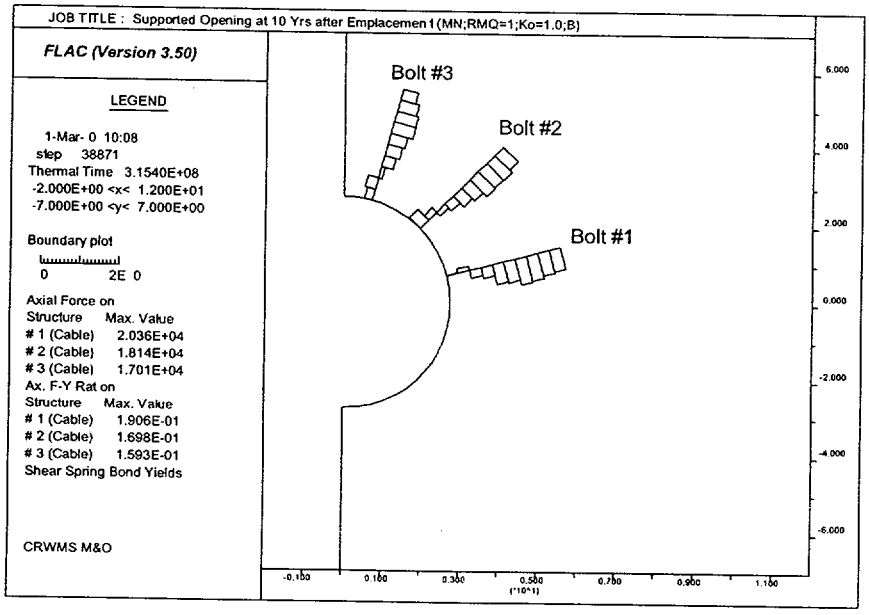

(b)

Figure 6-35. Distributions of Axial Force Along Rock Bolts for Emplacement Drift in Non-lithophysal Rock Under Combined In Situ and Thermal Loads for Different RMQ Categories and K_o: (a) RMQ=1 and K_o=0.3; (b) RMQ=1 and K_o=1.0; (c) RMQ=5 and K_o=0.3; (d) RMQ=5 and K_o=1.0

Note: MN=Middle Non-lithophysal Unit; B=Bolt.

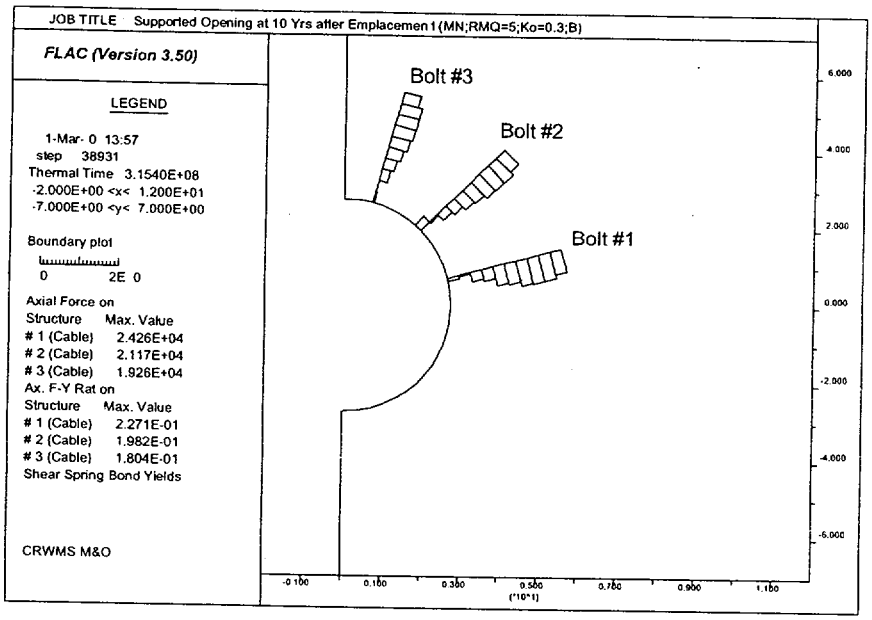

(c)

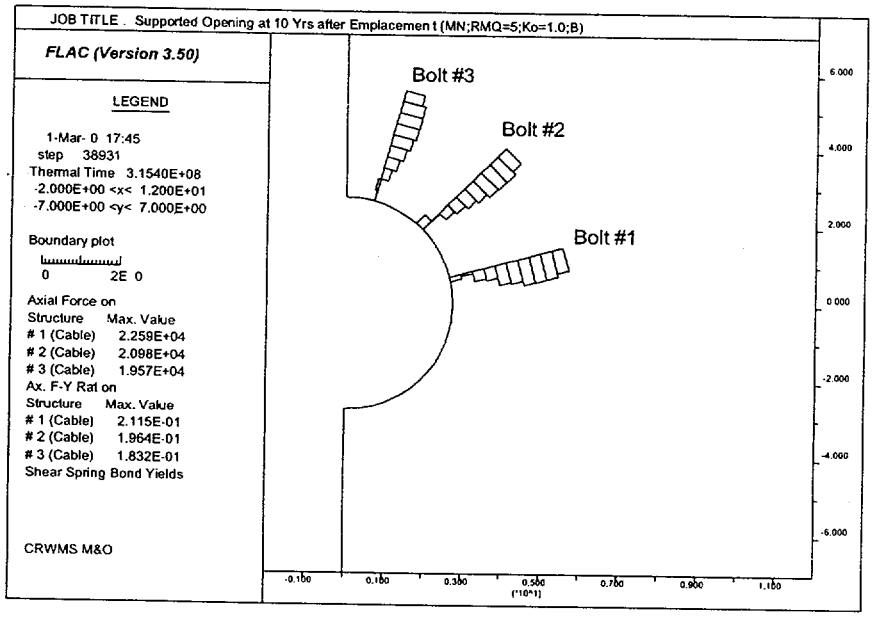

(d)

Figure 6-35 (Continued). Distributions of Axial Force Along Rock Bolts for Emplacement Drift in Non-lithophysal Rock Under Combined In Situ and Thermal Loads for Different RMQ Categories and K_o: (a) RMQ=1 and K_o=0.3; (b) RMQ=1 and K_o=1.0; (c) RMQ=5 and K_o=0.3; (d) RMQ=5 and K_o=1.0

Note: MN=Middle Non-lithophysal Unit; B=Bolt.

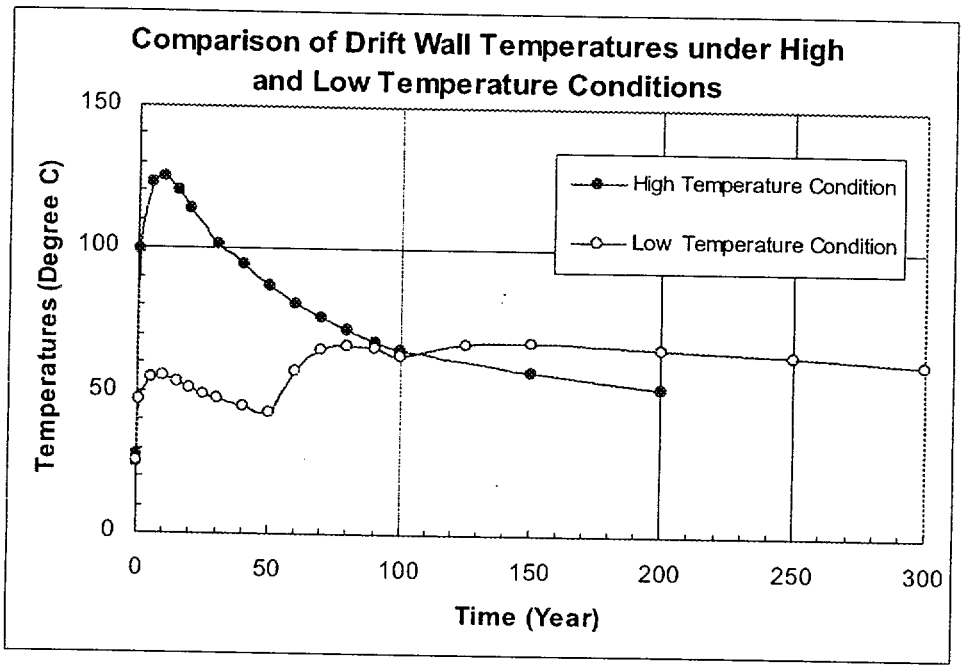

Figure 6-36. Comparison of Drift Wall Temperatures under High and Low Temperature Conditions

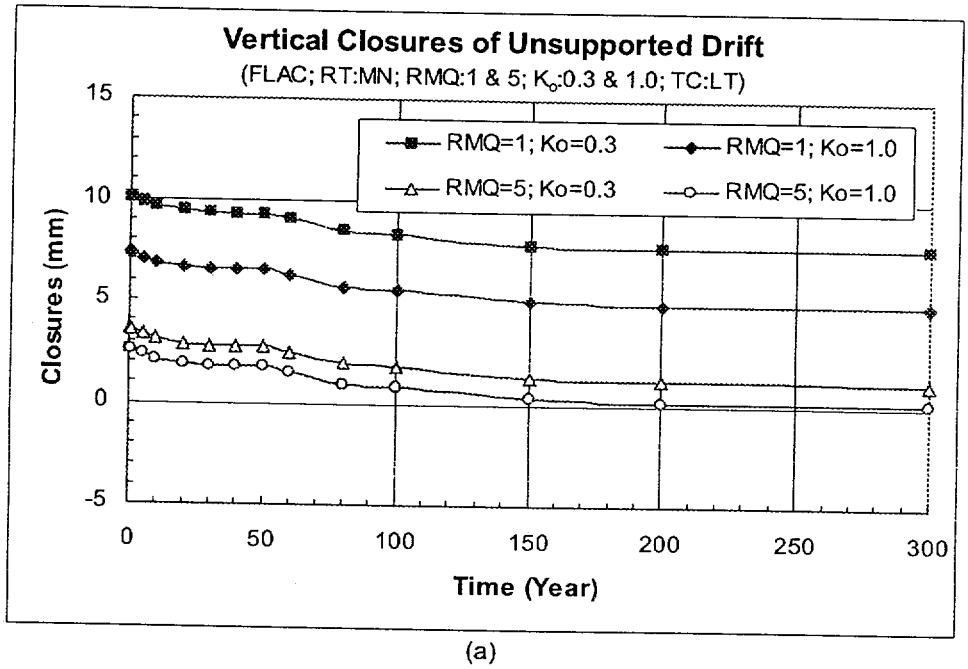

(a)

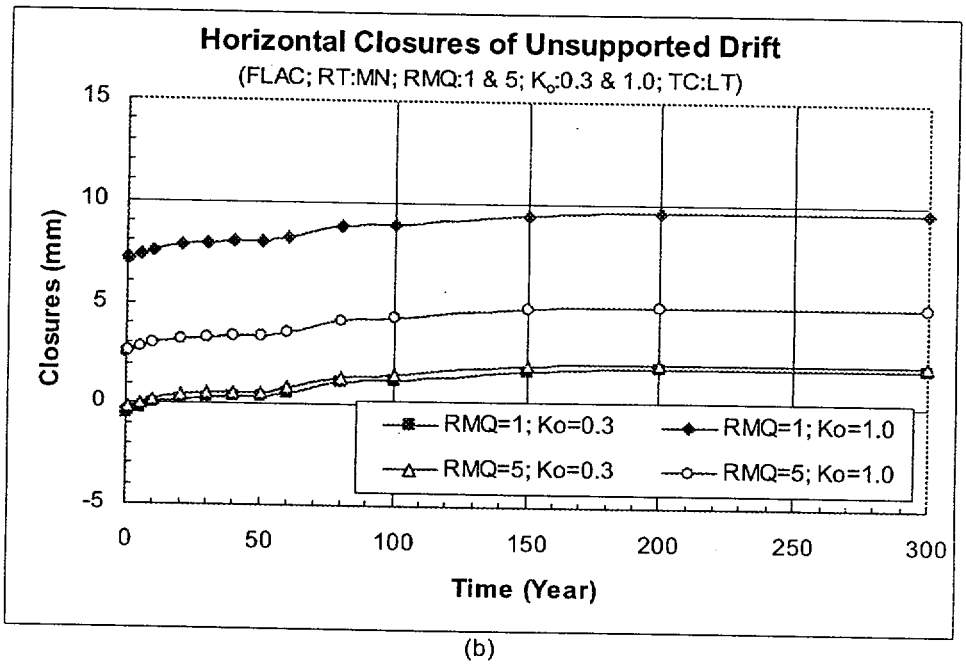

(b)

Figure 6-37. Time Histories of Drift Closures under Low Temperature Condition for Non-Lithophysal Rock, RMQ Categories of 1 and 5 and K_o of 0.3 and 1.0: (a) Vertical Closures; (b) Horizontal Closures

Note: RT=Rock Type; MN=Middle Non-Lithophysal Unit; RMQ=Rock Mass Quality Category; K_o=In Situ Horizontal to Vertical Stress Ratio; TC=Thermal Loading Condition; LT=Low Temperature.

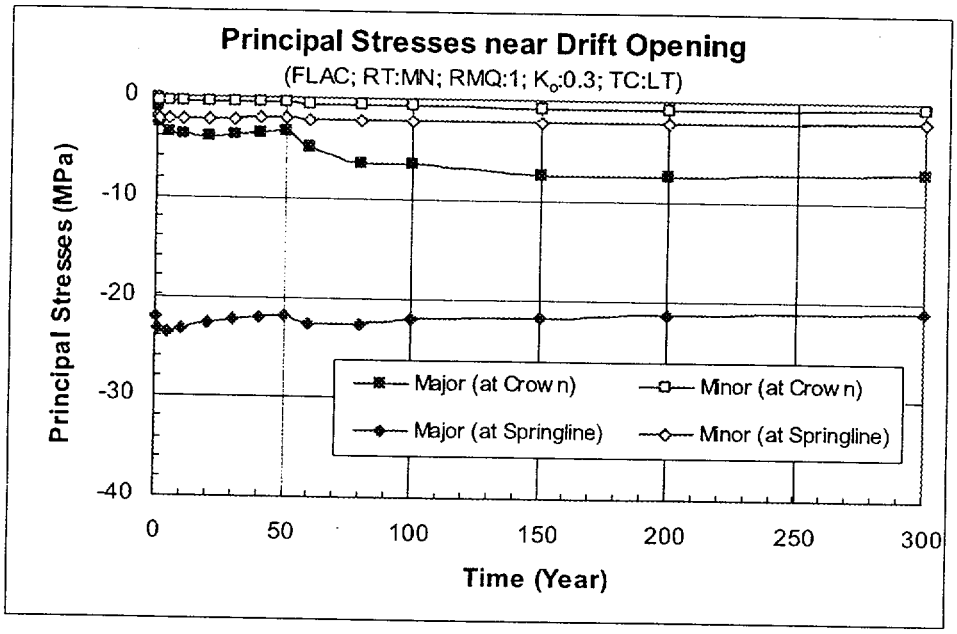

(a)

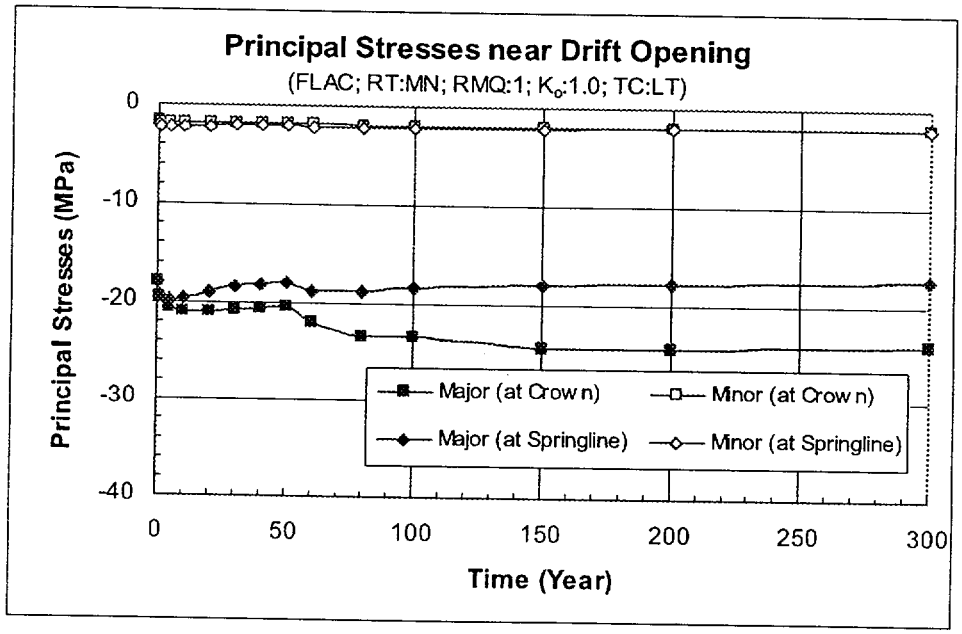

(b)

Figure 6-38. Time Histories of Principal Stresses near Drift Crown and Springline under Low Temperature Condition for Non-Lithophysal Rock, RMQ Category of 1, and K_o of 0.3 and 1.0: (a) K_o=0.3; (b) K_o=1.0

Note: RT=Rock Type; MN=Middle Non-Lithophysal Unit; RMQ=Rock Mass Quality Category; K_o=In Situ Horizontal to Vertical Stress Ratio; TC=Thermal Loading Condition; LT=Low Temperature.

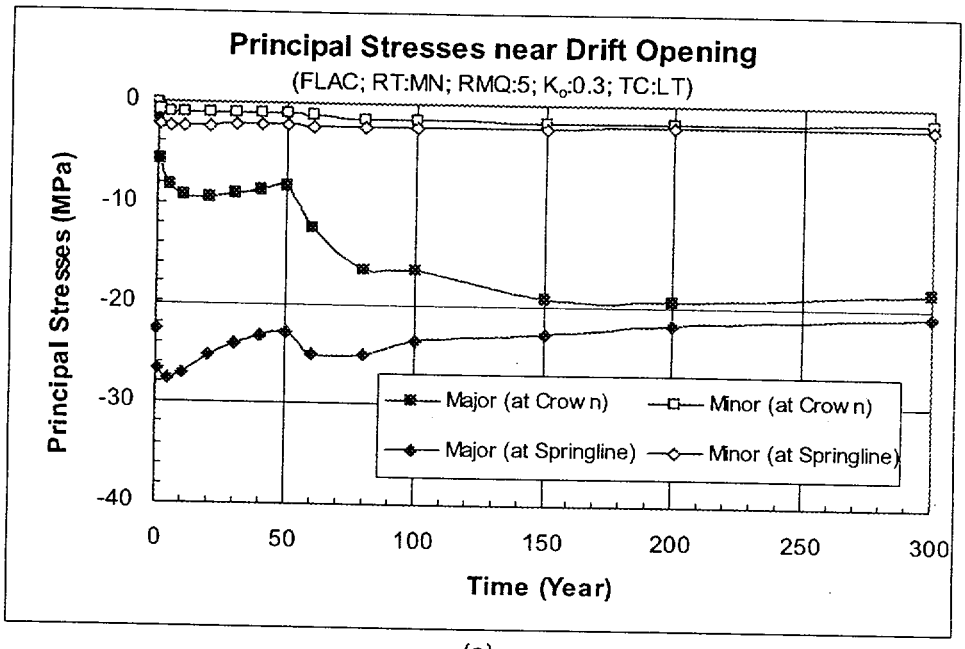

(a)

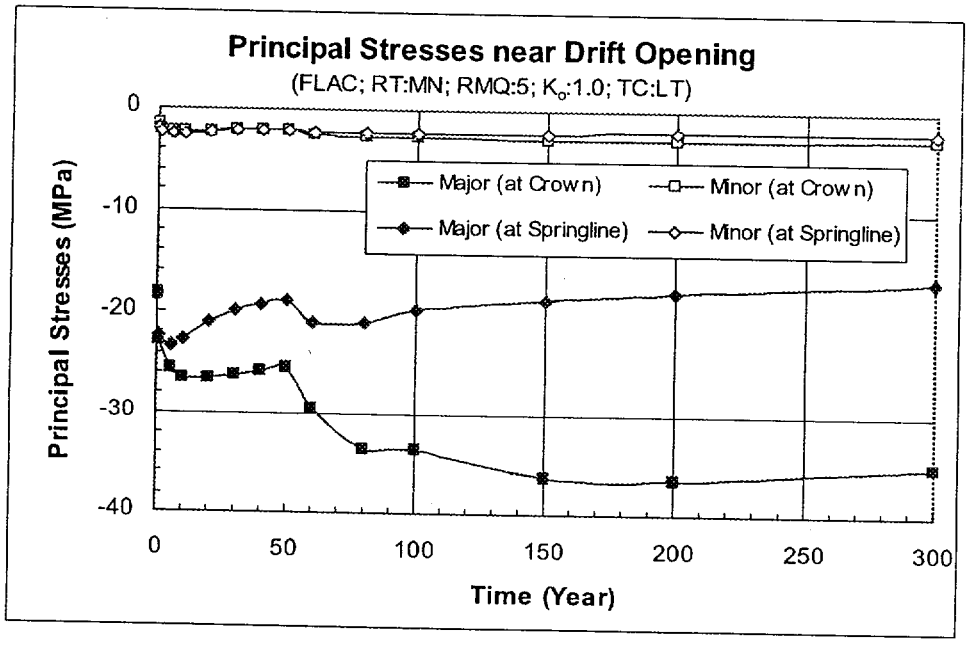

(b)

Figure 6-39. Time Histories of Principal Stresses near Drift Crown and Springline under Low Temperature Condition for Non-Lithophysal Rock, RMQ Category of 5, and Ko of 0.3 and 1.0: (a) Ko=0.3; (b) Ko=1.0

Note: RT=Rock Type; MN=Middle Non-Lithophysal Unit; RMQ=Rock Mass Quality Category; K_o=In Situ Horizontal to Vertical Stress Ratio; TC=Thermal Loading Condition; LT=Low Temperature.

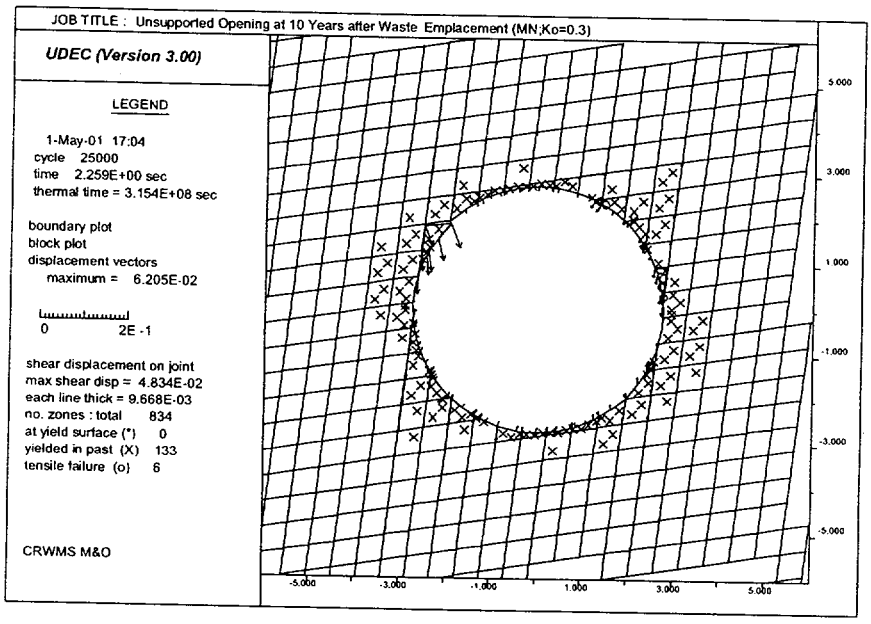

(a)

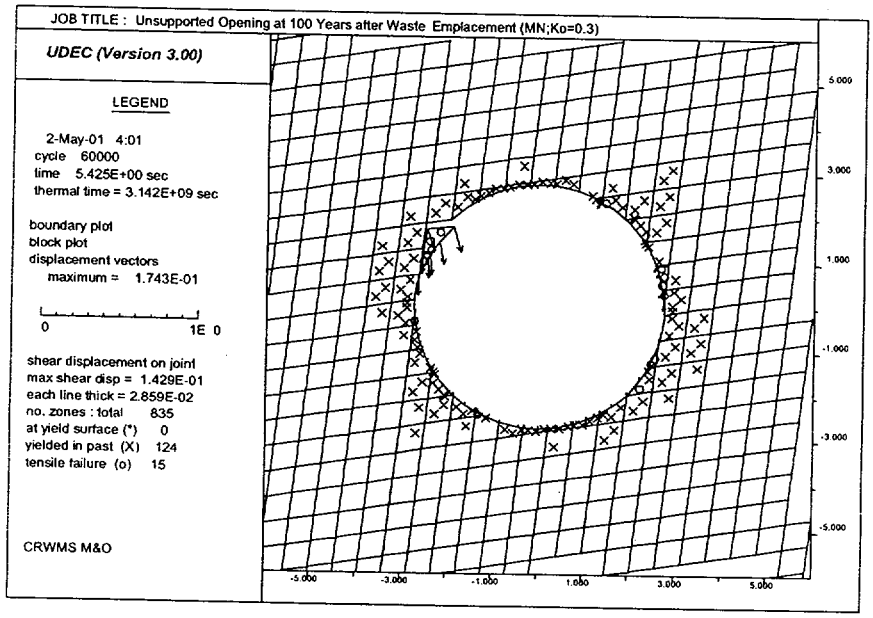

(b)

Figure 6-40. Rock Block Displacements, Shear Displacement on Joints, and Failure Zone Development Around an Emplacement Drift in Non-Lithophysal Rock Under Low Temperature Condition for K_o=0.3: (a) at 10 Years After Heating; (b) at 100 Years After Heating; (c) at 150 Years After Heating; (d) at 300 Years After Heating

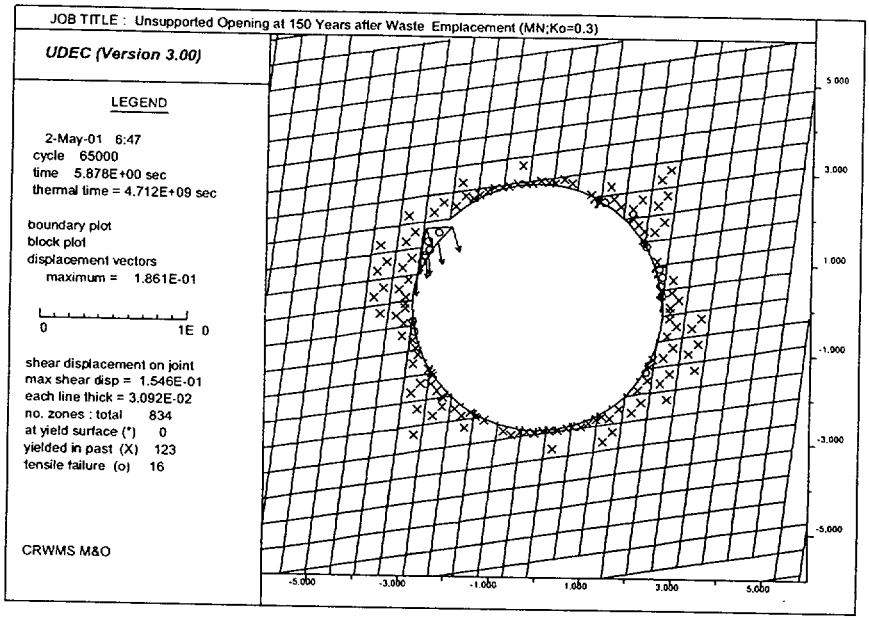

(c)

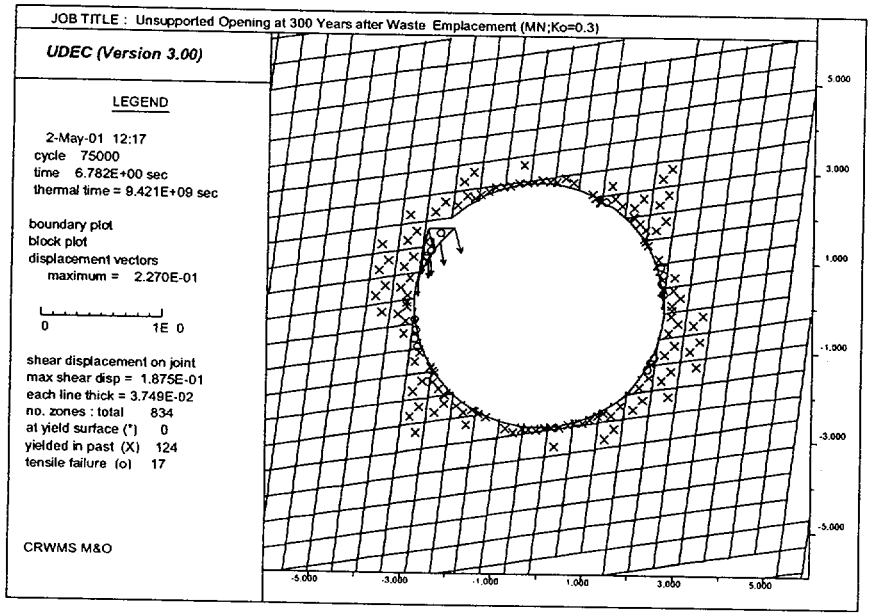

(d)

Figure 6-40 (Continued). Rock Block Displacements, Shear Displacement on Joints, and Failure Zone Development Around an Emplacement Drift in Non-Lithophysal Rock Under Low Temperature Condition for K_o=0.3: (a) at 10 Years After Heating; (b) at 100 Years After Heating; (c) at 150 Years After Heating; (d) at 300 Years After Heating

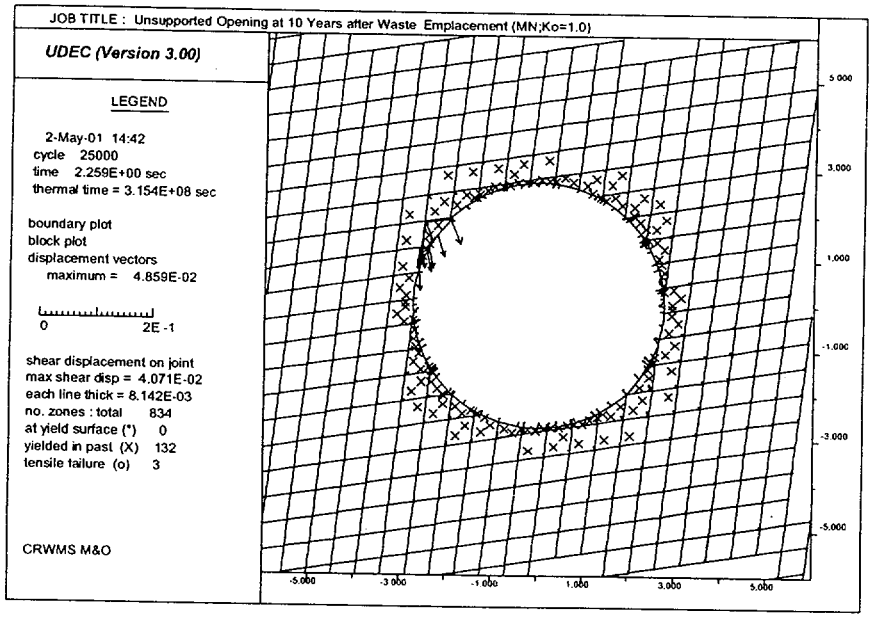

(a)

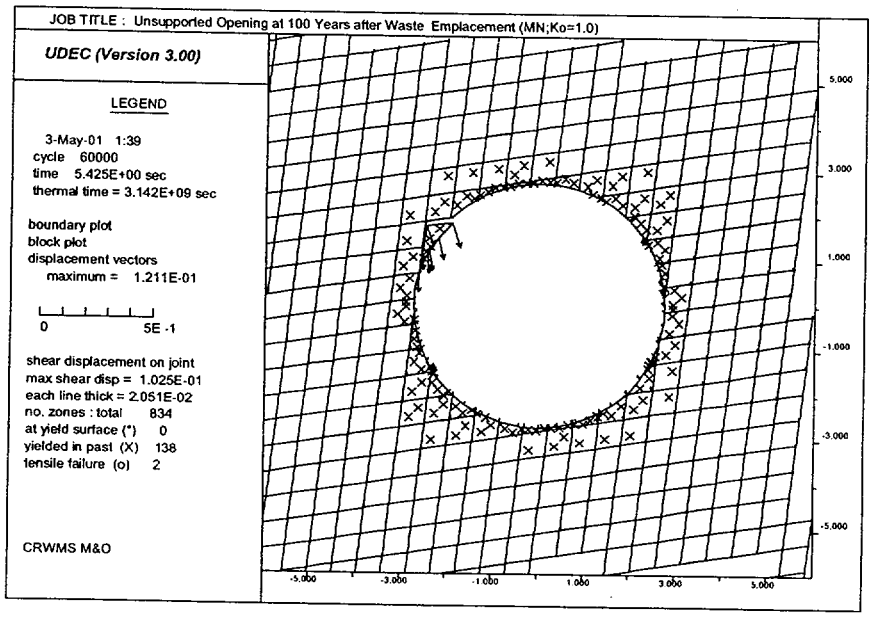

(b)

Figure 6-41. Rock Block Displacements, Shear Displacement on Joints, and Failure Zone Development Around an Emplacement Drift in Non-Lithophysal Rock Under Low Temperature Condition for K_o=1.0: (a) at 10 Years After Heating; (b) at 100 Years After Heating; (c) at 150 Years After Heating; (d) at 300 Years After Heating

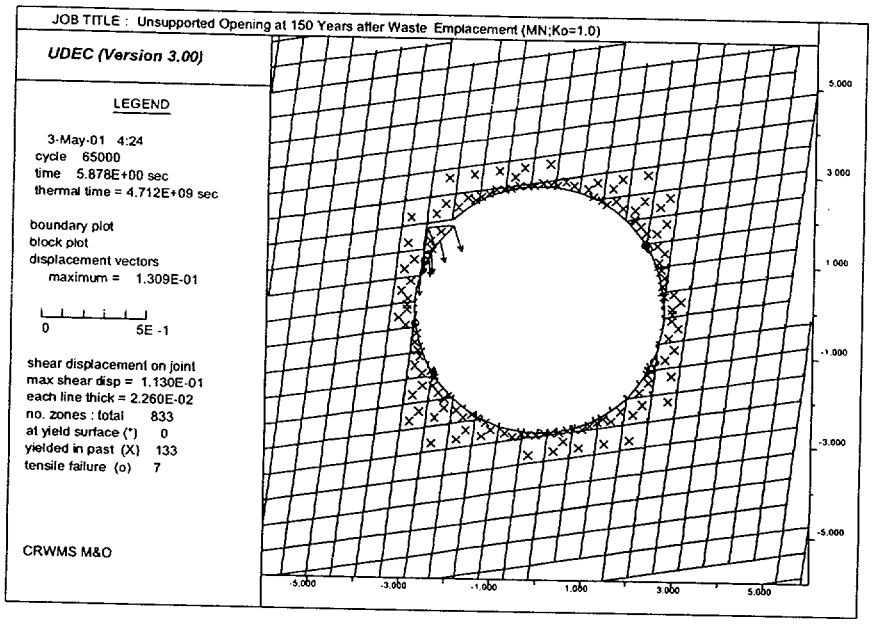

(c)

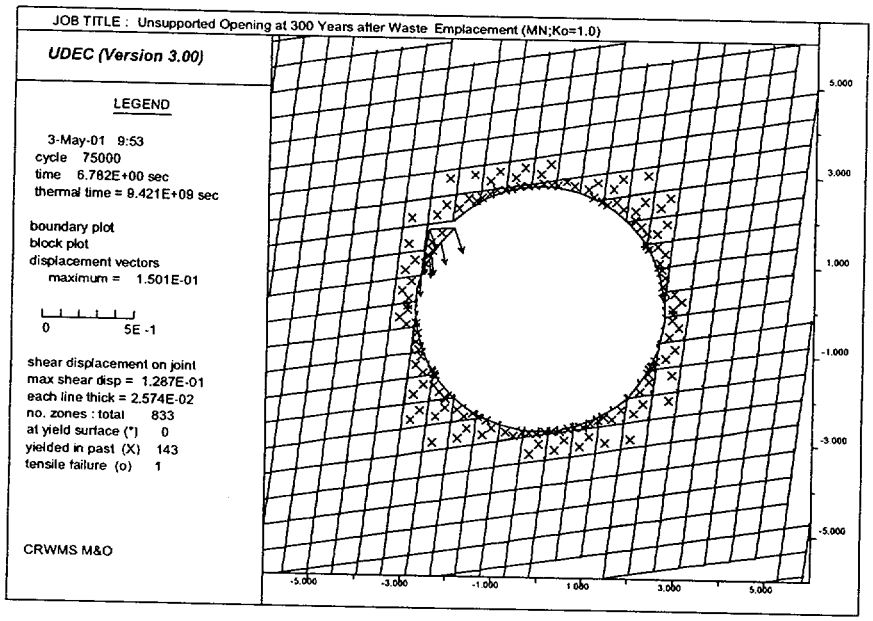

(d)

Figure 6-41 (Continued). Rock Block Displacements, Shear Displacement on Joints, and Failure Zone Development Around an Emplacement Drift in Non-Lithophysal Rock Under Low Temperature Condition for K_o=1.0: (a) at 10 Years After Heating; (b) at 100 Years After Heating; (c) at 150 Years After Heating; (d) at 300 Years After Heating

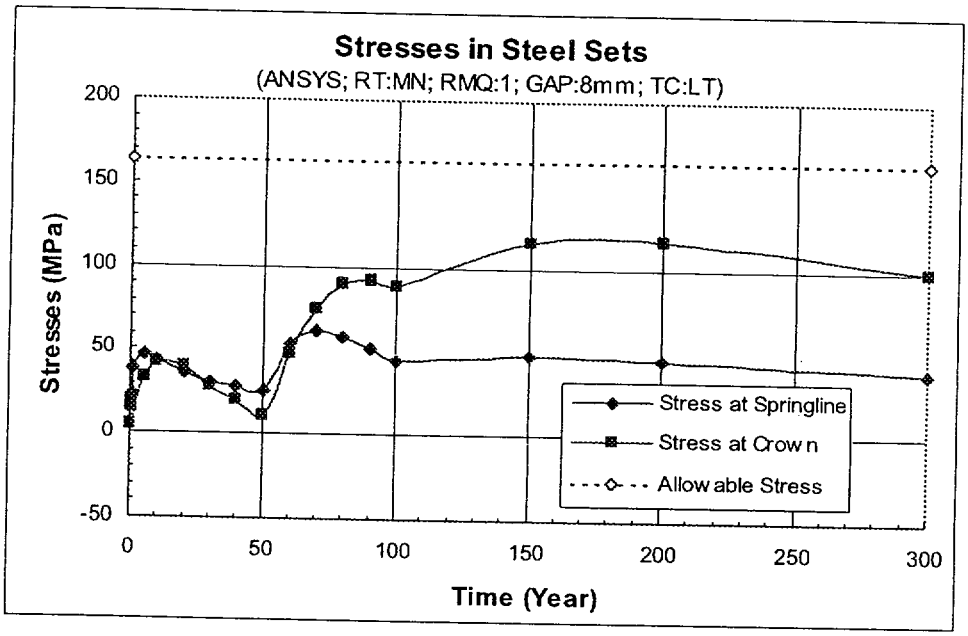

(a)

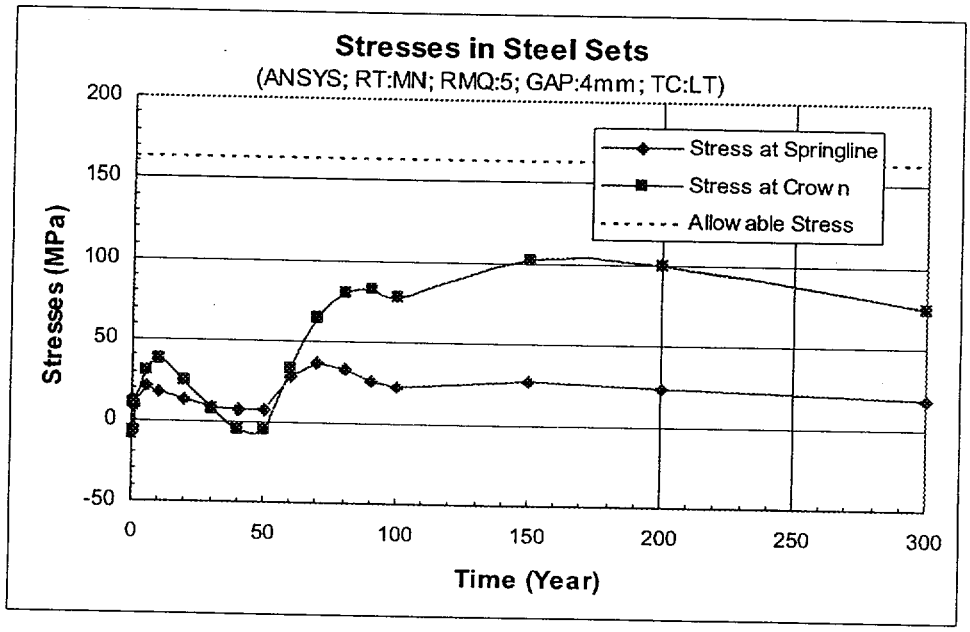

(b)

Figure 6-42. Time Histories of Stresses at Crown and Springline of Steel Sets with Initial Gaps of 4 and 8 mm under Low Temperature Condition for RMQ Categories of 1 and 5: (a) RMQ=1 and Gap=8mm; (b) RMQ=5 and Gap=4mm

Note: RT=Rock Type; MN=Middle Non-Lithophysal Unit; RMQ=Rock Mass Quality Category; TC=Thermal Loading Condition; LT=Low Temperature.

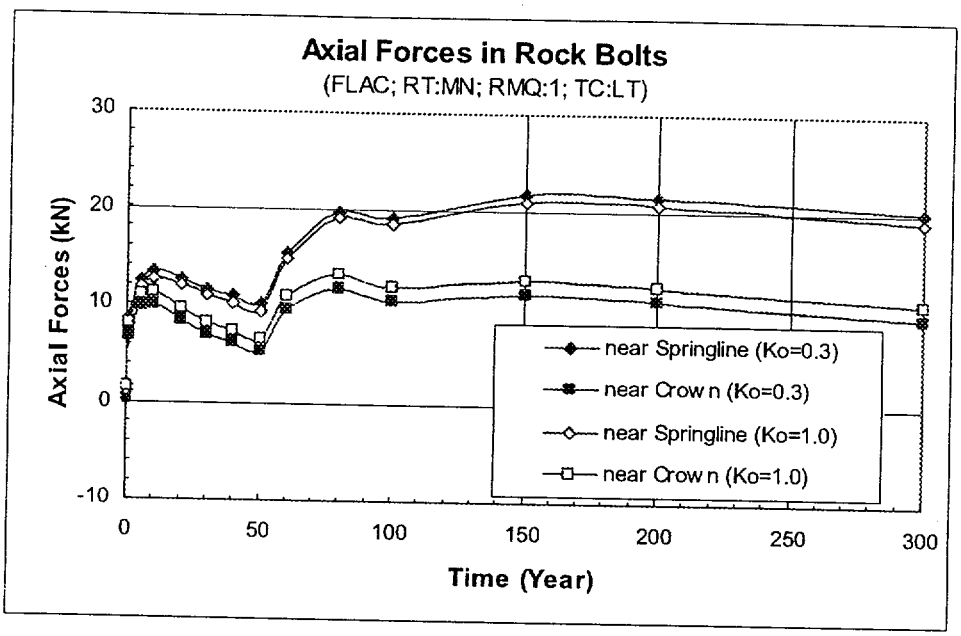

(a)

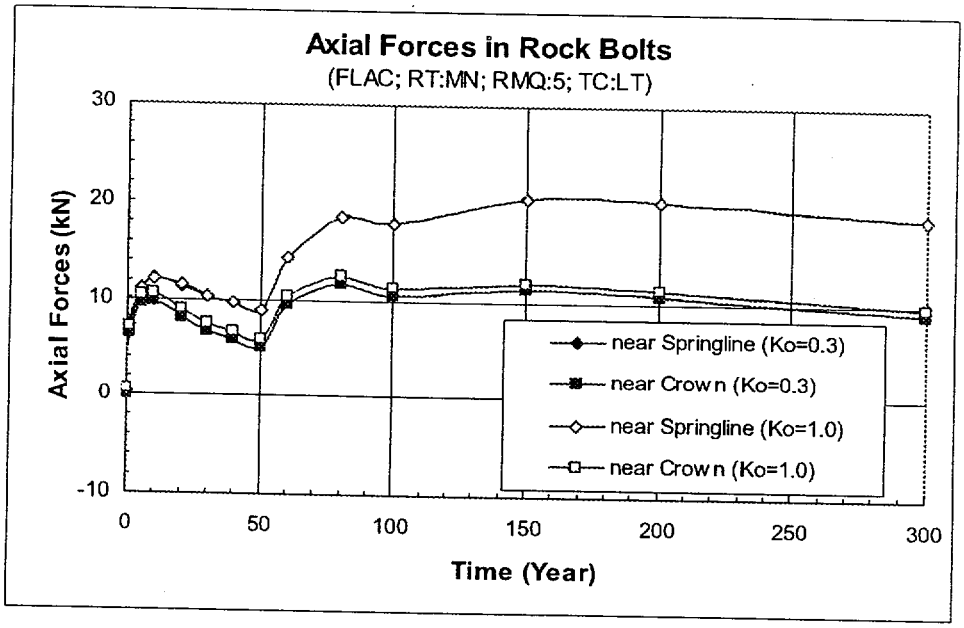

(b)

Figure 6-43. Time Histories of Axial Forces in Rock Bolts near Crown and Springline of Emplacement Drifts under Low Temperature Condition for RMQ Categories of 1 and 5 and K_o=0.3 and 1.0: (a) RMQ=1; (b) RMQ=5

Note: RT=Rock Type; MN=Middle Non-Lithophysal Unit; RMQ=Rock Mass Quality Category; TC=Thermal Loading Condition; LT=Low Temperature.

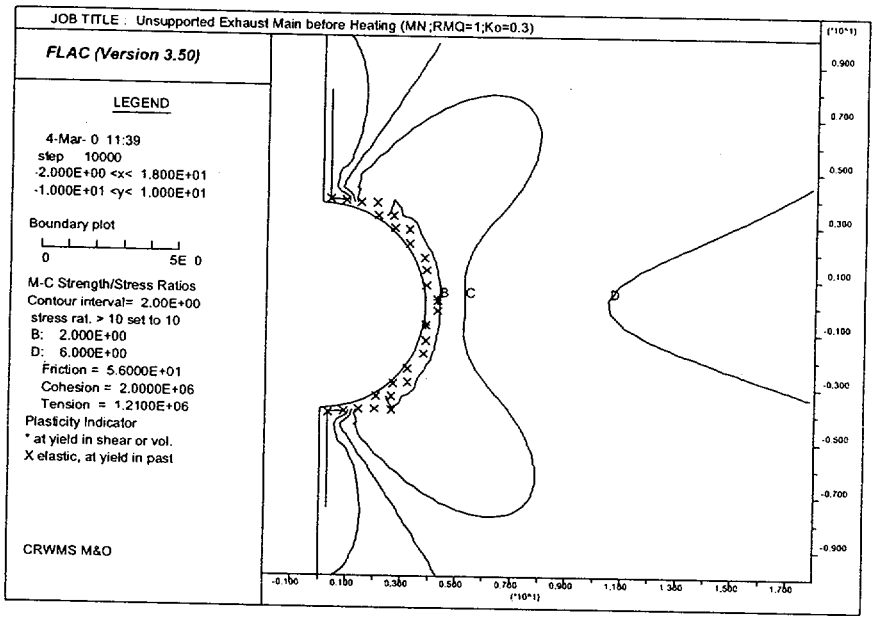

(a)

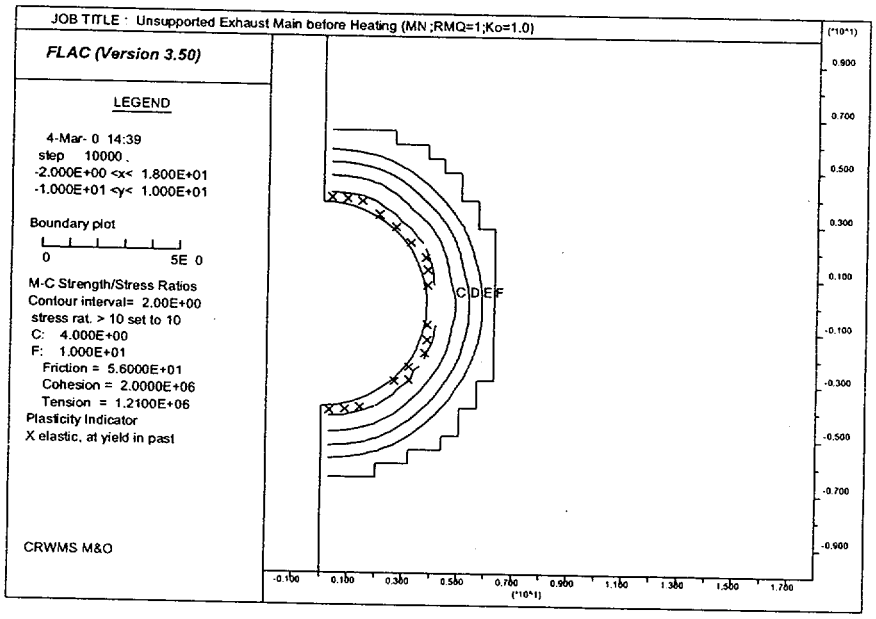

(b)

Figure 6-44. Strength/Stress Ratio Contours and Plasticity Indicators Around Unsupported Exhaust Main for In Situ Stress Load, RMQ Categories 1 and 5, and In Situ Stress Ratio K_o of 0.3 and 1.0: (a) RMQ=1 and K_o=0.3; (b) RMQ=1 and K_o=1.0; (c) RMQ=5 and K_o=0.3; (d) RMQ=5 and K_o=1.0

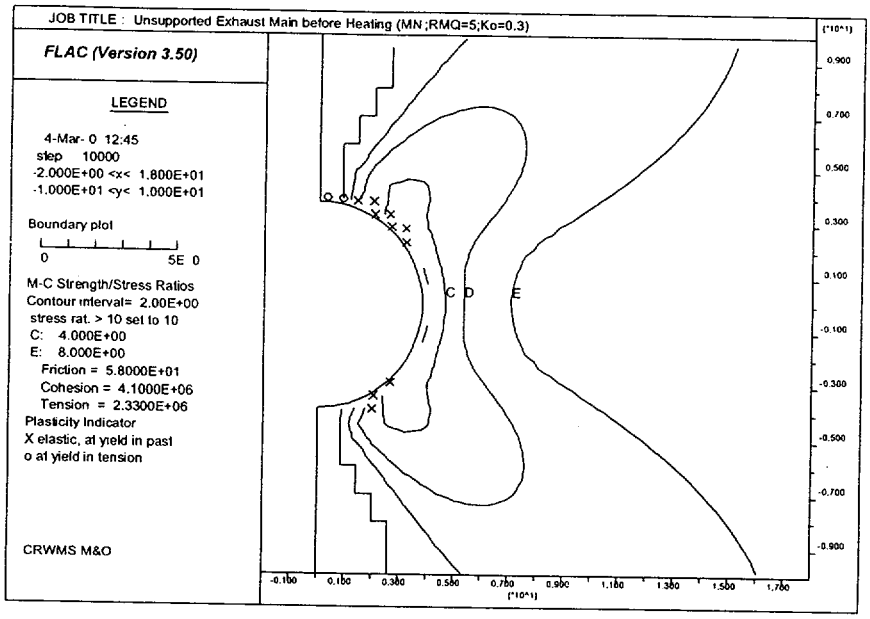

(c)

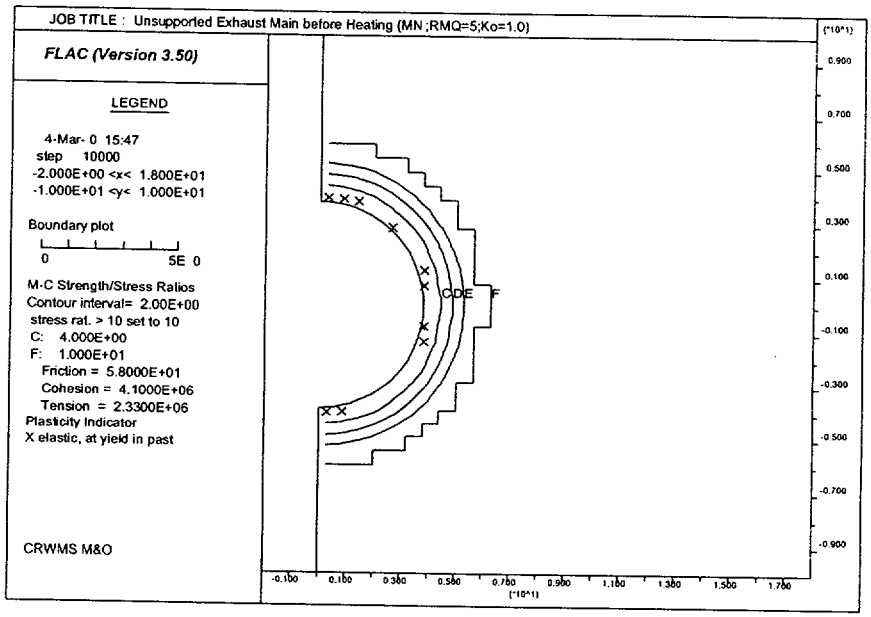

(d)

Figure 6-44 (Continued). Strength/Stress Ratio Contours and Plasticity Indicators Around Unsupported Exhaust Main for In Situ Stress Load, RMQ Categories 1 and 5, and In Situ Stress Ratio K_o of 0.3 and 1.0: (a) RMQ=1 and K_o=0.3; (b) RMQ=1 and K_o=1.0; (c) RMQ=5 and K_o=0.3; (d) RMQ=5 and K_o=1.0

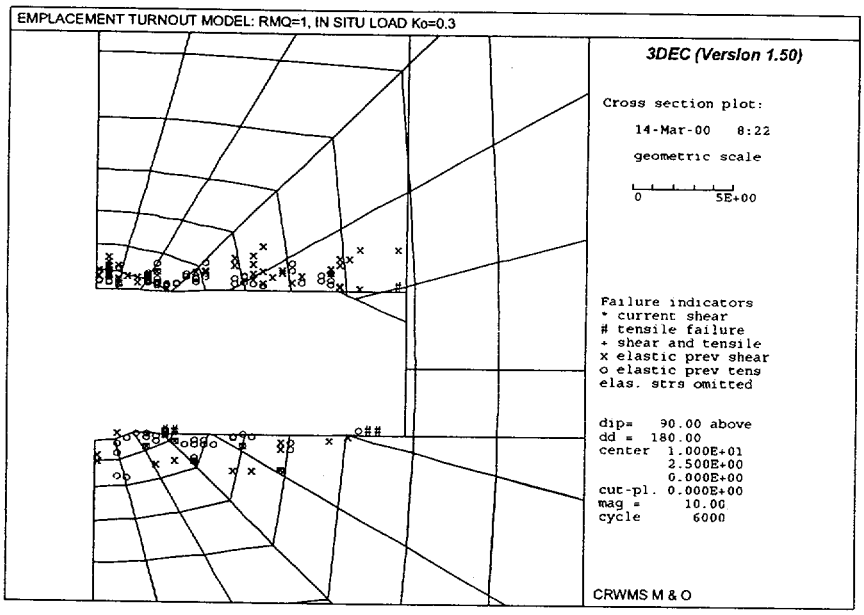

(a)

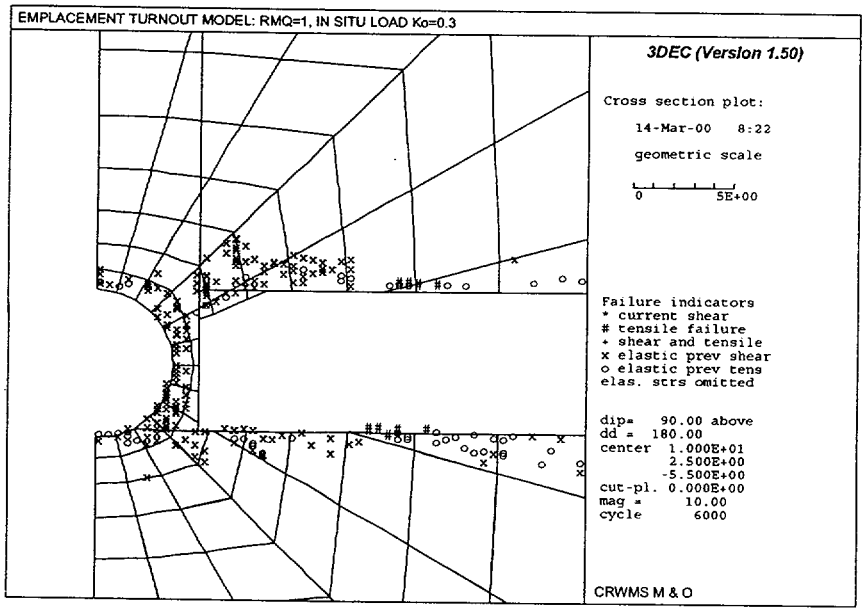

(b)

Figure 6-45. Sectional Views of the Static Response to Excavation of the Intersection of Access Main (AM) and Emplacement Drift Turnout (EDT) Using the 3DEC Model: (a) Cross-Section at Intersection; (b) Cross-Section at 5.5 m Away From Intersection Along AM; (c) Cross-Section at 6 m Away From Intersection Along AM; (d) Cross-Section at 8 m Away From Intersection Along AM

Note: Both Geometric and Vector Scales in Meters.

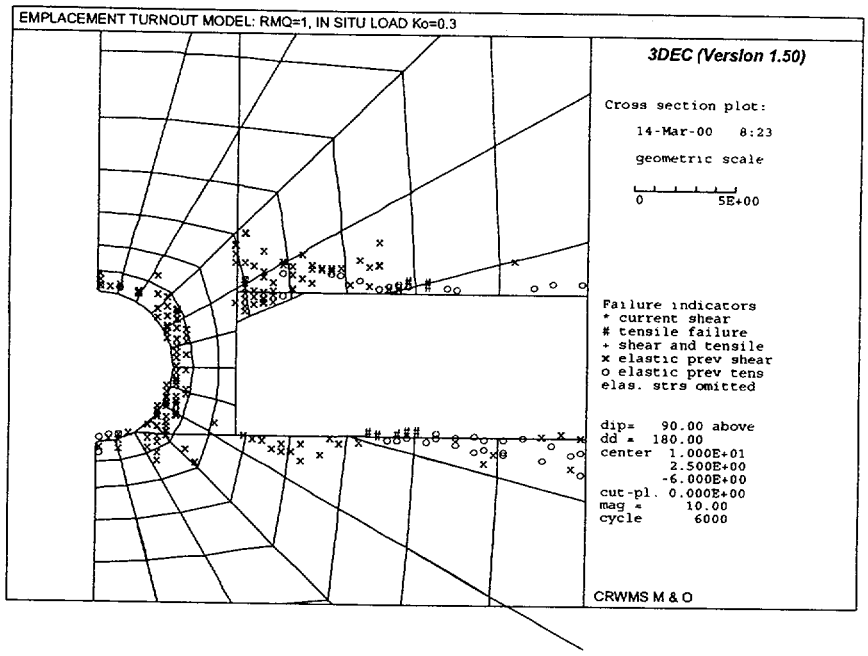

(c)

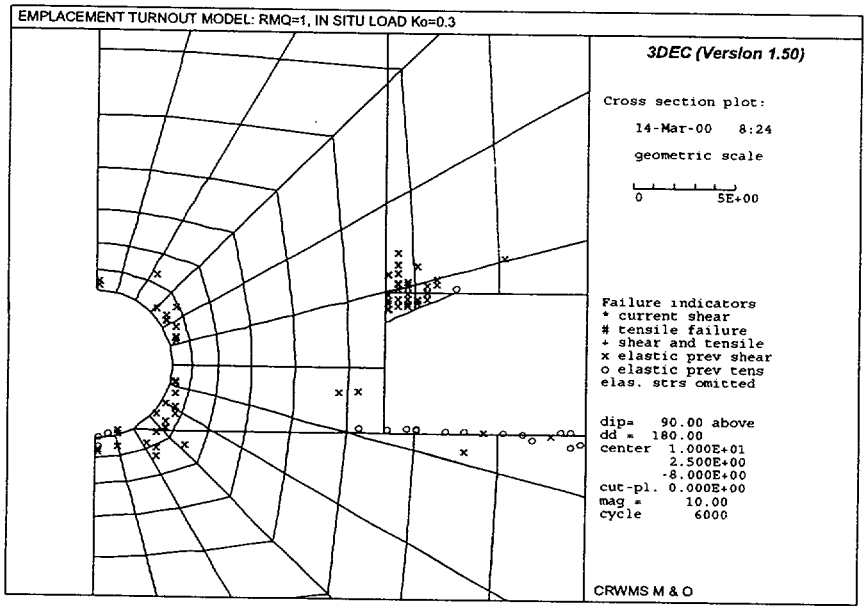

(d)

Figure 6-45 (Continued). Sectional Views of the Static Response to Excavation of the Intersection of Access Main (AM) and Emplacement Drift Turnout (EDT) Using the 3DEC Model: (a) Cross-Section at Intersection; (b) Cross-Section at 5.5 m Away From Intersection Along AM; (c) Cross-Section at 6 m Away From Intersection Along AM; (d) Cross-Section at 8 m Away From Intersection Along AM

Note: Both Geometric and Vector Scales in Meters.

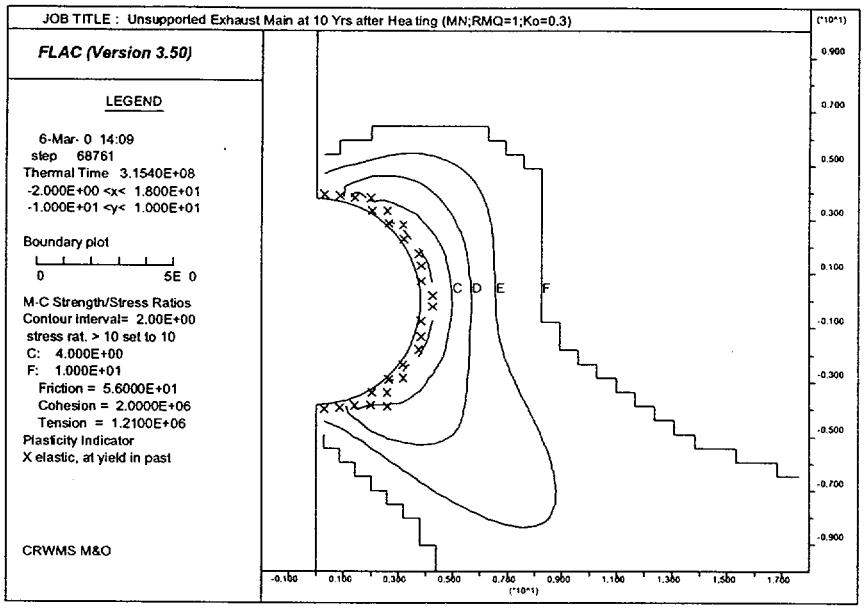

(a)

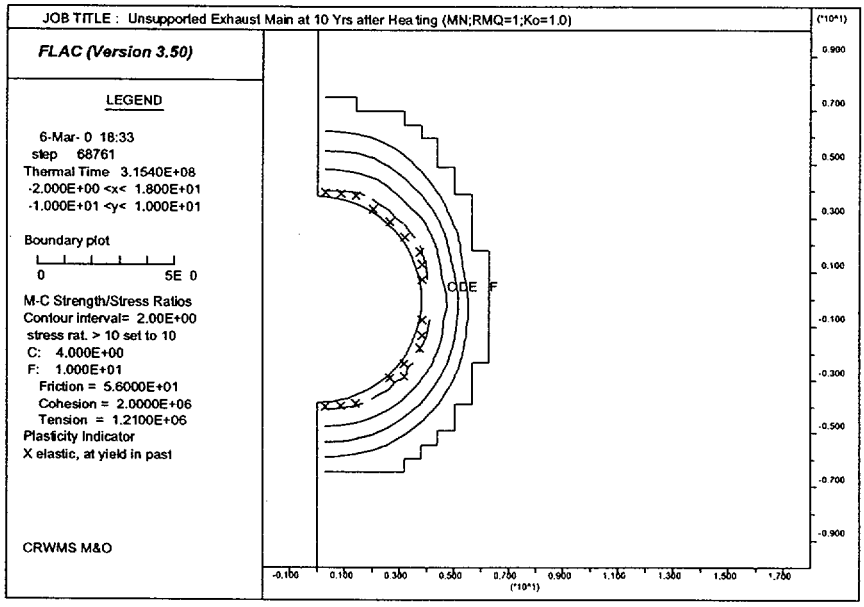

(b)

Figure 6-46. Strength/Stress Ratio Contours and Plasticity Indicators Around Unsupported Exhaust Main for Combined In Situ Stress and Thermal Loads, RMQ Categories 1 and 5, and In Situ Stress Ratio K_o of 0.3 and 1.0: (a) RMQ=1 and K_o=0.3; (b) RMQ=1 and K_o=1.0; (c) RMQ=5 and K_o=0.3; (d) RMQ=5 and K_o=1.0

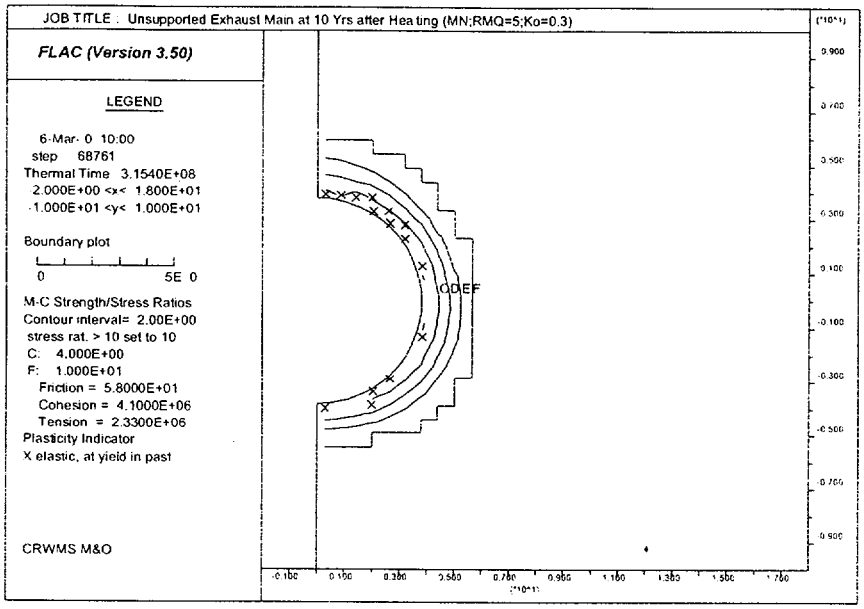

(c)

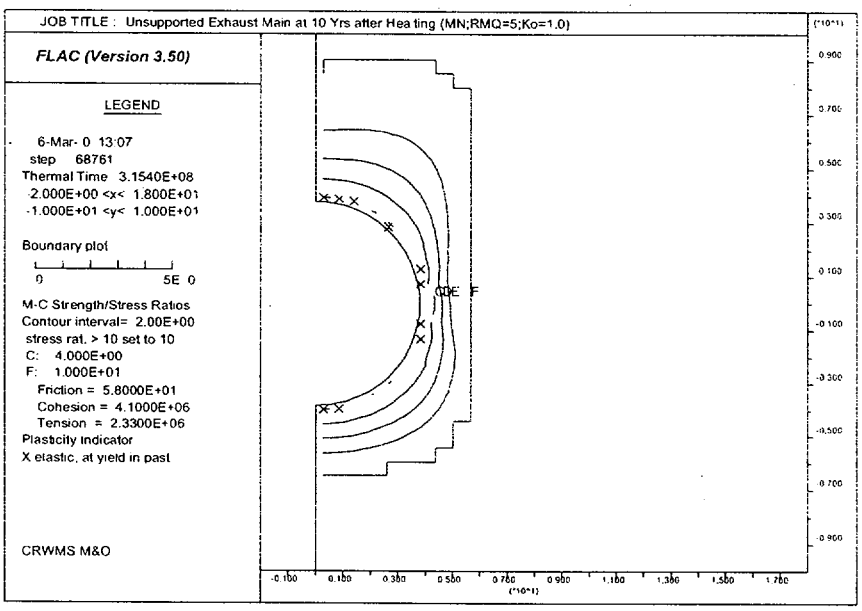

(d)

Figure 6-46 (Continued). Strength/Stress Ratio Contours and Plasticity Indicators Around Unsupported Exhaust Main for Combined In Situ Stress and Thermal Loads, RMQ Categories 1 and 5, and In Situ Stress Ratio K_o of 0.3 and 1.0: (a) RMQ=1 and K_o=0.3; (b) RMQ=1 and K_o=1.0; (c) RMQ=5 and K_o=0.3; (d) RMQ=5 and K_o=1.0

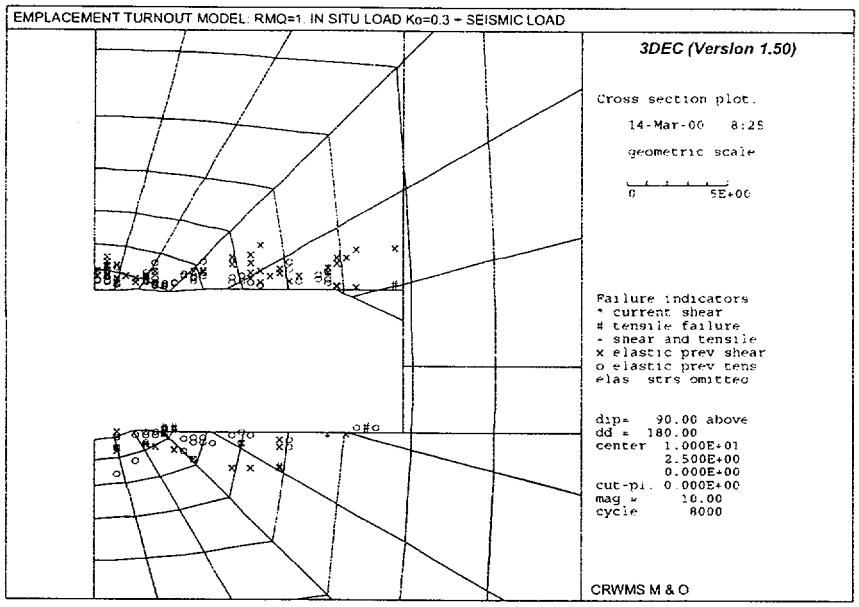

(a)

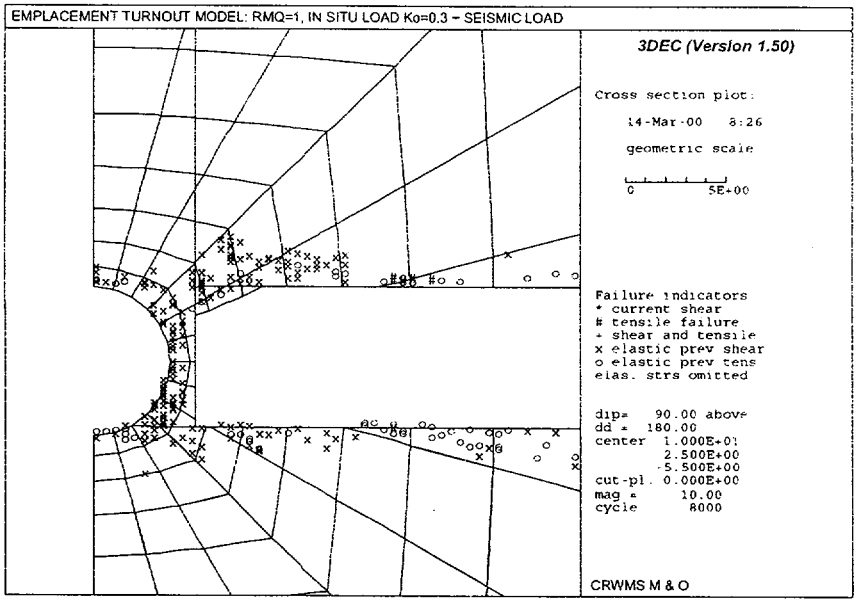

(b)

Figure 6-47. Sectional Views of the Static Response to Seismic Load for the Intersection of Access Main (AM) and Emplacement Drift Turnout (EDT) Using the 3DEC Model: (a) Cross-Section at Intersection; (b) Cross-Section at 5.5 m Away From Intersection Along AM; (c) Cross-Section at 6 m Away From Intersection Along AM; (d) Cross-Section at 8 m Away From Intersection Along AM

Note: Both Geometric and Vector Scales in Meters.

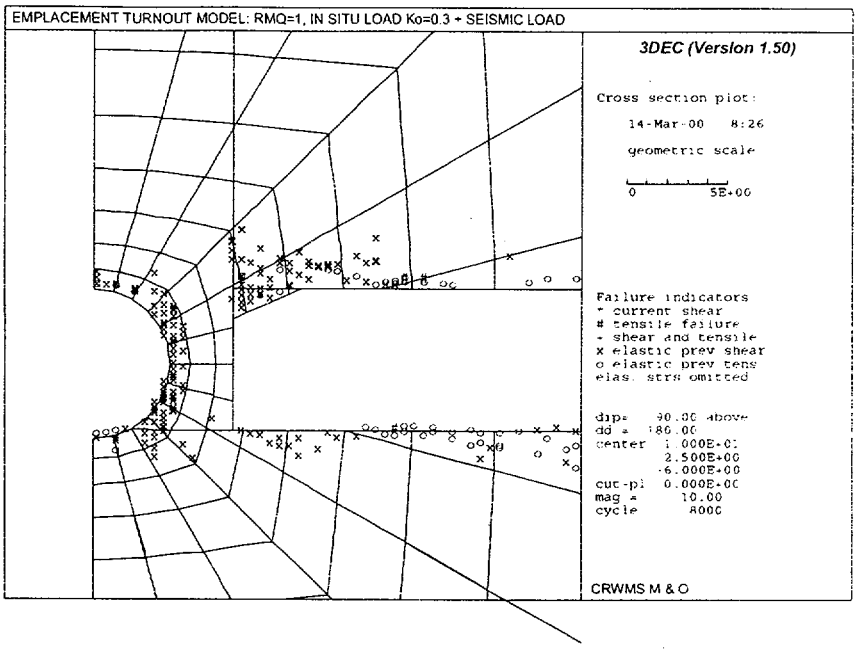

(c)

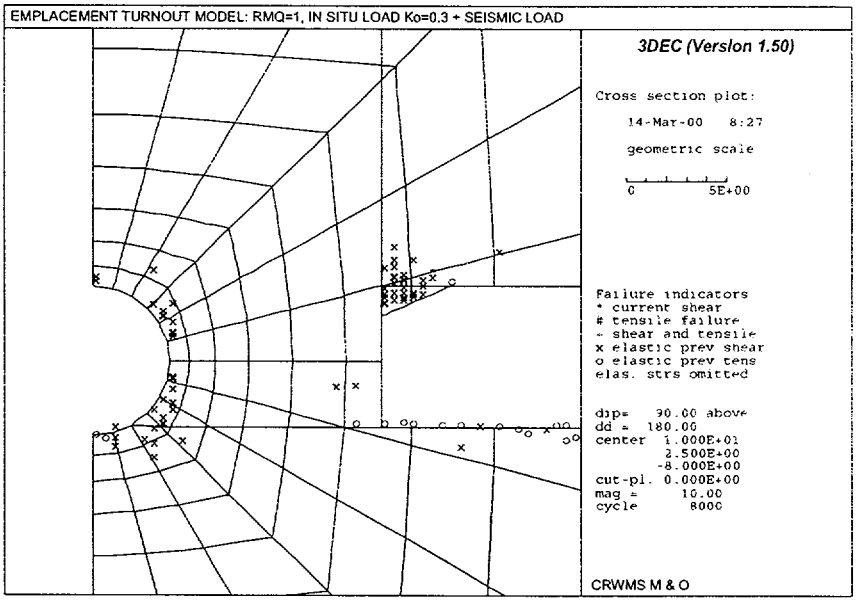

(d)

Figure 6-47 (Continued). Sectional Views of the Static Response to Seismic Load for the Intersection of Access Main (AM) and Emplacement Drift Turnout (EDT) Using the 3DEC Model: (a) Cross-Section at Intersection; (b) Cross-Section at 5.5 m Away From Intersection Along AM; (c) Cross-Section at 6 m Away From Intersection Along AM; (d) Cross-Section at 8 m Away From Intersection Along AM

Note: Both Geometric and Vector Scales in Meters.

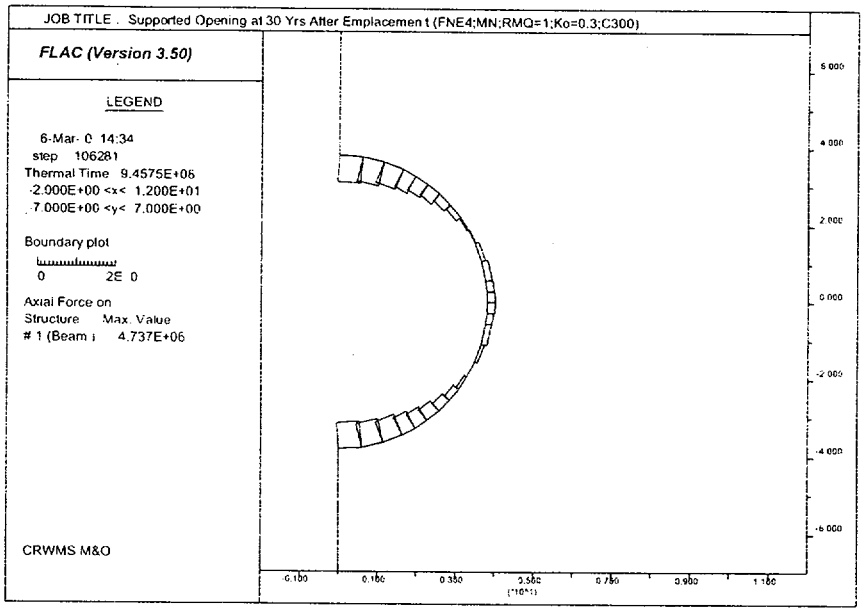

(a)

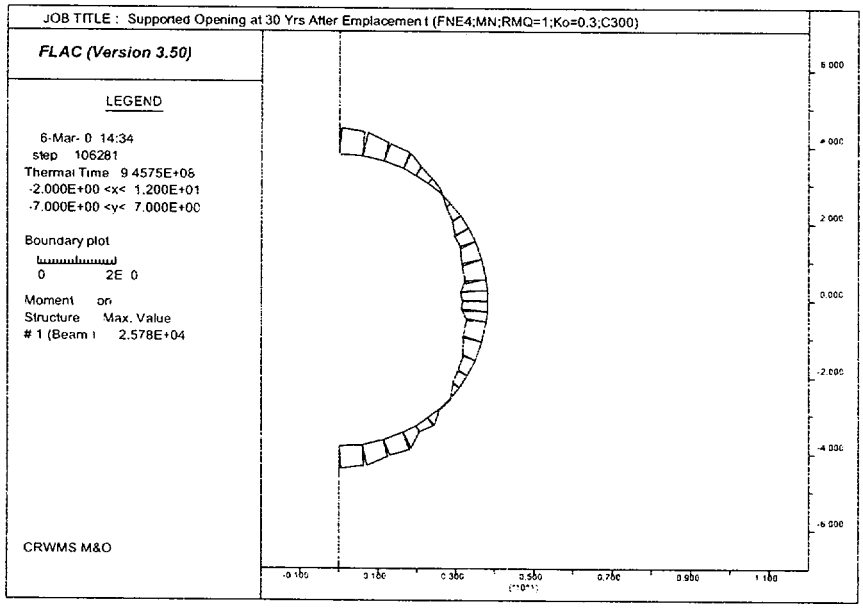

(b)

Figure 6-48. Distributions of Axial Force and Moment Along Cast-in-place Concrete Lining in Exhaust Main Under Thermal Loads, RMQ Category 1, and In Situ Stress Ratio K_o of 0.3 and 1.0: (a) Axial Force (K_o=0.3); (b) Moment (K_o=0.3); (c) Axial Force (K_o=1.0); (d) Moment (K_o=1.0)

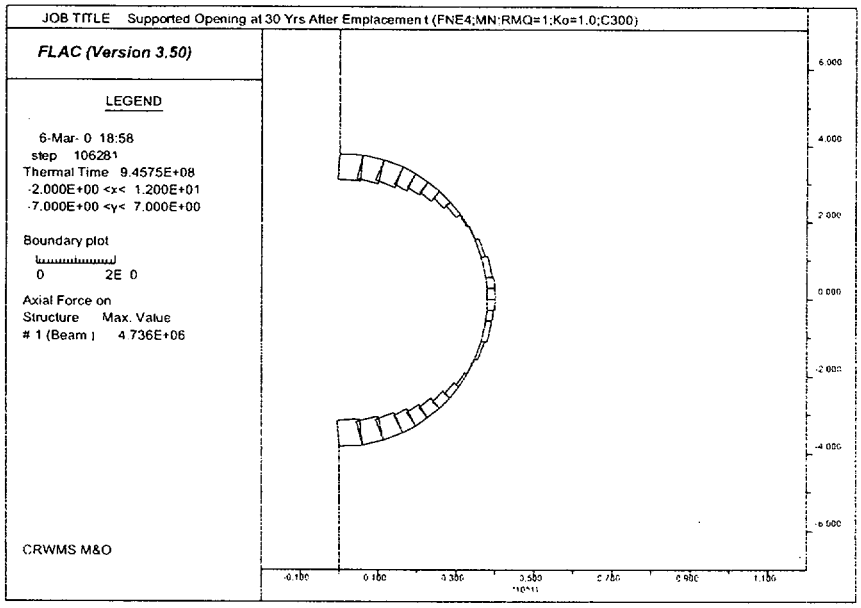

(c)

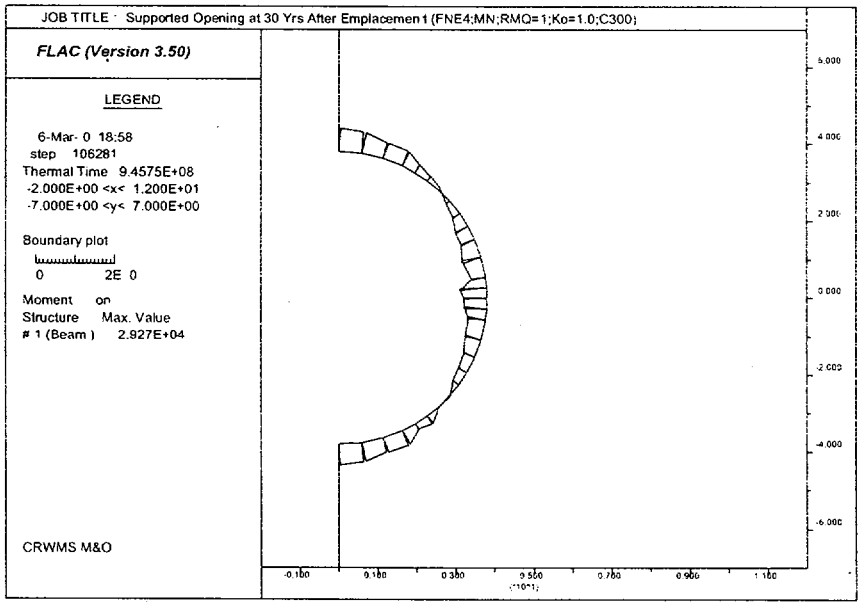

(d)

Figure 6-48 (Continued). Distributions of Axial Force and Moment Along Cast-in-place Concrete Lining in Exhaust Main Under Thermal Loads, RMQ Category 1, and In Situ Stress Ratio K_o of 0.3 and 1.0: (a) Axial Force (K_o=0.3); (b) Moment (K_o=0.3); (c) Axial Force (K_o=1.0); (d) Moment (K_o=1.0)

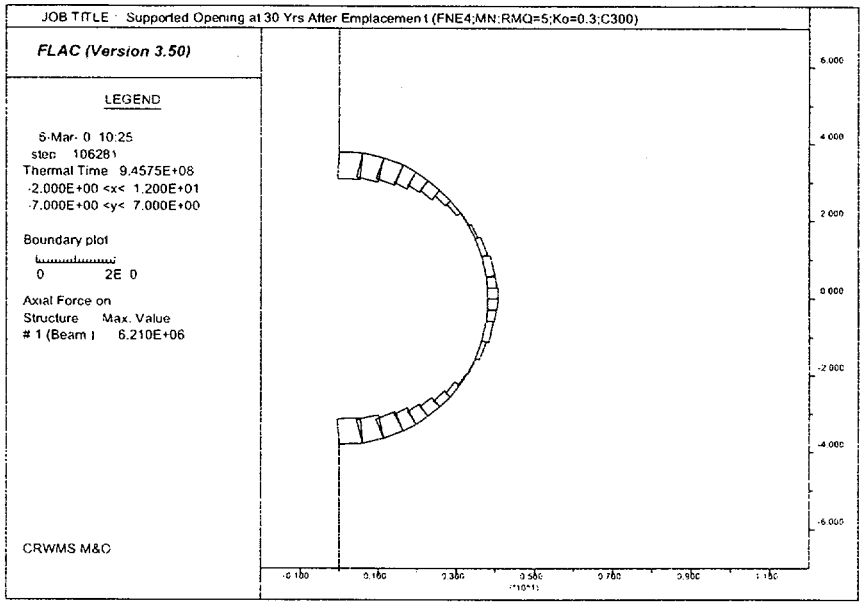

(a)

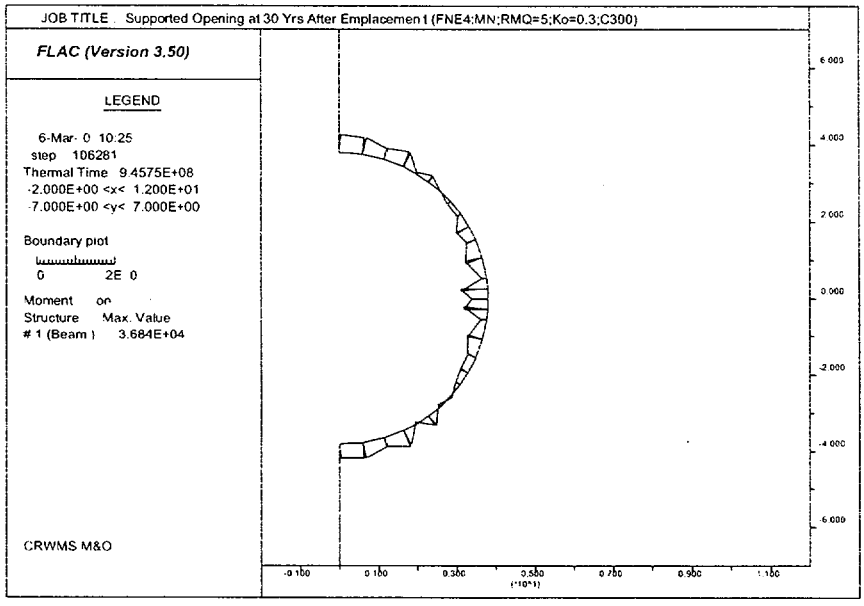

(b)

Figure 6-49. Distributions of Axial Force and Moment Along Cast-in-Place Concrete Lining in Exhaust Main Under Thermal Loads, RMQ Category 5, and In Situ Stress Ratio K_o of 0.3 and 1.0: (a) Axial Force (K_o=0.3); (b) Moment (K_o=0.3); (c) Axial Force (K_o=1.0); (d) Moment (K_o=1.0)

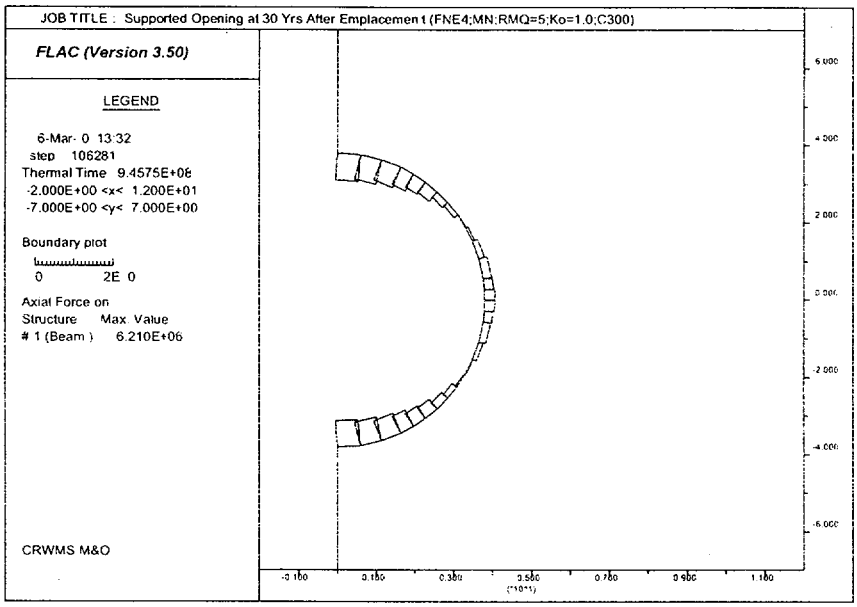

(c)

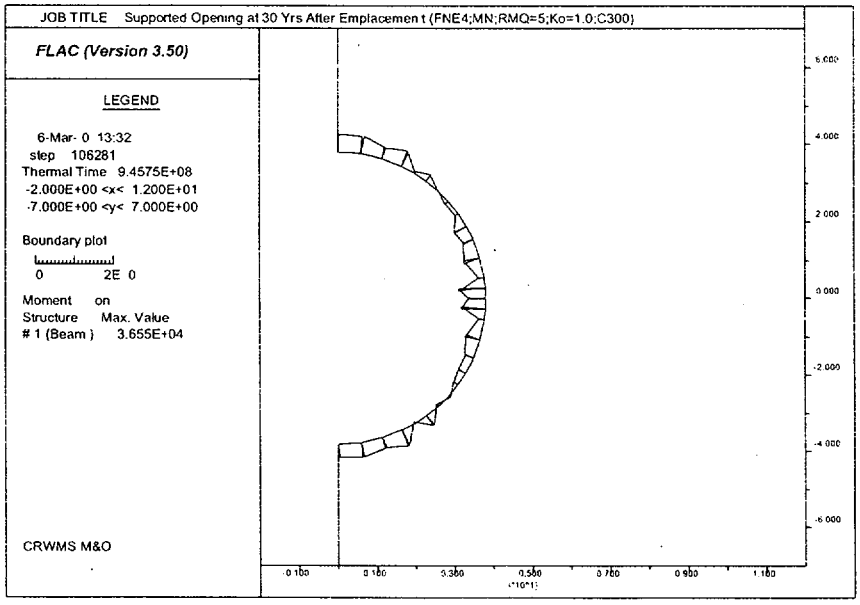

(d)

Figure 6-49 (Continued). Distributions of Axial Force and Moment Along Cast-in-Place Concrete Lining in Exhaust Main Under Thermal Loads, RMQ Category 5, and In Situ Stress Ratio K_o of 0.3 and 1.0: (a) Axial Force (K_o=0.3); (b) Moment (K_o=0.3); (c) Axial Force (K_o=1.0); (d) Moment (K_o=1.0)

8. INPUTS AND REFERENCES

8.1 DOCUMENTS CITED

ASM (American Society for Metals) 1978. *Properties and Selection: Irons and Steels.* Volume 1 of *Metals Handbook.* 9th Edition. Bardes, B.P., ed. Metals Park, Ohio: American Society for Metals. TIC: 209799.

ASM International 1990. *Properties and Selection: Irons, Steels, and High-Performance Alloys.* Volume 1 of *Metals Handbook.* 10th Edition. Materials Park, Ohio: ASM International. TIC: 245666.

Barton, N. 1988. "Rock Mass Classification and Tunnel Reinforcement Selection Using the Q-System." *Rock Classification Systems for Engineering Purposes.* Kirkaldie, L., ed. ASTM STP 984. 59-84. Philadelphia, Pennsylvania: American Society for Testing and Materials. TIC: 216484.

Beer, F.P. and Johnston, E.R., Jr. 1977. *Vector Mechanics for Engineers, Statics.* 3rd Edition. New York, New York: McGraw-Hill Book Company. TIC: 247391.

Bieniawski, Z.T. 1988. "The Rock Mass Rating (RMR) System (Geomechanics Classification) in Engineering Practice." *Rock Classification Systems for Engineering Purposes.* Kirkaldie, L., ed. ASTM STP 984. 17-34. Philadelphia, Pennsylvania: American Society for Testing and Materials. TIC: 216484.

BSC (Bechtel SAIC Company) 2001. *Requirements and Criteria for Implementing a Repository Design that can be Operated Over a Range of Thermal Modes.* Input Transmittal 00402.Ta. Las Vegas, Nevada: Bechtel SAIC Company. ACC: MOL.20010504.0296.

CRWMS M&O (Civilian Radioactive Waste Management System Management and Operating Contractor) 1994a. *Software Qualification Package for 3DEC Version 1.5 (SCP: N/A).* Las Vegas, Nevada: CRWMS M&O. ACC: MOL.19950329.0099.

CRWMS M&O 1995. *ESF Ground Support Analysis.* BABEE0000-01717-0200-00002 REV 00. Las Vegas, Nevada: CRWMS M&O. ACC: MOL.19960409.0355.

CRWMS M&O 1997a. *Yucca Mountain Site Geotechnical Report.* B00000000-01717-5705-00043 REV 01. Two volumes. Las Vegas, Nevada: CRWMS M&O. ACC: MOL.19971017.0736; MOL.19971017.0737.

CRWMS M&O 1997b. *Data Transmittal Package (DTP) for "Hydraulic Fracturing Stress Measurements in Test Hole: ESF-AOD-HDFR#1, Thermal Test Facility, Exploratory Studies Facility at Yucca Mountain.* DTN: SNF37100195002.001, TDIF 305878. Las Vegas, Nevada: CRWMS M&O. ACC: MOL.19970717.0005; MOL.19970717.0006; MOL.19970717.0007; MOL.19970717.0008.

CRWMS M&O 1997c. *Constructability Considerations for Repository Drifts for Viability Assessment.* BCAA00000-01717-0200-00005 REV 00. Las Vegas, Nevada: CRWMS M&O. ACC: MOL.19971229.0302.

CRWMS M&O 1997d. *Software Qualification Report for ANSYS Revision 5.2SGI.* CSCI: 30013 V5.2SGI. DI: 30013-2003, Rev. 00. Las Vegas, Nevada: CRWMS M&O. ACC: MOL.19970815.0536.

CRWMS M&O 1998a. *ESF Design Confirmation Steel Set Loads Analysis.* BABEE0000-01717-5705-00006 REV 00. Las Vegas, Nevada: CRWMS M&O. ACC: MOL.19981014.0001.

CRWMS M&O 1998b. *Repository Ground Support Analysis for Viability Assessment.* BCAA00000-01717-0200-00004 REV 01. Las Vegas, Nevada: CRWMS M&O. ACC: MOL.19980512.0714.

CRWMS M&O 1998c. *Drift Ground Support Design Guide.* BCAA00000-01717-2500-00001 REV 01. Las Vegas, Nevada: CRWMS M&O. ACC: MOL.19990326.0104.

CRWMS M&O 1999a. *Classification of the MGR Ground Control System.* ANL-GCS-SE-000001 REV 00. Las Vegas, Nevada: CRWMS M&O. ACC: MOL.19990928.0217.

CRWMS M&O 1999b. *Thermal Modeling Parameters by Stratigraphic Unit.* Input Transmittal SSR-NEP-99261.T. Las Vegas, Nevada: CRWMS M&O. ACC: MOL.19990910.0090; MOL.19990920.0109.

CRWMS M&O 1999c. *ANSYS Thermal Calculations in Support of Waste Quantity, Mix and Throughput Study.* CAL-EBS-MG-000001 REV 00. Las Vegas, Nevada: CRWMS M&O. ACC: MOL.20000119.0134.

CRWMS M&O 1999d. *Ground Control - 00 (FY 00 WP # 12012124M9).* Activity Evaluation, October 29, 1999. Las Vegas, Nevada: CRWMS M&O. ACC: MOL.19991202.0161.

CRWMS M&O 1999e. *Single Heater Test Final Report.* BAB000000-01717-5700-00005 REV 00 ICN 1. Las Vegas, Nevada: CRWMS M&O. ACC: MOL.20000103.0634.

CRWMS M&O 1999f. *Development Plan for Ground Control for Emplacement Drifts for SR.* TDP-EBS-GE-000001 REV 01. Las Vegas, Nevada: CRWMS M&O. ACC: MOL.19991115.0234.

CRWMS M&O 1999g. *Natural Environment Data for Engineered Barrier System (EBS) Base Case.* Input Transmittal EBS-NEP-99273.Ta. Las Vegas, Nevada: CRWMS M&O. ACC: MOL.19991005.0146.

CRWMS M&O 1999h. *TBV-332/TBD-325 Resolution Analysis: Geotechnical Rock Properties.* B00000000-01717-5705-00134 REV 00. Las Vegas, Nevada: CRWMS M&O. ACC: MOL.19991005.0235.

CRWMS M&O 2000a. *Ground Control System Description Document.* SDD-GCS-SE-000001 REV 01. Las Vegas, Nevada: CRWMS M&O. ACC: MOL.20000803.0355.

CRWMS M&O 2000b. *Drift Degradation Analysis.* ANL-EBS-MD-000027 REV 01. Las Vegas, Nevada: CRWMS M&O. ACC: MOL.20001206.0006.

CRWMS M&O 2000c. *Fracture Geometry Analysis for the Stratigraphic Units of the Repository Host Horizon.* ANL-EBS-GE-000006 REV 00. Las Vegas, Nevada: CRWMS M&O. ACC: MOL.20000918.0286.

CRWMS M&O 2001. *Technical Work Plan for Subsurface Design Section FY 01 Work Activities.* TWP-MGR-MG-000001 REV 01 ADDENDUM D. Las Vegas, Nevada: CRWMS M&O. ACC: MOL.20010417.0455.

Deere, D.U. and Deere, D.W. 1988. "The Rock Quality Designation (RQD) Index in Practice." *Rock Classification Systems for Engineering Purposes.* Kirkaldie, L., ed. ASTM STP 984. 91-101. Philadelphia, Pennsylvania: American Society for Testing and Materials. TIC: 216484.

DOE (U.S. Department of Energy) 2000. *Quality Assurance Requirements and Description.* DOE/RW-0333P, Rev. 10. Washington, D.C.: U.S. Department of Energy, Office of Civilian Radioactive Waste Management. ACC: MOL. 20000427.0422.

Dowding, C.H. 1979. "Earthquake Stability of Rock Tunnels." *Tunnels & Tunnelling, 11,* 15-20. London, England: Morgan-Grampian Publishing. TIC: 242115.

Goodman, R.E. 1980. *Introduction to Rock Mechanics.* New York, New York: John Wiley & Sons. TIC: 218828.

Hardy, M.P. and Bauer, S.J. 1991. *Drift Design Methodology and Preliminary Application for the Yucca Mountain Site Characterization Project.* SAND89-0837. Albuquerque, New Mexico: Sandia National Laboratories. ACC: NNA.19910808.0105.

Hudson, J.A. and Priest, S.D. 1979. "Discontinuities and Rock Mass Geometry." *International Journal of Rock Mechanics and Mining Sciences & Geomechanics Abstracts, 16,* 339-362. Oxford, United Kingdom: Pergamon Press. TIC: 240802.

Itasca Consulting Group 1994. *User's Manual.* Volume 1 of *3DEC 3-Dimensional Distinct Element Code.* Version 1.5. Minneapolis, Minnesota: Itasca Consulting Group. TIC: 232818.

Itasca Consulting Group 1996a. *FLAC, Fast Lagrangian Analysis of Continua, Version 3.3.* Four Volumes. Minneapolis, Minnesota: Itasca Consulting Group. TIC: 236418; 236419; 236420; 236421.

Itasca Consulting Group 1996b. *UDEC, Universal Distinct Element Code, Version 3.0.* Three Volumes. Minneapolis, Minnesota: Itasca Consulting Group. TIC: 247190.

Itasca Consulting Group 1998. *FLAC, Fast Lagrangian Analysis of Continua: User's Guide, Version 3.4.* Minneapolis, Minnesota: Itasca Consulting Group. TIC: 247064.

MacGregor, J.G. 1997. *Reinforced Concrete: Mechanics and Design.* Prentice Hall International Series in Civil Engineering and Engineering Mechanics. Upper Saddle River, New Jersey: Prentice Hall. TIC: 242587.

Merritt, F.S., ed. 1983. *Standard Handbook for Civil Engineers.* 3rd Edition. New York, New York: McGraw-Hill. TIC: 206892.

Onofrei, M.; Gray, M.N.; Pusch, R.; Borgesson, L.; Karnland, O.; Shenton, B.; and Walker, B. 1993. *Sealing Properties of Cement-Based Grout Materials Used in the Rock Sealing Project.* AECL-10815. Pinawa, Manitoba, Canada: Whiteshell Laboratories. TIC: 210964.

Owen, D.R. and Hinton, E. 1980. *Finite Elements in Plasticity: Theory and Practice.* Swansea, United Kingdom: Pineridge Press Limited. TIC: 208975.

Sass, J.H.; Lachenbruch, A.H.; Dudley, W.W., Jr.; Priest, S.S.; and Munroe, R.J. 1988. *Temperature, Thermal Conductivity, and Heat Flow Near Yucca Mountain, Nevada: Some Tectonic and Hydrologic Implications.* Open-File Report 87-649. [Denver, Colorado]: U.S. Geological Survey. TIC: 203195.

Swanson Analysis Systems 1995. *ANSYS User's Manual for Revision 5.2.* Four Volumes. Houston, Pennsylvania: Swanson Analysis Systems. TIC: 221933.

Terzaghi, K. 1968. "Introduction to Tunnel Geology." *Rock Tunneling with Steel Supports.* Proctor, R.V. and White, T., eds. 17-99. Youngstown, Ohio: Commercial Shearing and Stamping Company. TIC: 244417.

Wickham, G.E.; Tiedemann, H.R.; and Skinner, E.H. 1972. "Support Determinations Based on Geologic Predictions." *Proceedings: North American Rapid Excavation and Tunneling Conference, Chicago, Illinois, June 5-7, 1972.* 43-64. New York, New York: American Institute of Mining, Metallurgical, and Petroleum Engineers. TIC: 226274.

Williams Form Engineering Corporation. 1997. Rock Anchor Systems, No. 397. Grand Rapids, Michigan: Williams Form Engineering Corporation. TIC: 245370.

8.2 CODES, STANDARDS, REGULATIONS, AND PROCEDURES

ACI 318-99 (American Concrete Institute) 1999. *Building Code Requirements for Structural Concrete (ACI 318-99) and Commentary (ACI 318R-99).* Farmington Hills, Michigan: American Concrete Institute. TIC: 245142.

AISC (American Institute of Steel Construction) 1997. *Manual of Steel Construction - Allowable Stress Design.* 9th Edition, 2nd Revision, 2nd Impression. Chicago, Illinois: American Institute of Steel Construction. TIC: 240772.

AP-2.21Q, Rev. 1, ICN 0, BSCN 001. *Quality Determinations and Planning for Scientific, Engineering, and Regulatory Compliance Activities.* Washington, D.C.: U.S. Department of Energy, Office of Civilian Radioactive Waste Management. ACC: MOL.20010212.0018.

AP-3.10Q, Rev. 2, ICN 4. *Analyses and Models.* Washington, D.C.: U.S. Department of Energy, Office of Civilian Radioactive Waste Management. ACC: MOL.20010405.0009.

AP-3.15Q, Rev 2, ICN 1. *Managing Technical Product Inputs.* Washington, D.C.: U.S. Department of Energy, Office of Civilian Radioactive Waste Management. ACC: MOL.20010405.0011.

AP-SI.1Q, Rev. 3, ICN 1. *Software Management.* Washington, D.C.: U.S. Department of Energy, Office of Civilian Radioactive Waste Management. ACC: MOL. 20010515.0126.

AP-SV.1Q, Rev. 0, ICN 2. *Control of the Electronic Management of Information.* Washington, D.C.: U.S. Department of Energy, Office of Civilian Radioactive Waste Management. ACC: MOL.20000831.0065.

ASTM (American Society for Testing and Materials) A 36/A 36M-00a. 2000. *Standard Specification for Carbon Structural Steel.* West Conshohocken, Pennsylvania: American Society for Testing and Materials. TIC: 249500.

8.3 SOURCE DATA

CRWMS M&O 1994b. *Software Code: 3DEC.* V 1.5. PC. B00000000-01717-1200-30013.

CRWMS M&O 1999i. *Software Code: FLAC V3.5.* V 3.5. PC. 10167-3.5-00.

CRWMS M&O 1999j. *Software Code: UDEC V3.0.* V 3.0. PC. 10173-3.0-00.

CRWMS M&O 2000d. *Software Code: ANSYS. V5.2SGI.* Unix. 30013 V5.2SGI.

MO0001SEPSRMPC.000. Summary of Rock Mass Properties for Confining Stress Ranging from 0 to 42 MPA. Submittal date: 01/11/2000.

MO0002SPAFRA06.002. Fracture Geometry for Stratigraphic Units of Repository Host Horizon. Submittal date: 03/17/2000.

MO0003RIB00079.000. Rock Mechanical Properties. Submittal date: 03/30/2000.

MO0003SEPSDARS.002. Preliminary Seismic Design Acceleration Response Spectra for the Repository Level (Point B). Submittal date: 03/30/2000. Submit to RPC URN-0203

MO0003SEPSDATH.003. Preliminary Seismic Design Acceleration Time Histories for the Repository Level (Point B). Submittal date: 03/30/2000. Submit to RPC URN-0204

MO0004RIB00035.001. Rock Thermal Expansion. Submittal date: 04/07/2000.

MO0004SEPPGVRB.006. Preliminary Seismic Design Peak Ground Velocity for the Repository Level (Point B). Submittal date: 04/04/2000. Submit to RPC URN-0205

MO0007RIB00077.000. In Situ Rock Conditions. Submittal date: 07/18/2000.

MO0105MWDTHE05.009. Input and Output Files for Thermal Management Analysis for Low Temperature Repository Design for SR. Submittal date: 05/10/2001. Submit to RPC URN-0835

MO9911SEPGRP34.000. Geotechnical Rock Properties. Submittal date: 11/10/1999.

MO9911SPAWAQ01.000. Input and Output Files for ANSYS Thermal Calculations in Support of Waste Quantity, Mix and Throughput Study. Submittal date: 11/24/1999.

SN0003T0571897.013. Thermal Modeling Parameters by Stratigraphic Unit. Submittal date: 03/29/2000.

SN0011T0571897.014. Revised Thermal Modeling Parameters for Conduction-Only Models by Stratigraphic Unit. Submittal date: 11/29/2000.

SNF37100195002.001. Hydraulic Fracturing Stress Measurements in Test Hole: ESF-AOD-HDFR1, Thermal Test Facility, Exploratory Studies Facility at Yucca Mountain. Submittal date: 12/18/1996.

SNL02112293001.002. Results from Shear Stress Experiments on Natural Fractures from NRG-7. Submittal date: 03/10/1995.

SNL02112293001.003. Results from Shear Stress Experiments on Natural Fractures from NRG-4 & NRG-6. Submittal date: 03/13/1995.

SNL02112293001.005. Mechanical Properties of Fractures in Specimens from Drillhole USW SD-9. Submittal date: 07/15/1996.

SNL02112293001.007. Mechanical Properties of Fractures in Specimens from Drillholes USW NRG-7/7A and USW SD-12. Submittal date: 08/08/1996.

8.4 OUTPUT DATA

MO0004MWDEMP02.003. Input and Output Files for Ground Control for Emplacement Drifts for SR. Submittal date: 04/05/2000.

MO0105MWDGRO02.008. Input and Output Files for Ground Control for Low Temperature Repository Design. Submittal date: 05/10/2001.

ATTACHMENT I CALCULATION OF SPACING FOR VERTICAL JOINTS

CALCULATION OF SPACING FOR VERTICAL JOINTS

It is observed that two predominant sub-vertical joint sets exist in the Tptpmn and Tptpll units. Table I-1 presents the joint set orientation and mean joint spacing data based on DTN: MO0002SPAFRA06.002. In order to account both joint sets for the two-dimensional numerical analysis, a calculation was conducted to obtain the combined vertical joint spacing. The equation presented in Hudson and Priest (1979, p. 341) was used for this calculation as presented below.

$$\lambda_\theta = \sum_{i=1}^{n} \lambda_i \cos\theta_i \qquad \text{(Eq. I-1)}$$

where λ_θ = combined joint frequency, 1/m
λ_i = frequency of the ith set along the normal to the ith set, 1/m
θ_i = acute angle between the scanline and the normal to the ith set, degree

Calculation of the combined joint frequencies and joint spacings for various drift orientation are shown in Tables I-2 and I-3 for the non-lithophysal and lithophysal units, respectively. The results are graphically presented in Figures I-1 and I-2. For conservatism, the highest combined joint frequency, or the minimum combined joint spacing, was selected in the two-dimensional numerical analysis. The combined joint spacing selected are 0.54 m for the Tptpmn unit and 1.93 m for the Tptpll unit. The average orientations (dips) of the combined vertical joints are calculated using the mean values of the joint sets #1 and #2 for the corresponding rock units, and are equal to 83.5 degrees for the Tptpmn unit and 80.5 degrees for the Tptpll unit (see Table I-1).

Table I-1. Joint Set Orientation and Spacing Data

Rock Unit	Joint Set Number	Mean Strike Direction (degree)	Mean Dip (degree)	Mean Joint Spacing (m)
Non-lithophysal (Tptpmn)	1	131	84	0.60
	2	209	83	1.92
	3	329	9	0.56
Lithophysal (Tptpll)	1	145	82	3.38
	2	180	79	4.05
	3	315	5	2.94

Source: DTN: MO0002SPAFRA06.002

Table I-2. Calculation of Combined Joint Spacing for Non-Lithophysal Unit (Tptpmn)

Drift Orientation (degree)	θ_1 (degree)	θ_2 (degree)	Projected Frequency for Joint Set 1 (/m)	Projected Frequency for Joint Set 2 (/m)	Combined Joint Frequency (/m)	Combined Joint Spacing (m)
0	41	61	1.25	0.25	1.50	0.66
5	36	66	1.34	0.21	1.55	0.64
10	31	71	1.42	0.17	1.59	0.63
15	26	76	1.49	0.13	1.62	0.62
20	21	81	1.55	0.08	1.63	0.61
25	16	86	1.59	0.04	1.63	0.61
30	11	89	1.63	0.01	1.64	0.61
35	6	84	1.65	0.05	1.70	0.59
40	1	79	1.66	0.10	1.76	0.57
45	4	74	1.65	0.14	1.80	0.56
50	9	69	1.64	0.19	1.83	0.55
55	14	64	1.61	0.23	1.84	0.54
60	19	59	1.57	0.27	1.84	0.54
65	24	54	1.52	0.31	1.82	0.55
70	29	49	1.45	0.34	1.79	0.56
75	34	44	1.38	0.37	1.75	0.57
80	39	39	1.29	0.40	1.69	0.59
85	44	34	1.19	0.43	1.62	0.62
90	49	29	1.09	0.46	1.54	0.65
95	54	24	0.97	0.48	1.45	0.69
100	59	19	0.85	0.49	1.35	0.74
105	64	14	0.73	0.51	1.23	0.81
110	69	9	0.59	0.51	1.11	0.90
115	74	4	0.46	0.52	0.98	1.02
120	79	1	0.32	0.52	0.84	1.19
125	84	6	0.17	0.52	0.69	1.45
130	89	11	0.03	0.51	0.54	1.85
135	86	16	0.12	0.50	0.62	1.62
140	81	21	0.26	0.49	0.75	1.34
145	76	26	0.40	0.47	0.87	1.15
150	71	31	0.54	0.45	0.99	1.01
155	66	36	0.67	0.42	1.10	0.91
160	61	41	0.80	0.39	1.20	0.84
165	56	46	0.93	0.36	1.29	0.78
170	51	51	1.04	0.33	1.37	0.73
175	46	56	1.15	0.29	1.44	0.69

Table I-3. Calculation of Combined Joint Spacing for Lithophysal Unit (Tptpll)

Drift Orientation (degree)	θ_1 (degree)	θ_2 (degree)	Projected Frequency for Joint Set 1 (/m)	Projected Frequency for Joint Set 2 (/m)	Combined Joint Frequency (/m)	Combined Joint Spacing (m)
0	55	90	0.17	0.00	0.17	5.89
5	50	85	0.19	0.02	0.21	4.72
10	45	80	0.21	0.04	0.25	3.96
15	40	75	0.23	0.06	0.29	3.44
20	35	70	0.24	0.08	0.33	3.06
25	30	65	0.26	0.10	0.36	2.77
30	25	60	0.27	0.12	0.39	2.55
35	20	55	0.28	0.14	0.42	2.38
40	15	50	0.29	0.16	0.44	2.25
45	10	45	0.29	0.17	0.47	2.15
50	5	40	0.29	0.19	0.48	2.07
55	0	35	0.30	0.20	0.50	2.01
60	5	30	0.29	0.21	0.51	1.97
65	10	25	0.29	0.22	0.52	1.94
70	15	20	0.29	0.23	0.52	1.93
75	20	15	0.28	0.24	0.52	1.94
80	25	10	0.27	0.24	0.51	1.96
85	30	5	0.26	0.25	0.50	1.99
90	35	0	0.24	0.25	0.49	2.04
95	40	5	0.23	0.25	0.47	2.12
100	45	10	0.21	0.24	0.45	2.21
105	50	15	0.19	0.24	0.43	2.33
110	55	20	0.17	0.23	0.40	2.49
115	60	25	0.15	0.22	0.37	2.69
120	65	30	0.13	0.21	0.34	2.95
125	70	35	0.10	0.20	0.30	3.30
130	75	40	0.08	0.19	0.27	3.76
135	80	45	0.05	0.17	0.23	4.43
140	85	50	0.03	0.16	0.18	5.42
145	90	55	0.00	0.14	0.14	7.06
150	85	60	0.03	0.12	0.15	6.70
155	80	65	0.05	0.10	0.16	6.42
160	75	70	0.08	0.08	0.16	6.21
165	70	75	0.10	0.06	0.17	6.06
170	65	80	0.13	0.04	0.17	5.96
175	60	85	0.15	0.02	0.17	5.90

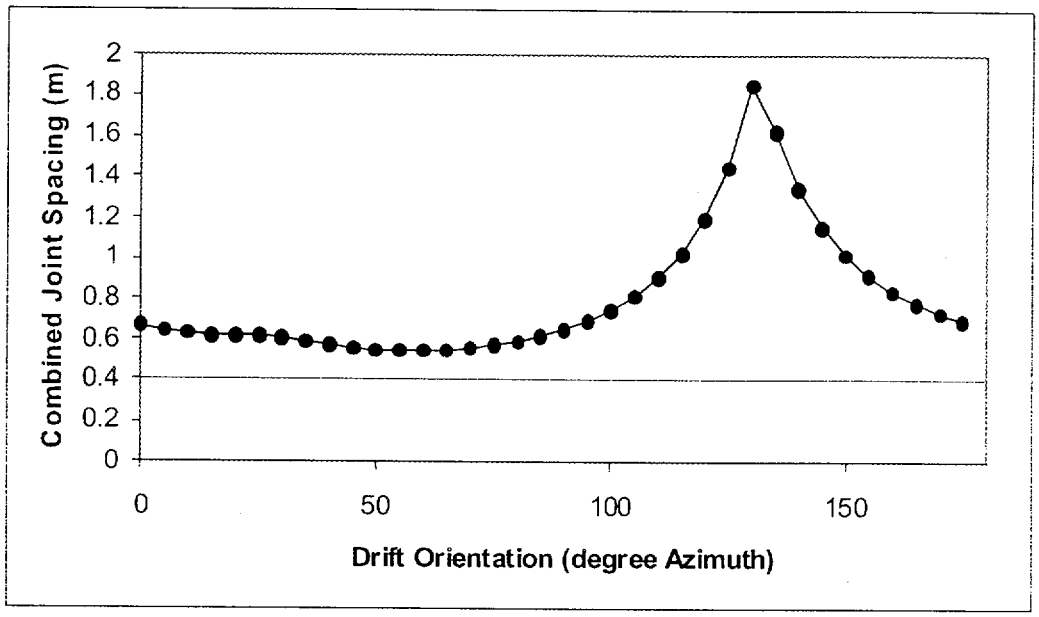

Figure I-1. Calculated Combined Joint Spacing for Various Drift Orientations for Non-Lithophysal Unit (Tptpmn)

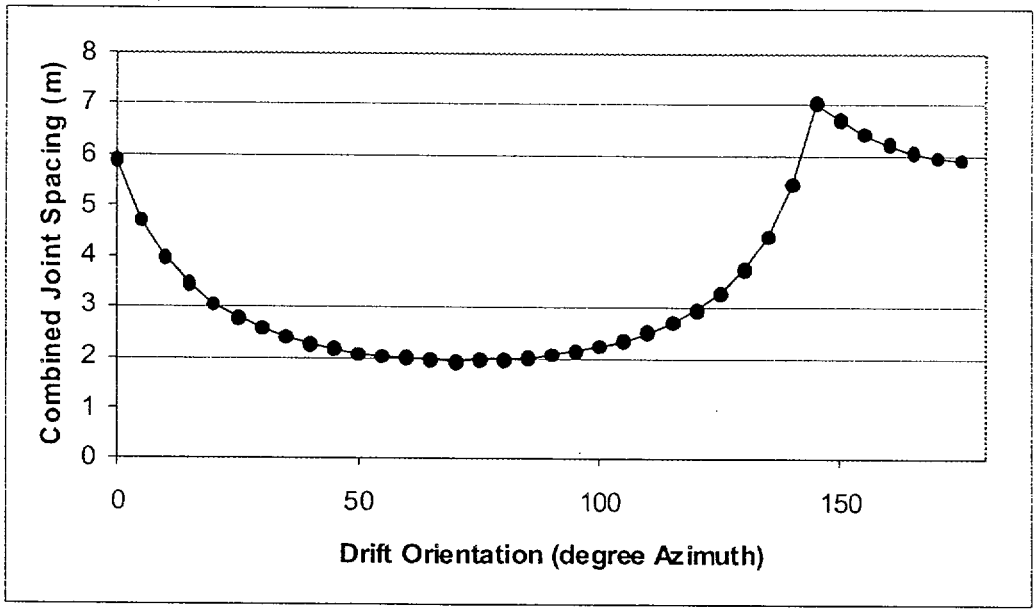

Figure I-2. Calculated Combined Joint Spacing for Various Drift Orientations for Lithophysal Unit (Tptpll)

ATTACHMENT II EFFECTS OF VARIATION OF ROCK MASS STRENGTH

EFFECTS OF VARIATION OF ROCK MASS STRENGTH

This attachment presents the results of a preliminary study on the effects of variation of rock mass strength, primarily cohesion and friction angle, on the drift displacements and stresses. The study is focused on the thermomechanical response of unsupported emplacement drifts subjected to in situ stress and thermal loads. Both the high and low temperature conditions were analyzed. The geometry and boundary conditions used are illustrated in Figure 6-4. The numerical analyses were performed using FLAC.

For purposes of comparison, the displacements and stresses were computed for values of cohesion and friction angle from Table 4-5a using the values for confining stress of 0-42 MPa for the Low Strength runs and the values for confining stress of 0-3 MPa for the High Strength runs. In addition, cases with a lower value in cohesion and friction angle in each rock category, for example a cohesion of 2.0 MPa combined with a friction angle of 37 degrees for RMQ category of 1, was also considered. Table II-1 lists the cases analyzed in this study.

Table II-1. Thermal Conditions and Strength Properties Used in Various Cases

Case ID	Thermal Condition	RMQ Category	Strength Property	
			Cohesion (MPa)	Friction Angle (degrees)
H1H	High Temperature	1	2.0	56
H1La	High Temperature	1	2.0	37
L1H	Low Temperature	1	2.0	56
L5H	Low Temperature	5	4.1	58
L1L	Low Temperature	1	8.1	37
L5L	Low Temperature	5	11.6	42
L1La	Low Temperature	1	2.0	37
L5La	Low Temperature	5	4.1	42

Under High Temperature Condition

Figures II-1a and II-1b show the comparisons of time histories of the vertical and horizontal closures between the cases H1H and H1La for the Category 1 rock and in situ horizontal to vertical stress ratio (K_o) values of 0.3 and 1.0 under the high temperature condition. Results show that the rock deformation is very sensitive to the rock mass friction angle, especially under the thermal loading condition. For example, the maximum horizontal closure increases from 2.9 mm to 7.9 mm for K_o=0.3 and from 10.6 mm to 17.0 mm for K_o=1.0 by reducing the friction angle from 56 degrees to 37 degrees.

Figures II-2a and II-2b show the comparison of time histories of major principal stresses near the drift opening between the cases H1H and H1La. Again, the stresses are also dependent on the friction angle, and are expected to be much lower when the friction angle is lower under the thermal loading condition.

Figure II-3a compares with Figure II-3b for the strength-to-stress ratios around the drift at 10 years after emplacement for the cases H1H and H1La. It is indicated that a decrease in the friction angle from 56 to 37 degrees would substantially increase the potential yield zone to depth of approximately 2.5 m into rock (see Figure II-3b), compared to less than 1 m when the friction angle is 56 degrees (see Figure II-3a).

Under Low Temperature Condition

Figures II-4a through II-5b show the comparisons of time histories of the vertical and horizontal closures among the cases L1H, L5H, L1L, and L5L for RMQ categories of 1 and 5 and in situ horizontal to vertical stress ratio (K_o) values of 0.3 and 1.0 under the low temperature condition. It appears that the combination of a low friction angle with a high cohesion is expected to have a nearly equivalent effect of a high friction angle combined with a low cohesion, especially for the weaker rock (RMQ=1). The cases with a low cohesion (L1H and L5H) show a slightly higher deformation.

Figures II-6a through II-7b show the comparisons of time histories of major principal stresses near the drift opening among the cases L1H, L5H, L1L, and L5L. Similar observations as those to the drift closures can be obtained.

Additional analyses were also conducted using lower values of cohesion and friction angle in each rock category for emplacement drifts under the low temperature condition. The time histories of drift closures and stresses adjacent to the drift opening are compared with those from the corresponding cases using the high strength rock property values in Figures II-8a through II-11b. These comparisons suggest that the effects of variation of rock mass strength properties on the thermomechanical response are also dependent on the rock mass modulus of elasticity, or the rock mass quality category. For a stronger rock with a higher modulus of elasticity, effects of the reduction in the strength property values appears to be less profound on the rock mass response.

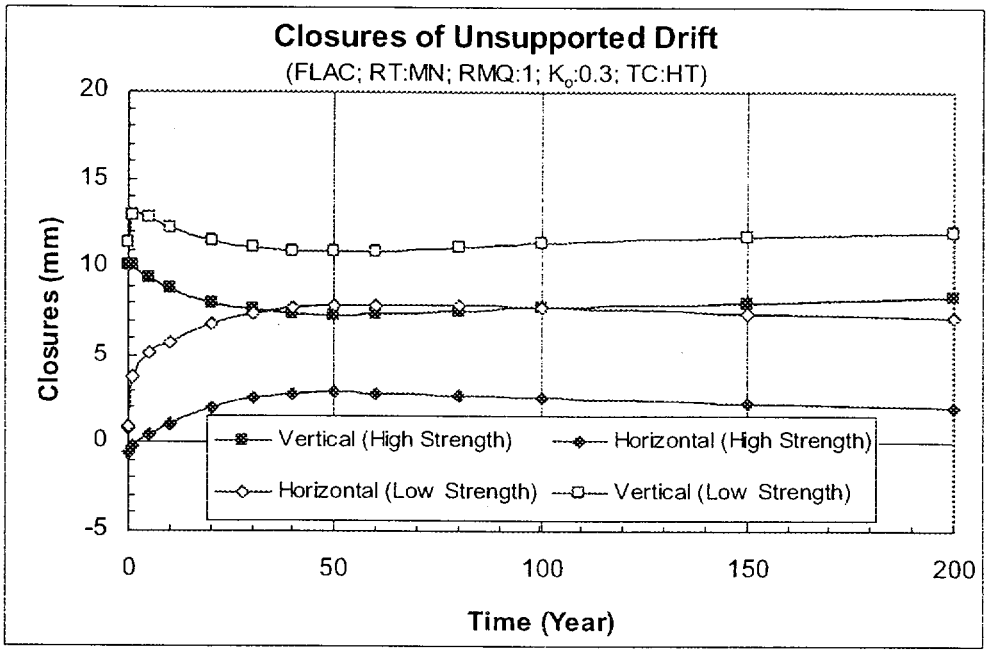

(a)

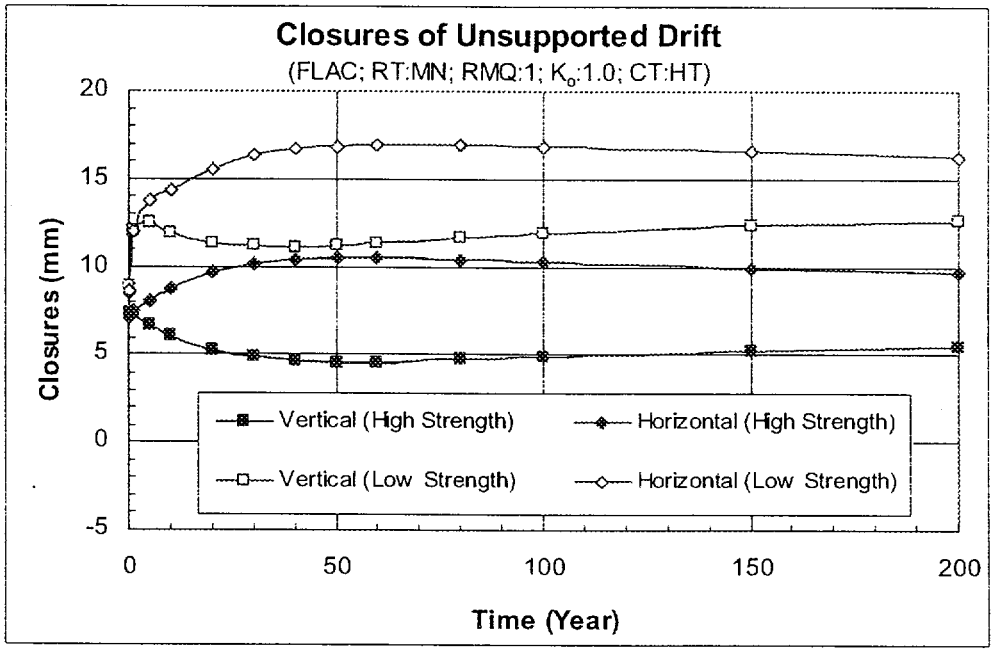

(b)

Figure II-1. Comparisons of Time Histories of Drift Closures Between Cases H1H and H1La under High Temperature Condition for Non-Lithophysal Rock and RMQ Category of 1: (a) K_o=0.3; (b) K_o=1.0

Note: RT=Rock Type; MN=Middle Non-Lithophysal Unit; RMQ=Rock Mass Quality Category; K_o=In Situ Horizontal to Vertical Stress Ratio; TC=Thermal Condition; HT=High Temperature.

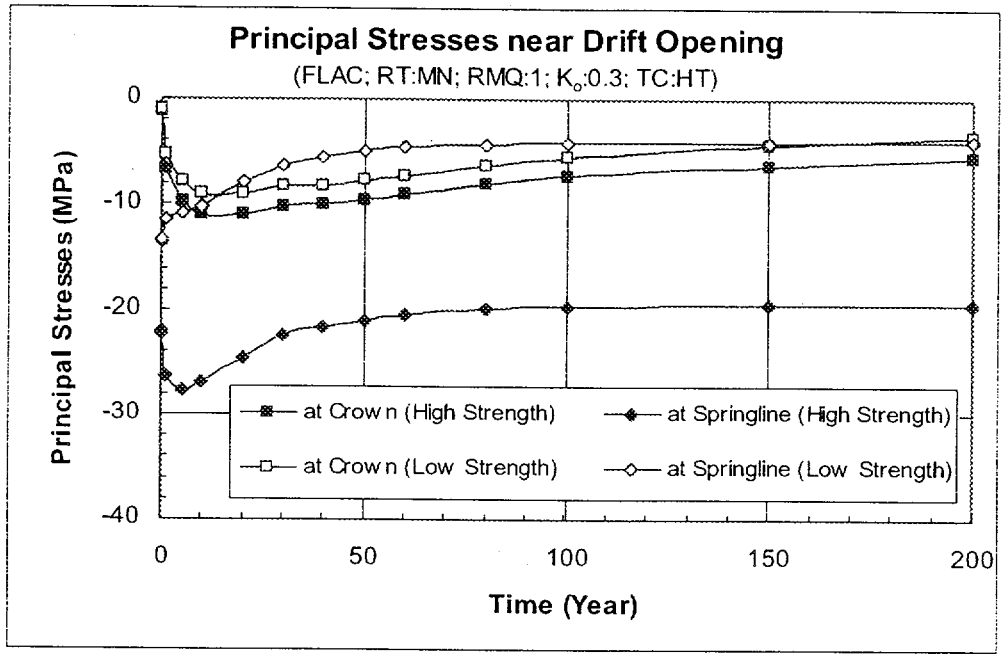

(a)

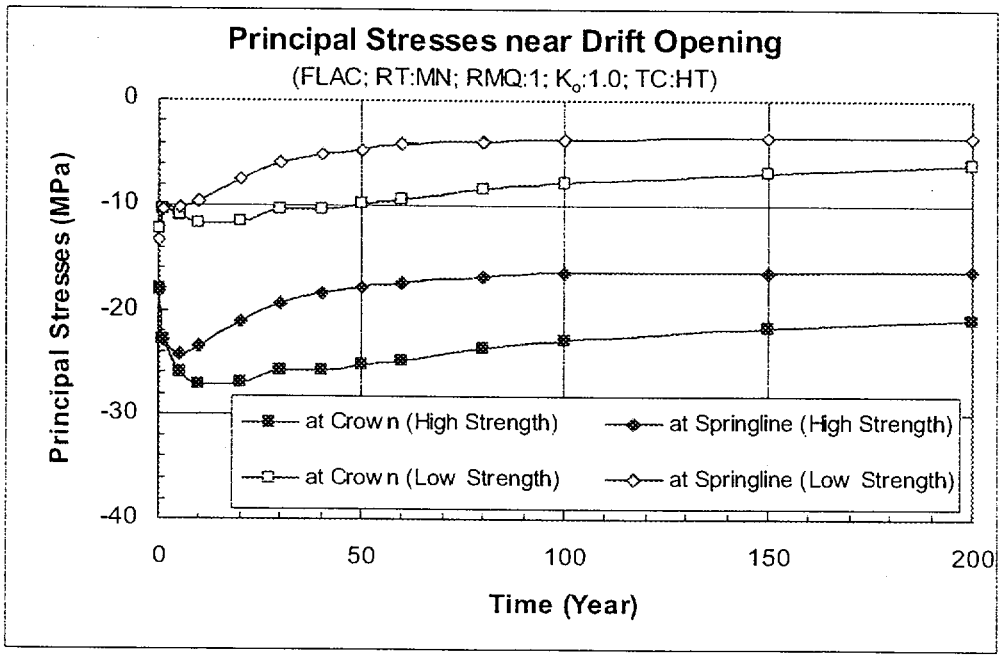

(b)

Figure II-2. Comparisons of Time Histories of Major Principal Stresses near Drift Opening Between Cases H1H and H1La under High Temperature Condition for Non-Lithophysal Rock and RMQ Category of 1: (a) K_o=0.3; (b) K_o=1.0

Note: RT=Rock Type; MN=Middle Non-Lithophysal Unit; RMQ=Rock Mass Quality Category; K_o=In Situ Horizontal to Vertical Stress Ratio; TC=Thermal Condition; LT=High Temperature.

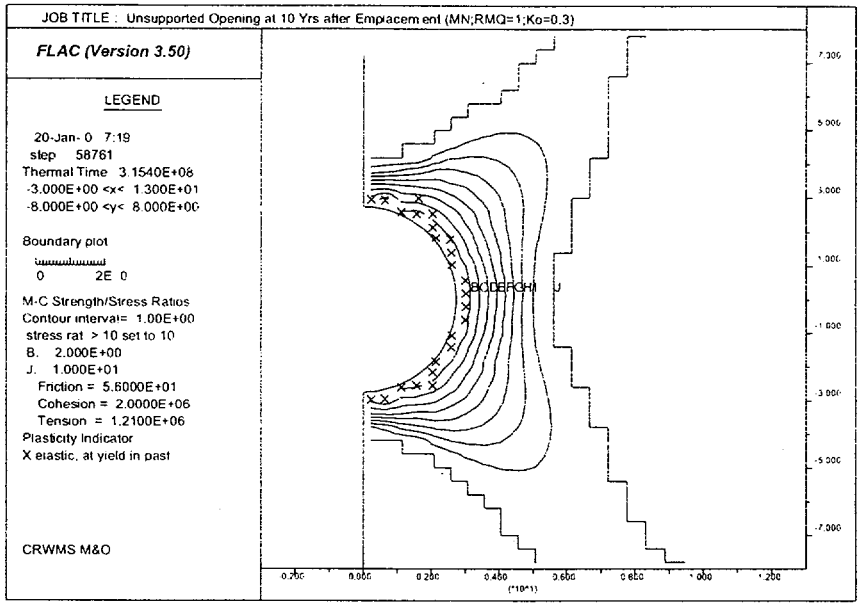

(a)

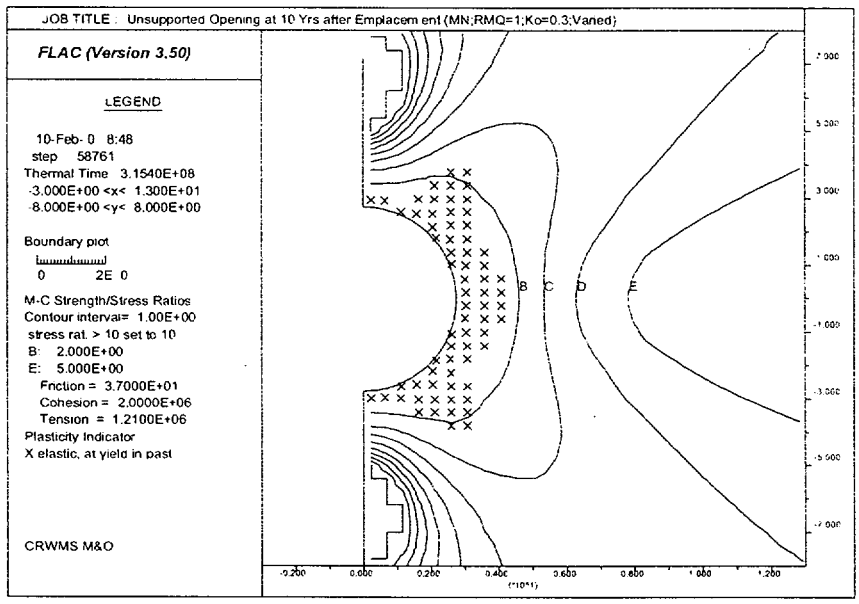

(b)

Figure II-3. Comparisons of Strength/Stress Ratio Contours and Plasticity Indicators Between Cases H1H and H1La for Unsupported Emplacement Drifts at 10 Years After Heating for Combined In Situ Stress and Thermal Loads, RMQ Category 1, and In Situ Stress Ratio K_o of 0.3: (a) High Strength (H1H Case); (b) Low Strength (H1La Case)

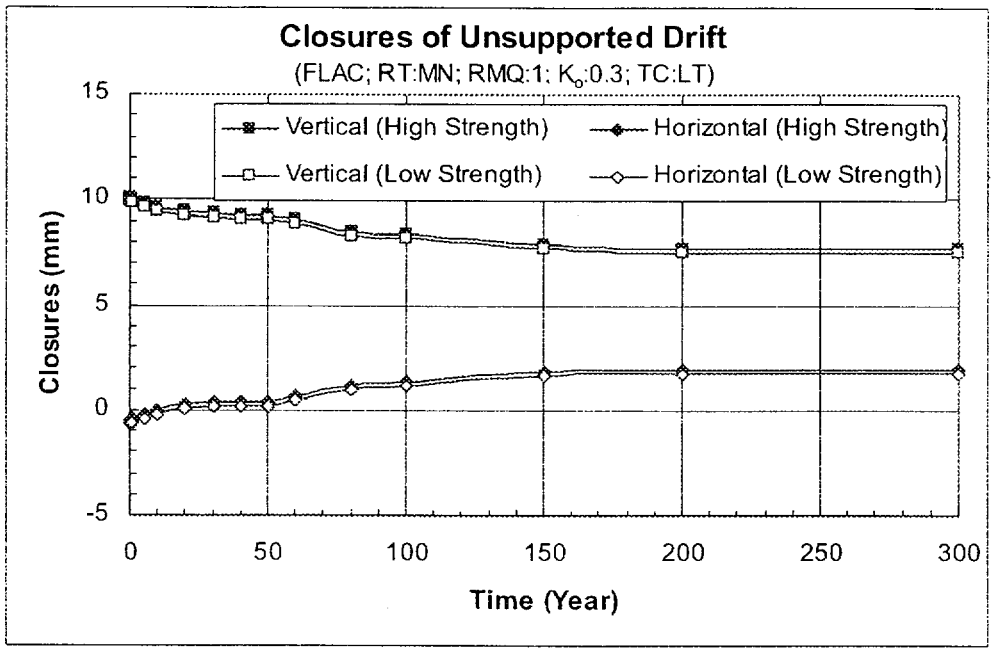

(a)

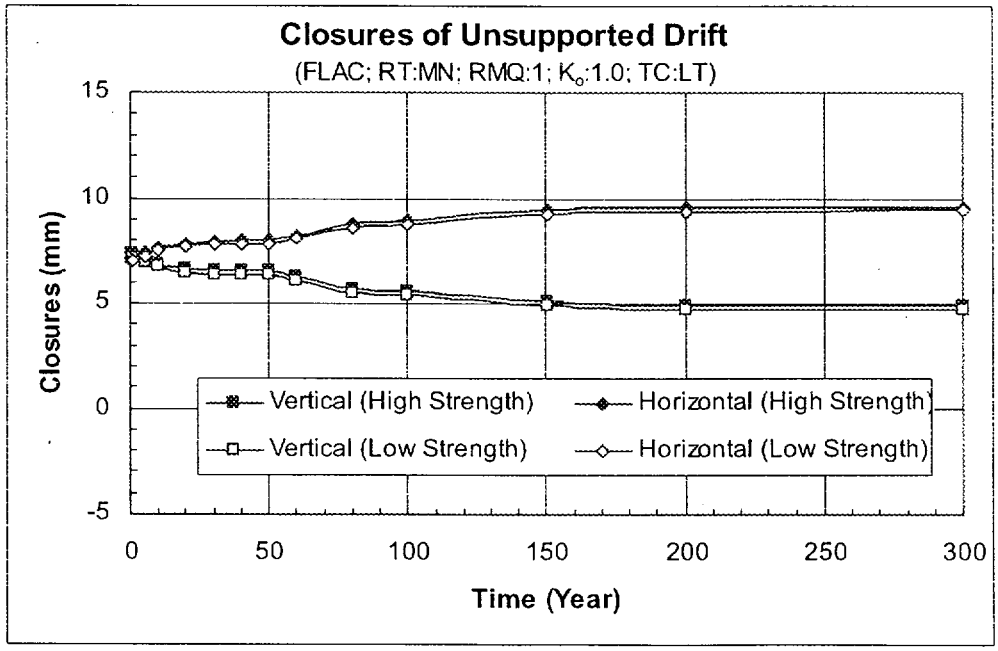

(b)

Figure II-4. Comparisons of Time Histories of Drift Closures Between Cases L1H and L1L under Low Temperature Condition for Non-Lithophysal Rock and RMQ Category of 1: (a) K_o=0.3; (b) K_o=1.0

Note: RT=Rock Type; MN=Middle Non-Lithophysal Unit; RMQ=Rock Mass Quality Category; K_o=In Situ Horizontal to Vertical Stress Ratio; TC=Thermal Condition; LT=Low Temperature.

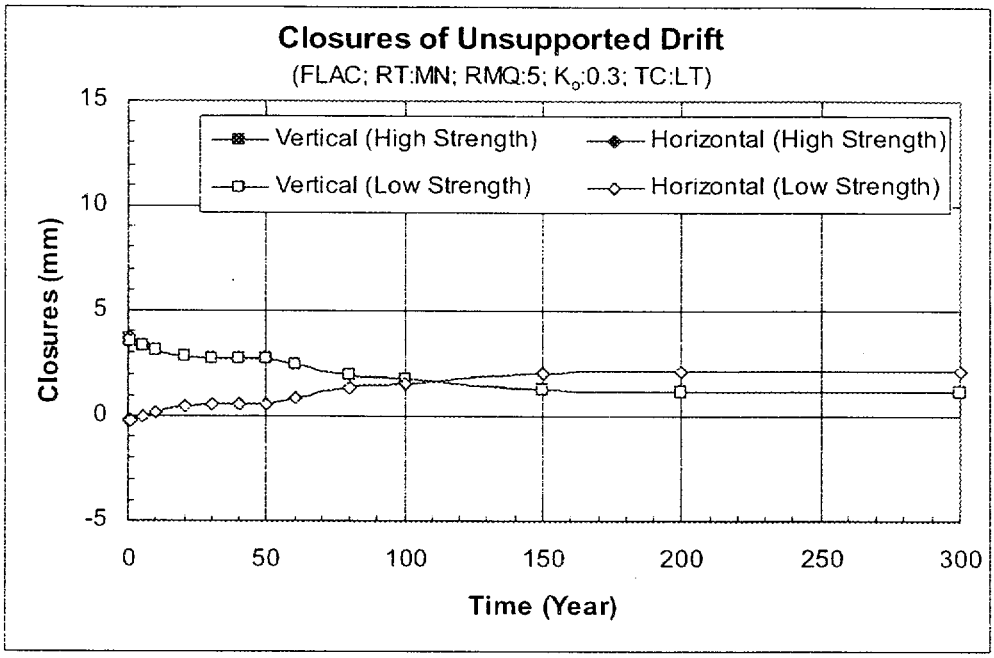

(a)

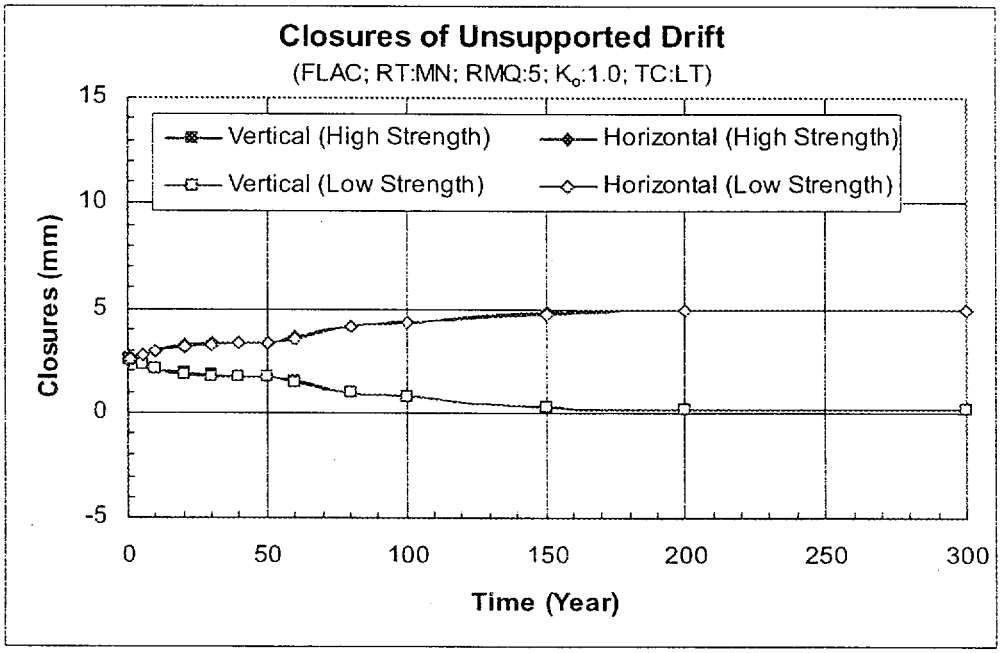

(b)

Figure II-5. Comparisons of Time Histories of Drift Closures Between Cases L5H and L5L under Low Temperature Condition for Non-Lithophysal Rock and RMQ Category of 5: (a) K_o=0.3; (b) K_o=1.0

Note: RT=Rock Type; MN=Middle Non-Lithophysal Unit; RMQ=Rock Mass Quality Category; K_o=In Situ Horizontal to Vertical Stress Ratio; TC=Thermal Condition; LT=Low Temperature.

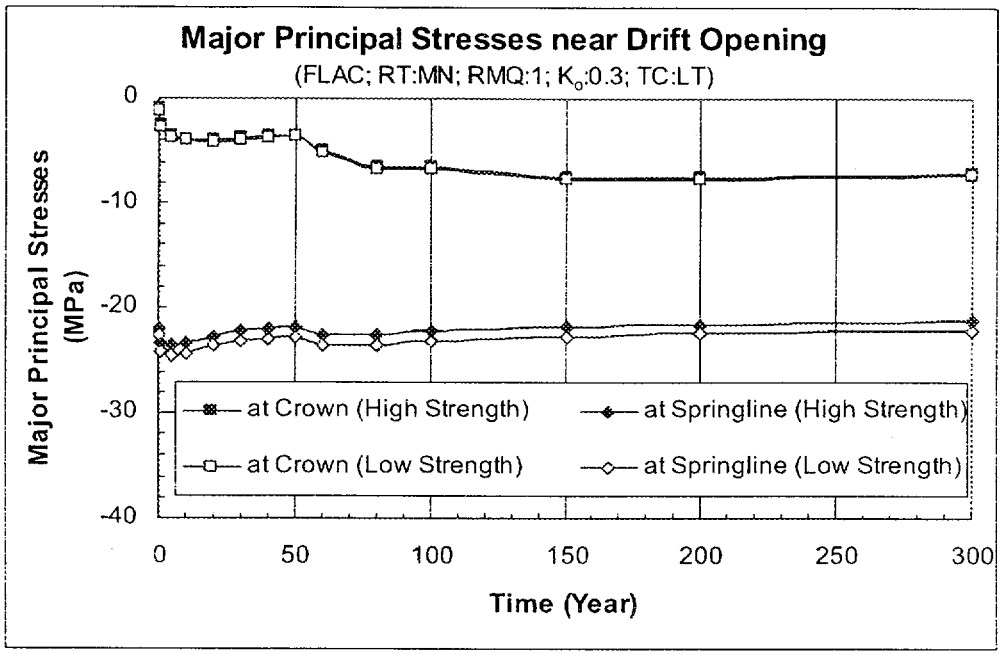

(a)

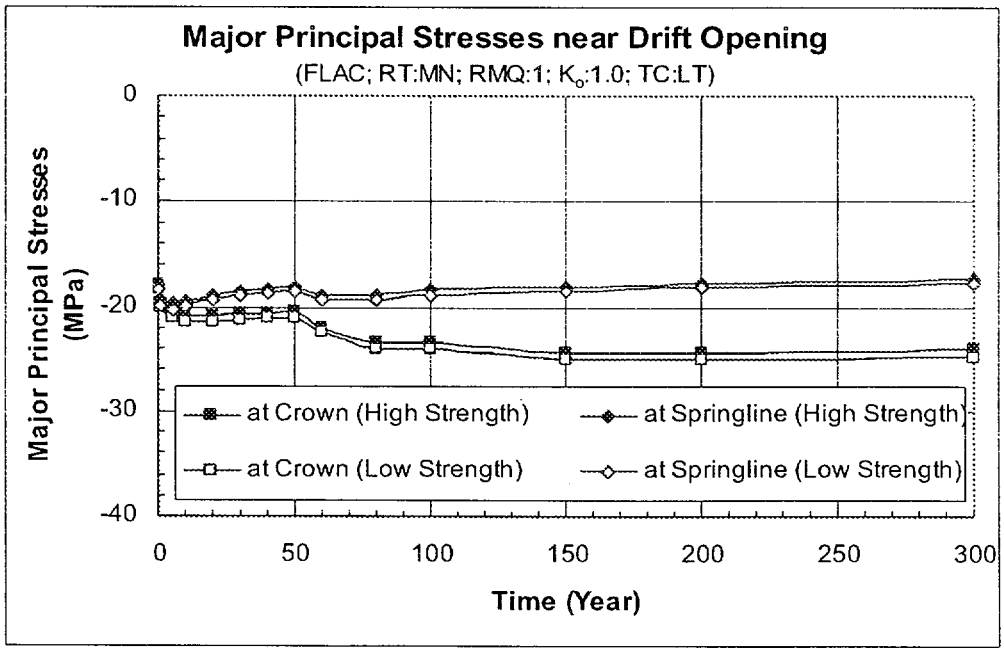

(b)

Figure II-6. Comparisons of Time Histories of Major Principal Stresses near Drift Opening Between Cases L1H and L1L under Low Temperature Condition for Non-Lithophysal Rock and RMQ Category of 1: (a) K_o=0.3; (b) K_o=1.0

Note: RT=Rock Type; MN=Middle Non-Lithophysal Unit; RMQ=Rock Mass Quality Category; K_o=In Situ Horizontal to Vertical Stress Ratio; TC=Thermal Condition; LT=Low Temperature.

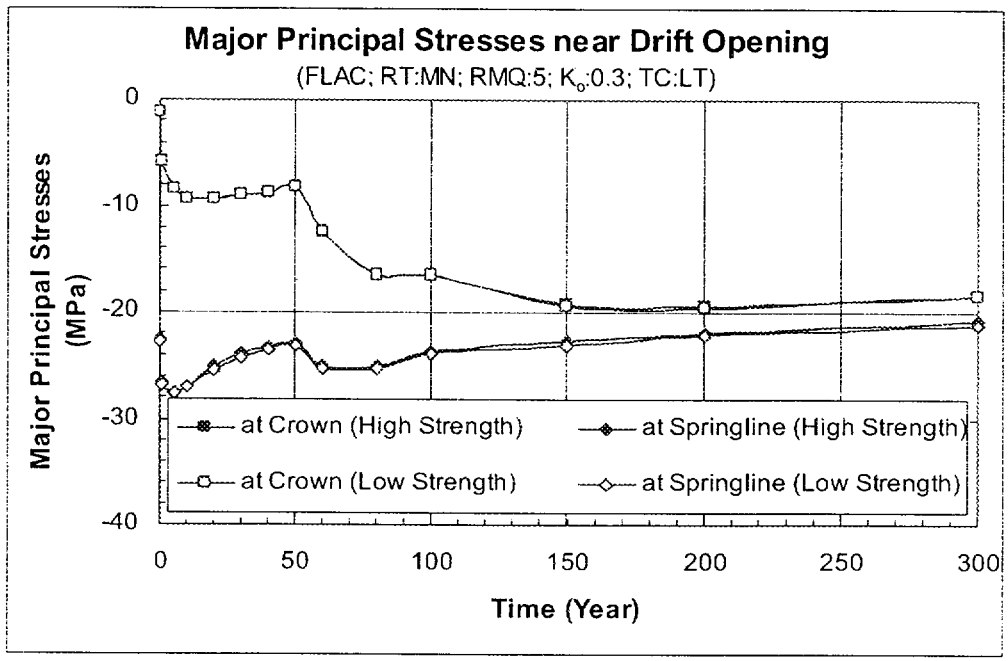

(a)

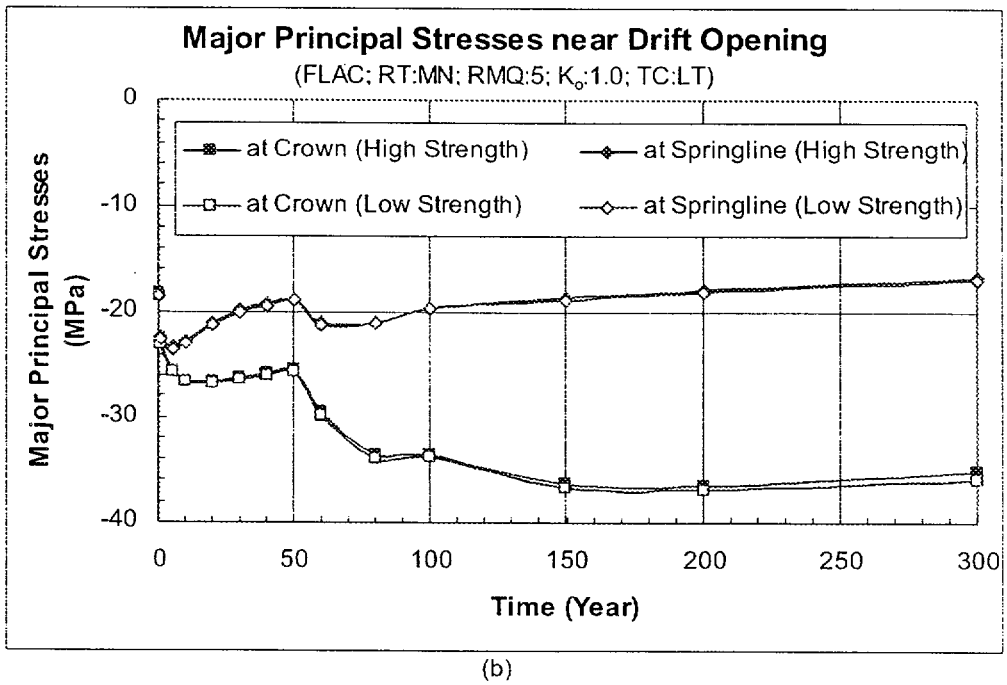

(b)

Figure II-7. Comparisons of Time Histories of Major Principal Stresses near Drift Opening Between Cases L5H and L5L under Low Temperature Condition for Non-Lithophysal Rock and RMQ Category of 5: (a) K_o=0.3; (b) K_o=1.0

Note: RT=Rock Type; MN=Middle Non-Lithophysal Unit; RMQ=Rock Mass Quality Category; K_o=In Situ Horizontal to Vertical Stress Ratio; TC=Thermal Condition; LT=Low Temperature.

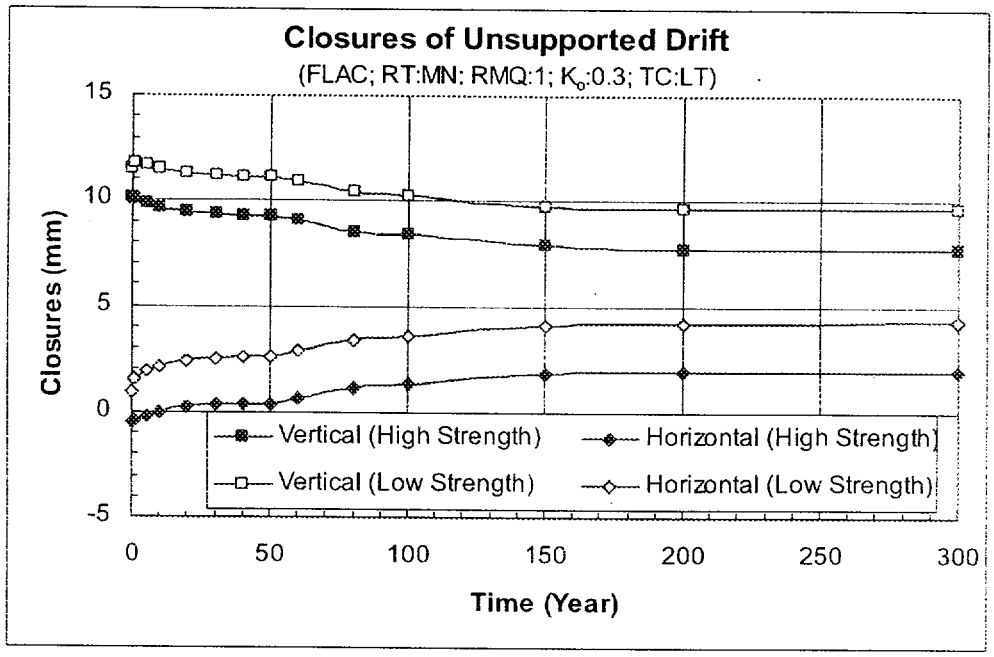

(a)

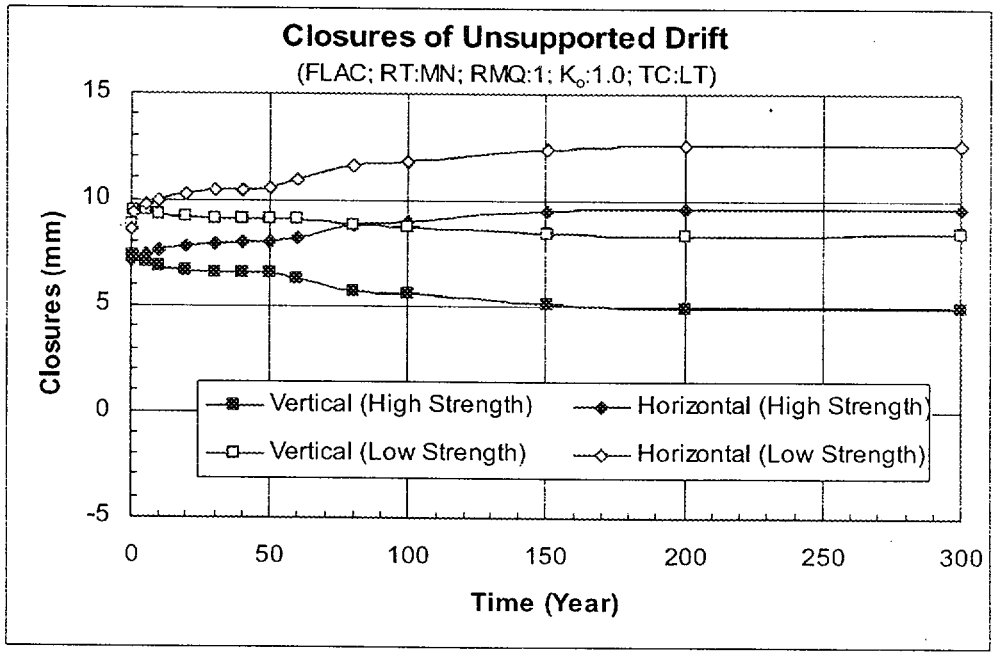

(b)

Figure II-8. Comparisons of Time Histories of Drift Closures Between Cases L1H and L1La under Low Temperature Condition for Non-Lithophysal Rock and RMQ Category of 1: (a) K_o=0.3; (b) K_o=1.0

Note: RT=Rock Type; MN=Middle Non-Lithophysal Unit; RMQ=Rock Mass Quality Category; K_o=In Situ Horizontal to Vertical Stress Ratio; TC=Thermal Condition; LT=Low Temperature.

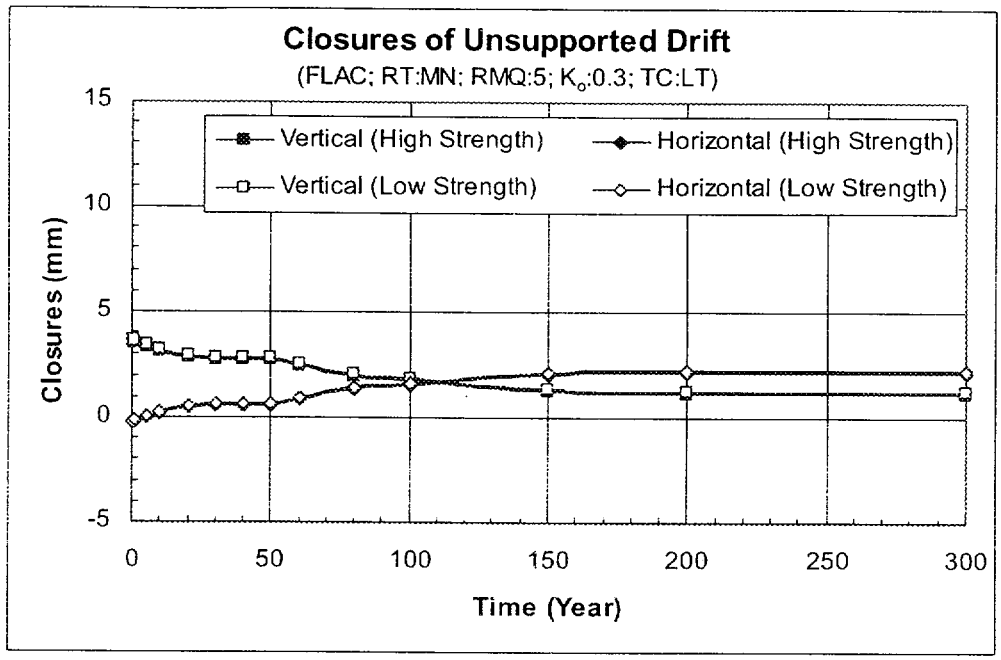

(a)

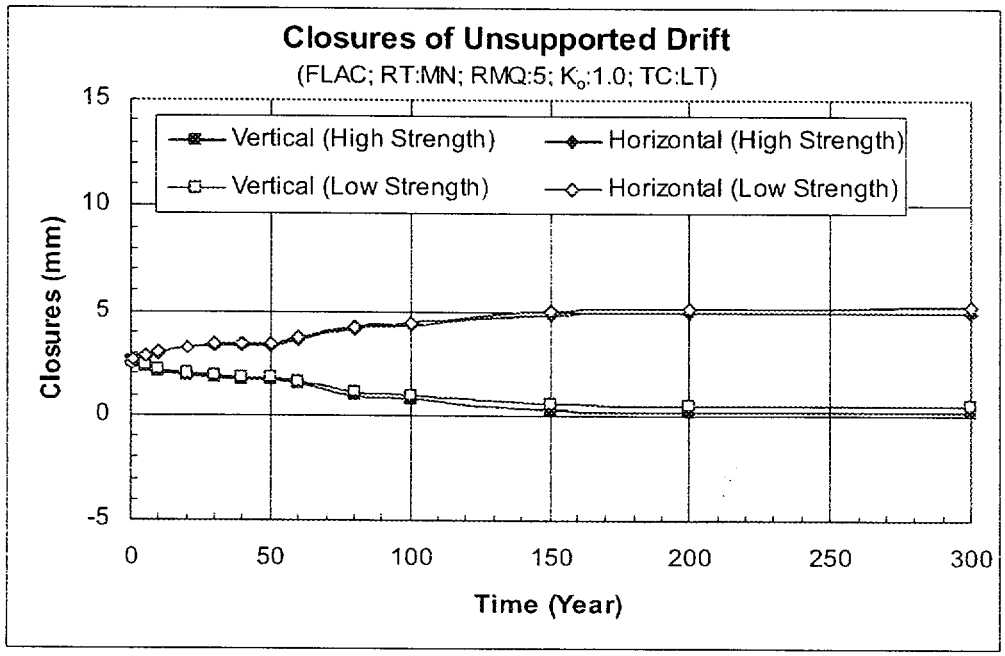

(b)

Figure II-9. Comparisons of Time Histories of Drift Closures Between Cases L5H and L5La under Low Temperature Condition for Non-Lithophysal Rock and RMQ Category of: (a) K_o=0.3; (b) K_o=1.0

Note: RT=Rock Type; MN=Middle Non-Lithophysal Unit; RMQ=Rock Mass Quality Category; K_o=In Situ Horizontal to Vertical Stress Ratio; TC=Thermal Condition; LT=Low Temperature.

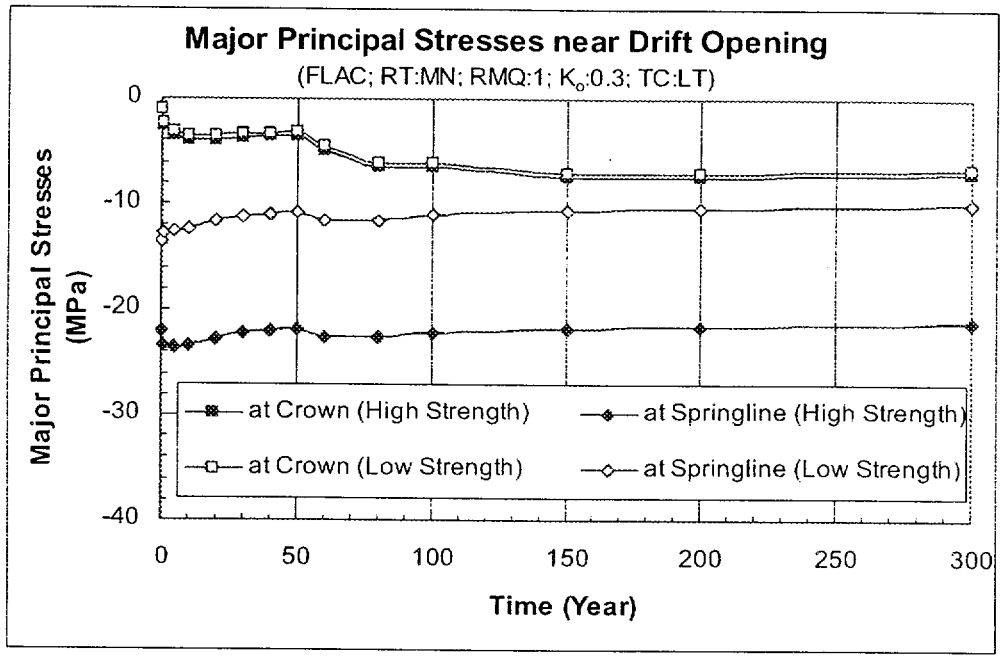

(a)

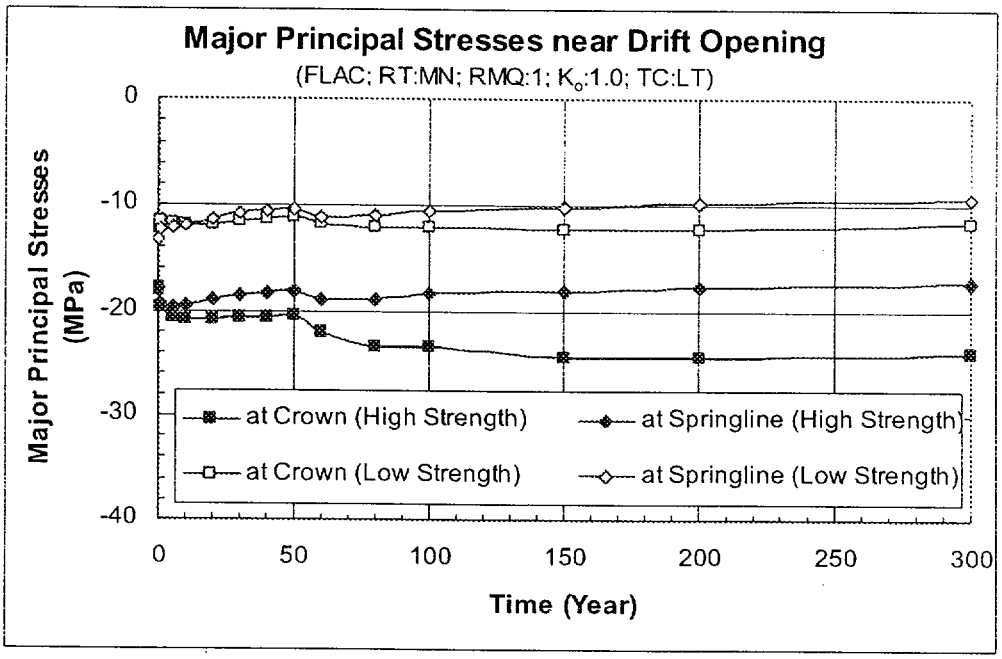

(b)

Figure II-10. Comparisons of Time Histories of Major Principal Stresses near Drift Opening Between Cases L1H and L1La under Low Temperature Condition for Non-Lithophysal Rock and RMQ Category of 1: (a) K_o=0.3; (b) K_o=1.0

Note: RT=Rock Type; MN=Middle Non-Lithophysal Unit; RMQ=Rock Mass Quality Category; K_o=In Situ Horizontal to Vertical Stress Ratio; TC=Thermal Condition; LT=Low Temperature.

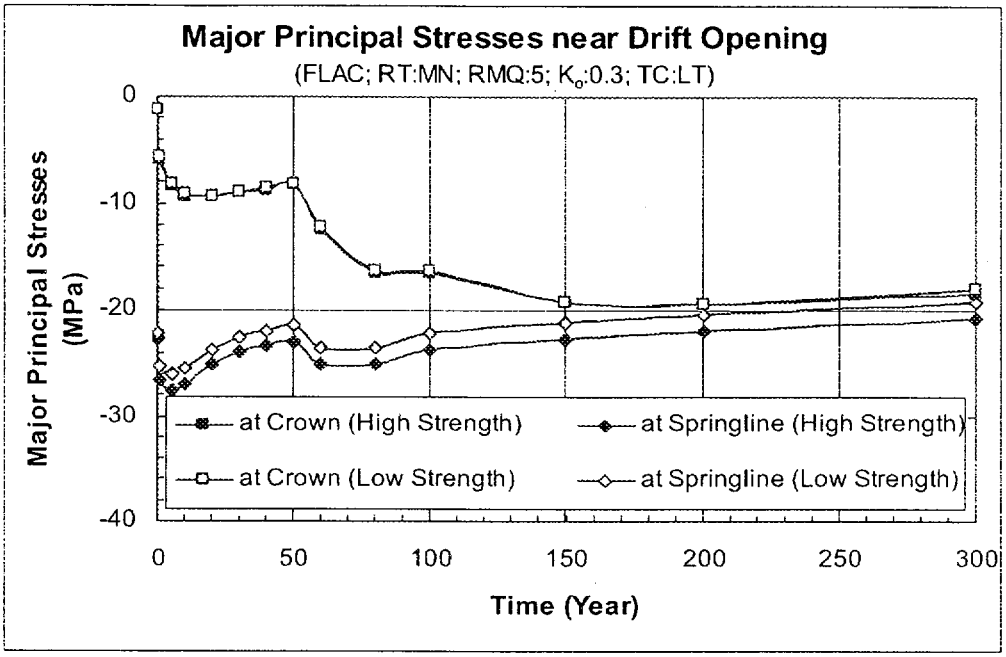

(a)

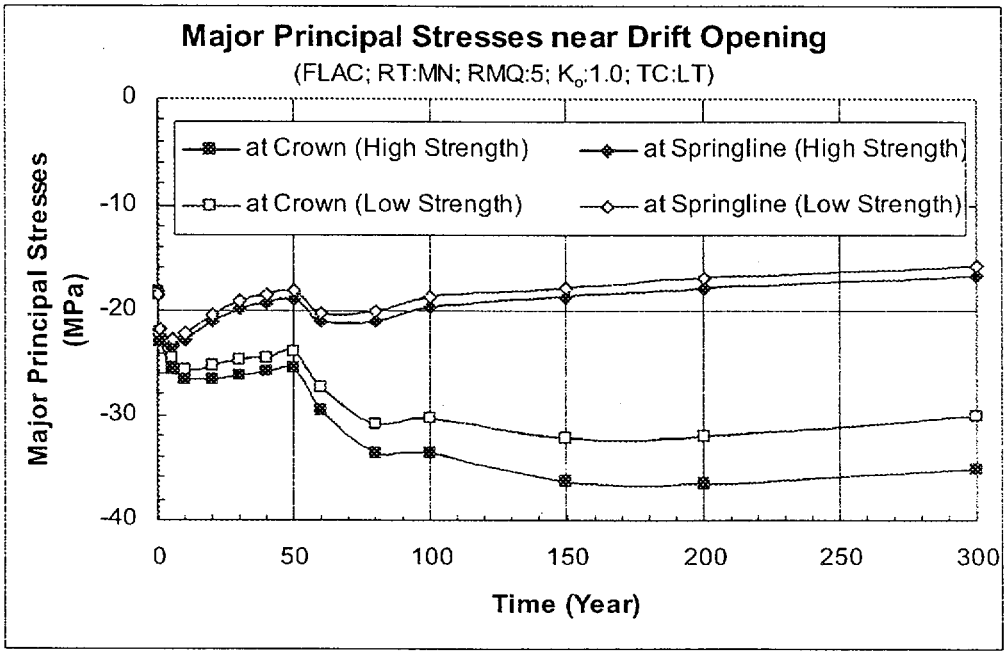

(b)

Figure II-11. Comparisons of Time Histories of Major Principal Stresses near Drift Opening Between Cases L5H and L5La under Low Temperature Condition for Non-Lithophysal Rock and RMQ Category of 5: (a) K_o=0.3; (b) K_o=1.0

Note: RT=Rock Type; MN=Middle Non-Lithophysal Unit; RMQ=Rock Mass Quality Category; K_o=In Situ Horizontal to Vertical Stress Ratio; TC=Thermal Condition; LT=Low Temperature.

ATTACHMENT III EFFECTS OF VARIATION OF MODEL DIMENSION

EFFECTS OF VARIATION OF MODEL DIMENSION

This attachment presents the results of preliminary study on the effects of variation of model vertical dimension on the displacements and stresses adjacent to emplacement drifts subjected to in situ stress and low temperature thermal loads. The study is based on numerical analyses using the FLAC code.

III.1 Model Configurations

For most of the thermomechanical models, the configuration used is illustrated in Figure 6-4. In this configuration, the vertical dimension is 100 m, and both the upper and lower boundaries are set at 50 m from the drift center. Though these boundaries are located at a distance about 10 times the drift diameter (5.5 m), the question remains whether this distance is adequate to limit or eliminate the boundary effect on the displacements and stresses near the drift openings. Therefore, additional analyses were conducted by extending the upper and lower boundaries. Two additional configurations were examined: (A) both the upper and lower boundaries were extended from 50 m to 100 m measured from the drift center; and (B) the upper boundary was extended to the ground surface, about 346 m from the drift center, and the lower boundary was set at the TSw2 and TSw3 contact, about 138 m from the drift center. These two configurations are illustrated in Figures III-1 and III-2, respectively. For convenience of discussion, the configuration shown in Figure 6-4 is called the Base Configuration.

Compared to Figure 6-4, most of conditions in Configurations A and B are identical, except the vertical dimension and the overburden. In Configuration A, the overburden is determined based on the rock bulk density and the vertical stress (10 MPa) at the drift center. This approach is similar to what is used for the Base Configuration. The in situ stress condition in Configuration A is essentially the same as that in the base configuration. In Configuration B, however, the overburden is set to be zero because the upper boundary is extended to the ground surface. The vertical stress component at any locations is calculated using Equation 6-1. Therefore, the in situ stress condition in Configuration B is different from that in the base configuration. For example, for the base configuration the vertical stress is 10 MPa at the elevation of the drift center, while for Configuration B it is about 7 MPa at the same elevation, about 30 percent lower than the former.

III.2 Results for Configuration A

Figures III-3a through III-4b show the comparisons of time histories of the vertical and horizontal closures of unsupported emplacement drifts using the Base Configuration (Figure 6-4) and Configuration A (Figure III-1). These results were calculated based on the rock mass properties of Tptpmn unit for RMQ of 1 and 5, listed in Table 4-5a, and the temperature histories presented in Table 4-12b. It is indicated that the differences in drift closures are very small, with the maximum of about 0.3 mm in the vertical closure for the case of RMQ=1 and K_o=0.3 (Figure III-3a). These differences are caused by in situ load, due to increased rock mass that contributes to the overall rock deformation, and not seen to increase with temperature. This suggests that thermomechanical response of emplacement drifts is not expected to be greatly affected by

extending the upper or lower boundaries as long as they are set far enough from the drift openings.

Figures III-5a through III-6b compare the time histories of major principal stresses near the crown and springline of unsupported emplacement drifts. The differences are shown to be minimal, further indicating that the effects of variation of model dimensions on the behavior of emplacement drift openings are negligible as long as the model boundaries are set far enough from the area of interest.

III.3 Results for Configuration B

Figures III-7a through III-8b compare the time histories of vertical and horizontal closures of unsupported emplacement drifts with the Base Configuration (Figure 6-4) and configuration B (Figure III-2). As expected, the calculated drift closures, especially the vertical, using the base configuration are much larger that those using Configuration B due mainly to differences in the in situ stress condition. For the cases with a horizontal-to-vertical stress ratio (K_o) of 0.3, the horizontal closures based on these two different configurations are very close to each other because the difference in the horizontal stresses between these two cases is reduced by this small ratio (K_o).

Time histories of the major principal stresses near the crown and the springline calculated using these two different configurations are compared in Figures III-7a through III-10b. Similar phenomena as those to the drift closures can be observed.

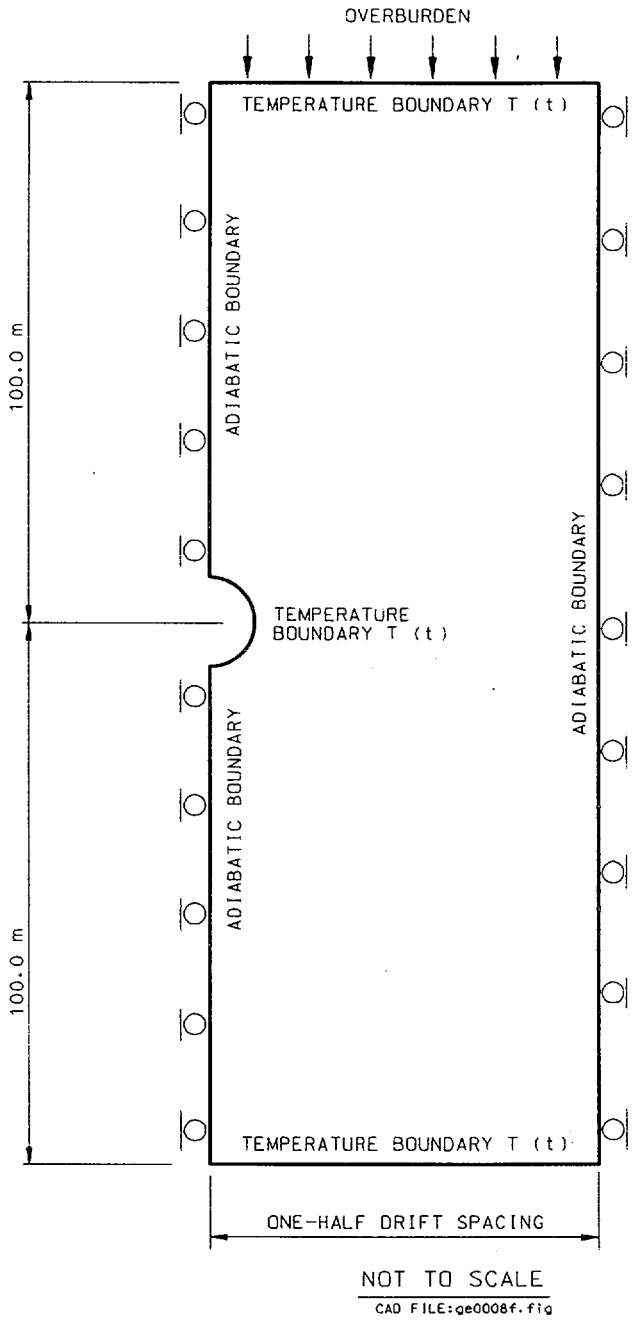

Figure III-1. Geometry and Boundary Conditions for Thermomechanical Modeling with Extended Upper and Lower Boundaries Using FLAC (Configuration A)

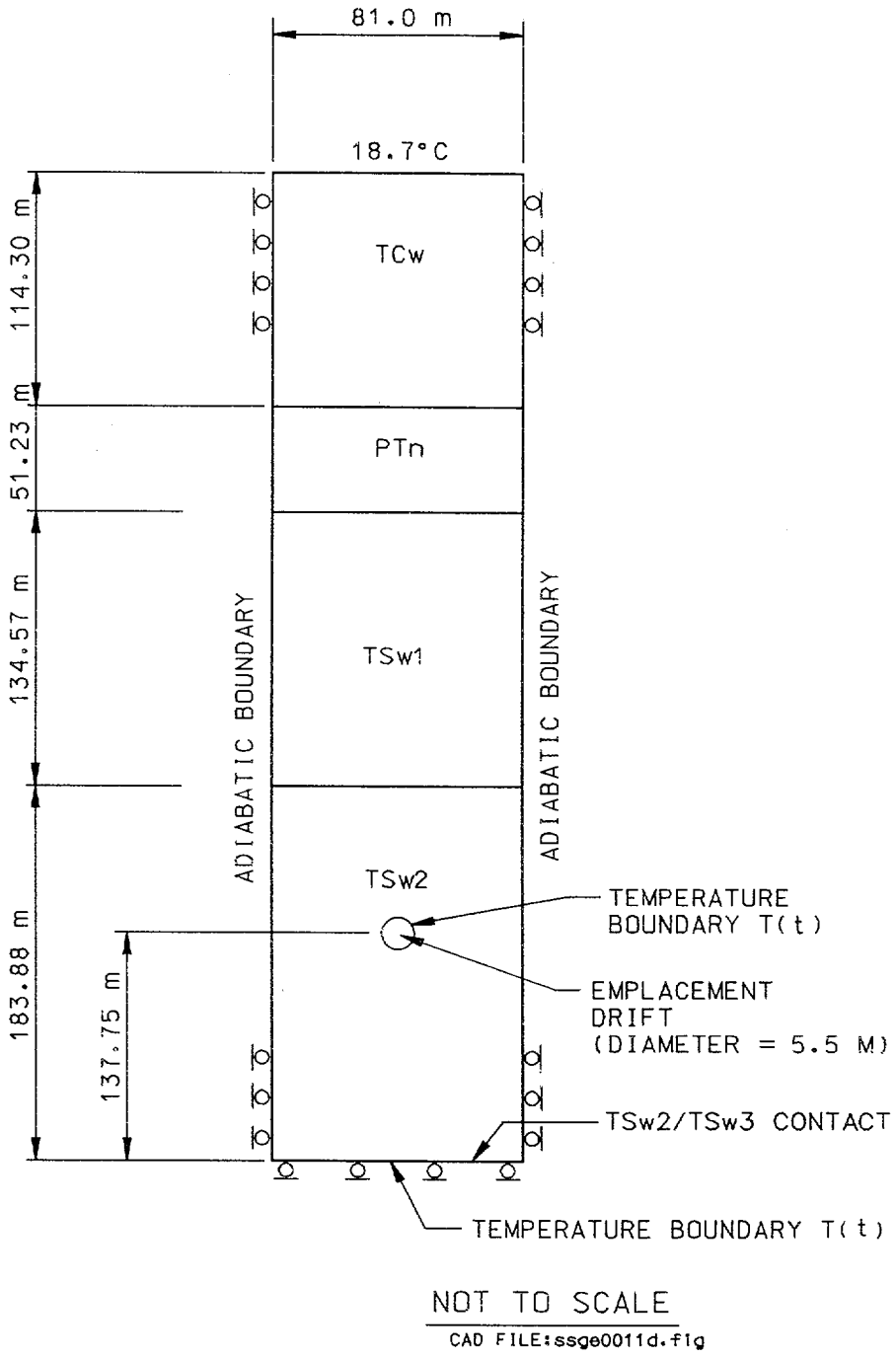

Figure III-2. Geometry and Boundary Conditions for Thermomechanical Modeling with Extended Upper and Lower Boundaries Using FLAC (Configuration B)

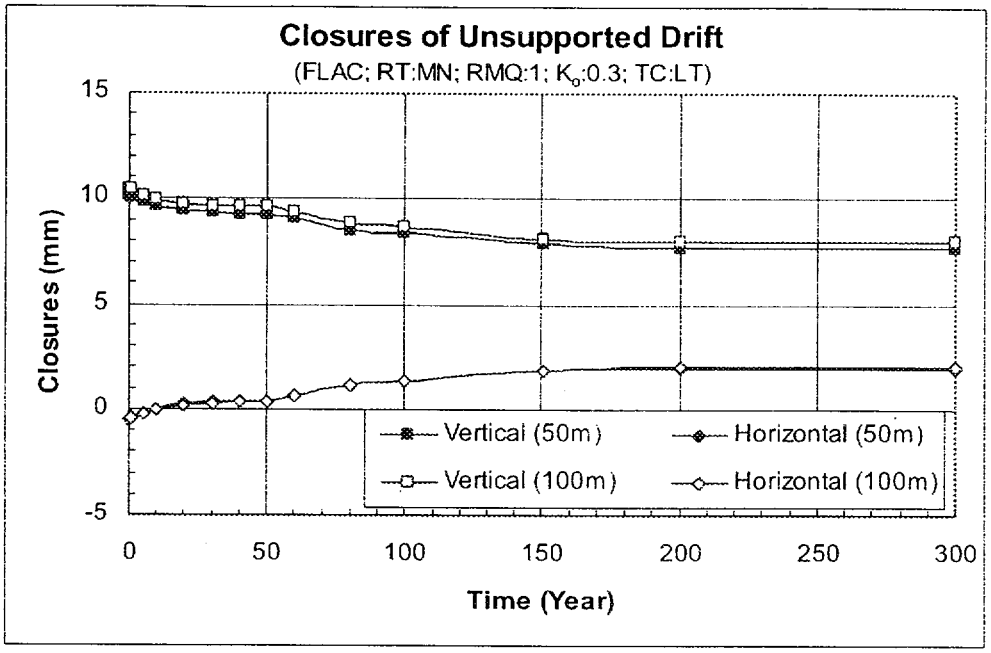

(a)

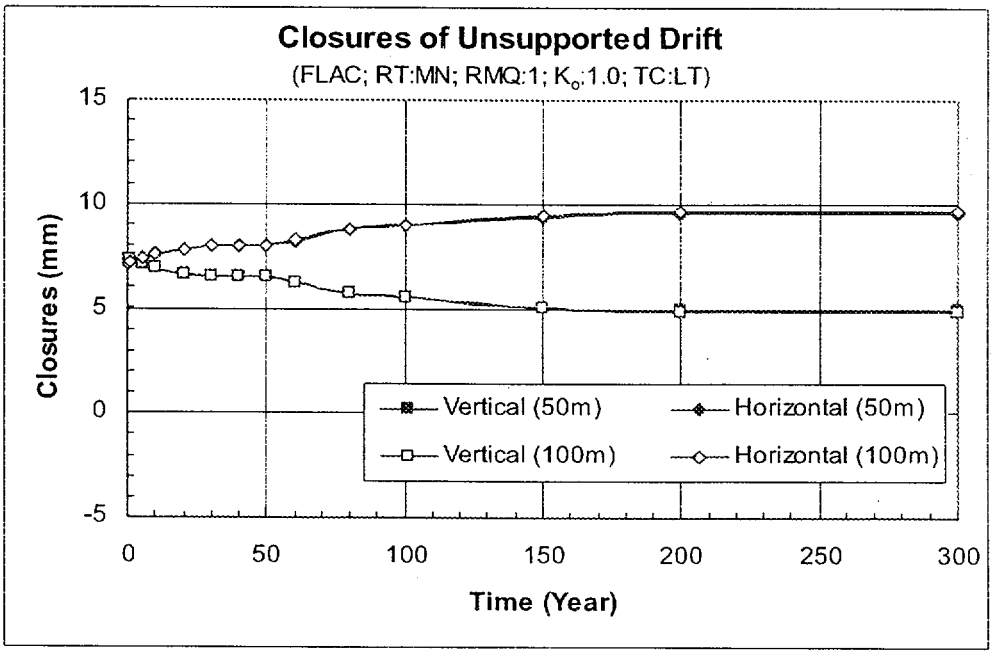

(b)

Figure III-3. Comparisons of Time Histories of Drift Closures under Low Temperature Condition for Non-Lithophysal Rock and RMQ Category of 1 with Different Model Dimensions: (a) K_o=0.3; (b) K_o=1.0

Note: RT=Rock Type; MN=Middle Non-Lithophysal Unit; RMQ=Rock Mass Quality Category; K_o=In Situ Horizontal to Vertical Stress Ratio; TC=Thermal Condition; LT=Low Temperature.

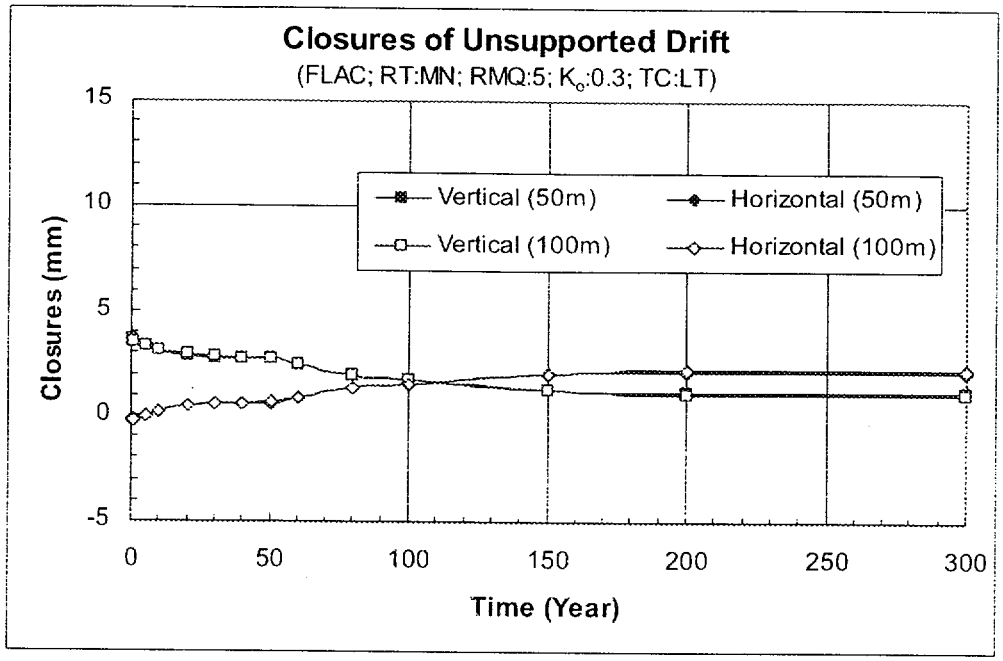

(a)

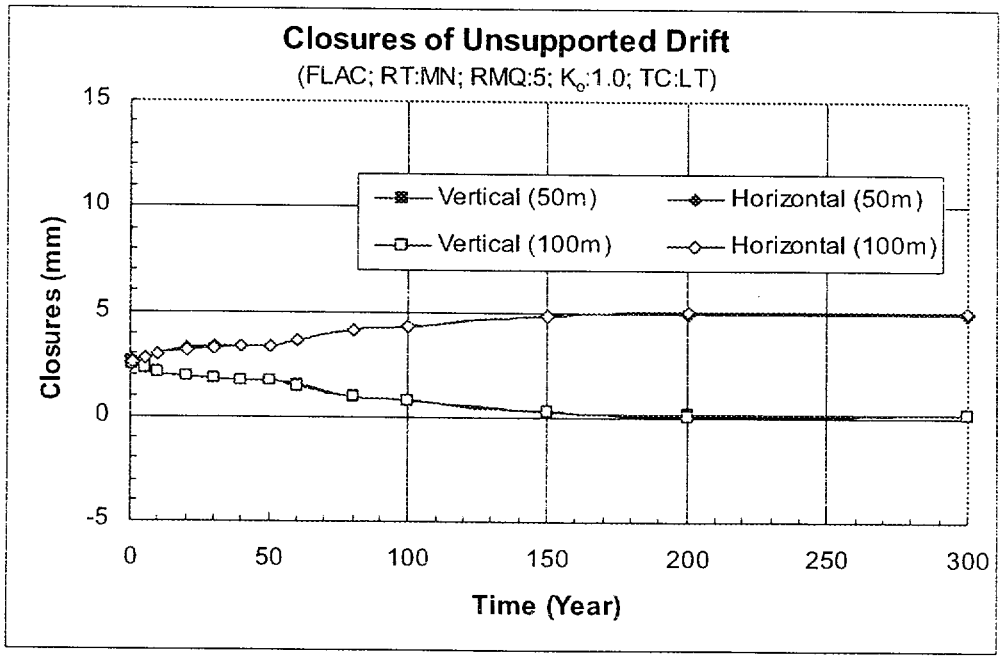

(b)

Figure III-4. Comparisons of Time Histories of Drift under Low Temperature Condition for Non-Lithophysal Rock and RMQ Category of 5 with Different Model Dimensions: (a) K_o=0.3; (b) K_o=1.0

Note: RT=Rock Type; MN=Middle Non-Lithophysal Unit; RMQ=Rock Mass Quality Category; K_o=In Situ Horizontal to Vertical Stress Ratio; TC=Thermal Condition; LT=Low Temperature.

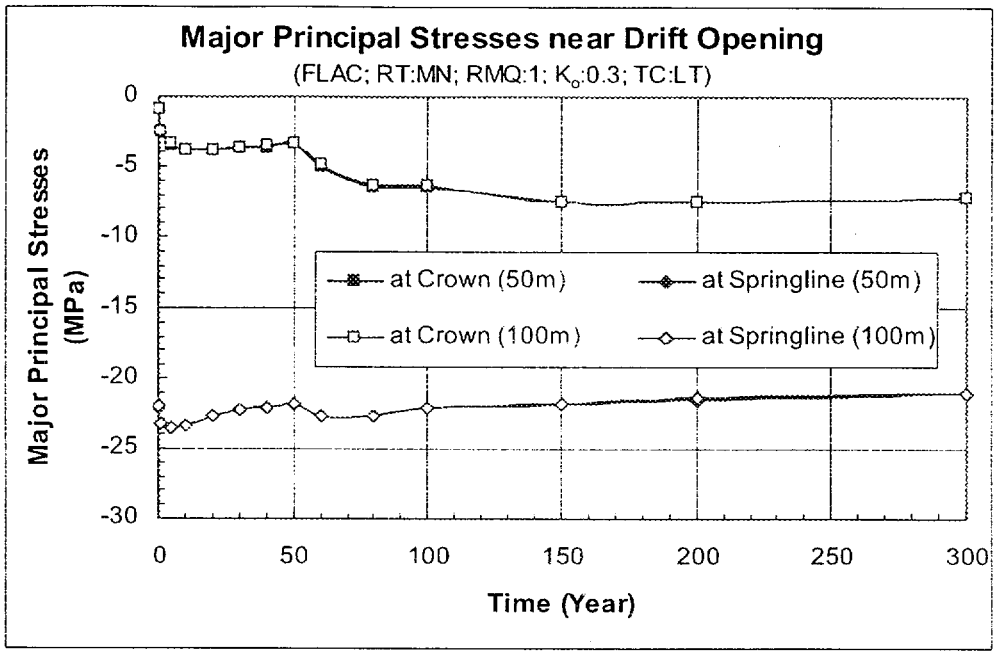

(a)

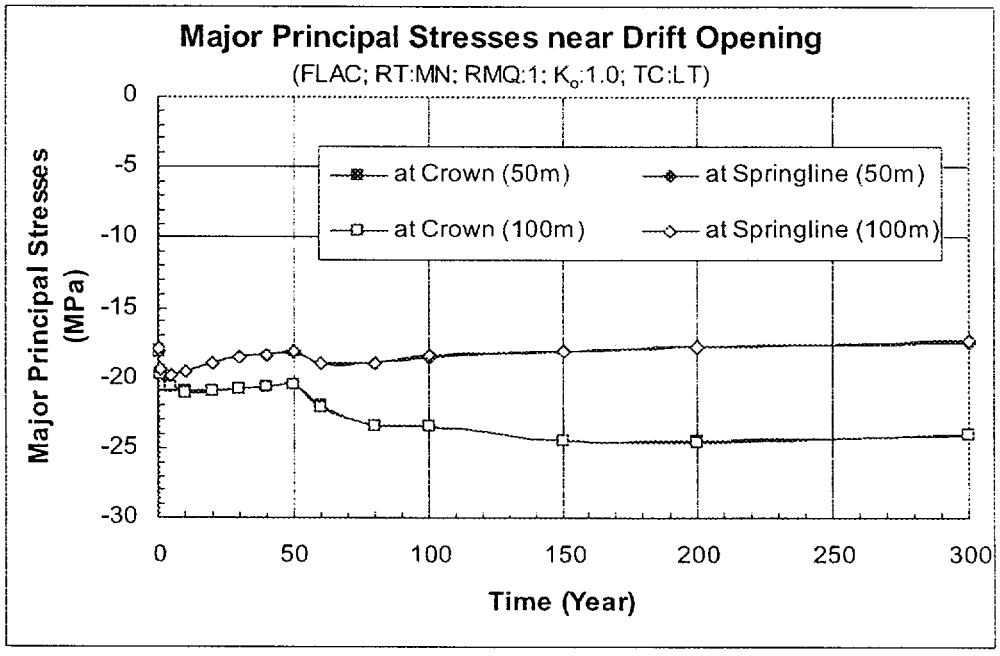

(b)

Figure III-5. Comparisons of Time Histories of Major Principal Stresses near Drift Opening under Low Temperature Condition for Non-Lithophysal Rock and RMQ Category of 1 with Different Model Dimensions: (a) K_o=0.3; (b) K_o=1.0

Note: RT=Rock Type; MN=Middle Non-Lithophysal Unit; RMQ=Rock Mass Quality Category; K_o=In Situ Horizontal to Vertical Stress Ratio; TC=Thermal Condition; LT=Low Temperature.

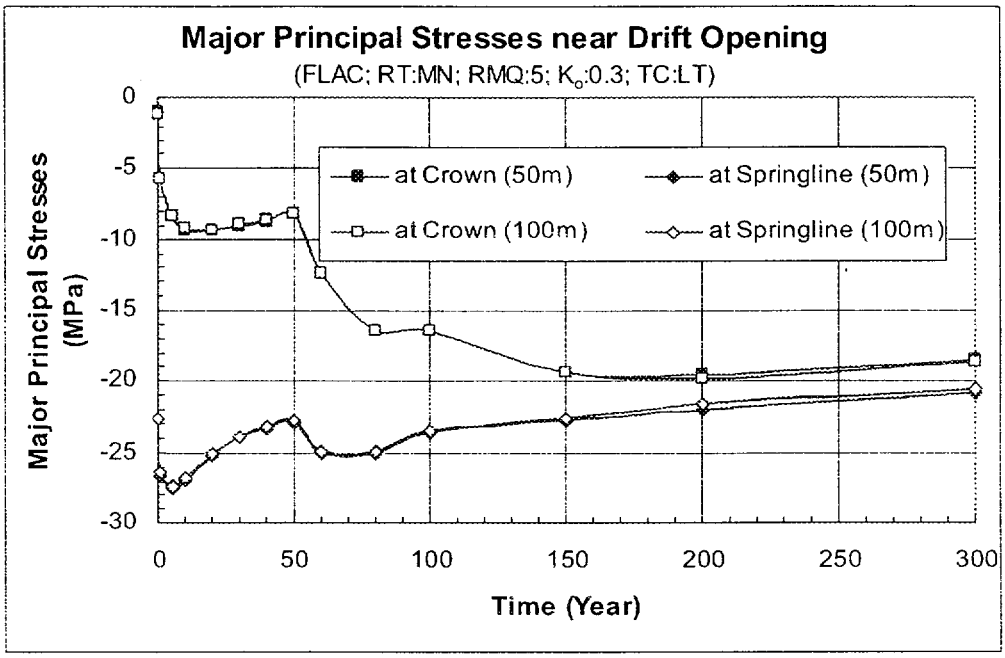

(a)

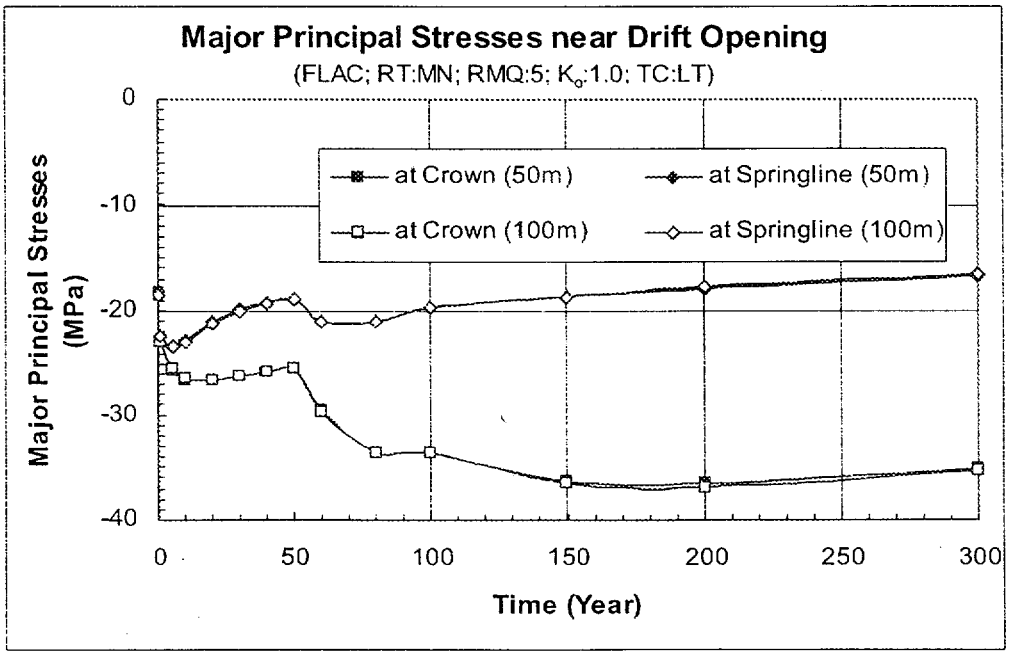

(b)

Figure III-6. Comparisons of Time Histories of Major Principal Stresses near Drift Opening under Low Temperature Condition for Non-Lithophysal Rock and RMQ Category of 5 with Different Model Dimensions: (a) K_o=0.3; (b) K_o=1.0

Note: RT=Rock Type; MN=Middle Non-Lithophysal Unit; RMQ=Rock Mass Quality Category; K_o=In Situ Horizontal to Vertical Stress Ratio; TC=Thermal Condition; LT=Low Temperature.

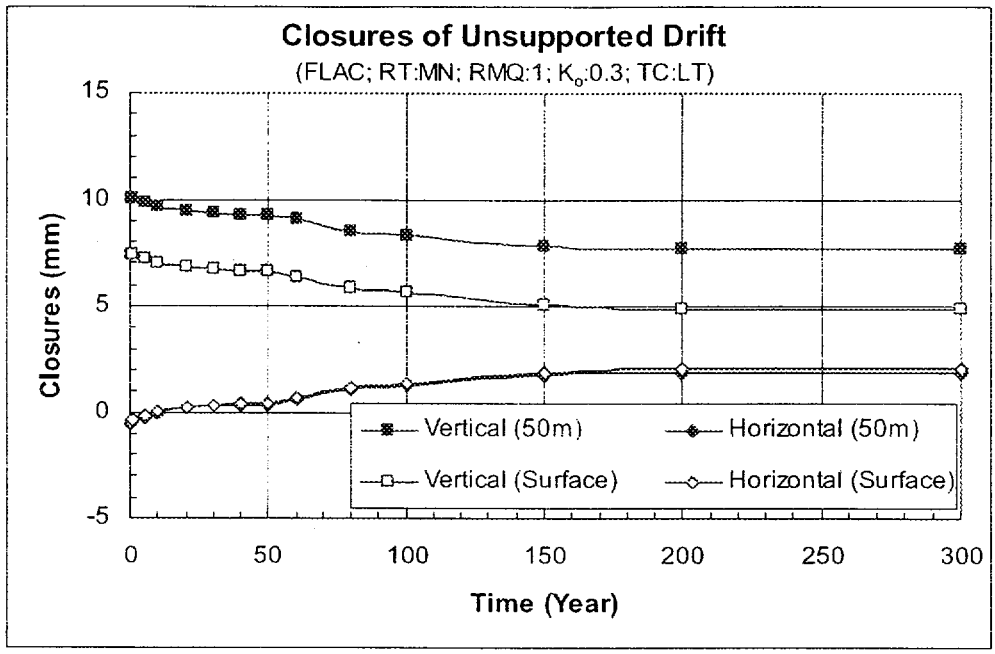

(a)

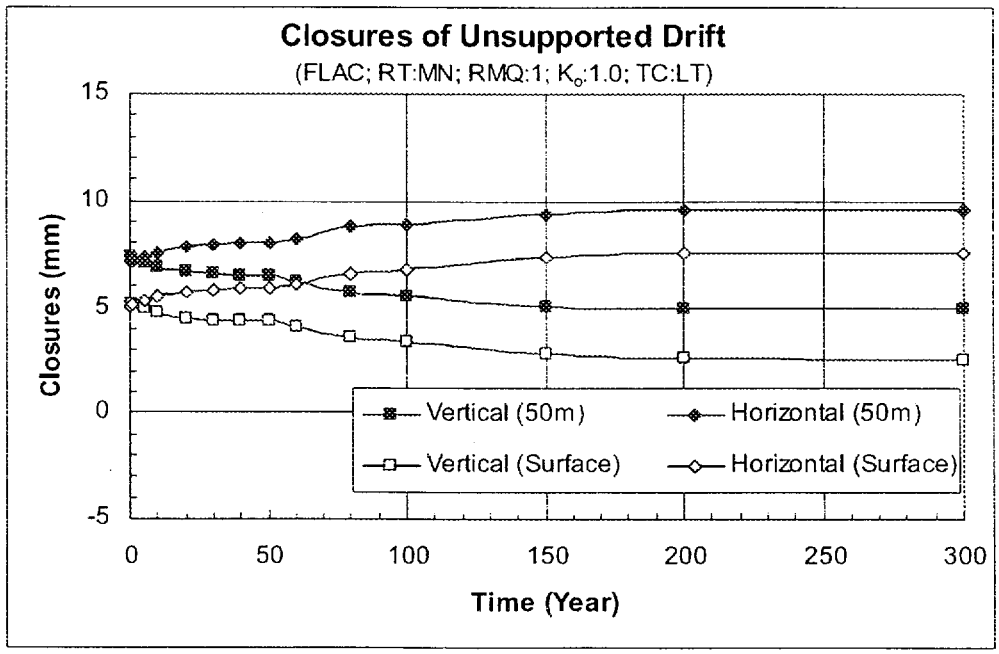

(b)

Figure III-7. Comparisons of Time Histories of Drift Closures under Low Temperature Condition for Non-Lithophysal Rock and RMQ Category of 1 with Different Model Dimensions: (a) K_o=0.3; (b) K_o=1.0

Note: RT=Rock Type; MN=Middle Non-Lithophysal Unit; RMQ=Rock Mass Quality Category; K_o=In Situ Horizontal to Vertical Stress Ratio; TC=Thermal Condition; LT=Low Temperature.

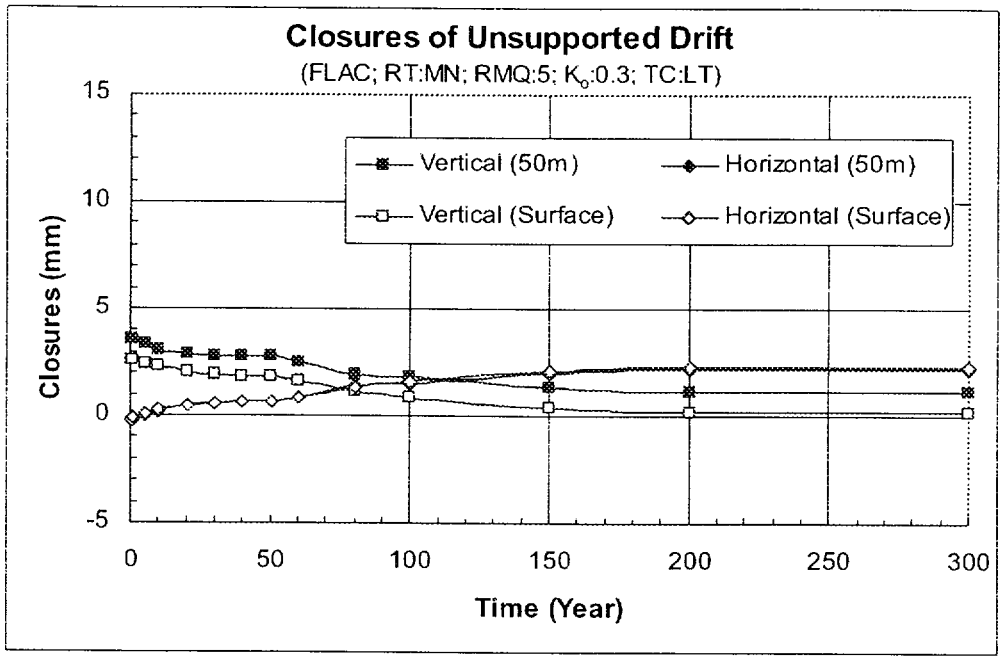

(a)

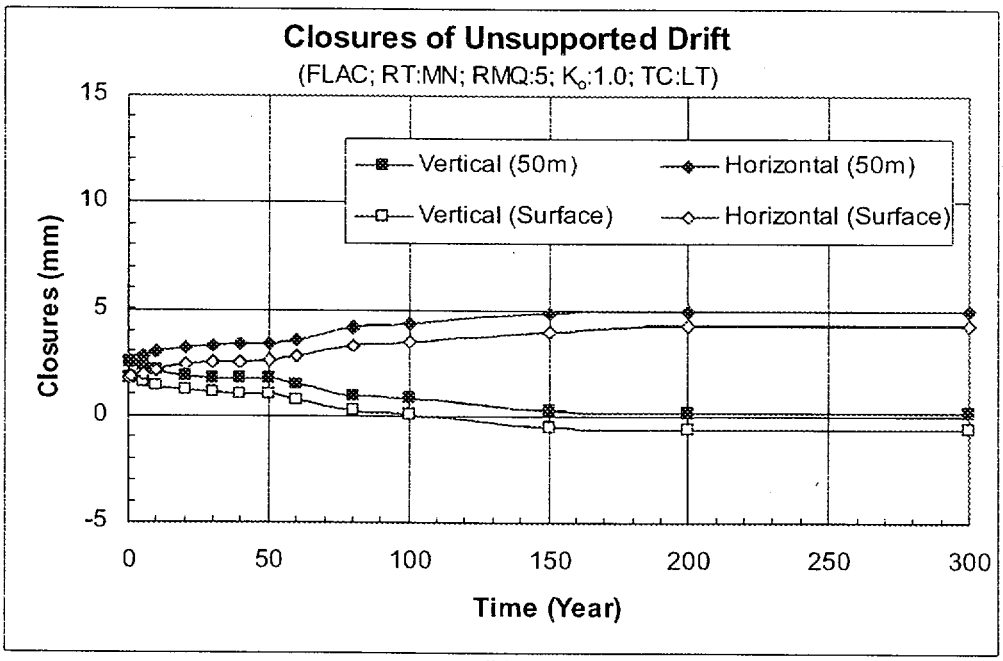

(b)

Figure III-8. Comparisons of Time Histories of Drift Closures under Low Temperature Condition for Non-Lithophysal Rock and RMQ Category of 5 with Different Model Dimensions: (a) K_o=0.3; (b) K_o=1.0

Note: RT=Rock Type; MN=Middle Non-Lithophysal Unit; RMQ=Rock Mass Quality Category; K_o=In Situ Horizontal to Vertical Stress Ratio; TC=Thermal Condition; LT=Low Temperature.

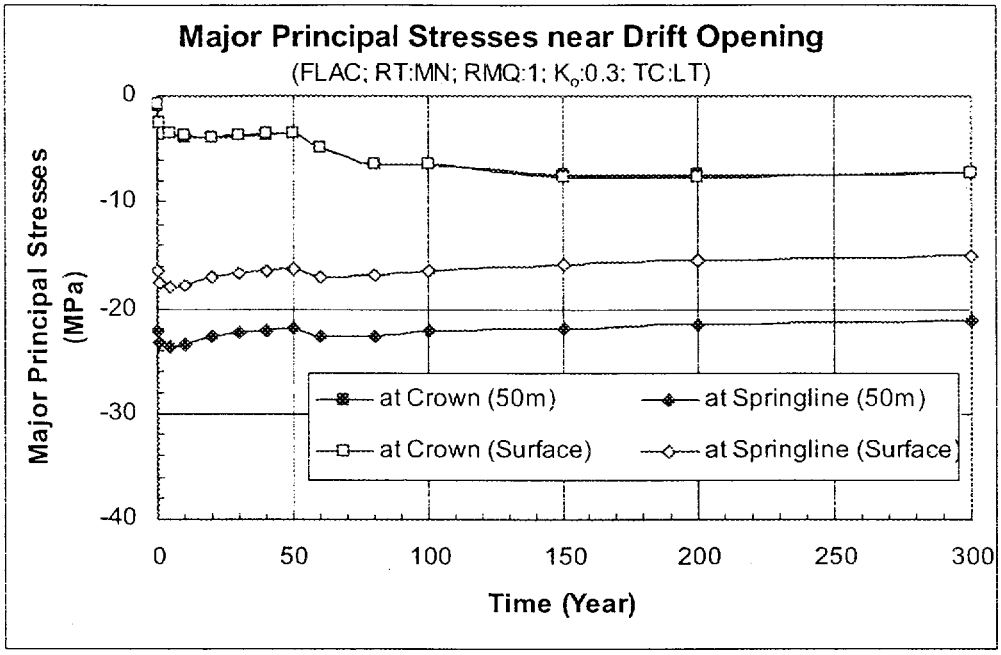

(a)

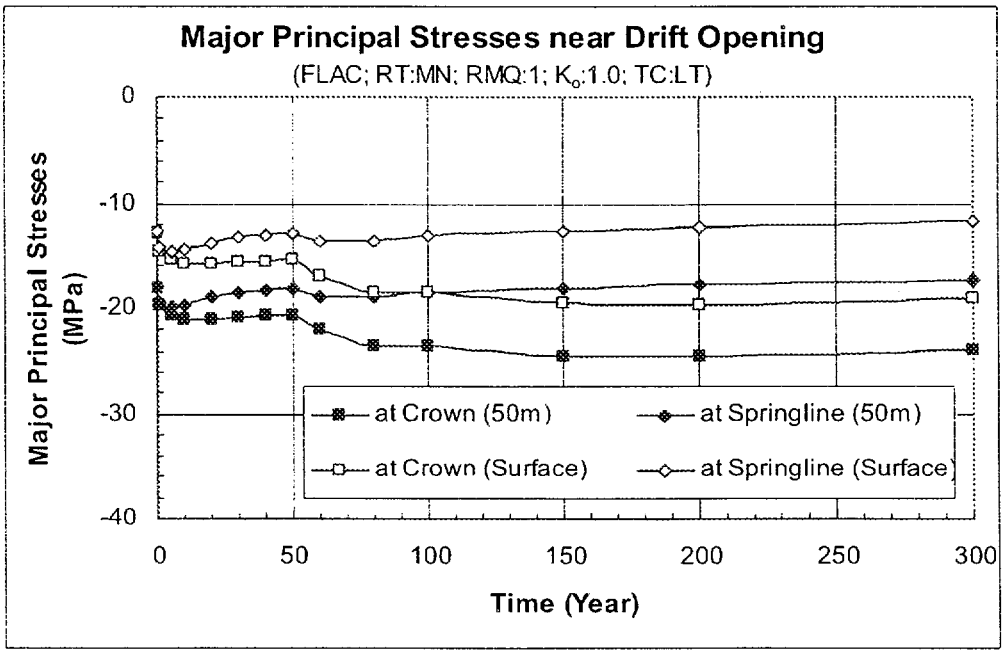

(b)

Figure III-9. Comparisons of Time Histories of Major Principal Stresses near Drift Opening under Low Temperature Condition for Non-Lithophysal Rock and RMQ Category of 1 with Different Model Dimensions: (a) K_o=0.3; (b) K_o=1.0

Note: RT=Rock Type; MN=Middle Non-Lithophysal Unit; RMQ=Rock Mass Quality Category; K_o=In Situ Horizontal to Vertical Stress Ratio; TC=Thermal Condition; LT=Low Temperature.

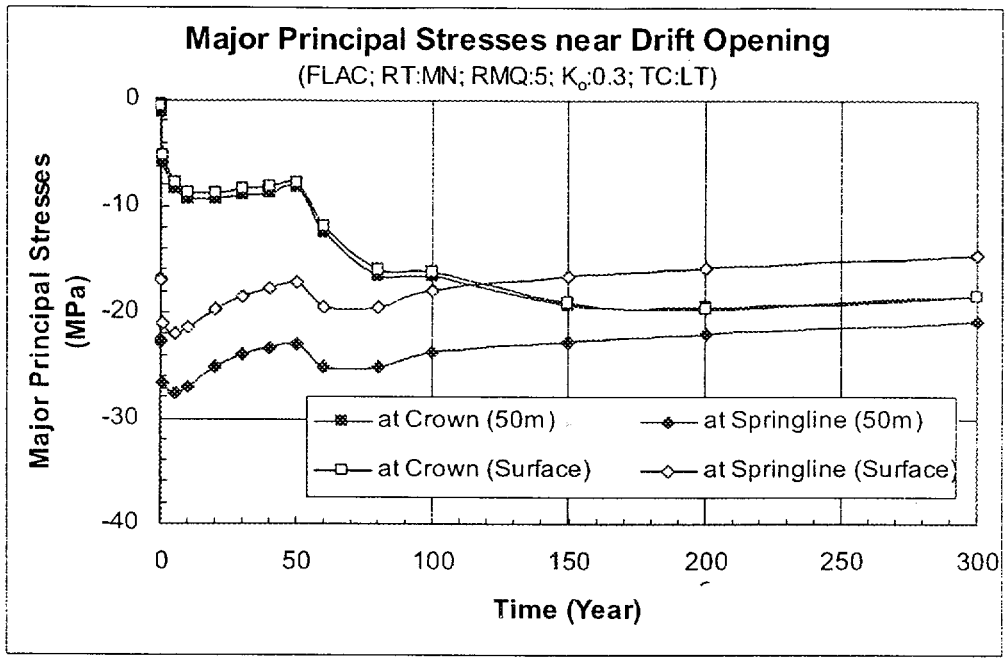

(a)

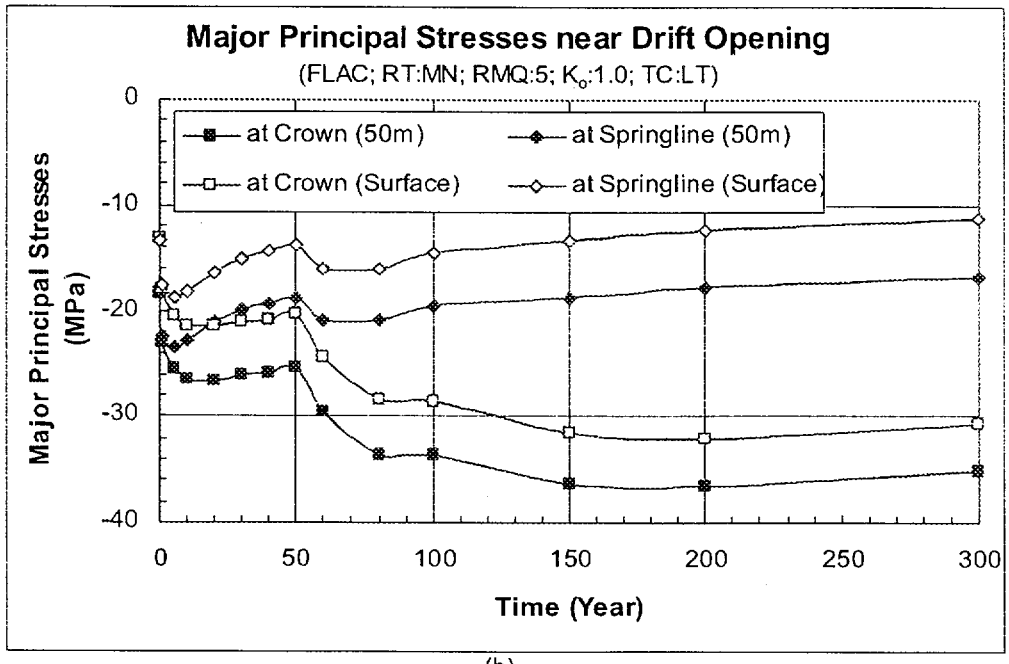

(b)

Figure III-10. Comparisons of Time Histories of Major Principal Stresses near Drift Opening under Low Temperature Condition for Non-Lithophysal Rock and RMQ Category of 5 with Different Model Dimensions: (a) K_o=0.3; (b) K_o=1.0

Note: RT=Rock Type; MN=Middle Non-Lithophysal Unit; RMQ=Rock Mass Quality Category; K_o=In Situ Horizontal to Vertical Stress Ratio; TC=Thermal Condition; LT=Low Temperature.

ATTACHMENT IV EFFECTS OF VARIATION OF JOINT PATTERN

EFFECTS OF VARIATION OF JOINT PATTERN

The ubiquitous joint pattern with through-going continuous fractures and constant joint spacing is used for the discontinuum UDEC analyses as shown in Figure 6-5. The projected joint spacings for various drift orientations are calculated in Attachment I.

The lowest joint spacing value, i.e. the most frequent joint pattern, was selected as input in the analysis as described in Attachment I. This attachment provides justification for using the ubiquitous joint pattern in UDEC analyses. The results of thermomechanical analyses using two sets of random joint patterns were used to compare with the results using the ubiquitous joint pattern.

In order to evaluate the impact of the variation of joint continuity and joint orientation, the statistical joint-set generator in UDEC was used to generate more realistic joint pattern. A joint set is characterized by eight generation parameters: four of these control mean geometric properties, and four control the standard deviation of random fluctuation about the mean (Itasca Consulting Group 1996b, p. E-1). The parameters given are a_m, a_d, t_m, t_d, g_m, g_d, s_m, s_d, where a is the angle of joint track to x-axis, t is the trace length of joint segment, g is the gap length between joint segments, and s is the spacing normal to joint tracks (see Figure IV-1). For each pair of values, the first entry with subscript m is the mean value and the second with subscript d is the maximum deviation from the mean (for uniform probability distribution).

The two sets of joint set generation parameters for Tptpmn unit used in this attachment are listed in Table IV-1. Parameter values for the ubiquitous joint pattern are also included in Table IV-1 for comparison. The mean dip angles are consistent with values listed in Table I-1, whereas the spacing values are taken from Tables I-2 for drift orientation of 70-degree azimuth. Source of the fracture trace length data is from mapping of the ESF main drift and the ECRB cross drift (DTN: MO0002SPAFRA06.002). The mean and median trace length values are listed in Table IV-2, based on the *Fracture Geometry Analysis for the Stratigraphic Units of the Repository Host Horizon* (CRWMS M&O 2000c, Table 13). The modeled trace lengths listed in Table IV-2 are assumed to be 4 times the mean trace lengths as listed in Table IV-1 (Assumption 5.6) following the conservative approach for accounting fracture trace length in the *Drift Degradation Analysis* (CRWMS M&O 2000b, Section 5.1, p. 24). Data for the continuity of fracture, defined as the trace length divided by the total length, was reported in the *Drift Design Methodology and Preliminary Application for the Yucca Mountain Site Characterization Project* (Hardy and Bauer 1991, p. 12-12 and Table 12-8) based on the joint trace photographs of pit walls excavated in TSw2. The reported mean continuity for the horizontal and vertical joint set are 41.5 and 51.8 percent, respectively. The continuity of joints is conservatively assumed to be within 80 to 90 percent (Assumption 5.6). Continuity data from the ESF mapping are not directly available. Based on the visual inspection of the joint trace maps, the range of 80 and 90 percent continuity is considered to be conservative. The values for the maximum deviation were assumed to be approximately 10 to 20 percent of the mean values for the dip angle, trace length, and spacing. Zero deviation was assumed for gap length to enhance the computational efficiency.

The generated joint patterns based on the parameters listed in Table IV-1 are shown in Figure IV-2. The initial and boundary conditions, material properties, and the thermal loading

for the three sets of analyses are identical. Ground support of the opening was not included in the model. The results for 50 years and 300 years after waste emplacement are presented in this Attachment. Figures IV-3 to IV-5 show the block displacement, joint shear slip, and the principal stresses at 50 years after waste emplacement for the three joint patterns respectively. Blocks sliding over the upper-left corner of the opening are predicted for both the ubiquitous joint pattern and the first random pattern. The stresses around the opening are in general similar with comparable magnitude. Figures IV-6 to IV-8 are the results for 300 years after waste emplacement. In general, the rock mass responses predicted at 300 years after waste emplacement are similar to the prediction for 50 years. Figure IV-9 compares the horizontal and vertical closure for the drift opening at 50 years after waste emplacement. The vertical closures are estimated to be in the range of 10 to 30 mm, whereas the horizontal closures slightly over 1 mm. The closures for the ubiquitous pattern are higher than those predicted for the random patterns. Figure IV-10 presents the calculated horizontal and vertical closures at 300 years. The vertical closure increases to the range of 30 to 60 mm and the horizontal closure extends to around 3 mm. The closures at 50 years for the ubiquitous pattern are higher than those predicted for the random patterns.

Rock mass responses depicted in Figures IV-3 to IV-10 indicate that the model based on the ubiquitous joint pattern in general predicts similar stress results but higher displacement values when comparing to the model using the random patterns generated for this study. Therefore, using the ubiquitous joint pattern is concluded to be conservative for predicting rock mass response under thermal loading. Due to the stochastic nature of joint network, it is impossible to model all combinations of joint patterns. The limited number of simulations in this study is intended to represent the best estimate of the joint footprints on two-dimensional cross section.

Table IV-1. List of the joint set generation parameters

Case	Joint Set	Dip Angle (degree)		Trace Length (m)		Gap Length (m)		Joint Spacing (m)	
		Mean	Deviation	Mean	Deviation	Mean	Deviation	Mean	Deviation
Ubiquitous Joint Pattern	1st + 2nd Sub-Vertical Set	83.5	0	through – going	0	0	0	0.54	0
	Sub-Horizontal Set	9	0	through – going	0	0	0	0.56	0
Random Joint Pattern 1	1st Sub-Vertical Set	84	10	10	1	1	0	0.7	0
	2nd Sub-Vertical Set	83	10	11	1	1	0	3	0
	Sub-Horizontal Set	9	2	13	1	1	0	0.6	0
Random Joint Pattern 2	1st Sub-Vertical Set	84	10	10	1	2	0	0.7	0
	2nd Sub-Vertical Set	83	10	11	1	2	0	3	0
	Sub-Horizontal Set	9	2	13	1	2	0	0.6	0

Table IV-2. Joint Set Trace Length in Tptpmn Unit

Joint Set	Strike/Dip (degree)	Mean Trace Length (m)	Median Trace Length (m)
1st Sub-Vertical Set	131/84	2.54	2.03
2nd Sub-Vertical Set	209/83	2.71	1.73
Sub-Horizontal Set	329/9	3.23	2.06

Sources: DTN: MO0002SPAFRA06.002 and CRWMS M&O 2000c, Table 13.

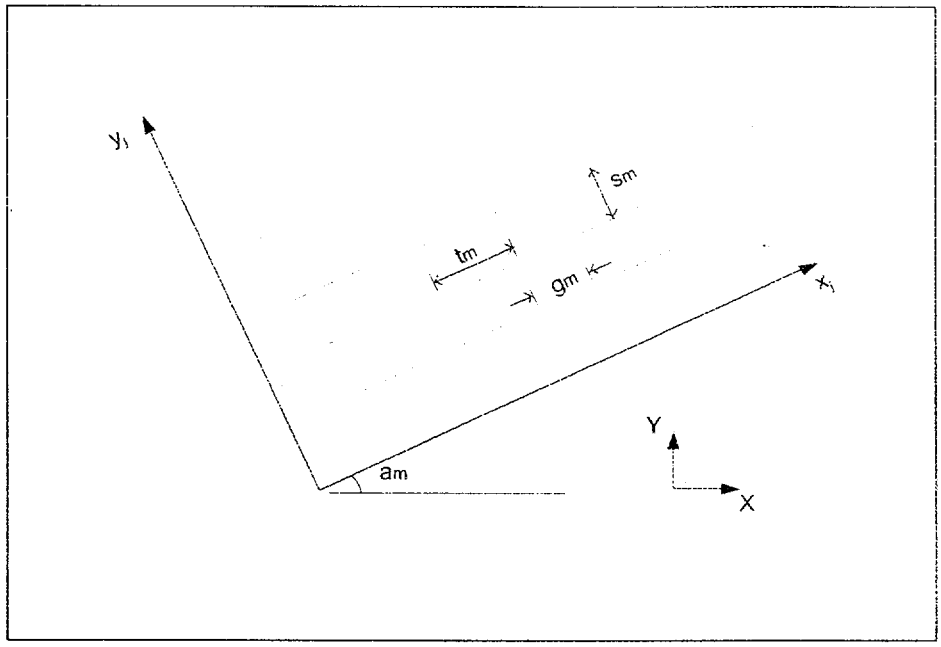

Figure IV-1. UDEC Joint Set Generation Parameter

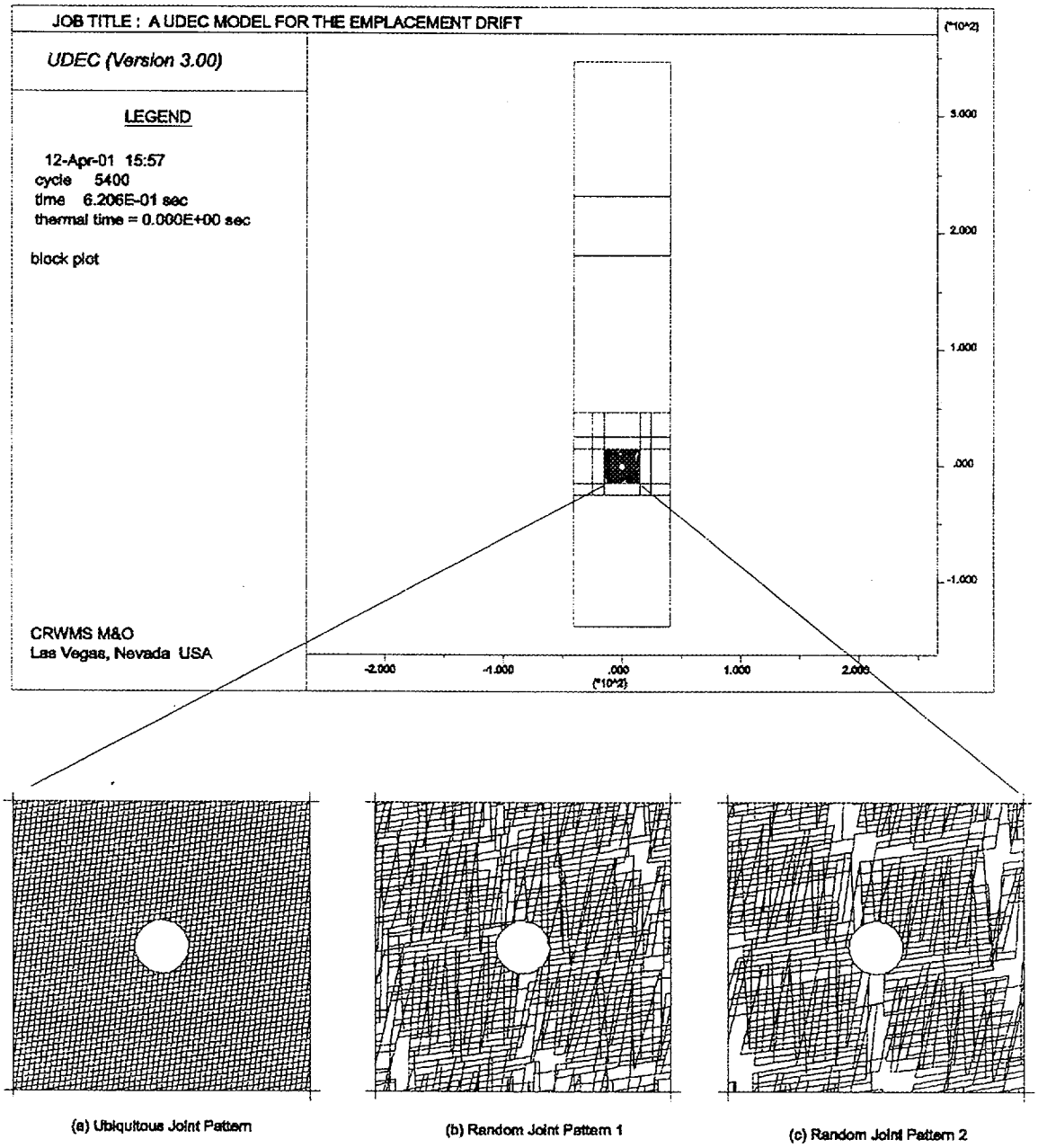

Figure IV-2. Generated Joint Pattern for UDEC Analyses

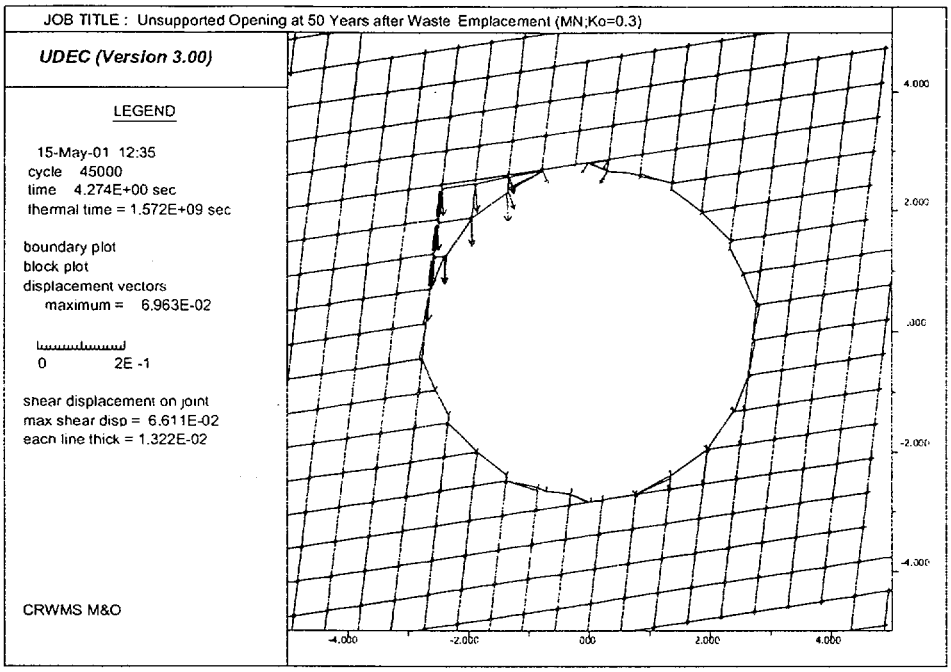

(a)

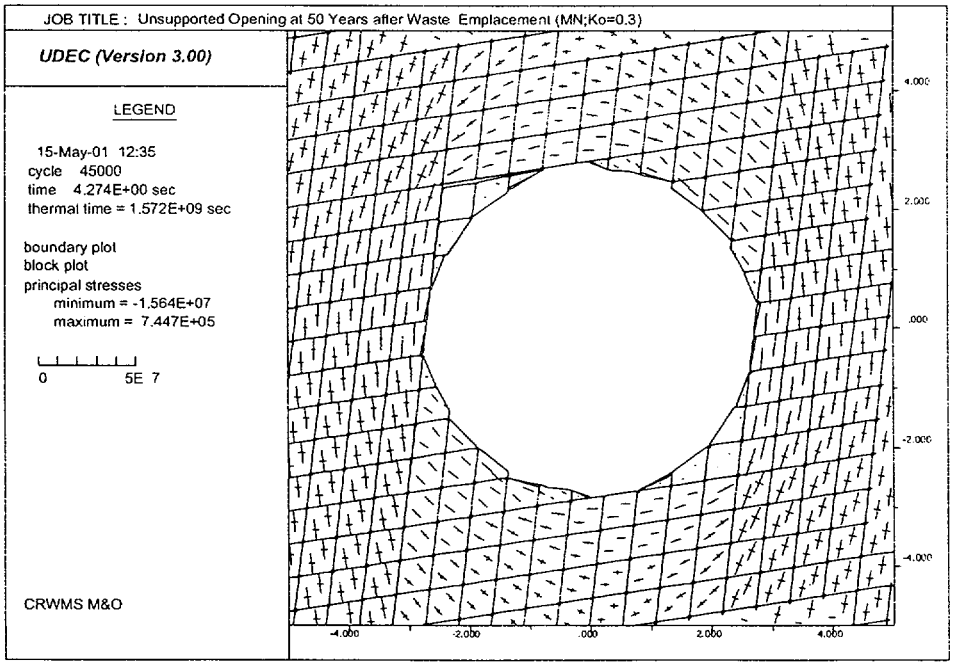

(b)

Figure IV-3. UDEC Analysis Results for (a) Block Displacement, Joint Shear Slip, and (b) Principal Stresses, Ubiquitous Joint Pattern, 50 Years after Waste Emplacement

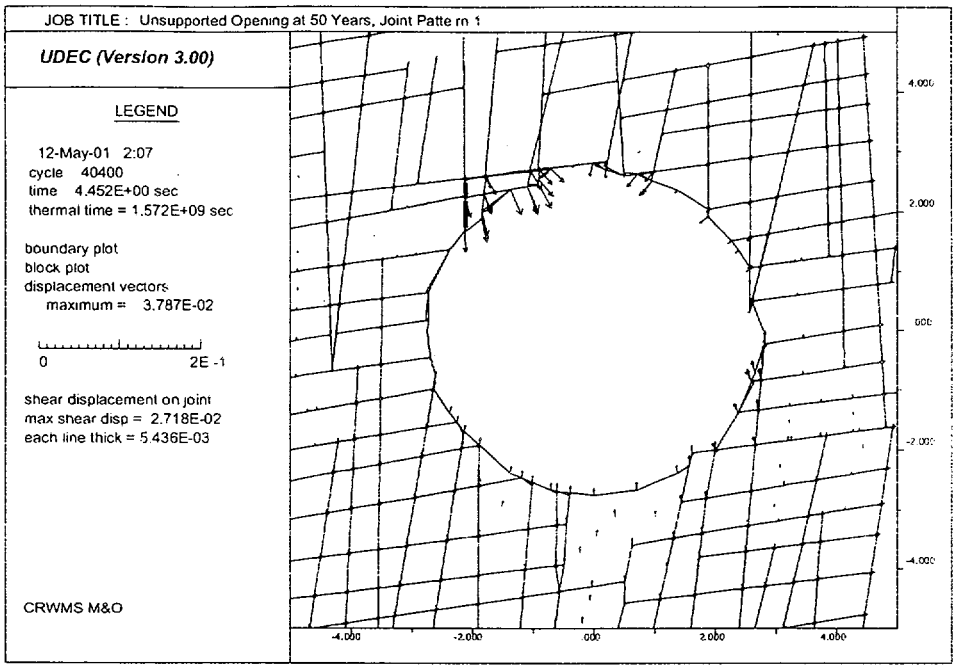

(a)

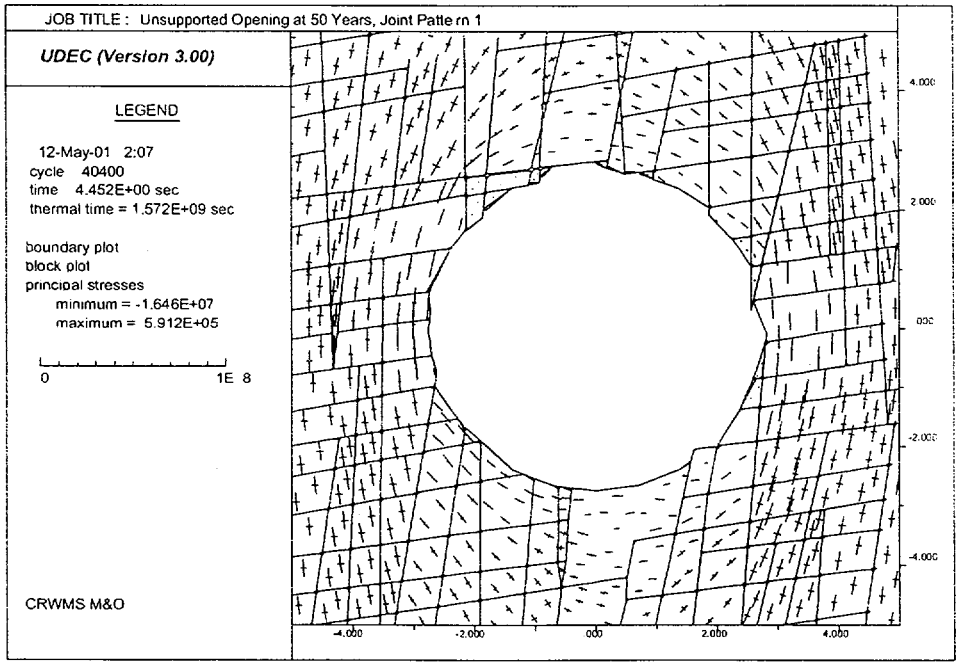

(b)

Figure IV-4. UDEC Analysis Results for (a) Block Displacement, Joint Shear Slip, and (b) Principal Stresses, Random Joint Pattern 1, 50 Years after Waste Emplacement

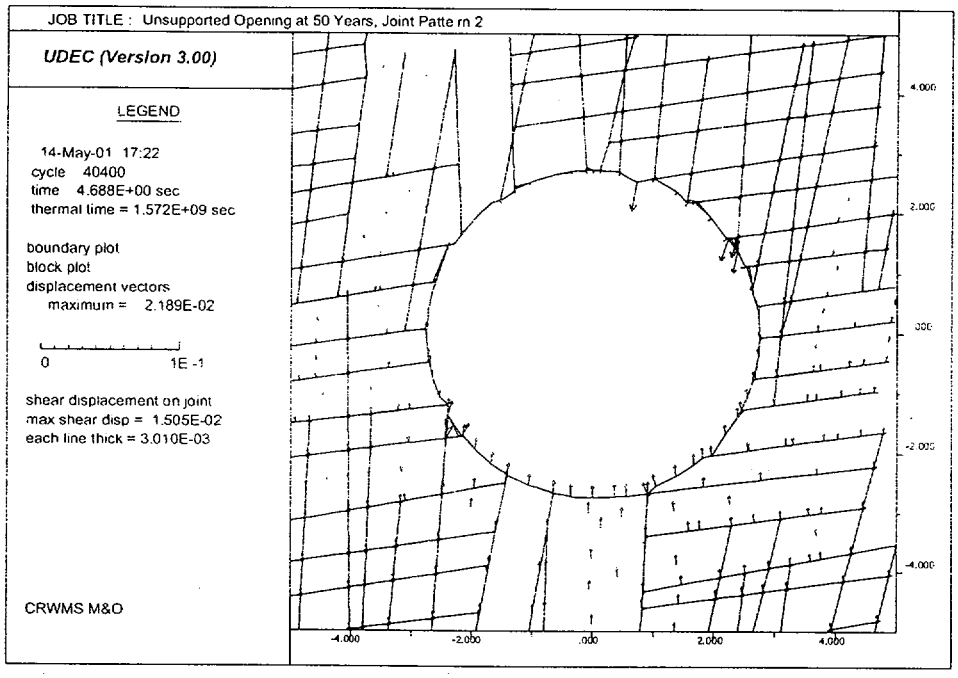

(a)

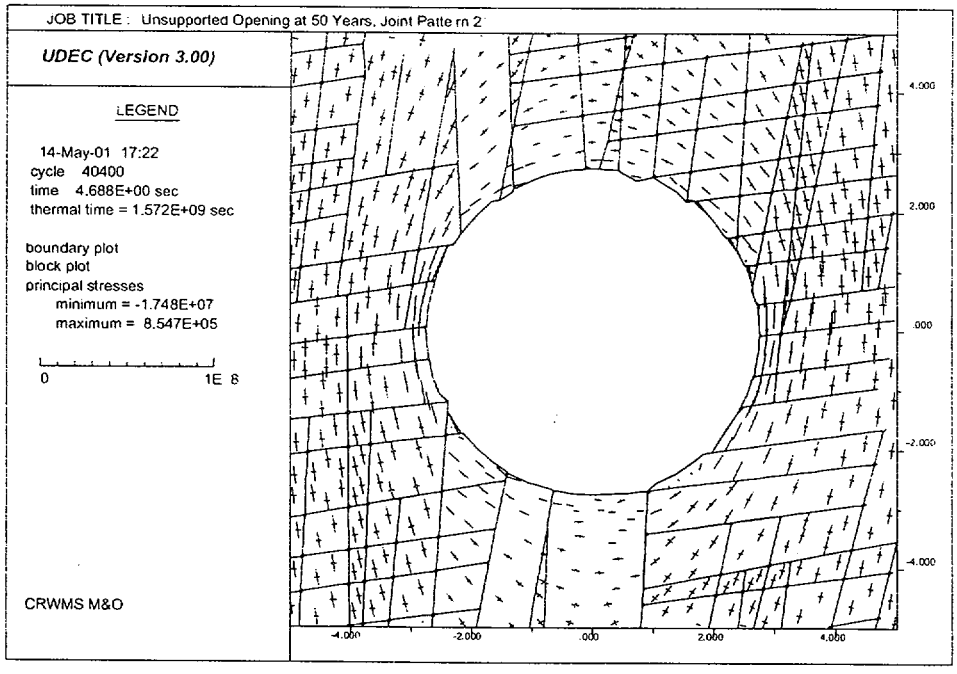

(b)

Figure IV-5. UDEC Analysis Results for (a) Block Displacement, Joint Shear Slip, and (b) Principal Stresses, Random Joint Pattern 2, 50 Years after Waste Emplacement

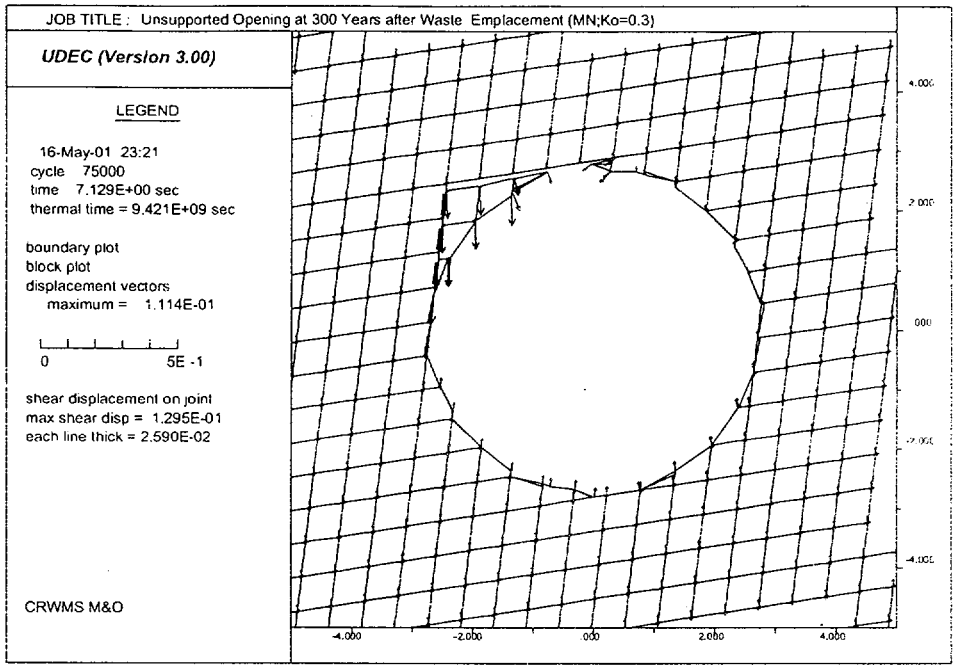

(a)

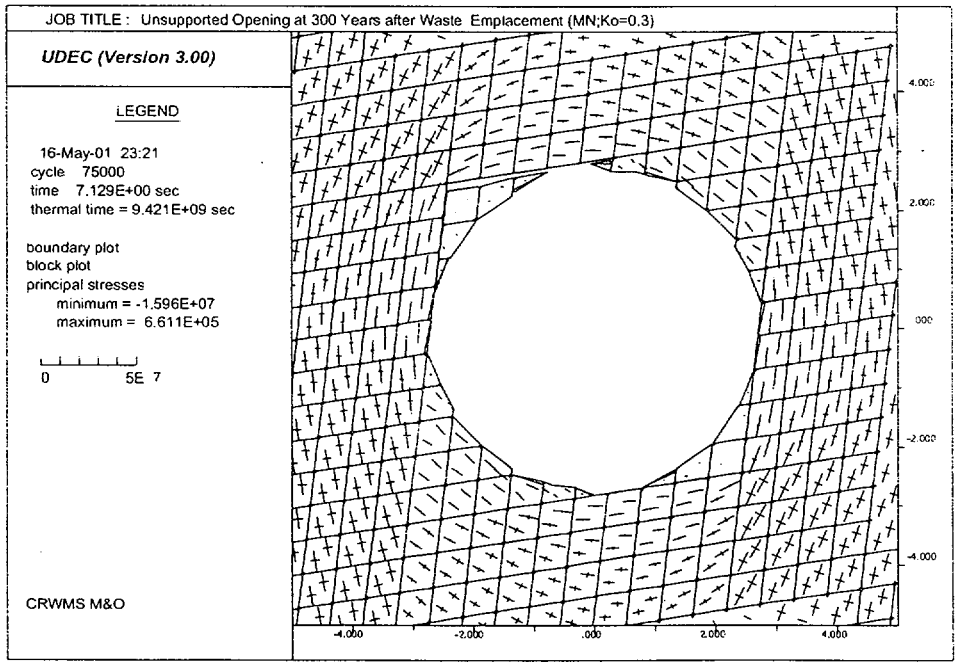

(b)

Figure IV-6. UDEC Analysis Results for (a) Block Displacement, Joint Shear Slip, and (b) Principal Stresses, Ubiquitous Joint Pattern, 300 Years after Waste Emplacement

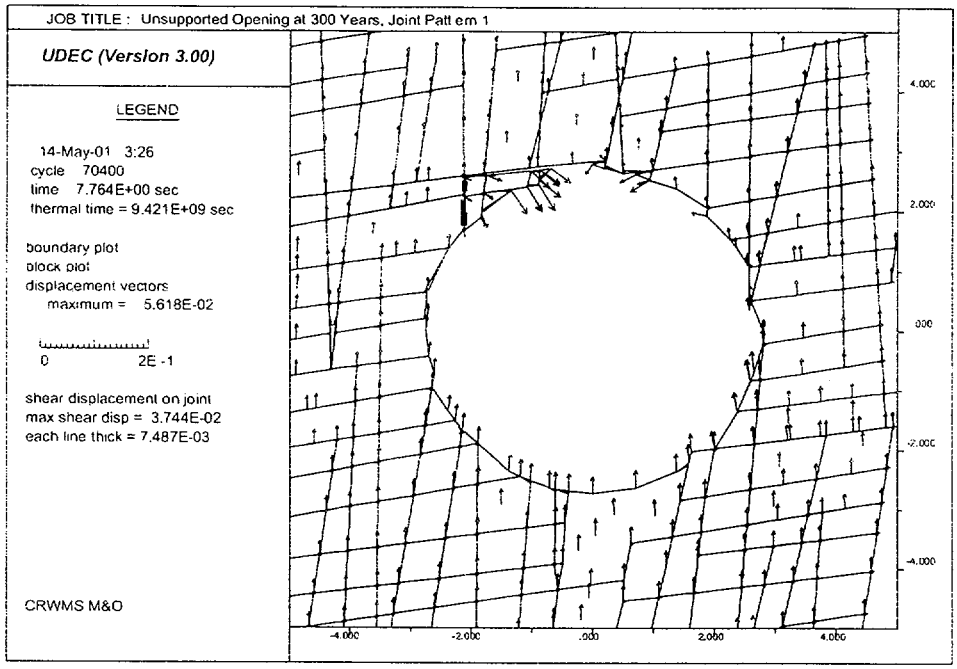

(a)

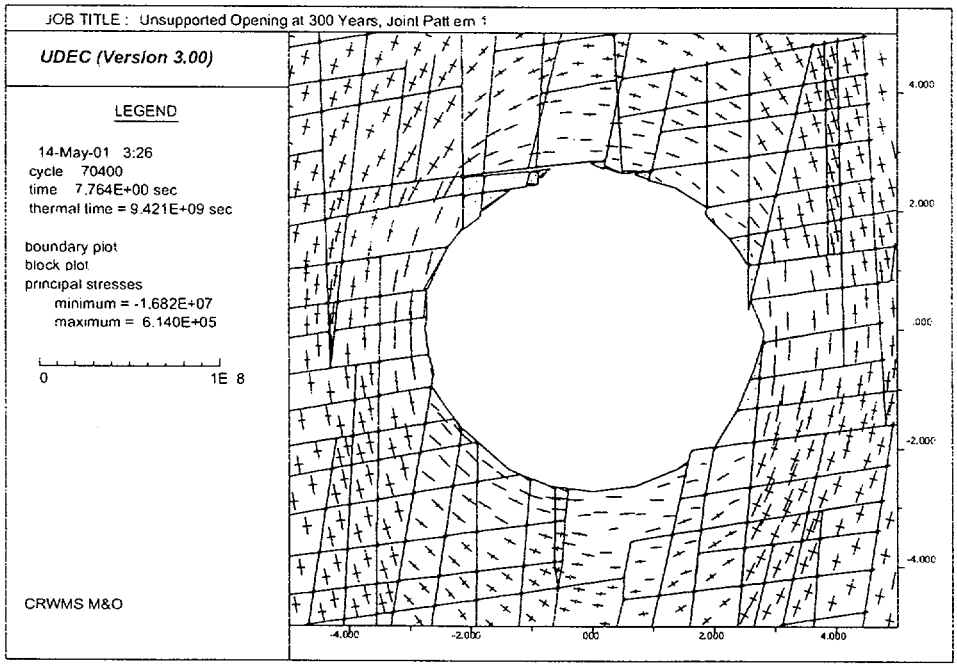

(b)

Figure IV-7. UDEC Analysis Results for (a) Block Displacement, Joint Shear Slip, and (b) Principal Stresses, Random Joint Pattern 1, 300 Years after Waste Emplacement

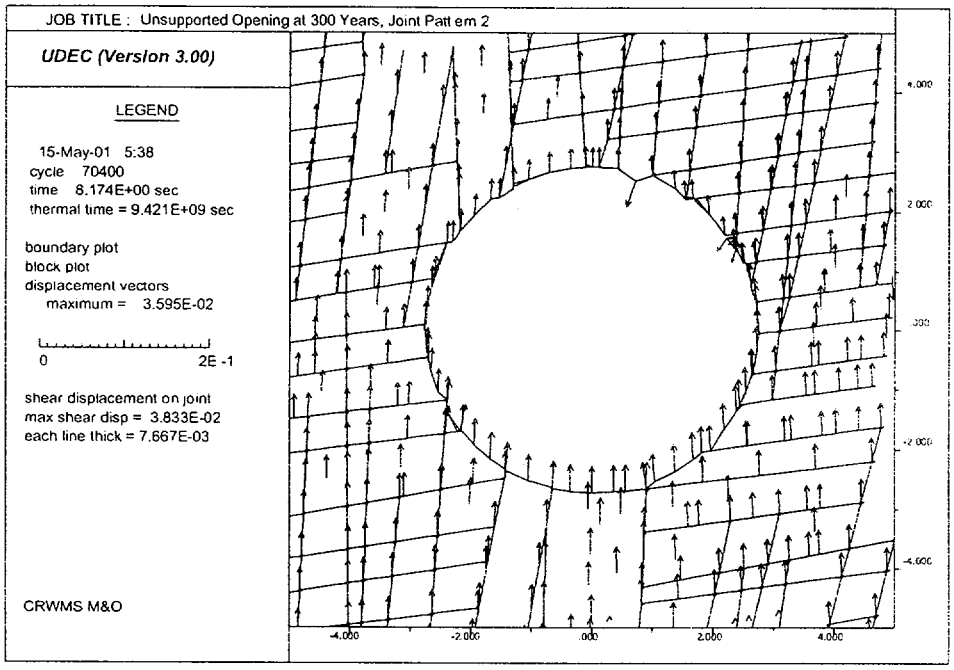

(a)

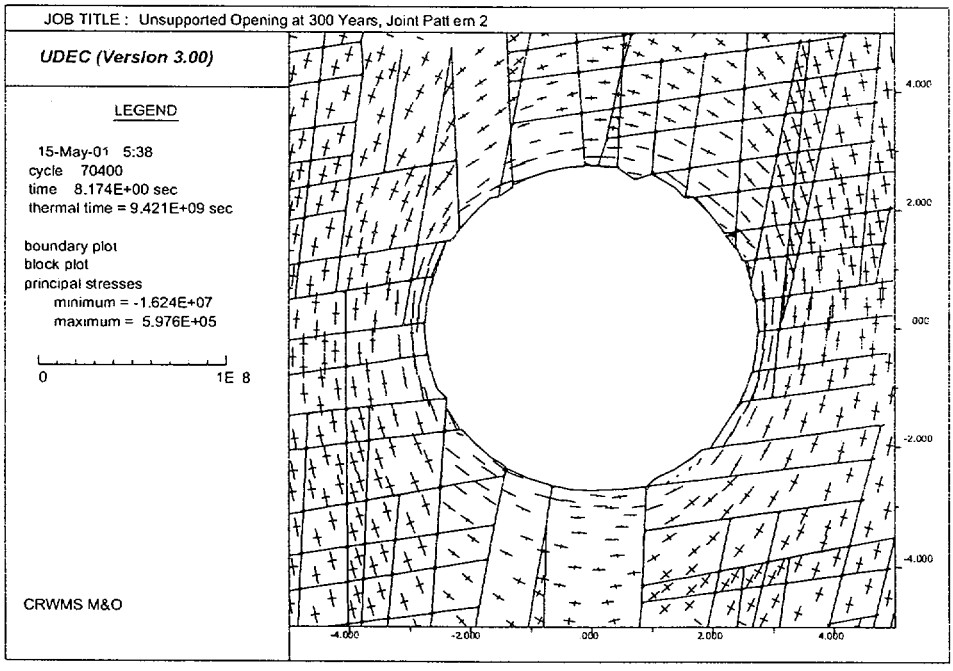

(b)

Figure IV-8. UDEC Analysis Results for (a) Block Displacement, Joint Shear Slip, and (b) Principal Stresses, Random Joint Pattern 2, 300 Years after Waste Emplacement

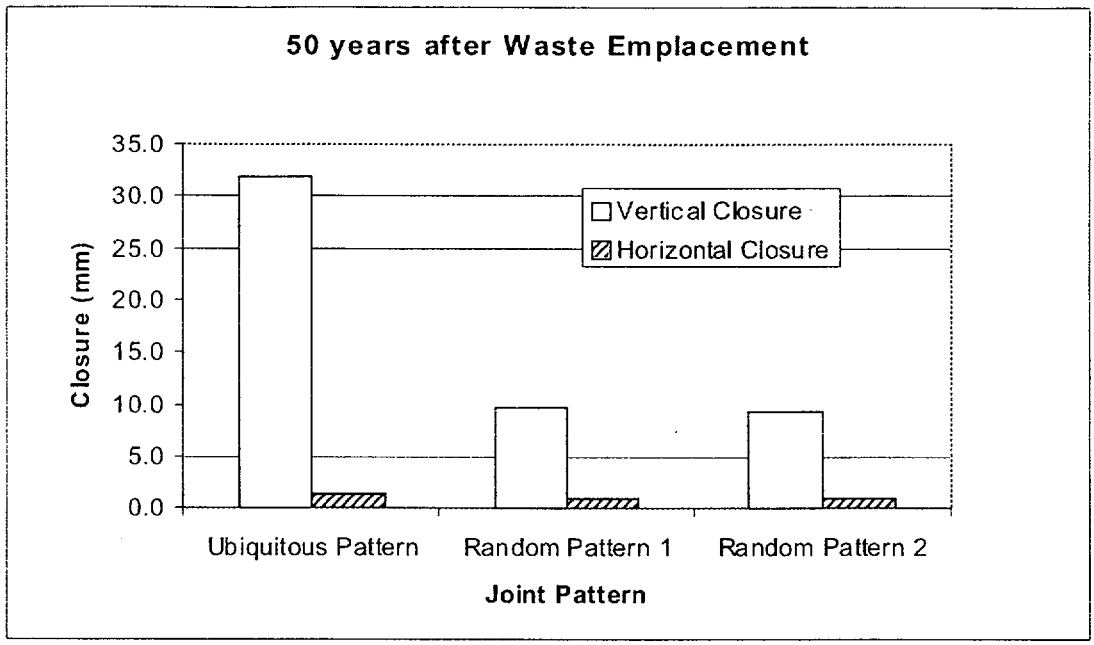

Figure IV-9. Predicted Drift Closures, 50 Years after Waste Emplacement

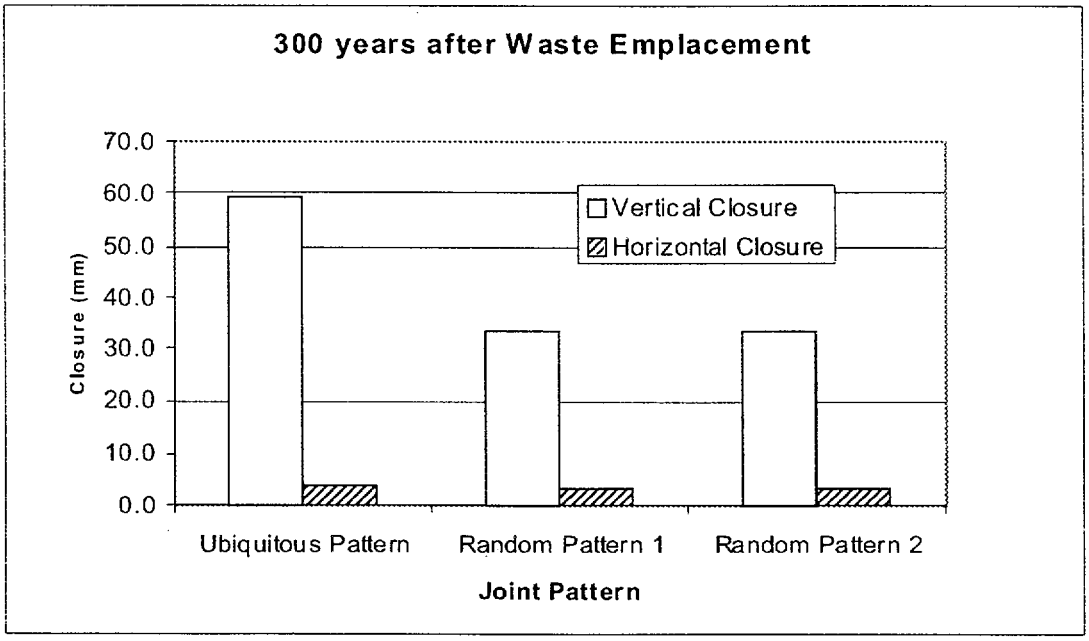

Figure IV-10. Predicted Drift Closures, 300 Years after Waste Emplacement